ACTIVATION OF SIGMA-1 RECEPTORS INCREASES EXPRESSION, TRAFFICKING, AND SURFACE LEVELS OF NMDA RECEPTORS

MOHAN PABBA

Thesis submitted to the Faculty of Graduate and Postdoctoral studies

in partial fulfillment of the requirements for the Doctorate in Philosophy degree in

Neuroscience

Department of Neuroscience

Faculty of Medicine

University of Ottawa

ABSTRACT

Sigma-1 receptors (σ-1Rs) are chaperone-like proteins that are broadly distributed throughout the central nervous system and in other tissues. They have been implicated in several physiological and pathological processes, primarily by their ability to modulate certain voltage- and ligand-gated ion channels. Growing evidence suggests that σ-1Rs regulate the functions of ion channels, such as voltage-gated K^+ 1.2 (Kv 1.2) and the human *Ether-à-go-go*-Related Gene (hERG) ion channels, by modulating their expression, trafficking, and targeting.

While it is well documented that σ-1Rs enhance the function of *N*-methyl-D-aspartate receptors (NMDARs), the mechanisms of this enhancement remain poorly understood. Using biochemical methods, we show that 90 minutes after intraperitoneal (i.p.) injection of σ-1R agonists such as (+)-SKF 10,047 (SKF) or (+)-Pentazocine (PTZ) (2 mg/kg), there is an increase in the expression of GluN2 subunits of NMDARs and postsynaptic density protein-95 (PSD-95) in the rat hippocampus. Following activation of σ-1Rs, co-immunoprecipitation (Co-IP) experiments reveal an increased interaction between σ-1Rs and NMDAR subunits; sucrose gradient centrifugation demonstrates an increase in the protein levels of GluN2 subunits in vesicular compartment; and biotinylation shows an increase in the surface levels of GluN2A-containing NMDARs.

Taken together, our results suggest σ-1Rs may enhance NMDARs function by increasing their expression, trafficking, and surface levels. This σ-1R-mediated increase in NMDAR expression and surface levels might be involved in several physiological processes such as learning and memory. Our findings also suggest that σ-1Rs could form a potential target for designing novel antipsychotics.

TABLE OF CONTENTS

ACKNOWLEDGEMENTS

First and foremost, I would like to thank **Dr. Richard Bergeron** for providing me with the guidance and opportunity to pursue my PhD studies in his laboratory. It has truly been my pleasure and a great experience to work with him. Dr. Bergeron's laboratory has not only provided me with an inspiring training environment to acquire the skills in the field of neuroscience, but I have also gained life skills that I carry forward with me forever. Dr. Bergeron has been an extremely supportive mentor throughout my studies in providing his scientific expertise and insightful ideas, without a doubt, I could not have accomplished progress in my studies. I would like to express my sincere and whole-hearted gratitude to Dr. Bergeron for providing me a platform to settle in science, life, and in Canada.

I would like to thank the PhD advisory committee members **Dr. Paul Albert, Dr. Johnny Ngsee**, **Dr. Leo Renaud** for their encouragement, time, guidance and perceptive. I especially like to thank Dr. Ngsee for his support in providing me letters of recommendation. I also like to thank **Dr. Stephen Gee** and **Dr. Rae R. Matsumoto** for their input on my thesis.

Over the past 5 years, I have had the opportunity to work with many exciting and supportive individuals within and outside Dr. Bergeron's laboratory. I would like to thank all and every member of Richard's laboratory; former members that include: **Wafae Baker**, **Jean-Francois Bordaus, Dr. Chun Lei Ma**, **Dr. Marzia Martina, Christian Metivier**, **and Dr. Emilie Muller**. I would especially like to thank to Dr. Marzia, for her guidance and encouragement in personal and professional forefronts. It is her with whom I had my

interview in May 2007, Milan, Italy to pursue my PhD studies in Dr. Bergeron's lab: Thank you Marzia. I also like to thank Christian Metivier for your support and patience in placing orders for numerous chemicals, questions, turning my daily challenges in the lab into a smooth journey. I also like to extend my gratitude to the present lab members that include: **Nina Ahlskog**, **Samed Asmer**, **Dante Biscaro**, **Elitza Hristova**, **Pamela Khacho**, **Kirean Mccann**, **Wissam Nassrallah, Dr. C. Prakash, Alexandra Sokolovski**, **Jack Wang**, and **Dr. Adrian Wong**. I would especially like to thank Adrian for his helpful suggestions, numerous discussions and criticisms in the progress of my project. Thank you Adrian, for your patience while correcting my progress reports and comprehensive exam. I also like to thank Dante for helping me in carrying out several experiments. In addition, I would like to thank **Dr. Jean-Claude Béïque** and his lab members: **Saleha Assadzada**, **Denise Cook, Sean Geddes**, **Kevin Lee**, **Cary Soares**, **Dr. Tina Qin**, and **Ling Tian**, for creating an exciting working environment and numerous discussions during my presentations at our joint lab meetings.

I like to thank my friends: **Syed Anwar**, **Dinesh Kumar**, **Raju Nallagonda**, **Pradeep Reddy, Srinath**, **Munender Vodanala**, and **Patrik Whalberg** for keeping me motivated in pursuing Ph.D. I would especially like to thank Anwar and Raju for having tons of discussions about research in the field of science that has stemmed me to decide my career in the field of research. I am also grateful to Dinesh for his encouragement, which generated curiosity and many discussions on personal and professional grounds often during difficult times.

I like to thank **Paul Andre David, Nella Bianconi,** and **Linda Richard** for their academic assistance during my training. I would especially like to thank **Linda Richard** for providing me support in several grounds for settling in Canada. I would also like to thank Linda and **Kelsey Oldland** for editing my thesis. I am also thankful to **Kim Roper** for editing my revised thesis.

I like to thank the University of Ottawa for providing me a PhD scholarship to perform this research.

This work would not have been accomplished without the support of my family. I would like to thank my mom, dad and brother: **Nagamani**, **Omprakash,** and **Mahesh** for their love and support. I also like to thank my father-, mother-, and sister-in-law: **Guru Prasad**, **Ratna Mangari,** and **Supriya** for their curiosity and support in the progress of my studies. Finally, my deepest and most heartfelt thanks goes to my wife **Anupama**: You have respected my schedule and provided me constant feedback and encouragement. I would also like to thank my daughter **Manaswini** for providing me time to work at home.

DEDICATION

I dedicate this thesis to my family.

LIST OF FIGURES

PAGE NUMBER

LIST OF TABLES

PAGE NUMBER

LIST OF ABBREVIATIONS

4-PPBP	4-Phenyl-1-(4-phenylbutyl)piperidine
σ-1R	Sigma-1 receptor
AMPA	α-Amino-3-hydroxy-5-methyl-isoxazole-4-propionic acid
AMPAR	α-Amino-3-hydroxy-5-methyl-isoxazole-4-propionic acid receptor
BD1047	N'-[2-(3,4-dichlorophenyl)ethyl]-N,N,N'-trimethylethane-1,2-diamine
BD1063	1-[2-(3,4-dichlorophenyl)ethyl]-4-methylpiperazine
BiP	Binding immunoglobulin protein
c-FOS	a proto-oncogene
Clozapine	8-Chloro-11-(4-methyl-1-piperazinyl)-5*H*-dibenzo[*b*,*e*][1,4]diazepine
Co-IP	Co-immunoprecipitation
CREB	cAMP response element-binding protein
DMT	N,N-Dimethyltryptamine
DTG	1,3-Di-(2-tolyl)guanidine
E-5842	(4-(4-fluorophenil)-1,2,3,6-tetrahydro-1-[4-(1,2,4-triazol-1-il)butyl] pyridine citrate)
EPSCs	Excitatory postsynaptic currents
EPSPs	Excitatory postsynaptic potentials
ERK1/2	Extracellular signal-regulated kinases
ER	Endoplasmic reticulum
ERPF	ER/microsomes/mitochondrial pellet fraction
EZ-link sulfo-NHS-SS-biotin	

	sulfosuccinimidyl-2-[biotinamido]ethyl-1,3-dithiopropionate
GluA1	AMPA receptor subunit 1
GluA2/3/4	AMPA receptor subunits 2/3/4
GluN1	NMDA receptor subunit 1
GluN2A	NMDA receptor subunit 2A
GluN2B	NMDA receptor subunit 2B
GlyR	Glycine receptor
Haloperidol	4-[4-(4-Chlorophenyl)-4-hydroxy-1-piperidyl]-1-(4-fluorophenyl)-butan-1-one
hERG	the human *Ether-à-go-go*-Related Gene
IgG	Immunoglobulin type G
IP3	Inositol 1,4,5 triphosphate
i.p.	Intraperitoneal
i.v.	Intravenous
K_i	Inhibition constant of the ligand-receptor complex
K_d	Dissociation constant of the ligand-receptor complex
Ketamine	2-(2-Chlorophenyl)-2-(methylamino) cyclohexanone hydrochloride
Kv1.2	Voltage gated K^+ 1.2 ion channel
LP1 fraction	Crude synaptosomal membrane fraction
LTP	Long-term potentiation
MAM	Mitochondria associated ER-membrane
NOS	Nitric oxide synthase
nNOS	neuronal Nitric oxide synthase

NMDA	*N*-methyl-D-aspartate
NMDAR	*N*-methyl-D-aspartate receptor
PCP	Phencyclidine [1-(l-phenylcyclohexyl)piperidine]
PDZ	PSD95, Discs large, Zona occludens 1
PRE-084	2-(4-Morpholinethyl) 1-phenylcyclohexanecarboxylate hydrochloride
PSD-93	Postsynatic density protein-93
PSD-95	Postsynaptic density protein-95
P or PTZ	(+)-Pentazocine (2*RS*,6*RS*,11*RS*)-6,11-dimethyl-3-(3-methylbut-2-en-1-yl)-1,2,3,4,5,6-hexahydro-2,6-methano-3-benzazocin-8-ol hydrochloride
SAP97	Synapse associated protein 97
SAP102	Synapse associated protein 102
s.c.	Subcutaneous
SEM	Standard error of the mean
SGC	Sucrose gradient centrifugation
S or SKF	(+)-SKF10,047 (*N*-allyl-normetazocine) 2*S*-(2α,6α,11*R**]-1,2,3,4,5,6-hexahydro-6,11-dimethyl-3-(2-propenyl)-2,6-methano-3-benzazocin-8-ol hydrochloride (N-allylnormetazocine)
SMF	Synaptosomal membrane fraction
VesF	Vesicular fraction
V or Veh	Vehicle

THESIS FORMAT

As per guidelines from the Faculty of Graduate and Postdoctoral studies, this thesis is presented as a monograph. This thesis has a general introduction providing a review of current literature as relevant to the field of study. Sections such as materials and methods, and present findings follow the introduction of the thesis. The thesis ends with a discussion that discusses the presented findings, and how these findings fit into advances in the field of study.

INTRODUCTION

1. SIGMA-1 RECEPTORS (σ-1Rs)

Sigma receptors (σ-Rs) were originally proposed in 1976 by Martin et al. based on the psychotomimetic actions of the drug (±)-SKF-10,047 (SKF) in morphine-dependent and non-dependent chronic spinal dogs (109). The name "sigma" (σ) was derived from the first letter "S" of SKF, a prototypic ligand for these receptors. σ-Rs were formerly thought to be a subtype of opioid receptors due to the complex pharmacology of the (-)-isomer of SKF as it binds to μ and κ opioid receptors (186). However, σ-Rs were subsequently found to exhibit enantioselectivity for the (+)-isomers and their actions were resistant to naloxone, an antagonist of opioid receptors (195). The σ-Rs were henceforth classified as a unique, non-opioid family of receptors (190).

Autoradiographic, electrophysiological, and behavioral studies using either [^{3}H]-labeled or non-labeled different σ-R ligands have revealed subtypes of σ-Rs (15, 20, 75, 100). Two subtypes have been proposed, σ-1 and σ-2 receptors (σ-1R and σ-2R, respectively) (161). These subtypes differ primarily in their drug selectivity, tissue distribution, molecular weights, and functions (52, 210).

σ-1Rs are the main focus of this thesis, being well-known and the only subtype of σ-Rs that have been sequenced and cloned from a number of species (including mouse, rat, guinea pig, and human) (56, 84, 127, 149, 157, 177, 179). Further, growing evidence from cellular and preclinical studies indicate that σ-1Rs are involved in a variety of neuronal disorders such as schizophrenia, amnesia, depression, and stroke (119).

1.1 Molecular biology of σ-1Rs

Initial characterization of the σ-1R gene was performed via a two-step process: First, membranes were treated with [^{3}H]-labeled selective σ-1R agonists to allow a partial σ-1R

amino acid sequence to be determined from the extracted protein; then, the corresponding cDNA sequence was cloned using reverse transcriptase PCR.

As summarized in **Table I**, the σ-1R gene locus in humans, mice, and rats is on chromosome 9, 4, and 5, respectively. In humans and mice, the σ-1R gene length is ~ 7 kbp and contains four exons and three introns. The coding region of the σ-1R gene is flanked by 5'- and 3'- noncoding regions of varying lengths of base pairs (56, 84, 127, 149, 157, 177, 179). Of particular note, the nucleotide sequence upstream of the σ-1R gene lacks the classical promoter element TATA box; however, three GC boxes are present within 100 nucleotides upstream of the σ-1R gene. Such GC boxes, in the absence of a TATA box, are known to play a critical role in binding to various transcription factors, thus promoting transcription of the gene (157).

Alternative splice variants and gene polymorphisms have been described for the σ-1R. Two mRNA splice variants have been described, one lacking exon 2 and the other lacking exon 3 (48, 182, 218). σ-1R gene polymorphisms have been implicated in certain neuropsychiatric disorders, particularly schizophrenia, addiction, and alcoholism (72, 141, 194). Polymorphisms in the σ-1R gene are also linked to certain neurodegenerative disorders, such as amyotrophic lateral sclerosis and Alzheimer's disease (3, 206); however, due to conflicting reports, it remains to be clarified whether this is a causal association. For example, the σ-1R gene polymorphism exists at two regions (GC-241-240TT and Gln2Pro) which were predicted to have connections with TT/Pro22 haplotype of schizophrenia (72), but several other reports have demonstrated that there is no such association between σ-1R gene polymorphism and schizophrenia (142, 175, 205).

1.2 Structure, pharmacology, and endogenous ligands of σ-1R

σ-1Rs are integral membrane proteins consisting of 223 amino acids with a molecular mass of ~ 28 kDa (56, 84, 127, 177, 178). The amino acids of σ-1R proteins across mammalian species are 94% identical and 95% similar (127) (**Fig 1** and **Table II**). σ-1Rs do not show sequence homology with any of the known classical neurotransmitter or neuropeptide receptors, but they share 30% sequence identity with a non-mammalian protein, the fungal sterol C8-C7 isomerase (56). Hence, σ-1Rs were predicted to have a role in sterol synthesis (131).

Like most cellular proteins, certain amino acid residues of σ-1Rs undergo post-translational modifications such as phosphorylation and myristolyation (84, 149, 157) (**Table II**). It remains unclear whether these modifications have any influence on the σ-1R structure, ligand binding properties, and physiology.

Hydropathy analysis on the σ-1R protein sequence has predicted that σ-1Rs could have two different membrane topologies consisting of either one or two transmembrane domains (56, 84, 127, 178). Studies performed by Aydar et al. and Hayashi et al. have confirmed that σ-1Rs consists of two transmembrane domains, one at the N-terminus (amino acid position 11–29) and another one in the middle of the protein (amino acid position 91–109) (9, 61) (**Fig 2**).

The ligand-binding domains of σ-1Rs have also been identified (188). Photoaffinity labeling and site-directed mutagenesis on recombinantly purified σ-1Rs have provided evidence for the existence of at least three ligand-binding domains: steroid binding domain-like I (SBDLI) (amino acids 91–109), steroid binding domain-like II (SBDII) (amino acids 176–194), and N-terminal transmembrane domain (30, 146, 147, 168). Furthermore, the

region from the initial portion of the second transmembrane domain (STD) to the middle portion of the σ-1R C-terminus is believed to be a part of the ligand-binding site (178). Support for this assumption comes from studies using the σ-1R mRNA splice variant lacking exon 3 (amino acids 119–149), where [^{3}H]-PTZ did not bind to σ-1R (48, 218). As well, Yamamoto et al. have shown that the amino acid substitutions (S99A, T103P and di-L105,106-di-A) in the STD of σ-1R is critical for ligand binding (218). Consequently, it appears that the binding of ligands to σ-1Rs requires two transmembrane domains and the amino acids spanning between 119–149 and 176–194 (**Fig 2**). The crystal structure of σ-1Rs in agonist bound conformational state would provide more concrete evidence regarding the residues and domains involved in ligand binding.

σ-1Rs has been extensively characterized in drug-binding studies (210). Several classes of high affinity, chemically- and structurally-unrelated drugs bind to σ-1Rs. These drugs can be grouped into following categories: (a) psychotomimetic benzomorphans (e.g., SKF, PTZ); (b) psychostimulants (e.g., cocaine, amphetamine and their derivatives, N,N-Dimethyltryptamine (DMT)); (c) arylcyclohexylamines (e.g., PCP); (d) N,N'-diaryl-substituted guanidines (e.g., DTG); (e) neuroactive steroids (e.g., progesterone); (f) neuroleptics (e.g., haloperidol, many new atypical antipsychotic agents); (g) peptides (e.g., neuropeptide Y); and (h) antidepressants (e.g., fluvoxamine) (32, 119, 210). Several studies suggest steroids (e.g., progesterone) are the endogenous ligands of σ-1Rs (187, 190). A recent study has shown that the hallucinogen DMT also acts as endogenous ligand for σ-1Rs (46). However, the potential role of steroids and DMT acting as endogenous ligands for σ-1Rs is not yet clear since the concentration of these compounds in *in vivo* might not be high enough to act in this way (24, 40, 176). This could be particularly true for DMT, which is

rapidly metabolized by the body (24, 40).

1.3 Distribution of σ-1Rs

σ-1Rs are distributed throughout the brain, localized in brain regions such as those involved in memory, emotion, sensory, and motor functions (52). They are also present throughout the body, for example, in peripheral organs such as heart, liver (52). However, the pattern of σ-1R distribution varies by region, from high to moderate levels. High levels of σ-1Rs are present in the pyramidal layers and dentate gyrus of the hippocampus, the granular layer of the olfactory bulb, and the hypothalamic nuclei (4). Immunohistochemical studies show that σ-1Rs are not only present in neurons but also in many other cell types, e.g., oligodendrocytes (148) and retinal cells (81).

At the subcellular level, σ-1Rs are localized mainly at the nuclear envelope, endoplasmic reticulum (ER), mitochondria-associated ER membrane (MAM), and at low levels at the post-synaptic thickenings of the neuron (4, 66). σ-1Rs at the MAM target clustered globular structures enriched with cholesterol and neutral lipids (60, 63), and σ-1R levels at the ER or MAM undergo dynamic changes depending on conditions such as agonist treatment, Ca^{2+} depletion, and ER stress (61).

1.4 Mechanisms of σ-1R action

The ubiquitous, yet specialized distribution of σ-1Rs in the brain indicate that σ-1Rs execute their physiological actions via distinct mechanisms (188, 189).

1.4.1 Translocation

The physiological role(s) of σ-1Rs remains unclear. Su et al. have identified that σ-1Rs act as a ligand-operated chaperone at the MAM, i.e., they assist in the proper folding of newly synthesized proteins (61). Under basal conditions at the MAM, σ-1Rs are associated

with a chaperone called binding immunoglobulin protein (BiP) (61).

Upon activation of σ-1Rs by agonists or endogenous ligands at concentrations ~ equal to, or less than, 10 times their K_i value, σ-1Rs dissociate from BiP. This dissociation modulates the function of inositol triphosphate receptors (IP3Rs), which in turn affects the Ca^{2+} influx and signaling into the mitochondria (61).

On the other hand, if σ-1R agonists or endogenous ligands are present in high concentrations (~ > 10 times their K_i value) or during ER stress, σ-1Rs dissociate from BiP and translocate (mobility speed ~ 8–10 μm/min (59, 83)) to the plasma membrane (92, 121, 134, 189). Recent investigations indicate that the translocating σ-1Rs could act as a trafficking scaffold and target several intracellular constituents (e.g., Kv1.4, Kv1.2 ion channels, and PKC β isoforms) to the plasma membrane (92, 121, 134). Once translocated to the plasma membrane, σ-1Rs can physically associate via protein-protein interaction with different classes of ion channels (e.g., voltage-gated Ca^{2+}, K^+, Na^+) and consequently modulate their activities (9, 46, 93, 223). Interaction of σ-1Rs with voltage-gated Ca^{2+} and K^+ channels causes either inhibition or enhancement of their activities, whereas σ-1R interaction with voltage-gated Na^+ channels results in the inhibition of sodium channel activity (35, 93). Thus, it is proposed that σ-1Rs act as inter-organelle signaling modulators serving locally at the MAM and remotely at the plasma membrane (188).

1.4.2 Alteration of mRNA or protein expression, lipid rafts, and cellular morphology

Ligand activation of σ-1Rs also triggers: (a) alteration in the mRNA or peptide/protein expression of several cellular constituents, especially ion channels (e.g., hERG ion channels, AMPARs, and NMDARs in various brain regions) (35, 53, 204); (b) formation and reconstitution of lipid-rafts (60); (c) different types of intracellular signaling

cascades that preserve cellular morphology (83); and (d) stabilization and suppression of proteins that are involved in apoptosis (65).

Various investigations have demonstrated that σ-1Rs are involved in the formation and reconstitution of lipid rafts (60)—specialized membrane microdomains of the ER or plasma membrane—although the exact relationship between them is unclear. Compared to the other membrane structures, lipid rafts contain greater amounts of cholesterol and lipids such as ganglioside and sphingomyelin. They subserve as signaling and trafficking platforms for ion channels, receptors, and kinases (67). In the ER of NG108 and PC12 cells, σ-1Rs are found in cholesterol-enriched, detergent-insoluble and ganglioside-enriched lipid rafts where the σ-1Rs compartmentalize ER-synthesized lipids (63, 193). In cultured hippocampal neurons, σ-1Rs are found in galactoceramide-enriched lipid rafts and promote oligodendrocyte differentiation (64). When animals are subjected to stroke, followed by recovery, σ-1Rs alter the lipid-raft-based trafficking of cholesterol in astrocytes and regenerating neurons (169).

The relationship between σ-1Rs and the maintenance of cellular morphology is indicated by studies showing that the overexpression of σ-1Rs or the activation of σ-1Rs with their ligands promote neurite sprouting, while knockdown of σ-1Rs causes deficiency in neurite sprouting and dendritic branching, and loss of spines and synapses (192, 193, 203). The aberrant loss of neuronal morphologies observed under the deficiency of σ-1Rs is due to the accumulation of reactive oxygen species and activation of caspase-3. These resultant changes consequently affect the machinery of neuronal dendritic sprouting and branching (203).

σ-1Rs also promote cell survival by stabilizing the anti-apoptotic protein, Bcl-2

(219), and by suppressing the expression and activation of pro-apoptotic proteins, Bcl-2-associated X protein (Bax) and caspase-3 (198). The level at which σ-1Rs exert their effects on these apoptotic proteins is currently unclear (i.e., the post-translational level or the gene level (119)); however, recent investigations indicate regulation at the gene level (128, 225).

Through their unique mechanisms of action, σ-1Rs play an important role in different physiological and pathological processes that occur in the brain. Important cognitive functions, such as learning and memory, and pathological conditions, such as addiction, amnesia, schizophrenia, depression, and Alzheimer's disease, are modulated by σ-1Rs (65, 83, 93, 119). σ-1Rs exert their modulatory role in learning and memory, and in disease conditions such as schizophrenia and depression, mainly by enhancing the function of NMDARs. However, the mechanism through which σ-1Rs potentiate the NMDARs function remains enigmatic (**Section 3**).

A substantial amount of evidence suggests that dysfunction of NMDARs leads to several neurodegenerative and neuropsychiatric disorders (e.g., Alzheimer's disease, amnesia, depression, and schizophrenia) (97). Consequently, gaining a better knowledge of the σ-1R modulation of NMDAR function is crucial and provides the prospect for designing therapeutic strategies against such debilitating disorders. Therefore, in the following section, we focus on NMDARs.

2. NMDARs

NMDARs are glutamate-gated cation channels that permit the flow of Ca^{2+} and Na^{+} ions, and are hetero-tetramers of subunits GluN1, GluN2 and or GluN3 (**Fig 2**) (151). A functional NMDAR ion channel complex requires an assembly of two obligatory GluN1 subunits together with either two GluN2 subunits or a combination of GluN2 and GluN3

subunits. Isoforms of the NMDAR subunits generate a large repertoire of NMDAR subunit combinations, giving rise to several functionally distinct NMDARs (145, 151). The GluN2 family includes four members (GluN2A through GluN2D) encoded by four different genes, while the GluN3 family includes two members (GluN3A and B) encoded by two separate genes (145, 151). Only one gene encodes the GluN1 subunit, but alternative mRNA splicing occurs at three regions of the gene, leading to eight possible isoforms for GluN1 (69, 151). Of all the NMDAR subtypes, those containing GluN2A and GluN2B subunits have received the most attention due to their distinctive spatiotemporal distribution and electrophysiological, molecular biology, and biochemical profiles (151).

2.1 GluN2A- and GluN2B-containing NMDARs distribution and electrophysiology

The GluN2A- and GluN2B-containing NMDARs are ubiquitously expressed in the brain. At the subcellular level, these NMDARs are distributed at synaptic, perisynaptic, and extra-synaptic sites of the post-synaptic neurons. The current hypothesis is that, in adults, GluN2A-containing NMDARs are present predominantly at synaptic sites, while GluN2B-containing NMDARs are at extra-synaptic sites (57).

Both GluN2A- and GluN2B-containing NMDARs carry large Ca^{2+} conductances and show high sensitivity to Mg^{2+} block (201). Of the two, GluN2A-containing NMDARs display currents with faster rising and decaying kinetics (217). At the single channel level, GluN2A-containing NMDARs exhibit higher open probability and faster deactivation time courses. Conversely, GluN2B-containing NMDARs at macroscopic and single channel level display slower kinetics, lower open probability, and slower deactivation time courses (217). However, many of these channel properties can vary according to the isoform of the GluN1 subunit in the NMDAR complex (201).

2.2 Molecular biology and biochemistry of GluN2A- and GluN2B-containing NMDARs

The NMDAR subunits' genes contain multiple transcription start sites with TATA and CAAT boxless promoter regions enriched with the GC content. The 5'-UTR region of NMDAR genes vary between 200 to over 1200 base pairs and contain several sites for binding promoters and transcription factors, such as NFκB, CREB, and REST, which regulate the transcription of NMDAR genes (201, 209).

NMDAR gene translation acts as one of the regulatory steps in determining NMDAR protein expression (201, 209). One study indicates that two pools of GluN1 mRNA with different translational rates exist, but whether the translation rate is determined by 5'-UTR or 3'-UTR of mRNA remains unexplored (8).

The expression of GluN2A and GluN2B subunits depends on the translation of their mRNA, especially GluN2A. The deletion or mutation of few base pairs in the 5'-UTR region of GluN2A subunit mRNA controls the level of its protein expression (29, 215).

While the pattern of NMDAR subunits gene expression appears to be relatively stable, the precise molecular mechanisms and components involved in several steps of the process are less well understood. This is probably because NMDAR gene expression at a given spatial and temporal scale is highly dependent on a wide range of factors, such as cell or tissue type, pharmacological manipulations (i.e., acute or chronic treatment with clinically relevant or non-clinical drugs), and pathological conditions (201, 209).

What *is* understood is that following transcription and translation, GluN2A- and GluN2B-containing NMDARs undergo several post-translational modifications such as glycosylation, nitrosylation, ubiquitination, phosphorylation, and palmitoylation (201). They

also interact with several intracellular proteins at their respective C-terminus tails. The GluN2A- and GluN2B-subunit C-terminus tail interacts with diverse classes of intracellular proteins: cytoskeletal, CaMKII, endocytosis machinery, PDZ-domain-containing family of proteins, PSD-95 family ((**Fig 2**) PSD-95 (91, 138), PSD-93 (22), SAP97 (85) and SAP102 (136)) and many others (201).

Alterations such as post-translational modifications and protein-protein interactions occurring to NMDAR subunits influence the trafficking and targeting of NMDARs to synaptic or extrasynaptic sites of the neuron (214). In particular, NMDAR phosphorylation and interaction with the PSD-95 family of proteins have distinct roles in tailoring the trafficking and targeting (surface expression), as well as removal of GluN2A- and GluN2B-containing NMDARs from the plasma membrane (214).

2.3 Mechanisms of GluN2A- and GluN2B-containing NMDARs trafficking and targeting

NMDARs are trafficked from the ER via Golgi apparatus to the plasma membrane in different kinds of vesicles (i.e., those containing large protein complexes of NMDARs, PSD-95 family of proteins, and several other proteins) (160).

The association between GluN2B-containing NMDARs, SAP102, SAP97, CASK, Sec8, and mPins in the ER drives these receptors to Golgi outposts (79, 172). Along the dendrites, the trafficking of GluN2B-containing NMDAR vesicles occurs in the form of a large protein complex containing GluN2B, KIF17, mLin-10, mLin-7/CASK, SAP97, SAP102 and PSD-95 (51, 79, 173, 180, 183, 213, 221). Disruption of this large protein complex results in reduced surface expression of GluN2B-containing NMDARs (172, 173).

The intracellular trafficking and sorting of GluN2A-containing NMDARs is less well

understood. However, it has been demonstrated that KIF17 plays an important role in the incorporation of GluN2A-containing NMDARs at synapses (221). As well, the interaction between GluN2A-containing NMDARs and SAP97 drives the trafficking of GluN2A-containing NMDARs through Golgi outposts and ultimately results in insertion into the plasma membrane (49, 112).

The plasma membrane insertion of GluN2A- or GluN2B-containing NMDARs can occur either directly (exocytosis) or mixed with endosomes that contain recycled NMDARs via involvement of myosin or actin filaments (5, 99). Disrupting the interaction between GluN2B-containing NMDARs and PSD-95 results in the removal of GluN2B-containing NMDARs from synaptic sites (158, 164, 174) and also could interfere with the insertion of the newly synthesized/recycled pool of these receptors (12, 153, 160, 172, 173). Thus, we see that highly complex and coordinated mechanisms control the trafficking and targeting of NMDARs, and they eventually influence the functions of NMDARs.

2.4 Functions of NMDARs

The GluN2A- and GluN2B-containing NMDARs are highly permeable to Ca^{2+} ions. As a result, they play an important role in several physiological processes occurring in the brain. For example, they are involved in synaptogenesis and synaptic plasticity (which brings long-lasting changes in synaptic efficacy, e.g., long-term potentiation (LTP)) (135, 200). Excessive activation of NMDARs (e.g., during ischemia) and subsequent Ca^{2+} influx into the postsynaptic neuron results in cell death (58, 103). Dysfunction of NMDARs leads to several neurodegenerative and neuropsychiatric disorders, e.g., Alzheimer's disease, amnesia, depression, and schizophrenia (97, 151). As a result, neurons modulate the functions of NMDARs via several extracellular (e.g., trans-synaptic) and intracellular

proteins (e.g., PSD-95 and σ-1Rs) to tailor the NMDARs role in numerous physiological and pathological processes.

3. σ-1R enhancement of NMDAR function

By employing electrophysiological techniques, various researchers have shown that σ-1R ligands enhance the frequency of NMDA-induced action potentials, the amplitude of NMDAR-mediated field excitatory postsynaptic potentials (fEPSPs), and NMDAR-mediated synaptic responses (excitatory postsynaptic currents (EPSCs) and potentials (EPSPs)) (27, 102, 108, 110, 133). Additionally, using behavioral models, Maurice's group has provided a large body of evidence that *in vivo* administration of several σ-1R ligands improve the behavior (learning and memory) of animals that are experiencing NMDAR-antagonism-induced amnesia (**Fig 3A**) (113, 114, 118, 120).

Based on both the electrophysiological and behavioral studies, three important observations can be summarized from the σ-1R enhancement of NMDAR function: (**a**) low doses of σ-1R agonists enhance NMDAR function (15, 114, 115), while high doses of σ-1R agonists do not enhance NMDAR function (44, 45). (**b**) The σ-1R action on NMDAR function is observed only when NMDARs are activated and the subsequent Ca^{2+} influx through NMDAR channel occurs (110, 117). (**c**) Following the activation of σ-1Rs, the facilitation of NMDAR-mediated responses or amelioration of learning and memory can be observed typically between 5–30 min, depending on the type of treatment (i.e., bath application of σ-1R agonists to tissue slices, 5–10 min; administration of σ-1R agonists to animals via different routes, 15–30 min). The amelioration effect can potentially be sustained as long as 90–120 min or, occasionally up to few days (14, 15, 50, 110, 114, 120). For example, Bergeron et al. reported that the increase in frequency of NMDA-induced action

potentials 15–30 min after i.v. administration of σ-1R agonists into anesthetized animals can be sustained as long as 90–120 min (13, 15). Maurice et al. demonstrated that subcutaneous administration of σ-1R agonists improved the short- and long-term memory (with time scales ranging between 30 min to hours/days) in mice experiencing NMDAR-antagonism-induced amnesia (113, 114, 120).

3.1 Mechanisms of σ-1R enhancement of NMDAR function

Although the σ-1R action on NMDAR function is well documented, the precise molecular mechanisms involved in the σ-1R enhancement of NMDAR function remain elusive.

Several laboratories using multidisciplinary approaches examined and suggested diverse mechanisms in the σ-1R enhancement of NMDAR function (**Fig 3B**). Using extracellular unitary recordings, Debonnel's group tested for the involvement of G-proteins in σ-1R-mediated enhancement in the frequency of NMDA-induced action potentials (132). They pretreated rats by injecting pertussis toxin (1 μg/2 μl) into the dorsal hippocampus (CA3 region), and then tested the efficacy of various σ-1R agonists in potentiating the NMDAR function. They noted that certain σ-1R agonists did not potentiate the frequency of NMDA-induced action potentials, suggesting the involvement of G-proteins in σ-1R action. Previous data from our lab show that σ-1Rs potentiate NMDAR EPSCs in the CA1 region of hippocampus by inhibiting SK channels (110).

Other laboratories have advocated for the involvement of intracellular signaling cascades in the σ-1R enhancement of NMDAR function. For example, Rho et al. (2011) proposed the participation of nitric oxide synthase (NOS) (165). Through an independent series of examinations, Chen's group and Kim et al. (2008) suggested the involvement of

Src-ERK1/2 signaling or protein kinase A- and protein kinase C-dependent phosphorylation of NMDAR subunits in the σ-1R's action on NMDARs function (86, 165, 166).

Nevertheless, the above-mentioned mechanisms do not completely explain the mechanisms of σ-1R action on NMDAR function. They do not clarify whether there are any changes in the protein expression and or surface levels of NMDARs in the σ-1R potentiation of NMDAR function.

The observation of enhancement in NMDAR function, especially at 90–120 min following σ-1R activation (13, 15) is most likely to occur via one, all, or combination of the following four plausible mechanisms, although several other possibilities and the above-mentioned mechanisms cannot be excluded. First, following σ-1R activation there could be an increase in the expression level (i.e., number) of NMDARs that leads to an increase in the levels of synaptic NMDARs. Second, there could be a change in NMDAR trafficking (redistribution) following σ-1R activation, resulting in an increase in surface NMDARs relative to the intracellular compartments (e.g., ER/Golgi), with or without any change in the expression of NMDARs. Third, an enhancement of NMDAR function by σ-1R could be due to alteration in the kinetics of NMDAR-mediated responses with a change in the surface levels of NMDARs. Fourth, consistent with the previous view of σ-1R modulation of several voltage-gated ion channels (**Section 1.4**), the potentiation of NMDAR function following σ-1R activation could occur due to the physical association between σ-1Rs and NMDARs that then consequently increase trafficking (redistribution) and surface presentation of NMDARs, similar to the σ-1R modulation of Kv1.2 ion channel function (92).

Taken together, the mechanisms of alteration in NMDARs protein expression, trafficking, and targeting underlying the σ-1R enhancement of NMDAR function still remain

unclear, so therefore requires further investigation. Understanding the potentiation of NMDAR function by σ-1Rs not only provides insights about functional association between σ-1Rs and NMDARs, but also affords opportunities to design counteractive measurements against NMDAR dysfunction in several neuropsychiatric and neurodegenerative disorders.

4. Aims of the thesis

By employing biochemical methods, the present study aims to investigate whether there is any increase in: (**A**) protein expression, (**B**) surface levels, and (**C**) trafficking of NMDARs in the rat hippocampus at 90 min following administration of σ-1R agonists (**Fig 3C**). We choose to investigate at this time point because electrophysiological studies indicated for the presence of σ-1R potentiation of NMDAR function at this time point in drug-treated rats (13, 15). Biochemical characterization of protein expression, surface levels, and trafficking of NMDARs provides the opportunity to identify and understand plausible mechanisms involved in σ-1R enhancement of NMDAR function, while overcoming certain technical limitations associated with several other forms of study.

5. Hypothesis

Acute activation of σ-1Rs increases protein expression, trafficking, and surface levels of NMDARs in the rat hippocampus (**Fig 3C**).

6. Model of study

It is clear that activation of σ-1Rs by agonists lead to an increase in the frequency and amplitude of NMDAR-mediated action potentials as well as the NMDAR-EPSCs in rat hippocampal neurons (13, 15, 110). Since these NMDAR-mediated events occur at synapses, it is appropriate to isolate and examine the aims of current study in neuronal synaptic compartments, i.e., synaptosomes. Therefore, rat hippocampal synaptosomes are mainly

used for elucidating the aims of the present study.

MATERIALS AND METHODS

1. Antibodies and Drugs

The following is a list of antibodies and their dilutions that were used in this study: rabbit polyclonal anti-c-FOS 1:2000 (LifeSpan Biosciences, WA, USA); rabbit polyclonal anti-pCREB 1:2000 (Cell Signaling, MA, USA); rabbit polyclonal anti-CREB 1:2000 (Santa Cruz, CA, USA); rabbit polyclonal anti-pERK 1/2 (42/44) 1:2000 (Cell Signaling, MA, USA); rabbit polyclonal anti-ERK 1:2000 (Cell Signaling, MA, USA); goat polyclonal anti-flotillin 1:250 (Santa Cruz, CA, USA); rabbit polyclonal anti-GluA1 clone C3T IgG 1:2500 (Upstate, MA, USA); rabbit polyclonal anti-GluA2/3/4 1:3500 (Cell Signaling, MA, USA); mouse monoclonal anti-GluN1 1:10,000 (Synaptic Systems GmbH, Germany); mouse monoclonal anti-GluN2A 1:750 (LifeSpan Biosciences, WA, USA); mouse monoclonal anti-GluN2B 1:750 (LifeSpan Biosciences, WA, USA); rabbit polyclonal anti-GluN2B 1:10,000 (Affinity BioReagents, MA, USA); rabbit polyclonal anti-α-1,2-GlyR 1:5000 (Affinity BioReagents, MA, USA); mouse monoclonal anti-PSD-95 1:10,000 (Affinity BioReagents, MA, USA); goat polyclonal anti-σ-1R 1:250 (Santa Cruz, CA, USA); rabbit polyclonal anti-β-tubulin 1:30,000 (Abcam, MA, USA).

SKF, BD1047, and BD1063 were purchased from Tocris, MN, USA; PTZ was purchased from Sigma Aldrich, MO, USA; anisomycin was purchased from Bioshop, ON, Canada. SKF, BD1047, and BD1063 were dissolved in PBS, whereas PTZ was initially dissolved in warm 0.1 N HCl and then diluted with buffer containing 0.029 M NaOH and 0.050 M KH_2P0_4, pH 7. Anisomycin was dissolved in DMSO and then diluted with buffer containing 0.029 M NaOH and 0.050 M KH_2P0_4, pH 7.

2. Drug treatments and isolation of hippocampi

All animals were handled in agreement with the guidelines of the Canadian Council

of Animal Care. Male Sprague Dawley® rats (4–6 weeks of age) were i.p. injected with vehicle (PBS), SKF (2 mg/kg), or PTZ (2 mg/kg), separately based on suggestions for the induction of σ-1R mediated effects on NMDAR function *in vivo* published in previous reports (76, 77). The hippocampi from these animals were collected at 30, 45, and 90 min after i.p. injection. For BD1047 and BD1063 treatment, animals were implanted subcutaneously with 100 µl osmotic mini-pumps (1 µl/h flow rate) (Alzet®, CA, USA) for 2 days at a concentration of 2 mg/kg. On the 2^{nd} day, the hippocampi were isolated 90 min after either SKF or PTZ injection. The dosage and delivery of BD1047 and BD1063 was guided by previously published report (222). For anisomycin treatment, anisomycin (30 mg/kg (212)) was injected i.p. 1 h prior to the injection of SKF or PTZ, and hippocampi were isolated after 90 min. The denotation "n" in the results and figure legends refers to the number of experiments (e.g., n = 9 represents 9 different experiments). For each experiment, a minimum of 3 or 4 hippocampi were obtained from separate rats (treated with either vehicle or drug) and were processed to isolate different cellular fractions, as described below (also see **Fig 4**).

3. Isolation of crude synaptosomal membrane fraction (LP1 fraction)

All steps were performed at 4^{o}C. The isolation of the LP1 fraction from vehicle and drug treated hippocampi were performed as previously described with minor modifications (54). Isolated hippocampi were homogenized using a Dounce tissue homogenizer in 1 ml of homogenization buffer: 20 mM Tris-HCl (pH 7.4), 320 mM sucrose, 5 mM EDTA, 1 mM EGTA, 10 mM NaF, 2 mM Na_3VO_4, 1 mM PMSF, 1x EDTA-free protease inhibitor cocktail tablet (Roche, Basel, Switzerland).

The total homogenate was centrifuged at 800 x g_{max} for 10 min. The resulting pellet

(P1) was discarded and the supernatant (S1) was subjected to further centrifugation for 15 min at 9,200 x g_{max}. This second pellet (P2) was subjected to hypoosmotic lysis by suspending it in homogenization buffer (0.75 ml) with the sucrose concentration maintained at 35.6 mM instead of 320 mM. The P2 suspension was left on ice for 30 min with occasional mixing.

Subsequently, the P2 suspension was subjected to centrifugation at 25,000 x g_{max} for 30 min. The resulting pellet (crude synaptosomal membrane) was solubilized in 0.3 ml homogenization buffer without sucrose but containing 1% NP40, 0.1% SDS, and 0.1% Na-deoxycholate for 30 min with end-over-end rotation, then centrifuged for 5 min at 16,000 x g_{max}. The resulting supernatant LP1 fraction was collected, and the protein concentration was determined using a Bradford assay. The samples were stored at -80^{o}C until further analysis.

4. Subcellular fractionation

Subcellular fractionation was performed on vehicle and SKF treated hippocampi as previously described, with certain modifications (18). All steps were performed at 4^{o}C.

LP1 pellets, described in Section 3, above, were resuspended in the homogenization buffer containing 320 mM sucrose. The suspension was layered on top of a discontinuous sucrose gradient containing 0.8M/1.0M/1.2M sucrose, and centrifuged for 2 h at 65,000 x g_{avg} in an SW 55 Ti rotor with slow acceleration and deceleration. The fractions yielded at the 0.8M/1.0M sucrose interface (fraction 1; vesicular fraction, VesF) and the 1.0M/1.2M sucrose interface (fraction 2; synaptosomal membrane fraction, SMF) were collected using a 3 ml syringe and 18½ gauge needle. Fraction 3 (ER/microsomes/mitochondrial pellet, ERPF) was collected using a pipette.

After collection, fractions were centrifuged for 30 min at 30,000 x g_{max}. The resulting

pellets were resuspended in 0.3 ml of homogenization buffer without sucrose and centrifuged again for 30 min at 30,000 x g_{max}. After the second centrifugation, the pellets were resuspended in 0.3 ml of homogenization buffer containing 5% glycerol. All fractions were stored at -80^{o}C until further analysis.

5. Co-immunoprecipitation (Co-IP)

P2 membranes from vehicle and drug treated (at 90 min after SKF or PTZ) hippocampi were isolated as described above, then Co-IP extractions were undertaken as noted in prior work (191).

The P2 membranes were solubilized in 0.2 ml of 50 mM Tris-HCl (pH 8.8), 2 mM EDTA, 1x EDTA free-protease inhibitor cocktail tablet, and 0.5% Na-deoxycholate, and incubated at 37^{o}C for 30 min. After incubation, 5 volumes of ice-cold 50 mM Tris-HCl (pH 6.7), 2 mM EDTA, 1x EDTA-free protease inhibitor cocktail tablet, and 0.1% Triton X-100 were added to produce lysates. The lysates were incubated at 4^{o}C for 30 min before being subjected to centrifugation at 25,000 x g_{max} for 30 min, then pre-cleared for 1 h at 4^{o}C using Protein A/G-UltraLink Agarose Resin (Pierce, IL, USA).

Antibodies (σ-1R, PSD-95, GluN2A, GluN2B, and GluN1) and Protein A/G UltraLink Agarose Resin (50 µl, of 50%) were added to the pre-cleared lysate at 5 µg/0.2-0.4 mg of protein. Following overnight incubation in end-over-end rotation, the beads were collected by centrifuging at 1,200 x g_{max} for 5 min at 4^{o}C. The beads were then washed four times with ice-cold wash buffer (50 mM Tris/HCl (pH 7.4), 2 mM EDTA, 0.1% Triton X-100, and 50 mM NaCl) and the protein complexes were eluted by adding SDS-PAGE loading buffer. The eluted protein complexes were saved at -80^{o}C until further analysis.

6. Surface biotinylation

Hippocampal slices (300 μm) were incubated with 1 mg/ml EZ-Link Sulfo-NHS-SS-Biotin (Pierce, IL, USA) for 30 min at 4^{o}C, with a gentle agitation to biotinylate surface proteins. The excess biotin was removed by washing slices 6–10 times with ice-cold Tris buffer saline containing 200 mM $MgCl_2$ and 200 mM $CaCl_2$ (TBS⊕) before homogenization in 1 ml of ice-cold homogenization buffer. The homogenate was centrifuged at 800 x g_{max} for 5 min at 4°C.

The supernatant (S1) was subjected to centrifugation at 9,200 x g_{max} for 15 min at 4°C to obtain the P2 pellet, which was then solubilized in 0.3 ml of ice-cold lysis buffer (50 mM Tris-HCl (pH 8.8), 2 mM EDTA, 1x EDTA free-protease inhibitor cocktail, and 0.5% Na-Deoxycholate) for 30 min at 37°C. The lysates were then incubated for 1 h at 4°C with (TBS⊕) pre-washed neutravidin beads to capture biotinylated surface proteins.

The neutravidin beads were collected by centrifugation at 2,000 x g_{max} at 4°C for 30 sec, and unbound materials were also collected (Internal). Then, the neutravidin beads were washed 6x with 1 ml of ice-cold (TBS⊕) containing 0.05 % SDS. Bound proteins were eluted from the beads with 0.4 ml of elution buffer (50 mM Tris-HCl, pH (6.6), 2 % SDS, and 1 mM dithiothretiol) by boiling them for 5 min at 100^{0}C. The eluted biotinylated proteins (surface) were saved at -80^{o}C until further analysis.

7. Cell culture

SH-SY5Y cells were maintained in Dulbecco's Modified Eagle's Medium (DMEM, Invitrogen, CA, USA) containing 50 μg/ml of penicillin and streptomycin (Invitrogen), 10% fetal bovine serum (Invitrogen), and gentamicin at 1 mg/ml final concentration. The cultures were incubated at 37 ^{o}C, 5% CO_2, and 100% humidity until they reached 80% confluency.

At that point, cDNAs of NMDAR subunits and GFP were added in a ratio of 1:2:1, with a final concentration 0.5 μg/ml GluN1 cDNA, then transient transfection was carried out using ESCORT™ II (Sigma Aldrich, MO, USA) in either a 6-well or a 12-well plate. In the case of transient transfection for PSD-95, GFP and PSD-95 at a ratio of 1:3 was used.

After 48 h of transfection, cells were washed three times with PBS, trypsinized (0.25% trypsin-EDTA, Invitrogen), and harvested with homogenization buffer containing detergents. The lysate was then incubated on a turntable for 30 min at 4^{o}C followed by centrifugation at 14,200 x g_{max} for 5 min. The supernatant was collected and saved at -80 ^{o}C until immunoblotting.

8. Immunoblotting

Immunoblot technique was chosen for the analysis of changes in NMDAR protein expression and surface levels following σ-1R activation. This technique has several advantages, such as ease of separation and quantification, sensitivity of detection, and lack of cross-reactivity.

Cellular fractions (10 μg protein) were resolved by SDS-PAGE (8% or 10%) and transferred to PVDF membranes. After blocking with 5% milk in TBS containing 0.1% Tween® 20 for 1 h, the membranes were incubated overnight with the corresponding primary antibodies at 4^{o}C on a rocking table. The membranes were then washed with TBS containing 0.2 % NP40 and incubated for 1-2 h at room temperature on a rocking table with a secondary antibody conjugated to HRP. Finally, the membranes were incubated with enhanced chemiluminescence solution (GE Healthcare, LC, UK) for 1 min, and the immunoreactive proteins on the membranes were visualized either on X-ray films or on LI-COR® imaging systems (NE, USA).

To avoid any potential bias and to remain within the linear range while collecting the immunoblot data from X-ray films, a saturation curve for each protein (i.e., band intensity versus exposure time in seconds) was generated for each experiment. The band intensities for each protein were obtained from ImageJ, in grayscale and 16-bit modes, after the X-ray films were scanned at a high resolution (typically 1200 dots per inch). An example saturation curve generated for the protein(s) of interest is shown in the **Figure 5**.

From the saturation curve, typically 3 or 4 band intensities falling under the linear range were collected for each protein and normalized against band intensities of the loading control (β-tubulin, unless otherwise stated) from the same experiment. Normalized data for each protein from each experiment (drug treatment condition) were averaged before performing a comparison to the vehicle. The initial results (as shown in the **Fig 7A, 90 min post-injection of SKF**) were further confirmed through analysis by using LI-COR® Odyssey® imaging systems (NE, USA) and its associated software, Image Studio (version 2.1.10). The analyses of subsequent experiments were performed using either ImageJ or Image Studio.

All data are presented as mean ± SEM and expressed as a percentage of vehicle. The statistical significance between vehicle and drug treatment for each protein was determined using an unpaired two-tailed or one-tailed Student's t-test, and a statistically significant result was defined as p being less than 0.05.

RESULTS

1. Immunoblot characterization of σ-1R, NMDAR, and PSD-95 antibodies

This study relies mainly on immunochemical techniques, in which the specificity of the antibodies plays an important role.

The σ-1R, NMDAR, and PSD-95 antibodies were tested on the total homogenate (**Fig 4**) of rat hippocampi using immunoblot technique. As seen in the **Figure 6**, the σ-1R antibodies recognized a single band at a predicted molecular weight of the σ-1R (~ 28 kDa) (177) (**Fig 6Ai**). Pre-incubating the σ-1R antibodies with a blocking peptide (bearing the short sequence of σ-1R C-terminus) resulted in the absence of the σ-1R band (**Fig 6Ai**). We also confirmed the specificity of the σ-1R antibodies by performing an immunoblot on hippocampal total homogenates from the wild type and σ-1R knockout mice (96). The panel **Aii** in **Figure 6** demonstrates the presence of σ-1Rs in the wild type but not in the σ-1R knockout mice.

NMDAR subunit (GluN1, GluN2A, and GluN2B) antibodies and PSD-95 antibodies also recognized the NMDAR subunits and PSD-95 as single bands at approximately their predicted molecular weights (GluN1: ~ 110 kDa; GluN2A and GluN2B: ~ 172 kDa; and PSD-95 ~ 95 kDa) on immunoblots containing the rat hippocampal total homogenate (**Fig 6Bi**). The specificity of these antibodies was tested further by probing the respective proteins on the whole-cell lysates of transiently transfected SH-SY5Y cells, with either GluN1/GluN2A or GluN1/GluN2B subunits, or PSD-95 alone (**Fig 6Bii**)**.** SH-SY5Y cells were used to transfect and test the antibodies of GluN subunits because these cells do not endogenously express NMDARs.

Thus, our immunoblot experiments demonstrate that the antibodies used in this study are specific in detecting their respective proteins on membranes.

2. Activation of σ-1Rs increases the protein levels of GluN2 subunits

We wanted to ascertain whether the enhancement in NMDAR function observed 90 min following the administration of σ-1R agonists is mediated by changes in the expression and or surface levels of NMDARs (**Section 3.1**). To investigate changes in the expression of NMDARs following activation of σ-1Rs, protein levels of NMDAR subunits (GluN1, GluN2A, and GluN2B) were initially examined in the rat hippocampal crude synaptosomal (LP1) fraction by immunoblotting (see Methods). Immunoblots shown in the **Figure 7** represent typical protein levels of the NMDAR subunits in the LP1 fraction. At 90 min after i.p. injection of the classical σ-1R agonist, SKF (2 mg/kg), there was a significant increase in the protein levels of GluN2A (205.5 ± 8.8% of vehicle, n = 9, $p < 0.05$) and GluN2B subunits (208 ± 13.6% of vehicle, n = 9, $p < 0.05$) when compared with vehicle (**Fig 7A**). A similar increase was also observed 90 min after the i.p. administration of another highly selective σ-1R agonist, PTZ (2 mg/kg), but to a lesser extent than SKF. In this case, the levels of GluN2A and GluN2B subunits were 136 ± 6.5% and 128 ± 2.9% of vehicle, n = 7, $p < 0.05$ (**Fig 7B**).

Since potentiation in NMDAR function was reported to occur at 30 min and, in some cases, 45 min following the administration of σ-1R agonists, we also performed immunoblot experiments at 30 and 45 min after i.p injection of σ-1R agonists SKF and PTZ (**Fig 7A** and **B**). We found no significant change in the expression level of any of the NMDAR subunits at these time points following injection of either SKF (e.g., GluN2A subunit: 100 ± 4% of vehicle at 30 min and 122 ± 12% of vehicle at 45 min) or PTZ (e.g., GluN2B: 95 ± 10% of vehicle at 30 min and 102 ± 9% of vehicle at 45 min). In all cases, n = 4–5 and $p > 0.05$ (see **Table III**).

Previous investigations have reported that AMPAR-mediated responses remain unaffected following σ-1R activation (15, 36). To confirm that our observations were specific to NMDARs, we performed immunoblot experiments to verify any change in the protein levels of AMPAR subunits (GluA1 and GluA2/3/4) after activation of σ-1Rs. As seen in **Figure 8**, the protein levels of GluA1 and GluA2/3/4 are similar to vehicle (**Table III**) at all tested time points after either SKF (**Fig 8A**) or PTZ (**Fig 8B**) administration. Thus, our data demonstrate that a specific and a robust increase in the protein levels of NMDAR subunits in LP1 fractions occurs at 90 min following the administration of σ-1R agonists. Accordingly, we used this time point in all subsequent experiments unless otherwise mentioned.

3. Pharmacological blockade of σ-1Rs prevents an increase in the protein levels of GluN2 subunits

To confirm whether σ-1Rs mediate the increase in protein levels of GluN2 subunits in our observations (**Fig 7**), σ-1Rs were pharmacologically blocked with a specific antagonist, BD1047 (111), before SKF or PTZ administration. The robust effect of SKF on the protein levels of GluN2 subunits (**Fig 7A**) was further examined by the use of a second σ-1R antagonist, BD1063 (111).

Rats were implanted with osmotic mini-pumps containing BD1047 or BD1063 (2mg/kg/day) for two days and then challenged with SKF or PTZ (**Fig 9A**). Administration of BD1047 or BD1063 alone did not alter the levels of GluN2A (for BD1047: 111 ± 4.2 % of vehicle, n = 5, $p > 0.05$; for BD1063: 101.6 ± 6.1 % of vehicle, n = 3, $p > 0.05$) and GluN2B (for BD1047: 97 ± 4.0 % of vehicle, n = 5, $p > 0.05$; for BD1063: 109.3 ± 10.2 % of vehicle, n = 3, $p > 0.05$) (**Fig 9Bi** and **E**). However, both BD1047 and BD1063 blocked an

increase in protein levels of GluN2 subunits 90 min after SKF administration. The protein levels of GluN2A and GluN2B were 128 ± 14% and 118 ± 6.5% of vehicle, in both cases n = 4, $p > 0.05$, respectively, in the presence of BD1047 (**Fig 9C**); the protein levels of GluN2A and GluN2B were 88.9 ± 11.8 and 88.3 ± 13.7% of vehicle, in both cases n = 4, $p > 0.05$, respectively, in the presence of BD1063 (**Fig 9F**). Similar results were obtained following PTZ administration in the presence of BD1047: The protein levels of GluN2A and GluN2B were 101 ± 14% and 118 ± 16% of vehicle, in both cases n = 4, $p > 0.05$, respectively (**Fig 9D**).

Thus, the blockade of σ-1Rs by the antagonists BD1047 or BD1063 effectively prevents an SKF- or PTZ-induced increase in protein levels of GluN2 subunits in LP1 fractions (**Fig 7**), indicating the increase was mediated through direct activation of σ-1Rs.

4. Activation of σ-1Rs leads to an increase in the surface levels of GluN2A-containing NMDARs

We examined whether the increased protein levels of GluN2 subunits (**Fig 7**) was accompanied by an increase in the surface expression of NMDARs, which may account for the previously reported σ-1R-mediated enhancement in NMDAR function ((13, 15) and **Section 3**). We performed surface biotinylation experiments to investigate the surface levels of NMDARs at 30, 45, and 90 min after i.p injection of vehicle (Veh) or SKF (**Fig 10A**). These experiments were performed after SKF activation of σ-1Rs because SKF has a pronounced effect on the protein levels of GluN2 subunits (**Fig 7**) when compared with PTZ.

We first validated our biotinylation procedure by evaluating the presence of β-actin in biotinylated samples (surface), since β-actin is an abundant intracellular protein. Our immunoblots reveal that there is a marginal presence of β-actin in the biotinylated samples

(surface), suggesting that only surface proteins are biotinylated in our experiments (**Fig 10A**). We used ionotropic glycine receptors (GlyRs) as a normalization control because our preliminary immunoblot experiments showed no alteration in the surface levels of GlyRs following SKF administration.

There was a significant increase in the surface levels of NMDARs containing the GluN1 (147 ± 7.5% of vehicle, n = 8, $p < 0.05$) and GluN2A subunits (122 ± 6.0% of vehicle, n = 8, $p < 0.05$) at 90 min following administration of SKF. In contrast, no alteration in the surface levels of GluN2B was observed (84 ± 11% of vehicle, n = 8, $p > 0.05$) **(Fig 10B)**.

To determine whether the activation of σ-1Rs specifically alters NMDARs surface levels, we repeated the biotinylation experiments to verify the surface levels of AMPARs. As seen in the **Figure 10C**, there was no significant change in the surface levels of GluA1 (125 ± 14% of vehicle) and GluA2/3/4 (117 ± 19% of vehicle, in both cases n = 8, $p > 0.05$).

If activated σ-1Rs mediate the increase in surface levels of GluN2A-containing NMDARs, then blocking the σ-1Rs should prevent this increase. To test this hypothesis, we performed SKF administration in the presence of BD1063 and subsequently examined the surface levels of NMDARs. Results shown in the **Figure 10D** suggest that there is no change in the surface levels of NMDARs following SKF activation of σ-1Rs in the presence of BD1063. The surface levels of NMDARs were: GluN1, 95 ± 11% of vehicle; GluN2A, 107 ± 11.2% of vehicle; and GluN2B, 106 ± 15% of vehicle, in all cases n = 3, $p > 0.05$. Also, the surface levels of NMDARs remained unchanged after BD1063 treatment alone when compared with vehicle (GluN1, 93.4 ± 11% of vehicle, GluN2A, 98.3 ± 3.2% of vehicle, and GluN2B, 98 ± 2.3% of vehicle, in all cases n = 3, $p > 0.05$) (**Fig 10D**).

Although our results demonstrate no change in the protein levels of NMDARs at 30 and 45 min following activation of σ-1Rs (**Fig 7**), they do not address whether there is any increase in the surface levels of NMDARs at these time points. To test this possibility, we performed surface biotinylation experiments on hippocampal slices isolated from animals at 30 and 45 min after i.p. administration of SKF (**Fig 10A**). As seen in the **Figure 10E** and **F**, there were no changes in the surface levels of NMDARs between vehicle and SKF treatment at these time points. At 30 min after SKF administration, the values of NMDARs were: GluN1, 83.6 ± 17% of vehicle; GluN2A, 79 ± 23.2% of vehicle; and GluN2B, 92 ± 6.8% of vehicle, in all cases n = 3, $p > 0.05$. Values at 45 min after SKF administration were: GluN1, 83.9 ± 30% of vehicle; GluN2A, 96 ± 23% of vehicle; and GluN2B 81.8 ± 3% of vehicle, in all cases n = 3, $p > 0.05$.

Thus, the data from immunoblot experiments on LP1 fractions and surface biotinylation suggest that the observed potentiation of NMDAR function *in vivo* at 30 and 45 min following administration of σ-1R agonists may be mediated via already proposed mechanisms (**see Fig 3B**). However, at 90 min the potentiation of NMDAR function by σ-1R agonists *in vivo* occurs through an increase in the protein (**Fig 7**) and surface levels (**Fig 10**) of NMDARs.

5. Increased protein levels of GluN2 subunits after activation of σ-1Rs is mediated *via* protein synthesis

The increase in protein levels of GluN2 subunits in the LP1 fraction at 90 min following σ-1Rs activation could arise from *de novo* synthesis or redistribution of existing NMDAR subunits from intracellular compartments. If the redistribution of existing NMDAR subunits is occurring in our experiments, then we should observe no change in the protein

levels of GluN2 subunits in total homogenate. To test this possibility, we examined the protein levels of GluN2 subunits in the hippocampal total homogenate after SKF administration. Our results show an increase in GluN2 subunit levels in the total homogenate (GluN2A, 122 ± 3% of vehicle; GluN2B, 150 ± 10% of vehicle; in both cases n = 3, $p < 0.05$) (**Fig 11A**). These results suggest the possibility of an increase in the synthesis of GluN2 subunits and, in general, enhanced protein synthesis process is occurring in our experimental conditions following administration of σ-1R agonists.

A previous study has demonstrated the induction of c-fos—an immediate early gene and a routinely used marker for protein synthesis (43)—in various brain regions after the i.p. administration of σ-1R agonists (181). Since there was a possibility for a general increase in protein synthesis process in our experimental conditions, we wanted to determine if there was any increase in the protein levels of c-FOS (the product of the c-fos gene) after the administration of SKF. As shown in the **Figure 11B**, the protein levels of c-FOS were significantly increased after SKF administration when compared with vehicle (157.12 ± 12% of vehicle, n = 6, $p < 0.05$), indicating increase in the protein synthesis process is occurring in our experimental conditions.

A recent study has shown that the activation of σ-1Rs regulates the protein expression of hERG ion channels (35). If the increase in GluN2 subunits in our observations is due to increased synthesis, then inhibiting the protein synthesis should prevent this response. We tested our hypothesis by administering the protein synthesis inhibitor anisomycin (30 mg/kg (212)) 1 h before challenging the animals with σ-1R agonists (**Fig 11C**). We validated the effect of anisomycin by monitoring the levels of the protein c-FOS. These protein levels were significantly reduced (73 ± 1% of vehicle, n = 4, $p < 0.05$) after

anisomycin administration when compared with vehicle (**Fig 11D**), indicating a decrease in *de novo* protein synthesis. Administration of anisomycin alone has no effect on the protein levels of GluN2 subunits in the LP1 fraction (GluN2A, 84.8 ± 6.0% of vehicle; GluN2B, 90.4 ± 16% of vehicle; n = 4, $p < 0.05$) (**Fig 11D**). We then administered SKF or PTZ to rats that were pre-treated with anisomycin (1 h previously) and isolated the LP1 fractions at 90 min post-injection (**Fig 11C**). As seen in the **Figure 11E** and **F**, pre-treatment with anisomycin abolished the SKF- or PTZ- induced increase in the protein levels of GluN2 subunits in the LP1 fractions. Here, the protein levels of GluN2A and GluN2B were 102 ± 7% and 116 ± 8% of vehicle, respectively, in both cases n = 6, $p > 0.05$ when SKF was administered in the presence of anisomycin, and 118 ± 8% and 115 ± 16% of vehicle, respectively, in both cases n = 4, $p > 0.05$ following PTZ administration in the presence of anisomycin.

We also tested the protein levels of c-FOS in the LP1 fractions after the SKF or PTZ administration in the presence of anisomycin to confirm whether the blockade of protein synthesis process was still occurring. Indeed, the levels of c-FOS underwent significant decrease in these conditions (**Fig 11E** and **F**, 67 ± 1.4% after SKF plus anisomycin and 62 ± 2% of vehicle after PTZ plus anisomycin, n = 5 and $p < 0.05$ in both cases). Altogether, our results indicate that the increase in protein levels of GluN2 subunits in the LP1 fraction following activation of σ-1Rs (**Fig 7**) could be due to the increased synthesis of GluN2 subunits.

6. Activation of σ-1Rs also leads to an increase in the protein synthesis of PSD-95

PSD-95 is associated with NMDARs, particularly the GluN2A- and GluN2B-subunits (91, 138). This association is thought to play a supportive role in the anchoring and

trafficking of NMDARs at the synapse (153, 183) (**Section 2.3**). To determine whether the σ-1R-agonist-induced increase in the protein levels of GluN2 subunits is accompanied by an increase in PSD-95 protein levels, we investigated PSD-95 levels in the LP1 fraction following SKF or PTZ administration at 30, 45, and 90 min. Similar to the protein levels of GluN2 subunits, the levels of PSD-95 remain unchanged at 30 and 45 min after the administration of σ-1R agonists SKF or PTZ (see **Table III**). However, as seen in the **Figure 7A,** there is a significant increase in the levels of PSD-95 at 90 min after SKF administration (161.7 ± 12.5% of vehicle, n = 9, $p < 0.05$).

The SKF-mediated increase in the PSD-95 protein levels was blocked following pre-treatment with σ-1R antagonists BD1047 or BD1063 (92 ± 2.8% of vehicle, n = 5, $p > 0.05$ after SKF plus BD1047, and 101 ± 8% of vehicle, n = 3, $p > 0.05$ after SKF plus BD1063) (**Fig 9C** and **F**) and after anisomycin (87 ± 7% of vehicle, n = 3, $p > 0.05$) (**Fig 11E**), showing that the acute activation of σ-1Rs also led to an increase in the synthesis of PSD-95. PTZ administration also significantly increased the levels of PSD-95 (153 ± 9.4% of vehicle, n = 6, $p < 0.05$) (**Fig 7B**), and this increase was abolished following pre-treatment with BD1047 (105 ± 2.1% of vehicle, n = 4, $p > 0.05$) (**Fig 9D**) or anisomycin (111 ± 3.8% of vehicle, n =3, $p > 0.05$) (**Fig 11F**). Thus, the activation of σ-1Rs by their agonists SKF and PTZ not only increased the expression of GluN2 subunits but also that of PSD-95, which may consequently facilitate the trafficking and synaptic plasma membrane localization of the newly synthesized NMDA receptors.

7. Increase in phosphorylation levels of ERK1/2 and CREB following σ-1Rs activation

Our results demonstrate the possibility of *de novo* synthesis of GluN2 subunits and

PSD-95 following administration of σ-1R agonists (SKF or PTZ) (**Figs 7** and **11**). The question is through what mechanisms do activated σ-1Rs promote the protein synthesis of GluN2 subunits and PSD-95? In other words, is there any alteration in the intracellular signalling cascades that could lead to an increase in the synthesis of these proteins?

Previous investigations have suggested that σ-1Rs work in conjunction with a variety of intracellular signalling cascades, such as extracellular signal regulated kinase (ERK1/2), phosphatidylinositide 3-kinase pathways, alter the expression of several proteins (34, 139, 193). Notably, increased phosphorylation levels of ERK1/2 and its downstream target, cAMP response element-binding protein (CREB), have been demonstrated to promote the protein synthesis of NMDAR subunits and PSD-95 (28, 156, 162, 221).

If activation of σ-1Rs promotes the protein synthesis of GluN2 subunits and PSD-95 in our observations (**Figs 7** and **11**) through this signalling pathway, then we should observe increased phosphorylation levels of ERK1/2 and its downstream target, CREB. As seen in the **Figure 12**, there is an increased phosphorylation level of p42 of ERK1/2 (136 ± 8% of vehicle, n = 3, $p < 0.05$) following administration of SKF. This increase in phosphorylation level of p42 of ERK1/2 was prevented when administrated in the presence of σ-1R antagonist BD1047 (107 ± 12% of vehicle, n = 3, $p > 0.05$) (**Fig 12B**). We then examined the phosphorylation level of CREB after SKF administration. Our results show an increased phosphorylation level of CREB after SKF activation of σ-1Rs (140 ± 6% of vehicle, n = 3, $p < 0.05$), which was otherwise not observed in the presence of BD1047 (80.4 ± 10% of vehicle, n = 3, $p > 0.05$). Hence, our results suggest that the increased phosphorylation levels of ERK1/2 and CREB following activation of σ-1Rs could lead to an increase in the protein synthesis of GluN2 subunits and PSD-95 (**Fig 7** and **11**).

8. Increased interaction between σ-1Rs and GluN2 subunits following activation of σ-1Rs

Results thus far suggest that the activation of σ-1Rs can lead to an increase in protein synthesis of GluN2 subunits and PSD-95 via the ERK1/2 pathway. However, the fate of these new proteins is still unclear. Are these newly synthesized proteins trafficked to the plasma membrane from the ER? It is well known that the σ-1Rs act as chaperone proteins (e.g., IP3 receptors (61)) as well as aid in the trafficking and surface presentation of certain types of voltage-gated potassium channels (e.g., Kv1.2 channel (92)). These major roles of σ-1Rs were mainly described based on the formation of protein-protein interactions between σ-1Rs and the respective ion channels/receptors. Also, as surface biotinylation data demonstrate, there is an increase in the surface levels of NMDARs following σ-1R activation (**Fig 10**). Taken together, we hypothesize that additional roles for σ-1Rs could be as a ligand-activated chaperone that aid in the trafficking and targeting of NMDARs to the plasma membrane (**Fig 10**). Additionally, a recent investigation has demonstrated the existence of an interaction between NMDAR subunits and σ-1Rs *within* cells as well as at their surfaces (11). Thus, in this model, following activation by agonists, σ-1Rs should associate with the NMDAR-PSD-95 complex at the ER, which is then trafficked to the plasma membrane. To test this hypothesis, we first performed Co-IP experiments to confirm any interaction between σ-1Rs, NMDARs, and PSD-95 following σ-1Rs activation (**Fig 13**). Next, sucrose gradient centrifugation (SGC) experiments were carried out to track the movement of these proteins between intracellular compartments (**Fig 16**).

Figure 13 displays representative blots from a typical Co-IP experiment, showing an immunoprecipitation (IP) with σ-1Rs and immunoblot (IB) with NMDAR subunits (**Figs**

13A, 13B, and **15A**). In all Co-IP experiments, there was either a weak or no interaction between the control IgG and the proteins under study. Co-IP experiments performed under basal conditions (i.e., vehicle injection) demonstrated a marginal interaction between the NMDAR subunits and σ-1Rs; however, following SKF administration, there is a significant increase in the interaction between σ-1Rs and GluN2 subunits (GluN2A, 163 ± 41% of vehicle; GluN2B, 142 ± 22% of vehicle, respectively, in both cases n = 3, $p < 0.05$) (red arrows in **Fig 13A** and **B**), suggesting a ligand-dependent enhancement in the interaction between σ-1Rs and the GluN2 subunits. An investigation of the interaction between σ-1Rs and PSD-95 also showed interaction under basal conditions, with a slight but not statistically significant increase (137 ± 14% of vehicle, n = 3, $p > 0.05$, **Fig 13C**) occurring between these two proteins following σ-1R activation. Similar results were also obtained when the Co-IP experiments were repeated with the GluN2 subunits (or PSD-95) and the resulting blots were IB with antibodies against σ-1Rs (**Fig 13E**). Surprisingly, the interaction between σ-1Rs and GluN2 subunits (or PSD-95) remained similar under basal conditions as well as after activation of σ-1Rs with PTZ (**Fig 15A**).

Our data show a significant increase in the interaction between σ-1Rs and GluN2A or GluN2B subunits following SKF administration, but no change in the interaction between σ-1Rs and PSD-95. This raises the question of testing the interaction between PSD-95 and the GluN2 subunits, since the possibility for σ-1Rs to alter PSD-95 interaction with NMDARs cannot be ruled out.

A representative blot from a Co-IP experiment investigating the interaction between GluN2 subunits and PSD-95 after SKF administration is shown in the **Figure 14A–C**. Here, PSD-95 has been IP and probed with antibodies against GluN2A (**Fig 14B**) or GluN2B (**Fig**

14C) subunits. Our data reveal no change in the interaction between PSD-95 and GluN2A subunits following SKF administration (114 ± 18% of vehicle, n = 3, $p > 0.05$, **Fig 14D**), suggesting that the binding of σ-1Rs to GluN2A subunits occurs without affecting PSD-95 binding to GluN2A. However, a significant decrease in the amount of GluN2B subunits and PSD-95 binding (50 ± 4.1% of vehicle, n = 3, $p < 0.05$) was observed following SKF administration (**Fig 14D**), suggesting that the binding of σ-1Rs to GluN2B subunits attenuates the binding of PSD-95 to GluN2B-NMDARs. Conversely, when GluN2 subunits were IP and IB with PSD-95 antibody under PTZ treated conditions, there was no change in the interaction between PSD-95 and GluN2 subunits (**Fig 15B**).

To ascertain any change in the interaction between GluN subunits (i.e., GluN1 and GluN2) following SKF administration, IP experiments were carried out using GluN antibodies and IB with GluN1, GluN2A or GluN2B subunits. As seen in the **Figure 14A–C,** there is no change in the interaction between GluN subunits, suggesting that activation of σ-1Rs with SKF alters the interaction between PSD-95 and GluN2B subunits. Nevertheless, following SKF activation of σ-1Rs, there is an increased association between σ-1Rs and GluN2 subunits, which could subsequently lead to increased trafficking and surface presence of NMDARs (**Fig 10**).

9. Activation of σ-1Rs increases the protein levels of GluN2 subunits and PSD-95 in the vesicular compartment of the LP1 fraction

Earlier investigations have suggested that σ-1Rs are involved in the trafficking and targeting of proteins such as β isoforms of protein kinase C and Kv1.2 ion channel from the ER to the plasma membrane (92, 134). Our results show that following activation of σ-1Rs, there is an increased protein synthesis of GluN2 subunits (**Figs 7, 11,** and **12**) and an

enhancement in the interaction between GluN2 subunits and σ-1Rs (**Fig 13**). Together, they raise the possibility that σ-1Rs may facilitate the transport of newly synthesized NMDARs from the ER compartment to the plasma membrane (**Fig 10**).

If our hypothesis is correct, then we would expect an increased presence of GluN2 subunits, PSD-95, and σ-1Rs following SKF administration in the subcellular compartments associated with transport vesicles and or postsynaptic membranes. To test this assumption, we subjected crude synaptosomal fractions (LP1) from vehicle and SKF to discontinuous sucrose gradient centrifugation (SGC), to isolate subcellular compartments enriched with transport vesicles (VesF) and synaptosomal membranes (SMF). If the VesF contains the newly synthesized NMDARs/PSD-95 then the amount of NMDARs/PSD-95 in the ER/microsomes/mitochondria (ERPF) compartment would be expected to decrease, so the ERPF compartment was also isolated along with VesF and SMF (In the fractionation, transport vesicles are enriched at the 0.8 M and 1.0 M sucrose interface, while synaptosomal membranes are enriched at the 1.0 M and 1.2 M sucrose interface, and the pellet fraction is ER/microsomes/mitochondria (**Fig 16A**)). The purity of the isolated fractions was assessed by the presence of proteins such as flotillin, synaptophysin, and calnexin in VesF, SMF, and ERPF, respectively.

We performed this subcellular fractionation experiment only on SKF-treated animals, since SKF administration resulted in the robust increase in GluN2 subunits, PSD-95 expression, (**Figs 7, 11** and **12**) and enhanced interaction between the σ-1Rs and GluN2 subunits (**Fig 13**) as compared with PTZ administration.

A representative blot after SGC experimentation is shown in the **Figure 16B**. As seen in the figure, both GluN2A and GluN2B subunits' levels were significantly enhanced in

VesF (151 ± 11% of vehicle for GluN2A and 213 ± 13% of vehicle for GluN2B, in both cases n = 5, $p < 0.05$). The levels of GluN2A and GluN2B subunits were unaltered in SMF (94.1 ± 5% of vehicle for GluN2A and 103 ± 5% of vehicle for GluN2B, n = 5, $p > 0.05$) following SKF administration. PSD-95 was also significantly increased in VesF (156.5 ± 12% of vehicle) as well in SMF (143 ± 10% of vehicle; n = 5, $p < 0.05$ in both cases) (**Fig 16B**). Furthermore, there was a significant decrease in the levels of all three proteins in the ERPF (72 ± 5.7% of vehicle for GluN2A, 51 ± 14% of vehicle for GluN2B, 52 ± 6% of vehicle for PSD-95; n = 5, $p < 0.05$) (**Fig 16B**) following SKF administration, suggesting movement of these proteins from the ER compartment.

Thus, SKF activation of σ-1Rs leads to an increase in the GluN2 subunits and PSD-95 levels in VesF, along with an increase in the PSD-95 levels in SMF. This increase in VesF is likely due to an enhanced export of the newly synthesized proteins following SKF treatment (**Figs 7, 11,** and **12**), as there is an increased surface presentation of NMDARs (**Fig 10**).

10. The protein levels of σ-1Rs are also increased in the vesicular compartment of the LP1 fraction

What is the distribution of σ-1Rs? Are they enriched in VesF along with GluN2 subunits and PSD-95? It is possible that σ-1Rs are enriched in VesF, as previously published reports suggested for the localization of σ-1Rs in vesicles during active conditions (59). Further, our Co-IP experiments showed an enhanced interaction between the σ-1Rs and GluN2 subunits following SKF administration (**Fig 13**). Therefore, we wanted to ascertain the presence of σ-1Rs in isolated VesF. First, though, we tested for the presence of σ-1Rs in the LP1 fraction under basal conditions and after administration of σ-1R agonists, since low

levels or absence of σ-1Rs in the LP1 fraction was suggested (4).

Figure 17 shows a representative immunoblot regarding the levels of σ-1Rs in the LP1 fractions at 30, 45, and 90 min under basal conditions as well as following SKF administration. The levels of σ-1Rs underwent a significant decrease at 30 and 90 min following SKF administration (84 ± 1% of vehicle at 30 min and 67 ± 4% of vehicle at 90 min, in both cases n = 4, $p < 0.05$), while the levels were significantly increased at 45 min (151 ± 4% of vehicle, n = 4, $p < 0.05$) (**Fig 17A**). To support these observations, we tested the levels of σ-1Rs in the LP1 fractions at the same time points following PTZ administration. The levels of σ-1Rs also underwent a significant decrease at 90 min (59 ± 5% of vehicle, n = 7, $p < 0.05$) without any change at the 30 or 45 min (118 ± 20% of vehicle at 30 min and 105± 20% of vehicle, in both cases n = 4, $p > 0.05$) (**Fig 17B**).

Why do the levels of σ-1Rs decrease following agonist treatment? The decrease in the LP1 levels of σ-1Rs could be due to multiple factors; however, we speculate two major possibilities: (a) down regulation of σ-1Rs and or (b) redistribution of σ-1Rs from the LP1 fraction to other subcellular compartments. If σ-1Rs undergo down regulation after agonist administration, then we should observe a decrease in overall levels of σ-1Rs (i.e., in the total homogenate) as opposed to a decrease only in the LP1 fraction. To test this hypothesis, an immunoblot experiment was performed on total homogenates of hippocampi isolated at 30, 45, and 90 min after SKF administration. We choose to perform this experiment following SKF administration since the levels of σ-1Rs in the LP1 fraction were highly variable under these conditions (**Fig 17A**). Results from our experiments (**Fig 17C**) demonstrate that the levels of σ-1Rs were significantly higher at all of the tested time points. The σ-1Rs levels were 130 ± 1.6% at 30 min, 144 ± 2% at 45 min, and 166 ± 5% at 90 min of vehicle (n = 3,

$p < 0.05$ in all cases), suggesting that the decrease in the LP1 levels of σ-1Rs following agonist administration could be due to redistribution, not because of down regulation.

If the decrease (redistribution) in levels of σ-1Rs in the LP1 fraction is mediated by the agonist treatment, then we should not observe the decrease in levels of σ-1Rs in the presence of σ-1R antagonist. We tested the levels of σ-1Rs in the LP1 fraction at 90 min following SKF or PTZ administration in the presence of BD1047. We chose to test the σ-1R levels at 90 min following SKF administration because, at this time point, σ-1R agonists increase the protein expression of GluN2 subunits (**Figs 7, 11** and **12**). Surprisingly, results from our immunoblot experiments showed that levels of σ-1Rs still underwent a significant decrease following SKF administration (51 ± 3% of vehicle, n = 5, $p < 0.05$) in the presence of BD1047 (**Fig 17E**). However, the levels of σ-1Rs remained unchanged after PTZ administration in the presence of BD1047 (101 ± 9% of vehicle, n = 4, $p > 0.05$) (**Fig 17F**), and with BD1047 treatment alone (85 ± 4% of vehicle, n = 7, $p > 0.05$) (**Fig 17D**).

To support the observed decrease in σ-1Rs levels after SKF administration in the presence of BD1047, we repeated similar immunoblot experiments in the presence of another σ-1R antagonist, BD1063. As seen in **Figure 17E**, the levels of σ-1Rs still underwent a significant decrease after SKF plus BD1063 but to a lesser extent than observed with SKF plus BD1047. The levels of σ-1Rs in the LP1 fraction were 85 ± 9% of vehicle, n = 3, $p < 0.05$ after SKF plus BD1063, while the levels of σ-1Rs remained unchanged after BD1063 treatment alone (106 ± 21% of vehicle, n = 3, $p > 0.05$) (**Fig 17D**).

If the decrease/redistribution in σ-1Rs level continues to occur after the SKF administration even in the presence of antagonists, then we should not observe any change in the overall levels of σ-1Rs. To test this hypothesis, we performed immunoblot experiments

on the total homogenates of hippocampi that isolated after SKF treatment but in the presence of BD1047 or BD1063. Intriguingly, we still observed a significant decrease in the levels of σ-1Rs in the total homogenates of SKF plus BD1047 or BD1063 (**Fig 17H**), suggesting that there may be down regulation of σ-1Rs instead of redistribution as the total homogenate levels of σ-1Rs in vehicle and BD1047 or BD1063 remained unchanged (**Fig 17G**). The levels of σ-1Rs were 80 ± 3.6% of vehicle, $p < 0.05$ after SKF plus BD1063; 63 ± 3.3% of vehicle, $p < 0.05$ after SKF plus BD1047; 86 ± 6.7% of vehicle and 86 ± 5% of vehicle, $p > 0.05$ after BD1063 and BD1047, n = 3 in all cases.

Several investigations have demonstrated that in addition to ER/MAM distribution, σ-1Rs are present on the perinuclear membranes of the cell (81, 128, 155). Because of the spatial dynamics of σ-1Rs within the cell, it is hypothesized that σ-1Rs could act as transcriptional factors, controlling genes encoding several ion channels, possibly by redistribution into the nucleus (34). Also, a recent investigation has suggested that σ-1Rs might shuttle between the nucleus and the cytoplasm i.e., ER membranes, depending on the conditions (130). Thus, it is possible that at 90 min following SKF administration, certain amount of σ-1Rs from the LP1 fraction redistribute to the nuclear compartment and, simultaneous association with ERK1/2 and CREB signalling pathways (**Fig 12**) promote the protein synthesis of GluN2 subunits and PSD-95.

If our assumption is correct, then in the presence of protein synthesis blocker anisomycin, σ-1R translocation from the LP1 fraction should not occur. We tested our hypothesis by performing immunoblot experiments on the LP1 fraction at 90 min following SKF or PTZ administration in the presence of anisomycin. As seen in the **Figure 17E** and **F**, the levels of σ-1Rs did not undergo any decrease following treatment with agonists in the

presence of anisomycin or following anisomycin treatment alone. The levels of σ-1Rs were 82 ± 10% of vehicle after SKF plus anisomycin, 99 ± 1% of vehicle after PTZ plus anisomycin, and 100 ± 7% of vehicle after anisomycin (n = 3, $p > 0.05$ in all cases). These results suggest that the agonist treatment could induce certain amount of σ-1Rs to translocate from the LP1 fraction (see **Table IV**).

We next tested the presence of σ-1Rs in VesF along the lines of GluN2 subunits and PSD-95 (**Fig 16**). Immunoblotting for σ-1Rs on isolated fractions of SGC following SKF administration (**Fig 17I**) showed that the levels of σ-1Rs were significantly increased in VesF (240 ± 16% of vehicle, n = 3, $p < 0.05$), while the levels underwent significant decrease in SMF (65 ± 4% of vehicle, n = 3, $p < 0.05$). In the ERPF, the levels of σ-1Rs did not undergo any change (123 ± 8% of vehicle, n = 3, $p > 0.05$), suggesting that a major proportion of σ-1Rs in the LP1 fraction are in VesF along with GluN2 and PSD-95.

Taken together with the Co-IP and SGC results, our data suggest that activated σ-1Rs associate with NMDAR-PSD-95 complex and then aid in the trafficking and targeting of the newly synthesized NMDARs from the ER to the plasma membrane (**Fig 10**).

DISCUSSION

The regulation of ion channels' expression, trafficking, and targeting is an emerging theme in the role of σ-1Rs in the functional modulation of these channels, at least in the case of voltage-gated K^+ ion channels (35, 92, 121). It has been well documented that activated σ-1Rs potentiate the function of NMDARs (**Section 3** and (13-15, 50, 114, 120)). However, there has been an open question as to whether activated σ-1Rs also alter the expression, trafficking, and surface levels of NMDARs. In this study, we show that, following activation of σ-1Rs, (a) there is an increase in the protein expression of GluN2 subunits, and (b) there is an increase in the trafficking and targeting of NMDARs from the ER to the plasma membrane. These resultant changes could underlie the σ-1R enhancement of NMDAR function (13, 15).

1. σ-1R-mediated increase in GluN2 subunits and PSD-95 protein expression

Our study shows that acute activation of σ-1Rs leads to an increase in the protein expression of GluN2 subunits and PSD-95 in the rat hippocampus (**Figs 7** and **11**). Several lines of evidence support our conclusion. First, σ-1Rs mediate the increase in protein levels of GluN2 subunits and PSD-95, since their levels remained unchanged when σ-1Rs were chronically blocked with BD1047 or BD1063 (**Fig 9**). Second, subsequent to the activation of σ-1Rs, the levels of c-FOS—a routinely used marker for protein synthesis (43)—increased significantly. This suggests that a detectable increase in the protein synthesis process occurred under our experimental conditions (**Fig 11**). Third, the observed increase in GluN2 subunits and PSD-95 protein levels after the activation of σ-1Rs was prevented in the presence of anisomycin (**Fig 11**).

Administration of σ-1R ligands either *in vivo* or *in vitro* has been shown to alter the mRNA or protein expression of several neuronal proteins: for example, hERG ion channels

and NMDAR subunits. The previously reported alteration in the protein expression of NMDAR subunits took place after the chronic administration of σ-1R ligands (53, 204). Ours is the first report to demonstrate changes in the NMDAR subunits and PSD-95 protein expression after acute activation of σ-1Rs. Thus, our results provide an important piece of evidence regarding the σ-1R-mediated alteration in the protein expression of NMDARs.

What are the mechanisms through which σ-1Rs increase the protein expression of GluN2 subunits and PSD-95? The precise molecular mechanisms underlying our observations are still unclear. Growing evidence suggests that σ-1Rs could translocate from the ER to the nucleus and could act as a transcriptional factor for the expression of several ion channels (34). A recent study using a multidisciplinary approach has shown that σ-1Rs could shuttle between the ER and nucleus (130). In addition, σ-1Rs are connected to several intracellular signalling cascades, e.g., ERK1/2 during active conditions (139, 193). Taken together, it is possible that acutely activated σ-1Rs translocate from the LP1 fraction to the nuclear compartment and—also in connection with signalling pathways such as ERK1/2 and its downstream target, CREB—increase the protein synthesis of GluN2 subunits and PSD-95 as in our observations. Indeed, the results shown in **Figs 17A, 17B,** and **12B** suggest a possible σ-1R translocation, with a simultaneous increase in the phosphorylation levels of ERK1/2 and CREB that could eventually lead to the promotion of GluN2 subunits and PSD-95 protein expression (**Fig 7**). Our results are in line with earlier reports that demonstrate increased phosphorylation levels of ERK1/2 and CREB promote GluN2 subunits and PSD-95 protein expression (28, 156, 162, 221).

Activated σ-1Rs specifically affect GluN2 subunits, as shown in our study. This specific effect of σ-1Rs on GluN2 subunits could be due to these subunits being an important

contributor for the assembly and formation of functional NMDAR complexes (151, 185). The increase in the expression of GluN2 subunits but not that of AMPAR subunits, as seen in our observations (**Fig 8**), also suggests that σ-1Rs specifically affect GluN2 subunits and PSD-95 expression. This observation is in agreement with electrophysiological experiments, where acute application of σ-1R ligands enhances the function of NMDARs but not that of AMPARs (16, 133). It is not surprising, then, that the acute activation of σ-1Rs did not alter the expression of GluN1 subunits in our study (**Fig 7**), because GluN1 subunits are already abundant in the neuron (70).

Thus, the translocation of σ-1Rs and the promotion of the ERK1/2-CREB signal transduction cascades may underpin the upregulation of GluN2 subunits and PSD-95 expression following activation of σ-1Rs in our observations.

2. Increased trafficking of GluN2 subunits and PSD-95 following activation of σ-1Rs

Previous studies have demonstrated that the activated σ-1Rs facilitate the trafficking of proteins such as β isoform of protein kinase C and voltage-gated K^+ ion channels (e.g., Kv1.2 and Kv1.4) from the ER to the plasma membrane (92, 121, 134). Our SGC and biotinylation results also suggest that activated σ-1Rs enhance trafficking and surface presentation of NMDARs (**Figs 16** and **10**).

The levels of GluN2 subunits and PSD-95 in VesF were significantly increased following activation of σ-1Rs with SKF (**Fig 16**). This increase could have been due to enhanced exocytic transport vesicles containing newly synthesized GluN2 subunits and PSD-95 (**Fig 7** and (51, 79, 173, 180, 183, 213, 221)), particularly since we observed a concomitant significant decrease in the protein levels of GluN2 subunits and PSD-95 in the

ER compartment (**Fig 16**). However, we observed differences in the protein levels of GluN2 subunits and PSD-95 between isolated fractions, and increases in the LP1 fractions (**Fig 7**). These differences could be due to multiple factors that are associated with SGC technique, such as loss of material while collecting fractions and rapid movement of proteins between different compartments when compared with isolation of LP1 fractions. Nevertheless, our SGC experiments provided us an opportunity to track the redistribution or movement of GluN2 subunits and PSD-95 between the VesF and the ERPF compartments following activation of σ-1Rs.

Interestingly, elevated levels of σ-1R were observed in the VesF after SKF administration (**Fig 17I**). This is in agreement with previous studies showing sorting of σ-1Rs to exocytic vesicles following administration of σ-1R agonists (93). Hence, it is likely that all three components (GluN2 subunits, PSD-95, and σ-1Rs) are present in the same transport vesicles that may be destined for the synaptic plasma membrane sites. It is also possible that our VesF includes endocytic vesicles that contain retrieved GluN2B-containing NMDAR complexes originating from the postsynaptic membrane. We believe this is unlikely because the surface levels of GluN2B were unaltered following SKF administration (**Fig 10**). SKF activation of σ-1Rs results in the enhanced surface presentation of GluN2A-containing NMDARs, probably at the postsynaptic density.

Therefore, σ-1Rs regulate NMDAR numbers via protein synthesis, and trafficking to the plasma membrane by facilitating exit from the ER compartment.

3. σ-1R-mediated increase in the surface levels of GluN2A-containing NMDARs

Electrophysiological studies demonstrate that following the administration of σ-1R agonists into animals, there is an enhancement in NMDAR-mediated responses and

improvement in learning and memory (the time between first observation of the effect and the return to baseline ranges between 30–120 min and several days) (**Section 3** and reference therein). Our data suggests that the facilitation of NMDAR function at 90 min after the activation of σ-1Rs is due to an increase in the surface NMDARs containing the GluN2A subunits (**Fig 10**), since these NMDARs are predominantly expressed at synaptic sites while those that contain the GluN2B subunits are enriched at extrasynaptic sites (57). Although we did not observe any changes in the surface or protein expressions of NMDARs at 30 and 45 min after injection of σ-1R agonists, we speculate that the enhancement of NMDAR function by σ-1Rs at these time points is mediated via already proposed mechanisms (see **Fig 3** and **Section 3.1**).

The increase in surface expression of GluN2A-containing NMDARs (**Fig 10**) is lower when compared with the increased expression observed in LP1 fractions (**Fig 7**). This can be explained in two different ways: First, the proportion of GluN2A subunits in the LP1 fraction that is not observed on the surface might serve as an intracellular reserve pool. Aoki et al., demonstrated the presence of a reserve pool of GluN2A subunits in intracellular compartments near synaptic regions (6). Second, it has been suggested that there is only a limited number of "slots" that can accommodate the synaptic NMDARs at the postsynaptic density, despite a high availability of receptors (159).

Intriguingly, the surface expression of GluN2B remains unaltered after SKF administration (**Fig 10**). Here, we assume that the σ-1R-mediated insertion of GluN2B-containing NMDARs into the postsynaptic membrane might occur at a slower rate than GluN2A-containing NMDARs. It has been shown that disrupting the interaction between GluN2B subunits and PSD-95 results in the removal of GluN2B-containing NMDARs from

the plasma membrane (158, 164, 174). Further, accumulating evidence suggests that a disruption of this interaction could also interfere with the plasma membrane insertion of newly synthesized and recycled pools of GluN2B-containing NMDARs (12, 153, 160, 172, 173). Our Co-IP experiments showed a disruption of the interaction between GluN2B subunits and PSD-95 after activation of σ-1Rs (**Fig 14D**). Thus, it is possible that σ-1R-mediated disruption of interaction between GluN2B subunits and PSD-95 delays the surface insertion of GluN2B-containing NMDARs. In this regard, a longer time course is needed to resolve the surface increase in GluN2B-containing NMDARs at the postsynaptic membranes.

4. σ-1Rs exhibit increased association with GluN2 subunits following activation

One of the striking features of activated σ-1Rs is their ability to translocate from the ER to the plasma membrane and modulate the functions of various types of voltage-gated ion channels (e.g., K^+ ion channels) via protein-protein interaction (144, 188). Our Co-IP data suggest a ligand (SKF)-dependent enhanced interaction between σ-1Rs and NMDARs (**Fig 13**). However, we also observed interactions between these proteins under basal conditions (**Figs 13** and **15A**). These observations are in line with previous studies investigating the interaction between σ-1Rs and voltage-gated ion channels e.g., Na^+, K^+, and Ca^{2+} (9, 10, 197). Based on this information, we can see two roles for σ-1Rs in the context of interaction with NMDARs. First, NMDARs are central proteins that are necessary for executing a multitude of neuronal functions, so there is constant production of NMDAR subunits in neurons (209). The newly synthesized NMDAR subunits (under basal conditions as well as after activation of σ-1Rs) require proper protein folding with the aid of cellular chaperones to form mature NMDARs (80, 125). The finding that σ-1Rs have chaperone

activity (61) raises the likelihood that σ-1Rs might act as chaperones for newly synthesized NMDAR subunits at the ER. Second, under basal conditions, σ-1Rs associate with NMDARs at the ER and help to cluster receptor complexes into the transport vesicles (VesF) and then facilitate their transport from the ER to the plasma membrane (**Fig 16**). Balasuirya et al. have shown that σ-1Rs can interact with NMDAR subunits at the ER and at the cell surface under basal conditions (11), which is consistent with our finding of basal interaction between σ-1Rs and NMDAR subunits (**Figs 13** and **15**). Further, a recent finding has shown that activated σ-1Rs exhibit a higher association with voltage-gated Kv1.2 ion channels at the ER, and target them to the plasma membrane regions of the neuron (92). Our SGC experiments demonstrated the increased presence of σ-1Rs along with the NMDAR subunits in the VesF after the activation of σ-1Rs (**Fig 16**). Thus, after activation, σ-1Rs show an enhanced interaction with NMDAR subunits, followed by a pronounced exit of NMDARs from the ER compartment. It is unclear why, under PTZ treatment conditions, σ-1Rs showed no difference in interaction with NMDAR subunits.

Our data from Co-IP experiments demonstrated an interaction between σ-1Rs and PSD-95 (**Figs 13** and **Fig 15A**) under basal conditions as well as after activation of σ-1Rs. The observation of interactions between σ-1Rs and PSD-95 was not surprising given the ability of PSD-95 to interact with multiple proteins, especially with NMDAR subunits. We can envisage the following significance for σ-1R interaction with the NMDAR-PSD95 complex (**Fig 13**): (a) σ-1Rs could be involved in aiding the interaction between NMDARs and PSD-95 under basal as well as activated conditions, similar to the role of mPins. mPins has been shown to interact with NMDARs and facilitate the interaction between NMDARs and PSD-95/SAP102 (173). (b) Zhang et al., demonstrated that PDZ domain proteins (e.g.,

PSD-95) that exhibit interaction with glutamate receptors undergo chaperoning in their inter-domains, but how this is achieved remains unclear (224). Given the fact that σ-1Rs have chaperone activity (61), the interaction between σ-1Rs and PSD-95 might help the proper folding of newly synthesized PSD-95. (c) It has been shown that PSD-95 plays a supportive role in the trafficking and targeting of NMDARs from the ER to the plasma membrane (42, 183). Thus, we believe that σ-1Rs interact with PSD-95 to promote the trafficking and targeting of NMDARs to the synaptic plasma membranes (**Fig 10**).

We expected to see an increased interaction between σ-1Rs and PSD-95 in SKF treated conditions, since we observed an enhanced interaction between σ-1Rs and GluN2 subunits (**Fig 13**). It is unclear why we did not detect an enhanced interaction between σ-1Rs and PSD-95 following activation of σ-1Rs (**Fig 13**). It could be for the following reasons: First, σ-1Rs interact with NMDAR subunits and PSD-95 in different stoichiometric proportions. In this case, after administration of SKF, there could be an alteration in the conformation of NMDARs via unknown mechanisms. This alteration of NMDARs could lead to enhanced binding to σ-1Rs. Alteration of NMDAR conformation and consequent enhancement in the binding of intracellular components to NMDARs is not unusual and was shown in recent work (55). Second, our observation of interaction between σ-1Rs and PSD-95 could be a consequence of σ-1R interaction with NMDAR subunits. The data from Balasuriya et al., support this possibility because σ-1Rs were shown to interact with NMDARs without the involvement of PSD-95 (11).

5. Distribution of σ-1Rs

Our SGC data clearly demonstrated the presence of σ-1Rs in various subcellular compartments of the LP1 fraction, along with NMDAR subunits and PSD-95 (**Figs 16** and

17I). However, several laboratories have observed the opposite, that the protein levels of σ-1Rs in the LP1 fraction is either minimal or absent (4, 122, 148, 155). Most of these studies investigated the distribution of σ-1Rs by employing [^{3}H]-labeled agonists/antagonists and or peroxidase-containing substances. The use of these substances for studying σ-1R distribution has several limitations: (1) high cross-reactivity and non-specificity of the radio-ligands; (2) a very narrow detection range for identifying σ-1R distribution at rest vs. after activation; and finally, (3) an unclear distinction between electron-dense regions of the neuron, e.g., PSD and the peroxidase-labeled regions defining σ-1R localization (4, 148).

Our immunoblot technique confirmed the presence of σ-1Rs at rest in the hippocampal LP1 fraction of the rat (**Figs 7** and **16**). Interestingly, in an agonist- and time-dependent manner, the levels of σ-1Rs in the LP1 fractions decreased after acute treatment of rats with SKF or PTZ. These observations are in agreement with, and further supported by, the earlier studies (4, 122, 148, 155). The decrease in σ-1R protein levels in the LP1 fraction cannot be explained by downregulation since the total homogenate levels of σ-1Rs increased after activation of σ-1Rs with agonist (**Fig 16**). The decreased σ-1R protein levels in the LP1 fraction after activation with agonist could be due to redistribution.

Surprisingly, agonist (SKF) activation of σ-1Rs in the presence of antagonist (BD1047 or BD1063) resulted in low levels of σ-1Rs in the total homogenates as well as the LP1 fractions (**Fig 16**). The σ-1R protein levels in both the LP1 fractions and the total homogenates remained unaffected after treatment with antagonist alone (**Fig 16**). Thus, it is possible that a two-day chronic treatment with antagonists could prime the σ-1Rs for downregulation (see **Table IV**). The molecular mechanisms behind the upregulation of σ-1Rs after agonist treatment and the decrease in σ-1Rs levels after agonist-plus-antagonist

treatment require future investigation. Several studies have also reported the bidirectional regulation of σ-1Rs after either acute or chronic treatment with σ-1R ligands (71, 73, 74, 90), implying that the regulation of σ-1R levels is a highly variable process that depends on drug type, length of treatment, and experimental conditions.

We must ask, though, in our observations, where and why do σ-1Rs redistribute from the LP1 fractions following activation with agonists? It is not clear to which compartments the σ-1Rs redistribute after activation with σ-1R agonists. We hypothesize that σ-1Rs might redistribute to the nuclear compartment and simultaneously, with intracellular signalling cascades such as ERK1/2 and CREB, promote the synthesis of NMDARs and PSD-95 (**Figs 7, 12** and **16**). Support for our hypothesis comes from the facts that: (a) σ-1R protein levels in the LP1 fraction remains unchanged in the presence of anisomycin (**Fig 16**); (b) earlier reports have hypothesized that σ-1Rs could redistribute to the nuclear compartment after activation with ligands and possibly act as a transcriptional factor to promote the ion channel expression (34); and (c) two recent, but separate, studies have demonstrated that σ-1Rs localize to the nucleus and shuttle between the nucleus and cytoplasm i.e., ER membranes depending on the conditions (3, 130). This type of retro-redistribution has been reported and is frequently observed in the receptor tyrosine kinases of epidermal growth factor receptor family members such as ErbB-2 and ErbB-3 (211). Therefore, σ-1Rs might redistribute to the nucleus upon activation in a time- and agonist-dependent manner, although future investigations are required to confirm our assumption.

The other possibility that could underlie in σ-1Rs redistribution from LP1 fraction following agonist treatment is that they may be transported down to soma for degradation. In this case, blocking the motor proteins such as kinesin with Adocia sulphate-2 (AS-2) in

presence of SKF might prevent the redistribution of σ-1Rs from LP1 fraction. However, this intriguing possibility needs to be tested.

6. Differences in SKF- and PTZ-mediated σ-1R action

SKF and PTZ are the two σ-1R agonists most commonly used for studying σ-1R-mediated actions, so we employed SKF and PTZ for investigating σ-1R mediated changes in the expression and surface levels of NMDARs. We found that SKF- and PTZ-activated σ-1Rs enhanced the expression and surface levels of NMDAR subunits (**Figs 7** and **10**). These results are in line with earlier electrophysiological and behavioral approaches demonstrating facilitation of NMDAR function post-administration of SKF or PTZ (14, 15, 114).

Although SKF and PTZ both upregulated the expression of NMDARs, the change in levels after treatment with each of these agonists was different. SKF treatment resulted in an enhanced interaction between σ-1Rs and NMDAR subunits, while we did not observe any change in interaction after PTZ treatment (**Figs 7**, **13,** and **15**). These differences could be due to multiple factors, such as concentration, method of administration, bioavailability, and efficacy.

The concentration (2 mg/kg) and method of SKF or PTZ (intraperitoneal (i.p.) injection) administration to the rats was guided by previously published reports, where they suggested for the induction of σ-1R-meditated effects on NMDAR function *in vivo* (76, 77). A valid criticism of our study is the method of drug administration to the rats i.e., i.p. injection of SKF or PTZ. The i.p. injection of any drug drives through first-pass metabolism before it enters into systemic circulation and then into the brain. The exact brain concentration of SKF or PTZ acting on σ-1Rs to elicit changes in NMDAR subunits and PSD-95 expression (**Fig 7**) is unknown.

We have reasons to believe that the brain concentrations of SKF and PTZ were within the range required for the σ-1Rs to execute their actions: (a) both SKF and PTZ (2 mg/kg) altered the expression of NMDAR subunits and PSD-95 at 90 min, and (b) the observed effect was prevented when the σ-1Rs were pharmacological blocked with BD1047 or BD1063. Based on the earlier investigation and theoretical calculation (**Table V**), we estimated the brain concentration of PTZ to have been within 4–6 μM. SKF and PTZ bear analogous structures (**Table V**) and both belong to the benzomorphan class of chemical compounds, so we predict that the brain concentration of SKF was also 4–6 μM. Our theoretical calculation of SKF or PTZ concentration is in line with, and falls within, the concentration range used by previous electrophysiological study (170), in which they showed σ-1R promotion of NMDAR function.

Thus, the major factor that is involved in our observations could be the efficacy of drugs. Functional studies (neuroprotective, behavioral, and electrophysiological) demonstrate that SKF has a higher efficacy when compared with PTZ (105, 108, 114, 143), although, both SKF and PTZ demonstrate similar binding to σ-1Rs (SKF: K_i or K_d = 19.4 □ 4.6 nM (122); and PTZ: K_i or K_d = 4.59 □ 0.26 nM (25, 122)). This is probably why we observed SKF to be more effective in enhancing the expression of GluN2 subunits and σ-1R interaction with GluN2 subunits when compared with PTZ.

7. Model for σ-1R-mediated increase in NMDARs expression and surface levels

Our study showed an increase in the expression, trafficking, and surface levels of NMDARs (GluN2A-containing NMDARs) (**Fig 18**). This mode of σ-1R action on NMDARs could account for the σ-1R potentiation of NMDAR function observed *in vivo* (**Section 3**). However, several other potential mechanisms could also contribute to the σ-1R

potentiation of NMDAR function besides the mechanisms identified in this study.

It is important to consider that an increase in the NMDAR-mediated responses following σ-1R activation may also be due to a change in the NMDAR channel properties (e.g. single-channel conductance) along with an increase in channel numbers. It is well established that σ-1R interactions with the pore region of recombinant $K_v1.3$ (88) and $Na_v1.5$ channels (82) and high-voltage activated Ca^{2+} channels (223), leads to modulation of the kinetics or activation curves of these ion channels with no change in channel conductance. To date, there has been no detailed examination of the effect of σ-1Rs on the single-channel conductance of ligand-gated ion channels. Therefore, an effect of σ-1R on the gating of NMDARs already expressed at the cell surface cannot be ruled out at this stage, although post-translational modifications (e.g. phosphorylation) of NMDARs are more probable contributors (87, 167).

σ-1R can modulate NMDAR functions through physical association, along with the increase in number of surface receptors (**Figs 10** and **13**). It is well established that the activation of σ-1Rs leads to modulation of the kinetics of voltage-gated ion channels (**Section 1.4**) such as Na^+, K^+, and Ca^{2+} via direct interaction between the σ-1R and the ion channel. In addition, σ-1Rs are known to potentiate IP3 receptors (61, 216) via the formation of a trimer between the IP3 receptor, ankyrin, and the C-terminus tail of a σ-1R, and inhibit acid-sensing ion channels (ASIC; (26, 68)) through direct binding of a σ-1R to each ASIC subunit. It remains to be discovered whether the interaction between σ-1Rs and NMDARs alters the kinetics of NMDAR ion channels. Our laboratory has previously shown that activated σ-1Rs potentiate the NMDARs function without altering the kinetics of the NMDAR currents (110). However, these experiments were done on hippocampal slices and

were not performed in a system that contains NMDARs and σ-1Rs alone, thus limiting us to conclude that the enhanced interaction between σ-1Rs and NMDARs alters the kinetics of NMDAR ion channels.

8. Functional implications of σ-1R enhancement in the expression and surface levels of NMDARs

Our observations could be involved directly in NMDAR-dependent processes such as the formation and maintenance of spine morphology, synaptic plasticity (e.g., LTP), and neuroprotection. Results from the current study also provide an opportunity to understand the plausible role of σ-1Rs in antidepressant drug action as well as presents the likelihood of designing novel antipsychotics.

8.1 Formation and maintenance of spine morphology

Dendritic spines, which are small protrusions of the dendritic tree, form important junctions of neuronal communication. These spines are heterogeneous in shape and size, and have been classified as mushroom, thin, and stubby spines (123). NMDARs, in association with the PSD-95-family of proteins and the Rho family of GTPases, are involved in the formation and maturation of dendritic spines and in the maintenance of spine morphology (41, 89, 171, 199). For example, a prominent member of the Rho family of GTPases, Tiam 1-Rac1, couples to NMDARs via PSD-95 and regulates spine formation and dendritic arborisation (199). Several studies have suggested that the formation and maintenance of dendritic spines requires a sufficient amount of NMDARs because either the pharmacological blockade or the reduction in protein expression of GluN2A- and GluN2B-NMDARs alter the density and morphology of dendritic spines (23, 207). Furthermore, protein expression of PSD-95 also plays an important role in the growth and maturation of

spines (41, 184).

σ-1Rs have also been shown to promote neurite development in PC12 cells (192, 193). More importantly, a study has shown that σ-1Rs facilitate the formation and maintenance of hippocampal dendritic spine morphology (203). The study demonstrated that σ-1Rs regulate dendritic spine formation and morphology via the TIAM1-Rac1-GTP signalling pathway. Authors have also shown that the deficiency of σ-1Rs in the neurons results in lack of mushroom-shaped spines as well as functional synapses (i.e., absence of NMDARs and PSD-95 at synapse) (203). So, based on the current findings, it is possible that by regulating the expression of NMDARs and PSD-95 (**Figs 7** and **11**), σ-1Rs are involved in the formation and maintenance of dendritic spines, at least in the above study.

A separate study has shown that new glutamatergic synapses/spines (that include NMDAR-PSD-95 complexes) can be formed in a period of 1–2 h, indicating that the production of NMDARs and PSD-95 can occur at a faster rate (47). Our finding that σ-1Rs can increase the expression of NMDARs and PSD-95 at 90 min (**Fig 7**) further supports the possible involvement of σ-1Rs in the formation of new glutamatergic synapses.

The formation, remodeling and maintenance of dendritic spines, which can occur over a time scale ranging from seconds to tens of minutes or days, represents an important mode of refining the neuronal circuitry in the brain (123). Exposure to addictive compounds (e.g., cocaine, an agonist of σ-1Rs (30)) increases the dendritic spine arborization through unclear mechanisms (171). Thus, σ-1Rs could be involved in the formation and maintenance of dendritic spines via enhancement of the expression of NMDARs and PSD-95.

8.2 Synaptic plasticity

The LTP form of synaptic plasticity is well characterized and forms an important

molecular correlate of learning and memory (107). Processes such as induction, expression, and persistence of LTP are highly dependent on the function of NMDARs (19, 33, 135). Typically, LTP can be divided into two phases: A long-lasting LTP (L-LTP), which lasts for hours *in vitro* and for days *in vivo*, is dependent on protein synthesis (includes NMDARs and PSD-95); the other form of LTP that occurs early (in less than a hour) is called early-LTP (E-LTP) and is independent of protein synthesis (2, 154). Changes in the protein expression of NMDARs and PSD-95 by overexpression, gene knock-in or gene knockout studies have been shown to alter the LTP (including L-LTP and other classified LTP's) to a significant extent. For example, overexpression of GluN2B subunits in the hippocampus improves NMDAR function and LTP (196). This enhancement in NMDAR function was suggested to ameliorate the learning and memory in mice. The plasticity of ocular dominance was altered in response to the enhanced expression of GluN2A subunits in the visual cortex (163). Overexpression of PSD-95 enhances LTP in the hippocampus (129).

Our lab and several others have previously shown that σ-1R enhancement of NMDAR function alter LTP (27, 101, 104, 110). However, the molecular mechanisms of how σ-1Rs could bring changes to LTP remain unclear. In light of our current observations, we speculate that σ-1Rs contribute to the process of LTP by increasing the expression and surface levels of NMDARs (**Figs 7** and **10**). Support for our assumption comes from the fact that σ-1R agonists (e.g., DTG, SKF, PTZ and PRE-084) improve learning and memory in animal models with NMDAR-antagonism induced amnesia (114, 116, 120). Thus, it can be concluded that σ-1Rs alter synaptic plasticity by modulating the expression as well as surface levels of NMDARs in the hippocampus.

8.3 Neuroprotection

It is known that excessive calcium influx via NMDARs recruits and activates neuronal nitric oxide synthase (nNOS) that is attached to PSD-95. This complex of NMDARs/PSD-95/nNOS is the driving force for neurotoxicity (38). In this complex, PDZ-domain-based interactions create a ternary association composed of GluN2B C-terminal end amino acids (-ESDV)/PSD-95 (PDZ1 and PDZ2 domains) and PSD-95 (PDZ2 domain)/nNOS PDZ-domain amino acids (-ETTF) (31, 38). Current strategies against neurotoxicity in various models mainly include: (a) drugs acting as antagonists on NMDARs or nNOS; and or (b) disruption of the interactions between NMDAR/PSD-95 and/or PSD-95/nNOS using short peptides (38). Of interest, these short peptides bear similar amino acid sequences to those involved in the interaction between NMDARs/PSD-95/nNOS and compete for the endogenous interactions, thus providing neuroprotection (1).

Evidence from several laboratories suggests that many σ-1R ligands confer neuroprotection in different neurotoxicity models in multiple ways (119). Among them, altering the protein-protein interaction between PSD-95/nNOS is found to be the main mechanistic route for σ-1Rs to exert neuroprotection. For example, a study has shown that treatment with 4-PPBP, a σ-1R agonist, attenuates the coupling between nNOS and PSD-95, and thereby σ-1Rs exert neuroprotection towards neonatal ischemic degeneration in striatal neurons (220). However, in this study, it is unclear whether σ-1R alters the coupling between GluN2 subunits and PSD-95. Yang et al. demonstrated that treatment with 4-PPBP did not alter the interaction between GluN2 subunits and PSD-95, but their study has a limitation (220): They performed Co-IP experiments using a mixed GluN2A/GluN2B antibody to determine the interaction between GluN2 subunits and PSD-95, and concluded that they did

not observe any differences in the interaction between GluN2 subunits and PSD-95 (220). Previously, it was demonstrated that the interaction between GluN2B subunit and PSD-95 is critical in determining the toxicity levels to the neurons (1). In the present study, we demonstrated using Co-IP experiments that the interaction between PSD-95 and GluN2B subunit is reduced to 50% after acute activation of σ-1Rs (**Fig 14D**).

Although we did not perform our Co-IP experiments on tissue subjected to toxic conditions, when we consider the previous observations and the current results, we predict that in addition to altering the coupling between PSD-95 and nNOS (220), σ-1Rs also alter the coupling between NMDARs and PSD-95 to protect neurons against toxic/excessive calcium influx. Additionally, it is hypothesized that promotion of GluN2A-containing NMDARs results in neuroprotection, whereas the promotion of GluN2B-containing NMDARs results in the cell death (57). We have observed a significant increase in the surface expression of GluN2A-containing NMDARs after acute activation of σ-1Rs (**Fig 10**). Thus, the model could be that acutely activated σ-1Rs, by enhancing the surface expression of GluN2A-containing NMDARs, and by altering the coupling between GluN2B subunits and PSD-95 as well as PSD-95 and nNOS exert neuroprotection.

8.4 Increase in NMDARs and PSD-95 expression could be involved in rapid antidepressant drug action of σ-1R ligands

Several studies have suggested that the dysfunction of the glutamatergic system (especially NMDARs and their associated partners e.g., PSD-95) in the hippocampus and other brain regions is involved in the pathophysiology of depression (39). As a result, numerous antidepressants belonging to various chemical groups were designed to target NMDARs (137). Initially, the mechanism of action for many of the antidepressants targeting

NMDARs involved the antagonism of NMDARs (i.e., using ligands that bind to different sites within the NMDAR complex(202)), thus producing "antidepressant-like" behavior. More recent investigations have shown that several antidepressants modulate the NMDARs expression besides as NMDAR antagonists (39). For instance, antidepressant drugs that belong to all chemical groups produced a time- and dose-dependent change in the radio-ligand binding to NMDARs, which were assumed to be an adaptive change (increase) in the protein expression of NMDARs (21, 140, 152). Notably, many of the changes in NMDAR expression profiles were observed mainly after chronic treatment of animals with antidepressants (140, 152). However, the recent discovery that ketamine can produce a rapid antidepressant activity by modulating the NMDAR expression profile raised the possibility that antidepressants can alter the function of NMDARs under acute treatment conditions as well (7, 106).

Drugs such as SKF, PTZ, PCP, and ketamine belong to the category of psychotomimetic agents and were shown to act as antidepressants (17, 119). Coincidentally, the acute treatment of animals with σ-1R ligands improved the depressive symptoms rapidly i.e., σ-1R ligands acted as rapid antidepressants (37, 208). Nonetheless, it remained unclear whether there were any alterations in the expression profile of NMDARs and PSD-95 after acute treatment of animals with σ-1R ligands that exhibit rapid antidepressant actions. Our observation that the acute treatment of rats with σ-1R ligands increased the expression of NMDARs and PSD-95 (**Fig 7**) could be involved in the rapid antidepressant action of σ-1R ligands described in the above studies (37, 208). Also, our findings can be connected to a recent observation that a single dose of ketamine (acute i.p injection) alleviates the depressive behavior (after 30 min of injection) in mice (7). Two reasons might support our

assumption. First, several reports suggest that σ-1R ligands can act as rapid antidepressants by modulating NMDAR function when assessed through various behavioral paradigms (16, 95, 208). Second, Autry et al. demonstrated changes in the NMDAR expression profile at rest (7), similar to our observation of changes in NMDAR subunits and PSD-95 protein levels at rest, i.e., in the absence of depressive conditions. However, it is important to note that the mechanism of action described by Autry et al. differs from our observations. In the later study, the mechanism of ketamine action to bring rapid antidepressant effect in mice was suggested to occur due to the antagonism produced at the NMDARs. Conversely, our results demonstrated that the changes in expression profiles of NMDARs and PSD-95 in rats were not mediated through the antagonism of NMDARs. This is because SKF or PTZ treatment of rats in the presence of BD1047 or BD1063 (**Fig 9**) prevented the actions of SKF or PTZ treatment alone. Taken together, it is reasonable to assume that the results observed in our study could be involved in the rapid antidepressant action of several σ-1R ligands.

8.5 σ-1Rs as a potential target for designing novel antipsychotics

The proposal that NMDAR hypofunction could lead to positive symptoms and cognitive decline in schizophrenic patients came from the studies demonstrating the abnormalities in expression of NMDARs and their associated signalling proteins (e.g., PSD-95) (78, 94, 124). Thus, several drugs were designed and tested for promoting the expression and function of NMDARs in animal models of schizophrenia (94). However, studies performed on animals to evaluate many of the drugs (e.g., haloperidol, clozapine) as antipsychotic medication resulted in varied conclusions. This is because the efficacy of many of the drugs tested as antipsychotic medication was highly dependent on the type and length (acute vs. chronic) of treatment (94). In these studies, acute treatment with antipsychotics

resulted in downregulation of NMDARs, whereas chronic treatment upregulated the expression of NMDARs in a subunit- and region-specific manner. For example, one of the antipsychotic drugs, E-5842, that is selective towards σ-1R, altered the expression of NMDAR subunits differentially depending on the brain region under chronic treatment conditions (53). Similarly, several other antipsychotic drugs (e.g., clozapine, haloperidol) that mainly act as antagonists of σ-1Rs (62) showed improvement in the NMDARs function only after chronic treatment. Even so, it remained unknown whether there was any effect on the expression and function of NMDARs after acute treatment of animals with σ-1R agonists.

Our observation of an upregulation in the expression of NMDARs and PSD-95 (**Fig 7**) after acute treatment of rats with σ-1R agonists might act as an important route for improving NMDAR hypofunction/expression observed in schizophrenia. Further, electrophysiological and behavioral evidence demonstrate that the acute treatment of rats with σ-1R agonists enhances the function of NMDARs (**Section 3**). Thus, designing novel antipsychotic drugs that can act as σ-1R agonists might form a better therapeutic strategy and will help in deciphering the existing controversy regarding the association between σ-1Rs and schizophrenia (142, 175, 205).

CONCLUSIONS

Several lines of evidence demonstrate the functional interaction between σ-1Rs and NMDARs (**Section 3**). However, one of the most elusive roles described for σ-1Rs is the set of mechanisms through which σ-1Rs enhance the function of NMDARs. The results presented in this study provide novel mechanistic information (**Fig 18**) that could underlie the σ-1R enhancement of NMDAR function. Gaining substantial knowledge of the

molecular details of how σ-1Rs enhance the NMDARs function not only helps to decipher the σ-1R-NMDAR role in physiological and pathological conditions, it could form a venue for the development of novel therapeutic strategies to treat multiple disorders (e.g., schizophrenia, depression, amnesia, and stroke).

FIGURES AND TABLES

FIGURE AND TABLE LEGENDS

FIGURE 1. Identity of σ-1R amino acids across mammalian species

The underlined amino acid sequences of σ-1R from four mammalian species correspond to the predicted transmembrane domains. Amino acid sequences of σ-1R presented in the shaded area are identical. Modified from reference (127).

FIGURE 2. Molecular architecture of σ-1R, NMDAR, and PSD-95

(**A**) Domain organization of the σ-1R. σ-1R is proposed to have a short N-terminus, two transmembrane domains, and a long C-terminus tail. The numbers in the σ-1R structure correspond to the amino acids at the start and end of each predicted domain. (**B**) Domain organization of the NMDAR individual subunit. Each NMDAR subunit has an N-terminus domain (ATD, divided roughly into two halves, R1 and R2), a ligand-binding domain (LBD, formed from amino acid segments S1 and S2), a transmembrane domain (formed from four domains (M1-M4) and a P-loop), and a C-terminus tail (CTD). Functional NMDARs are tetrameric assembles of two obligatory GluN1 subunits with either two GluN2 subunits (different combinations of GluN2 subunits) or GluN3 subunits (not shown in the figure). For convenience, the dimer form of the NMDAR is presented. (**C**) Domain organization of the PSD-95. PSD-95 has three PDZ domains, one SH3 domain, and a GK domain. Additionally, PSD-95 possesses two palmitoylation residues at the N-terminus tail. Structures of σ-1R, NMDAR, and PSD-95 are adapted and modified from references (42, 61, 150).

FIGURE 3. σ-1R enhancement of NMDAR function: Proposed vs. hypothesized mechanisms

(**A**) Administration of σ-1R agonists via different routes (e.g., i.p., i.v., s.c., and bath application) to either *in vivo* or *ex vivo* potentiates different types of NMDAR-mediated responses, as listed in the table along with their representative references. (**B**) Multiple mechanisms have been put forward to describe the potentiation effect on NMDAR function by σ-1R agonists. Three major possible routes—(**a**) G-proteins, (**b**) SK channels, and (**c**) intracellular kinases—have been proposed to mediate the action of σ-1R agonists on NMDAR function (for details see **Section 3.1**). (**C**) Alternatively, we hypothesize that subsequent to acute activation of σ-1Rs, an increase in protein expression, trafficking, and surface presentation of NMDARs occurs, which could be involved in enhancement of NMDAR function by σ-1R. The current study aims to test the hypothesized mechanisms to gain insights on the σ-1R-NMDAR functional association.

FIGURE 4. Schematic diagram of hippocampal biochemical fractionation used in this study

The insulated hippocampi from rats either after vehicle or drug treatment were subjected to homogenization and subsequently to differential centrifugation steps (as shown in the figure) to isolate various cellular fractions. For each individual experiment, a minimum of 3 or 4 hippocampi except in **discontinuous sucrose gradient centrifugation** (**Fig 16**), where 10–12 hippocampi were used. The schematic also shows the particular cellular fraction used for each experiment.

FIGURE 5. Immunoblot saturation curves of NMDARs, AMPAR subunits, PSD-95, σ-1Rs, and β-tubulin

Immunoblot band intensities of proteins—NMDAR subunits, AMPAR subunits, PSD-95, σ-1R, and β-tubulin—were collected from X-ray films using ImageJ and plotted against exposure times (in seconds) to generate saturation curves. An example saturation curve for these proteins is shown in the figure. Saturation curves for these proteins were generated for each experiment. After saturation curves were generated, data or band intensities of each protein falling under the linear range (indicated with dashed line) were collected and normalized against similarly obtained band intensities of loading control from the same experiment. Normalized band intensity data of all proteins (under vehicle and drug treatment conditions) from different experiments were averaged respectively before any comparison with vehicle was performed, to identify any statistical significance between vehicle and drug treatment.

FIGURE 6. Specificity of σ-1R, NMDAR, and PSD-95 antibodies in detecting the proteins on membranes

(**A**) Immunoblots demonstrating the specificity of σ-1R antibodies in recognizing the σ-1R as a single band at its predicted molecular weight, while pre-incubation of σ-1R antibodies with blocking peptide resulted in the absence of the σ-1R band (**left**). The specificity of σ-1R antibodies was also confirmed by the absence of the σ-1R band in σ-1R knockout mice (**right**). (**B**) Immunoblot characterization of NMDAR subunit and PSD-95 antibodies, which also recognize the respective proteins as single bands at approximately their predicted

molecular weights (**left**)**.** The specificity of the above antibodies was confirmed by performing immunoblotting on whole-cell lysates of transiently transfected SH-SY5Y cells with NMDAR subunits or PSD-95 (**right**)**.**

FIGURE 7. Increase in protein levels of NMDAR subunits and PSD-95 following activation of σ-1Rs

Hippocampi collected at 30, 45, and 90 min from rats after single i.p. injection of vehicle, SKF (**A**), or PTZ treatment (**B**) (2 mg/kg) was subjected to isolation of LP1 fractions. Immunoblot experiments on extracted LP1 fractions showed a significant increase in the protein levels of GluN2A, 2B subunits of NMDARs, and PSD-95, at 90 min after SKF (**A**) or PTZ (**B**) administration. The protein levels of GluN2 subunits and PSD-95 remained unchanged in the LP1 fractions at 30 and 45 min after SKF or PTZ administration. β-tubulin is shown as the loading control in this and subsequent experiments. Band intensity values of each protein were normalized to band intensity values of β-tubulin of respective treatment and experiment. The results demonstrating the changes in GluN2 subunits and PSD-95 protein levels at 90 min after administration of SKF or PTZ are from 9 (SKF) and 7 (PTZ) different experiments, with two animals in each group for each experiment. Bar graphs represent mean ± SEM. Asterisks denote statistical significance (*$p < 0.05$, **$p<0.01$, and ***$p<0.001$ two-tailed distribution, unpaired t-test).

FIGURE 8. No change in protein levels of AMPAR subunits following σ-1Rs activation

Insulated hippocampi at 30, 45, and 90 min from rats after single i.p. injection of SKF or PTZ (2 mg/kg) were subjected to isolation of LP1 fractions. IB on these LP1 fractions

showed no significant changes in protein levels of AMPAR subunits GluA1 and GluA2/3/4 at any of the tested time points following administration of either SKF (**A**) or PTZ (**B**). Bar graphs represent mean ± SEM of at least 3 different experiments for each treatment at each time point. Statistical significance (p>0.05 in all cases) was determined using unpaired student's t-test, two-tailed distribution.

FIGURE 9. Prevention of increase in protein levels of GluN2 subunits and PSD-95 by σ-1R antagonists BD1047 and BD1063

A schematic diagram showing the experimental setup and collection of hippocampi following administration of SKF or PTZ, from animals that underwent to a two-day osmotic mini-pump treatment with σ-1R antagonist BD1047 or BD1063 (**A**). The protein levels of GluN2 subunits and PSD-95 in the LP1 fractions did not change following a two-day chronic treatment with σ-1R antagonist BD1047 (**B**). Representative immunoblots showing no change in the protein levels of GluN2 subunits and PSD-95 at 90 min after an i.p. injection of SKF (**C**) or PTZ (**D**) in the presence of BD1047. There was also no change in the protein levels of GluN2 subunits and PSD-95 in the LP1 fractions after treatment either with BD1063 (**E**) or BD1063 plus SKF (**F**). The bar graphs represent mean ± SEM from at least 3 or 4 different experiments. Statistical significance (p>0.05 in all cases) was determined using unpaired student's t-test, two-tailed distribution.

FIGURE 10. SKF activation of σ-1Rs results in increase in the surface levels of GluN2A-containing NMDARs

(**A**) The schematic explaining the isolation and procedure for surface biotinylation on

hippocampal slices obtained from rats at 30, 45, and 90 min after single i.p. injection of SKF. The process of surface biotinylation in our experimental paradigm was confirmed by the marginal presence of β-actin in surface samples. (**B**) Data showing an upregulation in surface levels of GluN1 and GluN2A without any changes in surface levels of GluN2B at 90 min after SKF administration. There were also no changes in the surface levels of AMPAR subunits (GluA1 and GluA2/3/4) at this time point (**C**). The surface levels of NMDARs remained unaltered at 90 min following SKF administration in the presence of BD1063 (**D**). (**E–F**) At 30 and 45 min following SKF administration, there were no changes in the surface levels of NMDARs. Ionotropic glycine receptors (GlyRs) were used as a loading control. The bar graphs represent mean ± SEM of at least 7 different experiments for 90 min time points, and 3 different experiments for 30 and 45 min time points. Asterisks denote statistical significance (*$p < 0.05$, two-tailed distribution, unpaired t-test) obtained after comparison between vehicle and SKF treatment.

FIGURE 11. Increase in protein levels of GluN2 subunits and PSD-95 following σ-1Rs activation, via increased protein synthesis

(**A**) Insulated hippocampi from rats at 90 min after single i.p. injection of SKF (2 mg/kg) were homogenized using homogenization buffer (see methods) to isolate total homogenates. At 90 min, following the activation of σ-1Rs with SKF, there was an increase in protein levels of GluN2 subunits and PSD-95 in the hippocampal total homogenate. This increase in GluN2 subunits and PSD95 could due to increase in *de novo* synthesis of these proteins, reflected in the increase in protein levels of c-FOS, a routinely used marker for protein synthesis (n = 5 experiments) (**B**). (**C**) A schematic illustrating the employed experimental

approach for testing the involvement of protein synthesis in our observations. (**D**) The protein levels of GluN2 subunits and PSD-95 remained unaffected following single i.p. injection of anisomycin alone. However, there was a significant decrease in the protein levels of c-FOS, demonstrating that anisomycin was blocking protein synthesis process at this time point. Administration of SKF (**E**) or PTZ (**F**) 1 h after anisomycin injection also blocked the SKF- or PTZ-induced increase (**Fig 7**) in the protein levels of GluN2 subunits and PSD-95 in the LP1 fractions. Bar graphs are mean ± SEM of at least 3 or 4 experiments. Asterisks indicate statistical significance (*p < 0.05, **p<0.01, two-tailed distribution, unpaired t-test).

FIGURE 12. Increase in phosphorylation levels of ERK1/2 and CREB following activation of σ-1Rs

(A) Increased phosphorylation levels of ERK1/2 and CREB following NMDAR activation promotes the synthesis of several proteins, including NMDARs (indicated with black arrows) (28, 156, 162, 221). Activation of σ-1Rs also increases phosphorylation levels of ERK1/2 (139, 193); however, it remains unknown if there was any change in the phosphorylation levels of ERK1/2 and CREB in σ-1R-mediated enhancement in the protein synthesis of NMDARs (indicated with purple arrows), i.e., in our observations (**Figs 7** and **11**). Hippocampi collected from rats at 90 min after an i.p. injection of SKF (2 mg/kg) were homogenized and total homogenates were isolated. Subsequently, IB on these total homogenates was performed to detect any changes in phosphorylation levels of ERK1/2 and CREB. (**B**) The phosphorylation levels of p42 ERK1/2 and CREB were increased following SKF activation of σ-1Rs. These changes in phosphorylation levels of ERK1/2 and CREB

were prevented when SKF was administrated in the presence of BD1047. The bar graphs represent mean ± SEM of 3 different experiments. Asterisks indicate statistical significance (*$p < 0.05$, two-tailed distribution, unpaired t-test) obtained after comparison between vehicle and SKF treatment.

FIGURE 13. Increase in interaction between σ-1Rs and NMDAR subunits following activation of σ-1Rs with SKF

Isolated hippocampi from rats at 90 min after single i.p. injection of SKF (2 mg/kg) were homogenized and P2 fractions were isolated. Subsequently, Co-IP on these fractions was performed to investigate the interaction between σ-1Rs, NMDAR subunits, and PSD-95 (representative blots show in panels **A** and **B**). Arrows in panels **A** and **B** show an increased interaction between σ-1Rs and NMDAR subunits; however, the interaction between σ-1Rs and PSD-95 remained unchanged following SKF administration (**S**) when compared with vehicle (**V**). Lanes 1 and 2 in all panels represent input (0.05% of total protein quantity); lanes 3 and 4 in panel **A**, and lanes 2 and 5 in panel **B**, are IP with σ-1Rs. Lanes 5 and 6 in panel **A**, and lanes 3 and 6 in panel **B**, are IP with IgG, showing minimal non-specific binding. (**C**) Pooled data from 4 experiments, showing a significant increase in the interaction between σ-1Rs and GluN2 subunits following SKF administration. The interaction between σ-1Rs and PSD-95 was also slightly increased but is not statistically significant. (**D**) An illustration of multimeric protein complex containing σ-1Rs and NMDAR-PSD-95 complex. (**E**) Representative blot demonstrating the interaction between σ-1Rs, NMDAR subunits, and PSD-95 when IP was performed using NMDAR subunits and PSD-95 antibodies and probed (**IB**) with σ-1R antibodies. Bar graphs are mean ± SEM of 4

experiments. Asterisks indicate statistical significance ($p < 0.05$, two-tailed distribution, unpaired t-test).

FIGURE 14. Decrease in interaction between GluN2B subunits and PSD-95 following activation of σ-1Rs with SKF

Insulated hippocampi from rats at 90 min after single i.p. injection of SKF (2 mg/kg) were homogenized and P2 fractions were isolated. Subsequently, Co-IP on these fractions was performed to investigate the interaction between NMDAR subunits and PSD-95 (representative blots shown in panels **A-C**). There was no change in the interaction between NMDAR subunits and the interaction between PSD-95 and the GluN2A subunit. A significant decrease in the interaction between PSD-95 and the GluN2B subunit was observed after SKF administration (**D**). Bar graphs are mean ± SEM of 3 experiments. Asterisks denote statistical significance (*$p < 0.05$, two-tailed distribution, unpaired t-test).

FIGURE 15. No change in interaction between σ-1Rs, NMDAR subunits, and PSD-95 following activation of σ-1Rs with PTZ

Hippocampi collected from rats at 90 min after single i.p. injection of PTZ (2 mg/kg) were subjected to isolate P2 fractions. Co-IP experiments performed on these P2 fractions demonstrated no change in interaction (indicated with arrows, lanes 3 and 4) between σ-1Rs, GluN2A, GluN2B, and PSD-95 (**A**) following PTZ administration (**P**), when compared with vehicle (**V**). Lanes 1 and 2 represent input material (0.05% of total protein quantity), lanes 3 and 4 represent IP with σ-1Rs, and lanes 5 and 6 in panel **A** are IP with IgG. Panel **B** is a representative Co-IP blot showing the interaction between NMDAR subunits and PSD-95

following vehicle or PTZ administration. There was no change in the interaction between GluN2 subunits and PSD-95 following PTZ administration when IP with GluN2 subunits and IB with PSD-95.

FIGURE 16. SKF activation of σ-1Rs leads to a redistribution of GluN2 subunits and PSD-95 from the ER to vesicular compartment

(**A**) Schematic drawing showing the isolation of three fractions from the LP1 fraction, using discontinuous sucrose gradient centrifugation. The LP1 fraction was collected from hippocampi that were isolated from rats at 90 min after single i.p. injection of SKF (2 mg/kg). (**B**) Representative blots showing protein levels in the three different compartments after vehicle (**V**) or SKF (**S**) treatment. Pooled data from 5 experiments showing a significant increase in GluN2A (**Ci**), GluN2B (**Cii**) levels in the VesF, and a significant increase of PSD-95 protein levels in both VesF and SMF (**Ciii**) following SKF administration. There was also a significant decrease in the levels of all three proteins in ERPF. β-tubulin was used as a loading control for all fractions. The purity of the fractions was assessed by the absence of calnexin, an ER marker in VesF and SMF; synaptophysin in ERPF; and flotillin in SMF and ERPF. Bar graphs are mean ± SEM of 5 experiments. Asterisks indicate statistical significance ($p < 0.05$, two-tailed distribution, unpaired t-test).

FIGURE 17. Enrichment of σ-1Rs in the vesicular compartment following SKF administration

Immunoblots showing the levels of σ-1Rs in the LP1 fractions at 30, 45, and 90 min following one time SKF (**A**) or PTZ (**B**) (2 mg/kg) administration to rats. The σ-1R protein

levels underwent a significant decrease (n = 5-7, $p < 0.05$) at 30 and 90 min, while there was a significant increase at 45 min after SKF administration (**A**). The σ-1R protein levels underwent a significant decrease only at 90 min following PTZ administration (**B**). The total homogenate levels of σ-1Rs underwent a significant increase (n = 3, $p < 0.05$) at all tested points following SKF administration, as shown by the representative immunoblots (**C**). (**D**) There was no change in the protein levels of σ-1Rs in the LP1 fractions after BD1047, BD1063, and anisomycin. (**E**) Surprisingly, σ-1R levels decreased significantly (n = 4, $p < 0.05$) after SKF treatment in the presence of BD1047 or BD1063, while there was no change after the PTZ treatment in the presence of BD1047. (**E-F**) The σ-1R levels in the LP1 fractions remained unaffected following SKF or PTZ administration in the presence of anisomycin. (**G-H**) The total homogenate levels of σ-1Rs following SKF administration in the presence of either BD1047 or BD1063 underwent a significant decrease (n = 3, $p > 0.05$) without any difference observed between vehicle and BD1047 or BD1063 treatment alone. (**I**) SKF activation of σ-1Rs caused σ-1Rs to localize largely in the vesicular compartment (n = 4, $p < 0.05$) of the LP1 fraction, as demonstrated by discontinuous sucrose gradient centrifugation experiments (**Fig 16**). Bar graphs are mean ± SEM of at least 3 experiments. Asterisks denote the statistical significance ($p < 0.05$, two-tailed distribution, unpaired t-test) obtained after comparison between vehicle and respective drug treatment.

FIGURE 18. Model summarizing the σ-1R-mediated enhancement of NMDAR function in the rat hippocampus

At 90 min after acute agonist activation of σ-1Rs, there was an increase in the protein expression of NMDARs and PSD95 (indicated with black arrows) (**Figs 7**, **11** and **12**). SKF

activation of σ-1Rs increased the surface expression of GluN2A-conatining NMDARs (indicated with green and black upright arrows) (**Fig 10**) with concomitant enhanced vesicular trafficking (indicated with circles) (**Fig 16**). These σ-1R mediated facilitation in NMDARs expression, trafficking, and targeting could underlie the σ-1R enhancement of NMDAR function.

TABLE I. σ-1R gene structural information

The σ-1R gene lacks the classical TATA box at the start of the transcription site, and has four exons and three introns. The σ-1R genes from all four mammalian species have similar numbers of base pairs in the open reading frame, and approximately 1580 to 1850 base pairs in the cDNA library. However, many aspects of σ-1R gene structural information are currently unavailable, especially for species such as guinea pig and rat.

TABLE II. Posttranslational modifications of σ-1Rs

Characterization of σ-1R proteins from four mammalian species has revealed that the σ-1R proteins contain 223 amino acids with a molecular weight of ~ 28 kDa. These σ-1R proteins have highly similar amino acids (**Fig 1**). Some of the amino residues of σ-1Rs, such as serine (98 or 99 and 182 or 183) and tyrosine (142 or 143), undergo phosphorylation. σ-1Rs do not undergo glycosylation, but they undergo myristoylation.

Table III. Changes in protein levels of NMDARs, AMPARs, and PSD-95 at 90 min following i.p. injection of SKF or PTZ

The 30-, 45-, and 90-min post-injection columns are expressed as a percentage of the

corresponding vehicle column, with the experiments done in parallel. Data are mean ± SEM of at least 4–9 different experiments for SKF and 4–7 experiments for PTZ treatments. Numbers that are asterisked in bold and italic indicate significant differences from vehicle injection ($p < 0.05$, two-tailed distribution, unpaired t-test).

TABLE IV. Alterations in protein levels of σ-1Rs in the LP1 fractions and total homogenates, depending on treatment time and type of drug

The table summarizes the changes occurring to the protein levels of σ-1Rs in the LP1 fractions and total homogenates of hippocampi following different types of drugs at diverse time points. In the table, possible mechanisms that could be involved in altering the protein levels of σ-1Rs were also indicated. Immunoblot experiments were performed to measure the protein levels of σ-1Rs in the LP1 fractions and total homogenates.

TABLE V. Theoretical estimation of SKF and PTZ concentration in the brain

SKF and PTZ are the two commonly used σ-1Rs agonists for studying σ-1R-mediated actions. These compounds belong to the benzomorphan class of drugs, and bear analogous structures with only minor differences in molecular weight. The estimated brain concentration of these compounds at 90 min after an i.p. injection of 2 mg/kg is around 4–6 μM according to the calculation described in the table.


human MQWAVGRRWAWAALLLAVAAVLTQIVWLWLGTQSFVFQREEIAQLARQYA (50)
guniea pig MQWAVGRRWLWVALFLAAVAVLTQIVWLWLGTQNFVFQREEIAQLARQYA (50)
rat MPWAVGRRWAWITLFLTIVAVLIQAVWLWLGTQSFVFQREEIAQLARQYA (50)
mouse MPWAAGRRWAWITLILTIIAVLIQAAWLWLGTQNFVFSREEIAQLARQYA (50)
human GLDHELAFSRLIVELRRLHPGHVLPDEELQWVFVNAGGWMGAMCLLHASL (100)
guinea pig GLDHELAFSKLIVELRRLHPVHVLPDEELQWVFVNAGGWMGAMCLLHASL (100)
rat GLDHELAFSRLIVELRRLHPGHVLPDEELQWVFVNAGGWMGAMCLLHASL (100)
mouse GLDHELAFSRLIVELRRLHPGHVLPDEELQWVFVNAGGWMGAMCILHASL (100)
human SEYVLLFGTALGSRGHSGRYWAEISDTIISGTFHQWREGTTKSEVFYPGE (150)
guniea pig SEYVLLFGTALGSPRHSGRYWAEISDTIISGTFHQWREGTTKSEVFYPGE (150)
rat SEYVLLFGTALGSHGHSGRYWAEISDTIISGTFHQWREGTTKSEVYYPGE (150)
mouse SEYVLLFGTALGSHGHSGRYWAEISDTIISGTFHQWKEGTTKSEVFYPGE (150)
human TVVHGPGEATAVEWGPNTWMVEYGRGVIPSTLAFALADTVFSTQDFLTLF (200)
guniea pig TVVHGPGEATAVEWGPNTWMVEYGRGVIPSTLGFALADTVFSTQDFLTLF (200)
rat TVVHGPGEATAVEWGPNTWMVEYGRGVIPSTLAFALSDTIFSTQDFLTLF (200)
mouse TVVHGPGEATALEWGPNTWMVEYGRGVIPSTLFFALADTFFSTQDYLTLF (200)
human YTLRVYARGLRLELTTYLFGQDP 96.0 % identity (223)
guniea pig YTLRVYARALQLELTTYLFGQDP 93.7 % identity (223)
rat YTLRAYARGLRLELTTYLFGQDP (223)
mouse YTLRAYARGLRLELTTYLFGQDS 93.3 % identity (223)

FIGURE 1

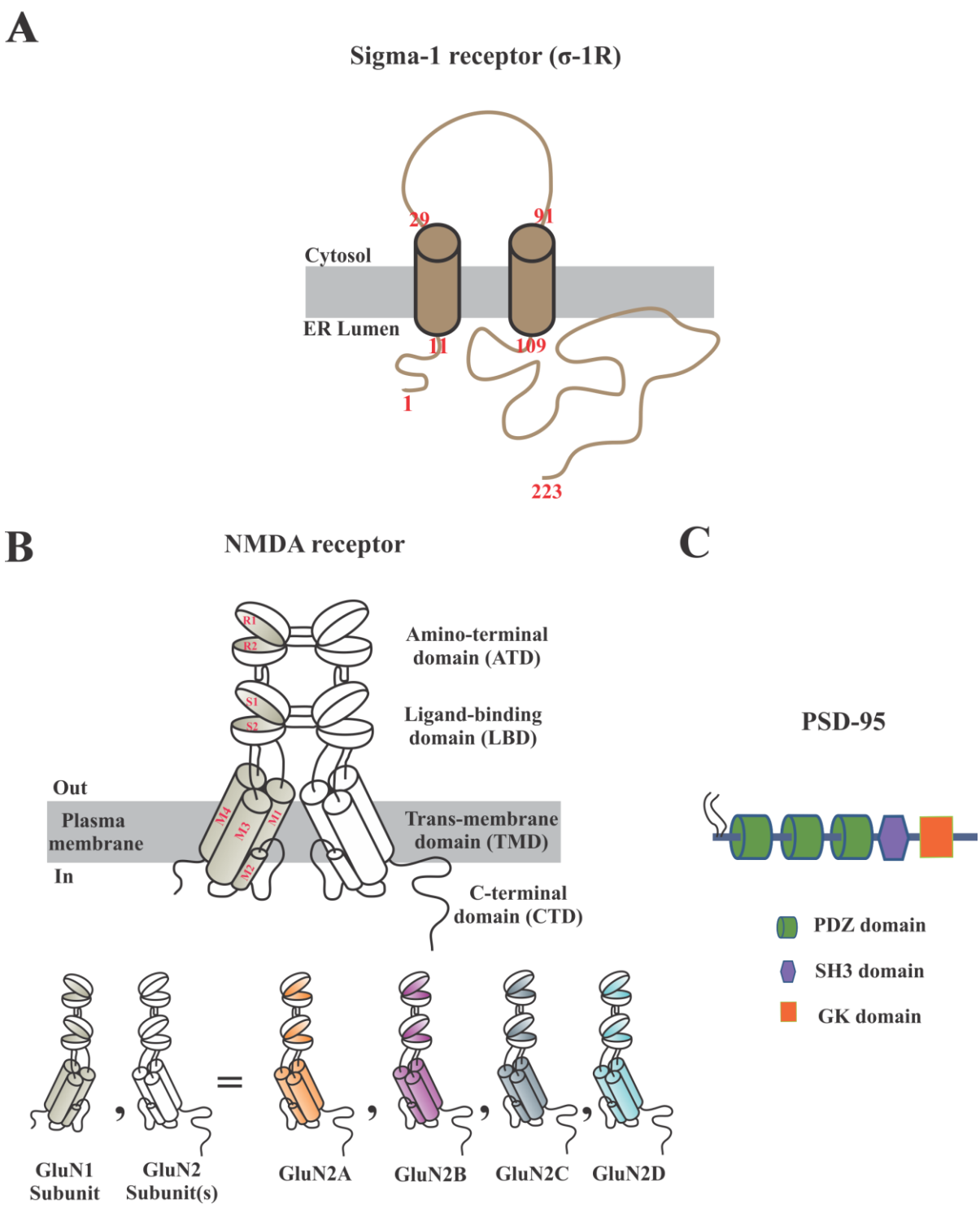
A
Sigma-1 receptor (σ-1R)
29
91
Cytosol
ER Lumen
111
109
1
223
B
NMDA receptor
R1
R2
S1
S2
Amino-terminal domain (ATD)
Ligand-binding domain (LBD)
Out
Plasma membrane
In
M4
M3
M1
M2
Trans-membrane domain (TMD)
C-terminal domain (CTD)
GluN1 Subunit
GluN2 Subunit(s)
GluN2A
GluN2B
GluN2C
GluN2D
C
PSD-95
PDZ domain
SH3 domain
GK domain

FIGURE 2

A

Potentiation of NMDAR mediated responses following σ-1R activation		
Response type	**Method**	**Representative reference(s)**
NMDA-induced frequency of action potentials	Extracellular unitary recordings/current-clamp recordings	(13)
fEPSPs	Extracellular field recordings	(27)
EPSPs	Whole cell current-clamp or voltage-clamp recordings	(102)
EPSCs		(110)
EEG spectrum	EEG recordings	(108)
NMDAR-dependent short- and long-term learning and memory	Y-maze for spatial working memory, step-down and step-through passive avoidance, and elevated plus-maze	(114)

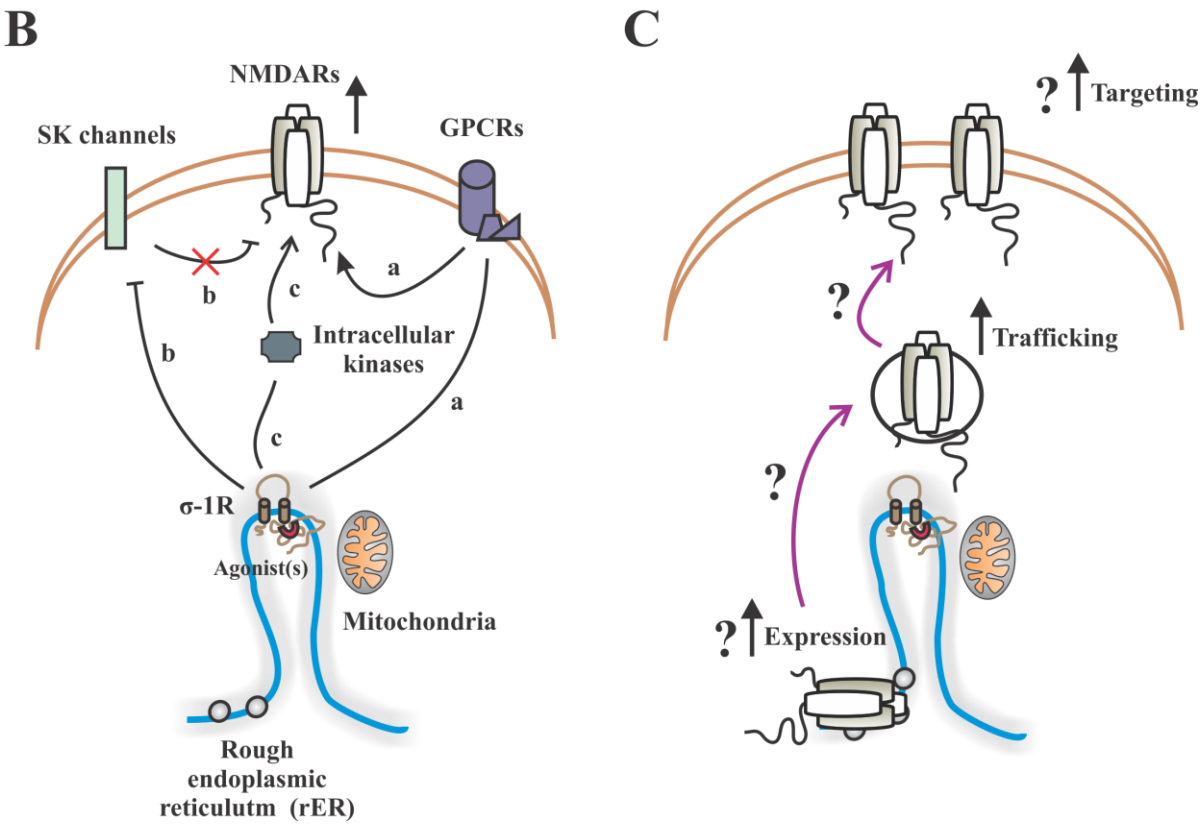

FIGURE 3

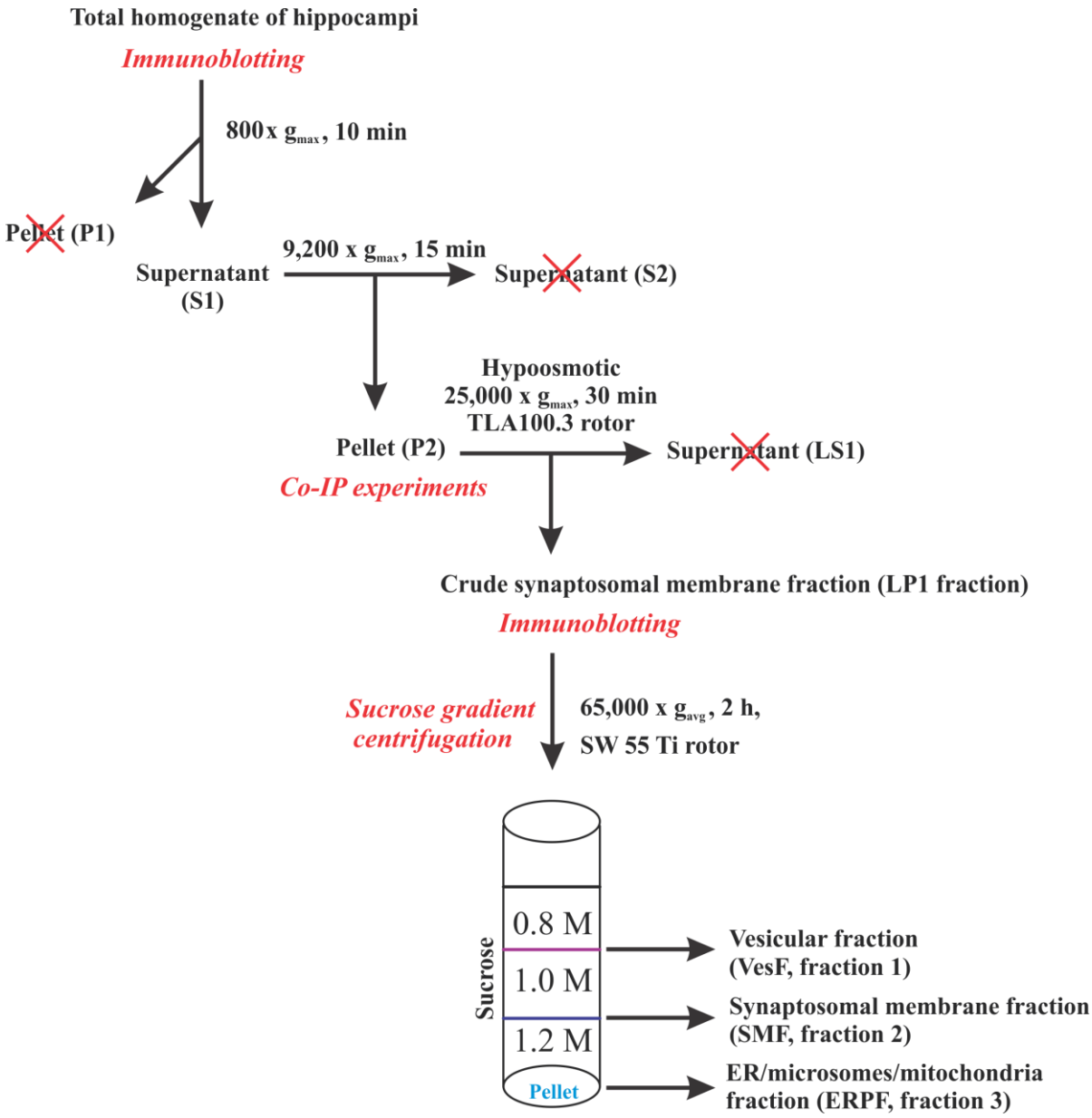
Total homogenate of hippocampi
Immunoblotting
800x g max, 10 min
Pellet (P1)
Supernatant (S1)
9,200 x g max, 15 min
Supernatant (S2)
Hypoosmotic
25,000 x g max, 30 min
TLA100.3 rotor
Pellet (P2)
Co-IP experiments
Supernatant (LS1)
Crude synaptosomal membrane fraction (LP1 fraction)
Immunoblotting
Sucrose gradient centrifugation
65,000 x g avg, 2 h,
SW 55 Ti rotor
Sucrose
0.8 M
1.0 M
1.2 M
Pellet
Vesicular fraction (VesF, fraction 1)
Synaptosomal membrane fraction (SMF, fraction 2)
ER/microsomes/mitochondria fraction (ERPF, fraction 3)

FIGURE 4

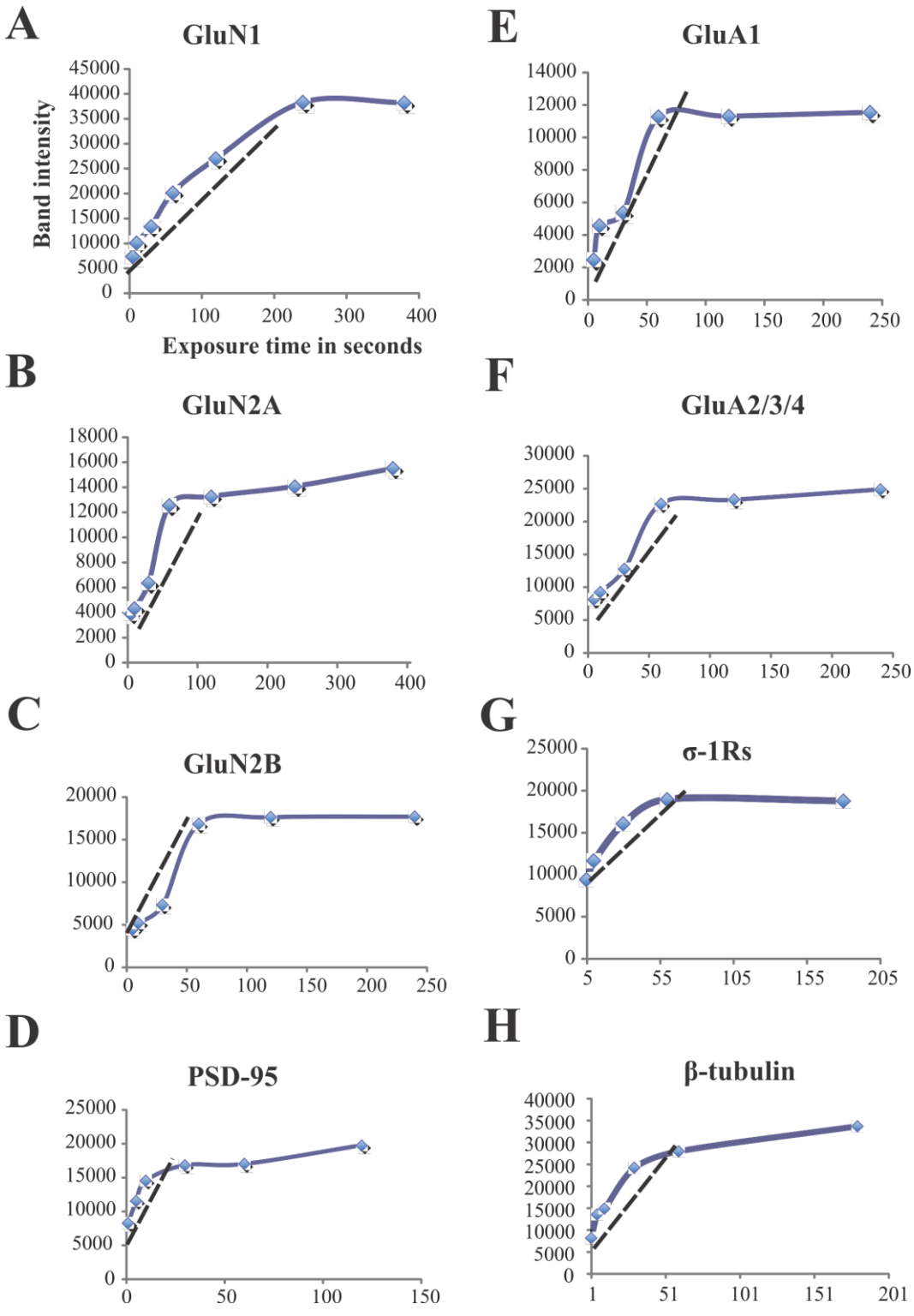
A
GluN1
Band intensity
Exposure time in seconds
B
GluN2A
C
GluN2B
D
PSD-95
E
GluA1
F
GluA2/3/4
G
σ-1Rs
H
β-tubulin

FIGURE 5

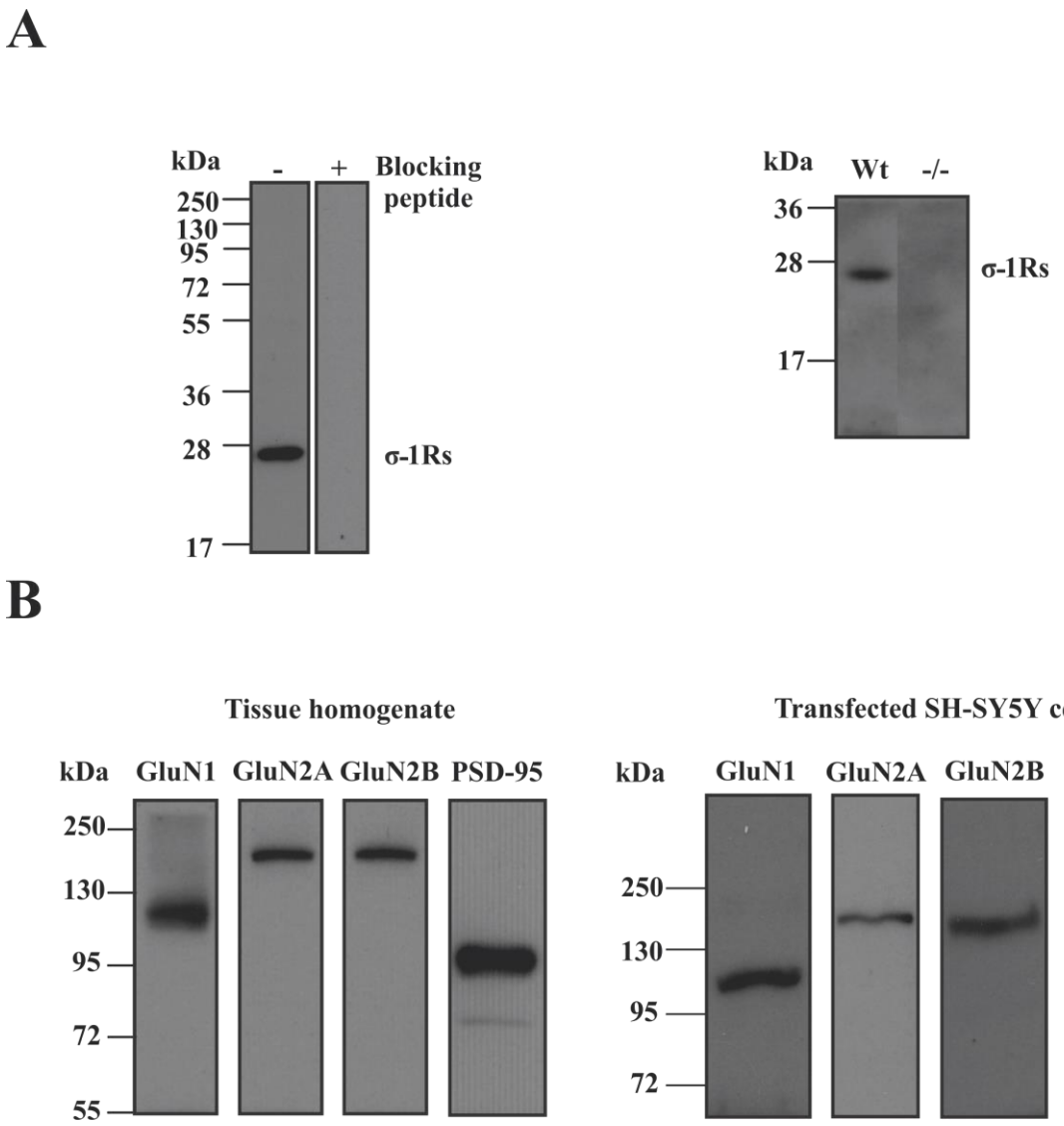
A
kDa
-
+
Blocking peptide
250
130
95
72
55
36
28
σ-1Rs
17
kDa
Wt
-/-
36
28
σ-1Rs
17
B
Tissue homogenate
kDa
GluN1
GluN2A
GluN2B
PSD-95
250
130
95
72
55
Transfected SH-SY5Y cells
kDa
GluN1
GluN2A
GluN2B
PSD-95
250
130
95
72

FIGURE 6

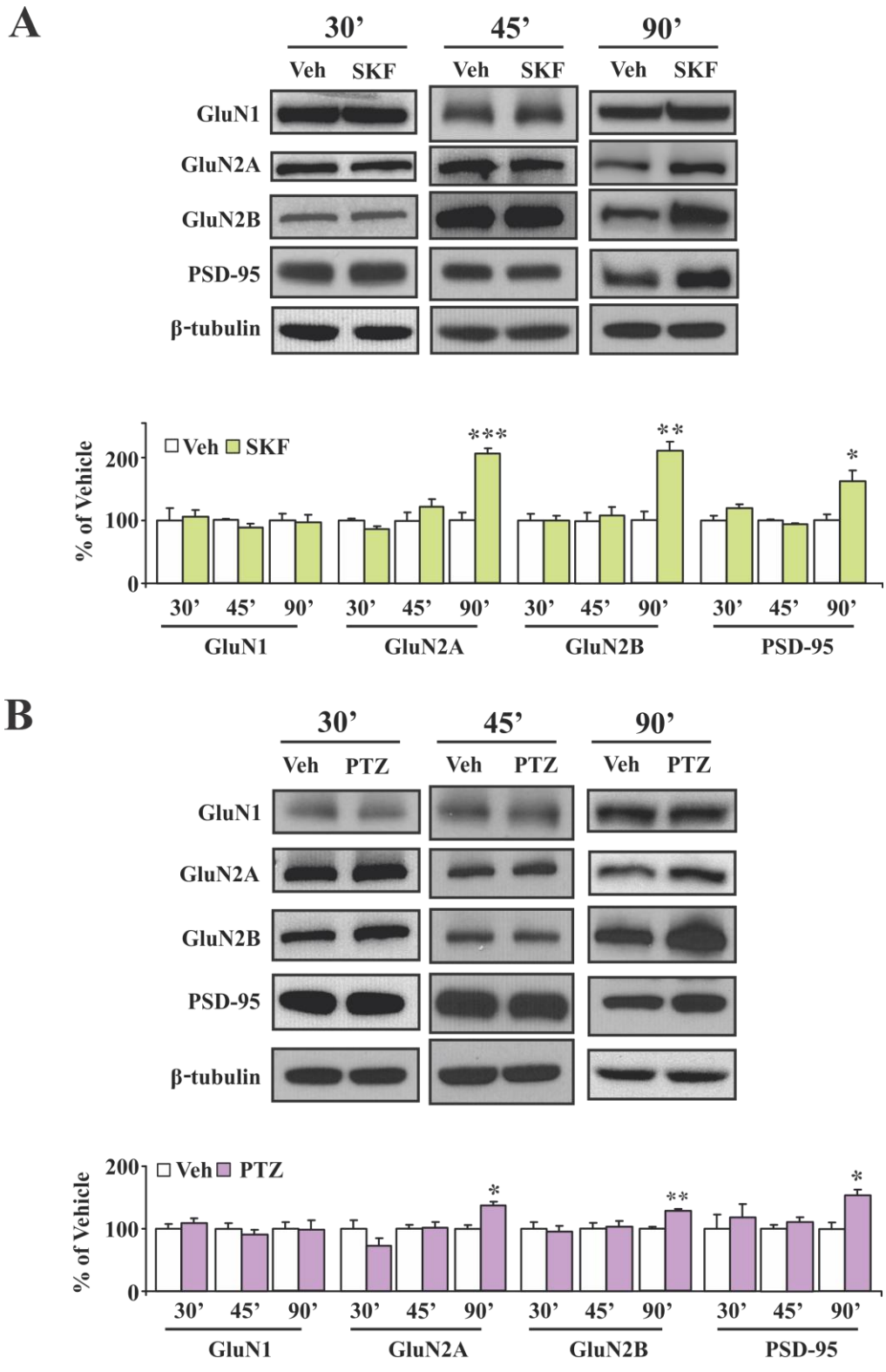
A
30'
45'
90'
Veh
SKF
GluN1
GluN2A
GluN2B
PSD-95
β-tubulin
Veh
SKF
% of Vehicle
200
100
0
***
**
*
30'
45'
90'
GluN1
GluN2A
GluN2B
PSD-95
B
PTZ

FIGURE 7

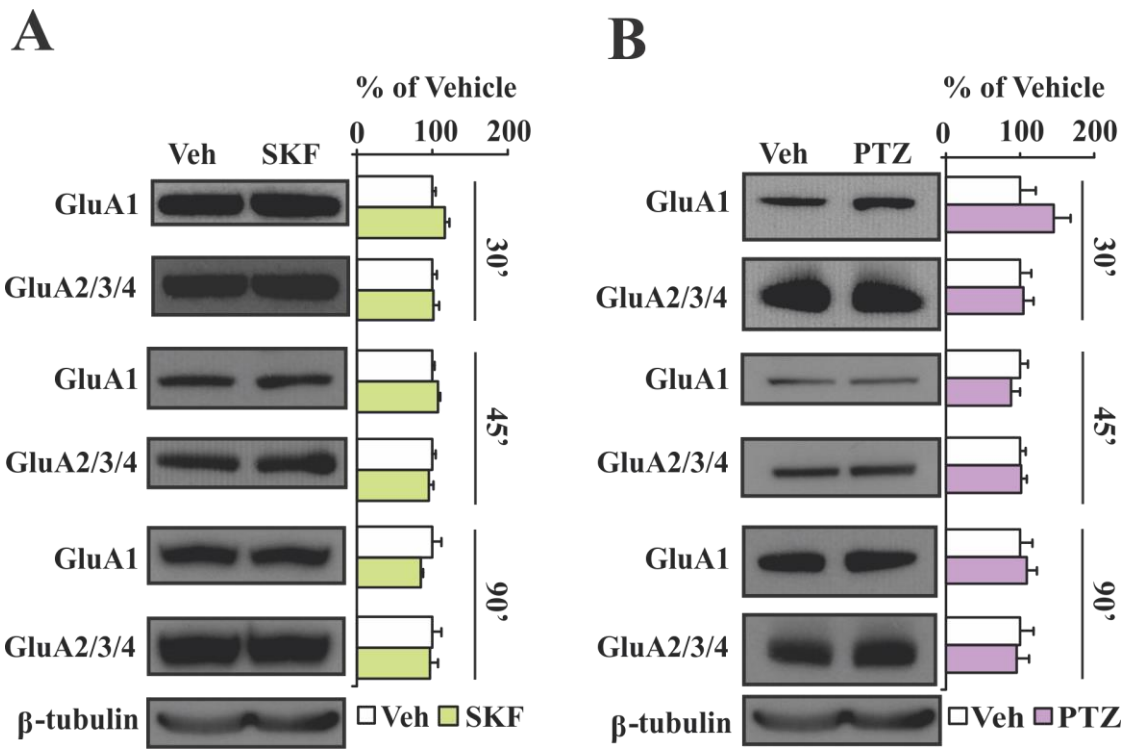
A
% of Vehicle
0
100
200
Veh
SKF
GluA1
GluA2/3/4
GluA1
GluA2/3/4
GluA1
GluA2/3/4
β-tubulin
30'
45'
90'
Veh
SKF
B
% of Vehicle
0
100
200
Veh
PTZ
GluA1
GluA2/3/4
GluA1
GluA2/3/4
GluA1
GluA2/3/4
β-tubulin
30'
45'
90'
Veh
PTZ

FIGURE 8

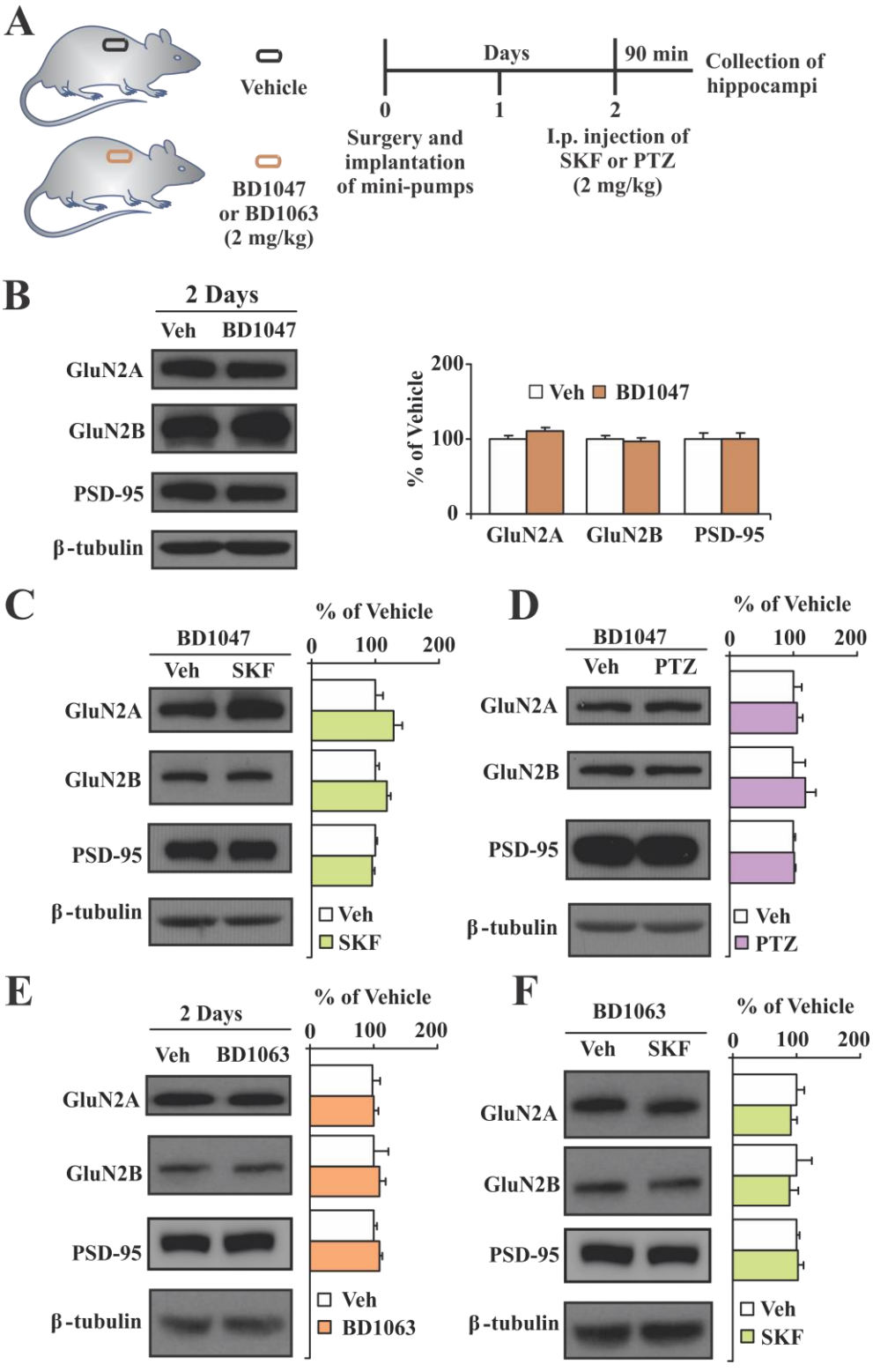
A
Vehicle
BD1047
or BD1063
(2 mg/kg)
Days
90 min
Collection of
hippocampi
0
1
2
Surgery and
implantation
of mini-pumps
I.p. injection of
SKF or PTZ
(2 mg/kg)
B
2 Days
Veh
BD1047
GluN2A
GluN2B
PSD-95
β-tubulin
% of Vehicle
200
100
0
Veh
BD1047
GluN2A
GluN2B
PSD-95
C
BD1047
Veh
SKF
% of Vehicle
0
100
200
Veh
SKF
D
BD1047
Veh
PTZ
Veh
PTZ
E
2 Days
Veh
BD1063
Veh
BD1063
F
BD1063
Veh
SKF
Veh
SKF

FIGURE 9

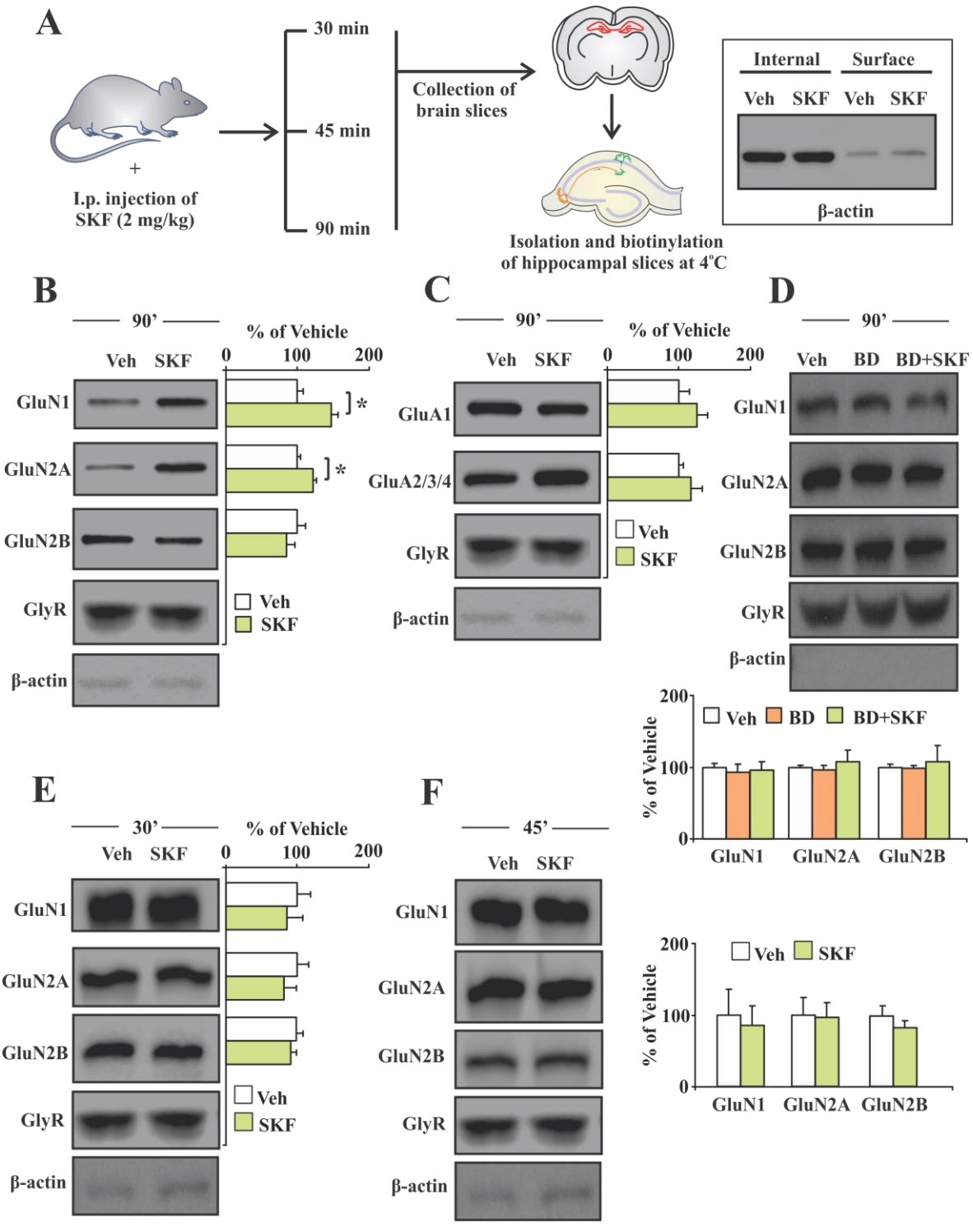
A
30 min
45 min
90 min
I.p. injection of SKF (2 mg/kg)
Collection of brain slices
Isolation and biotinylation of hippocampal slices at 4°C
Internal
Surface
Veh SKF Veh SKF
β-actin
B
90'
% of Vehicle
Veh SKF
0 100 200
GluN1
GluN2A
GluN2B
GlyR
β-actin
Veh
SKF
*
C
90'
% of Vehicle
Veh SKF
0 100 200
GluA1
GluA2/3/4
GlyR
β-actin
Veh
SKF
D
90'
Veh BD BD+SKF
GluN1
GluN2A
GluN2B
GlyR
β-actin
200
100
0
% of Vehicle
Veh BD BD+SKF
GluN1 GluN2A GluN2B
E
30'
% of Vehicle
Veh SKF
0 100 200
GluN1
GluN2A
GluN2B
GlyR
β-actin
Veh
SKF
F
45'
Veh SKF
GluN1
GluN2A
GluN2B
GlyR
β-actin
200
100
0
% of Vehicle
Veh SKF
GluN1 GluN2A GluN2B

FIGURE 10

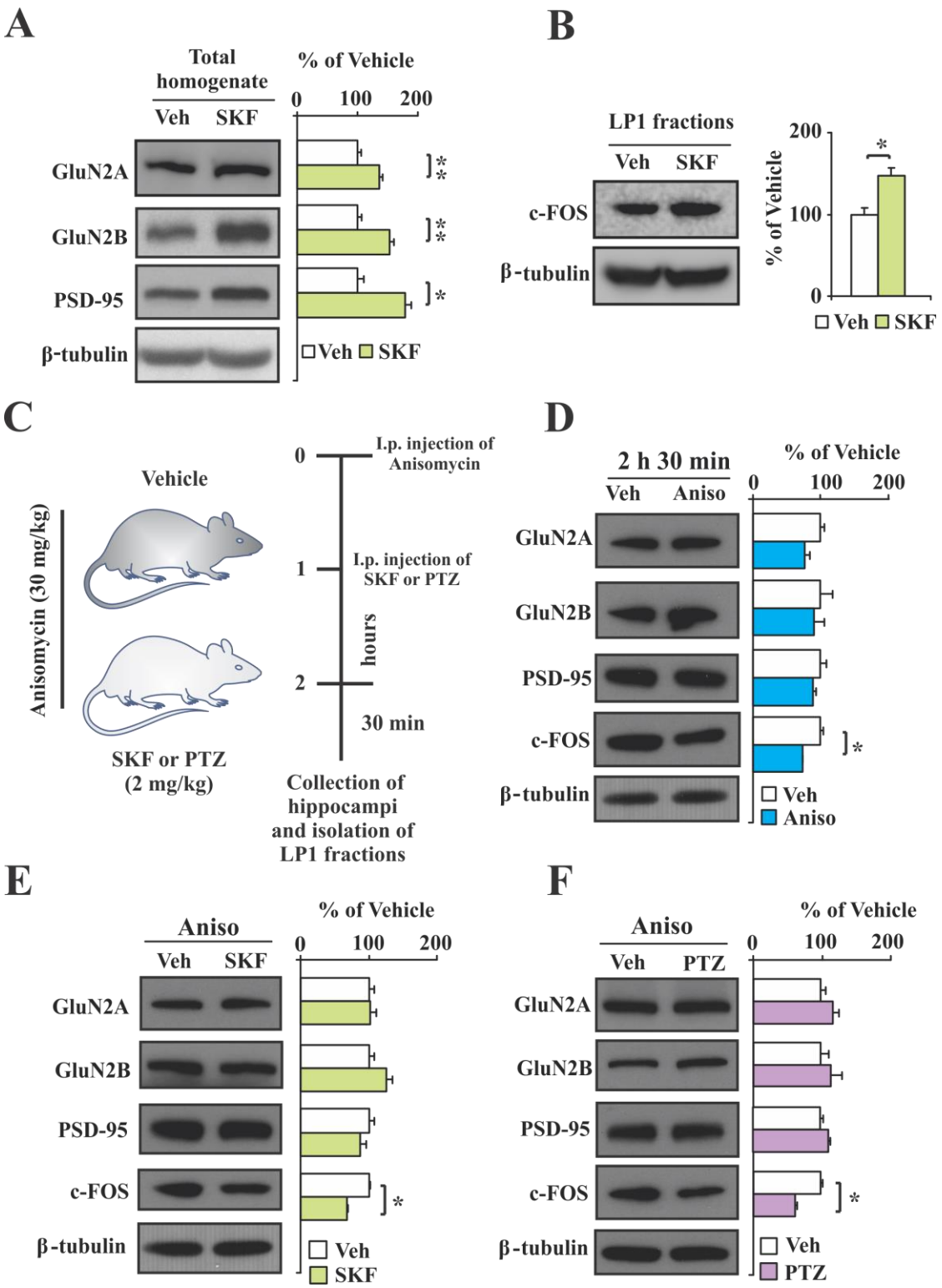
A
Total homogenate
% of Vehicle
Veh SKF
0 100 200
GluN2A
GluN2B
PSD-95
β-tubulin
Veh SKF
B
LP1 fractions
Veh SKF
c-FOS
β-tubulin
% of Vehicle
200
100
0
Veh SKF
C
Vehicle
Anisomycin (30 mg/kg)
SKF or PTZ
(2 mg/kg)
0
I.p. injection of Anisomycin
1
I.p. injection of SKF or PTZ
hours
2
30 min
Collection of hippocampi and isolation of LP1 fractions
D
2 h 30 min
% of Vehicle
Veh Aniso
0 100 200
GluN2A
GluN2B
PSD-95
c-FOS
β-tubulin
Veh
Aniso
E
Aniso
% of Vehicle
Veh SKF
0 100 200
GluN2A
GluN2B
PSD-95
c-FOS
β-tubulin
Veh
SKF
F
Aniso
% of Vehicle
Veh PTZ
0 100 200
GluN2A
GluN2B
PSD-95
c-FOS
β-tubulin
Veh
PTZ

FIGURE 11

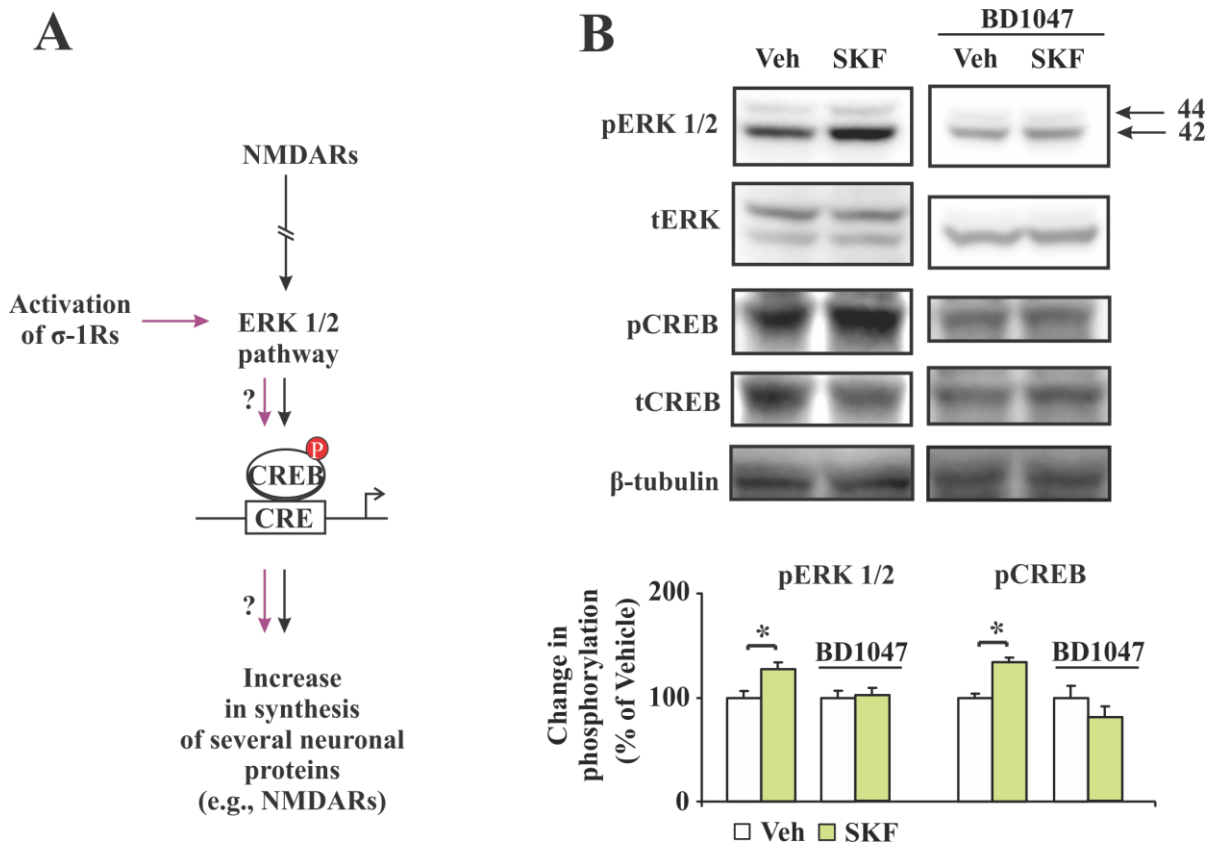
A
NMDARs
Activation of σ-1Rs
ERK 1/2 pathway
?
P
CREB
CRE
?
Increase in synthesis of several neuronal proteins (e.g., NMDARs)
B
BD1047
Veh
SKF
Veh
SKF
pERK 1/2
tERK
pCREB
tCREB
β-tubulin
44
42
pERK 1/2
pCREB
Change in phosphorylation (% of Vehicle)
200
100
0
*
BD1047
*
BD1047
Veh
SKF

FIGURE 12

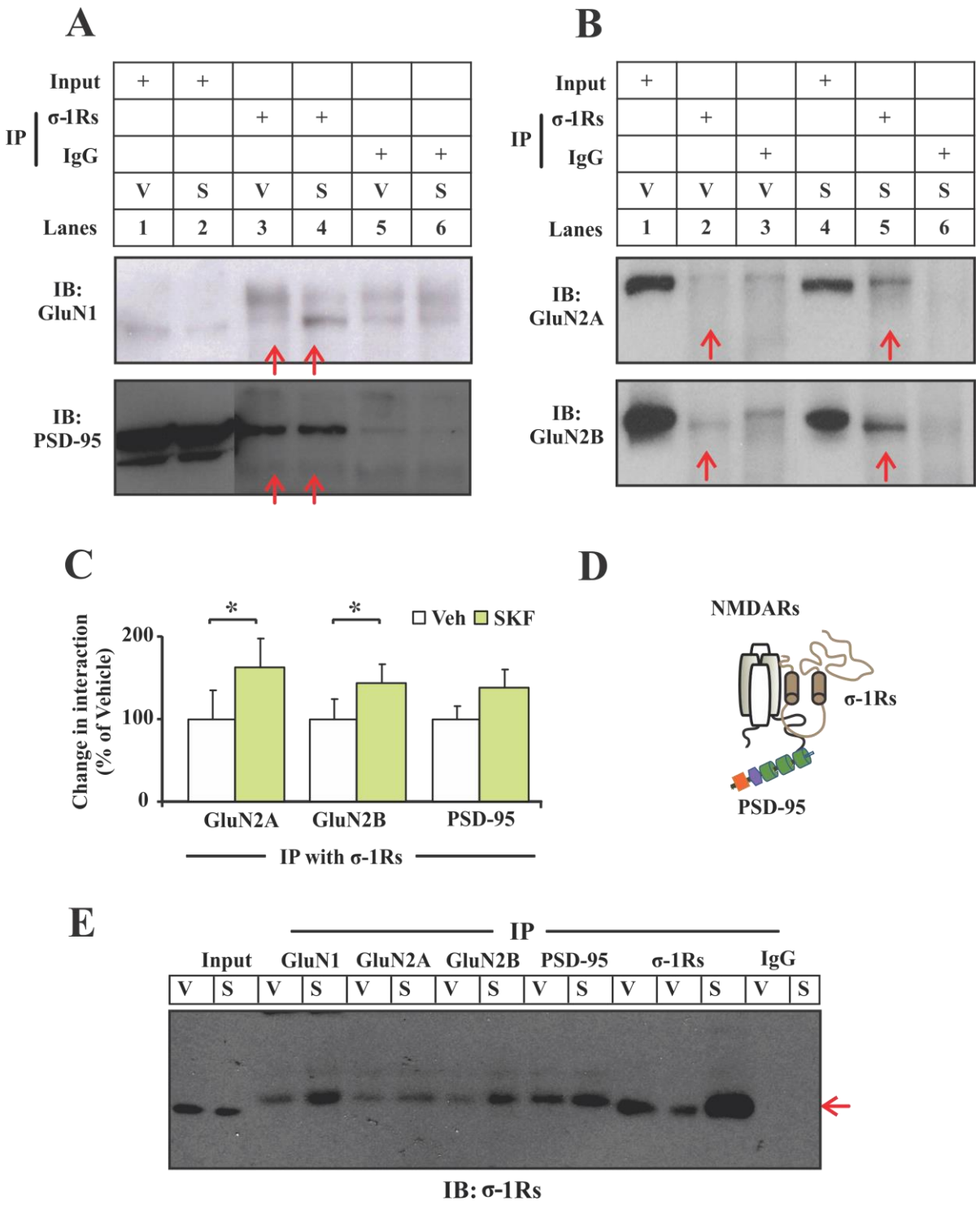
A
Input
IP
σ-1Rs
IgG
V S V S V S
Lanes 1 2 3 4 5 6
IB: GluN1
IB: PSD-95
B
Input
IP
σ-1Rs
IgG
V V V S S S
Lanes 1 2 3 4 5 6
IB: GluN2A
IB: GluN2B
C
Change in interaction (% of Vehicle)
200
100
0
*
*
Veh
SKF
GluN2A
GluN2B
PSD-95
IP with σ-1Rs
D
NMDARs
σ-1Rs
PSD-95
E
IP
Input
GluN1
GluN2A
GluN2B
PSD-95
σ-1Rs
IgG
V S V S V S V S V S V V S V S
IB: σ-1Rs

FIGURE 13

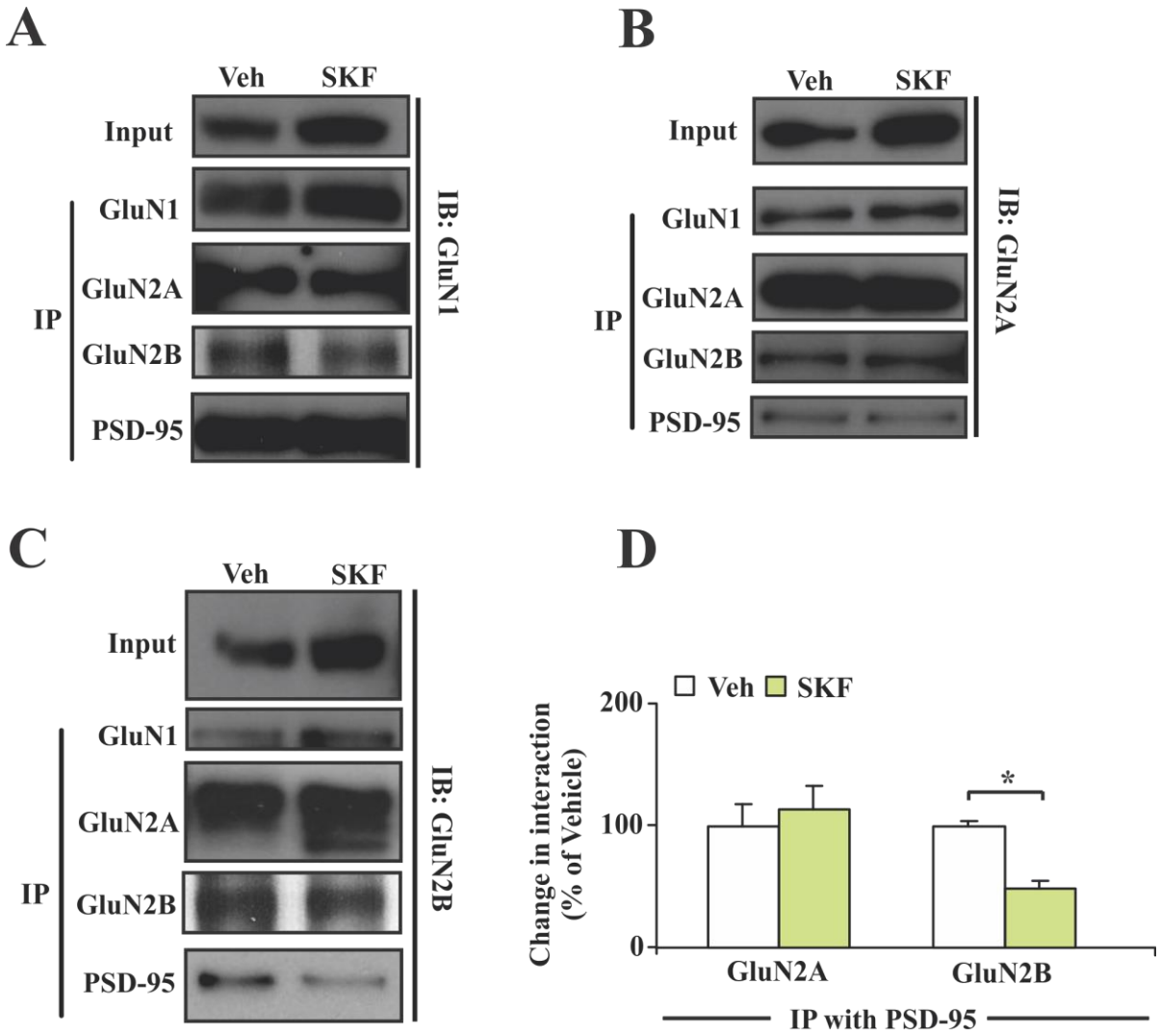
A
Veh
SKF
Input
GluN1
GluN2A
GluN2B
PSD-95
IP
IB: GluN1
B
Veh
SKF
Input
GluN1
GluN2A
GluN2B
PSD-95
IP
IB: GluN2A
C
Veh
SKF
Input
GluN1
GluN2A
GluN2B
PSD-95
IP
IB: GluN2B
D
Veh
SKF
Change in interaction (% of Vehicle)
200
100
0
*
GluN2A
GluN2B
IP with PSD-95

FIGURE 14

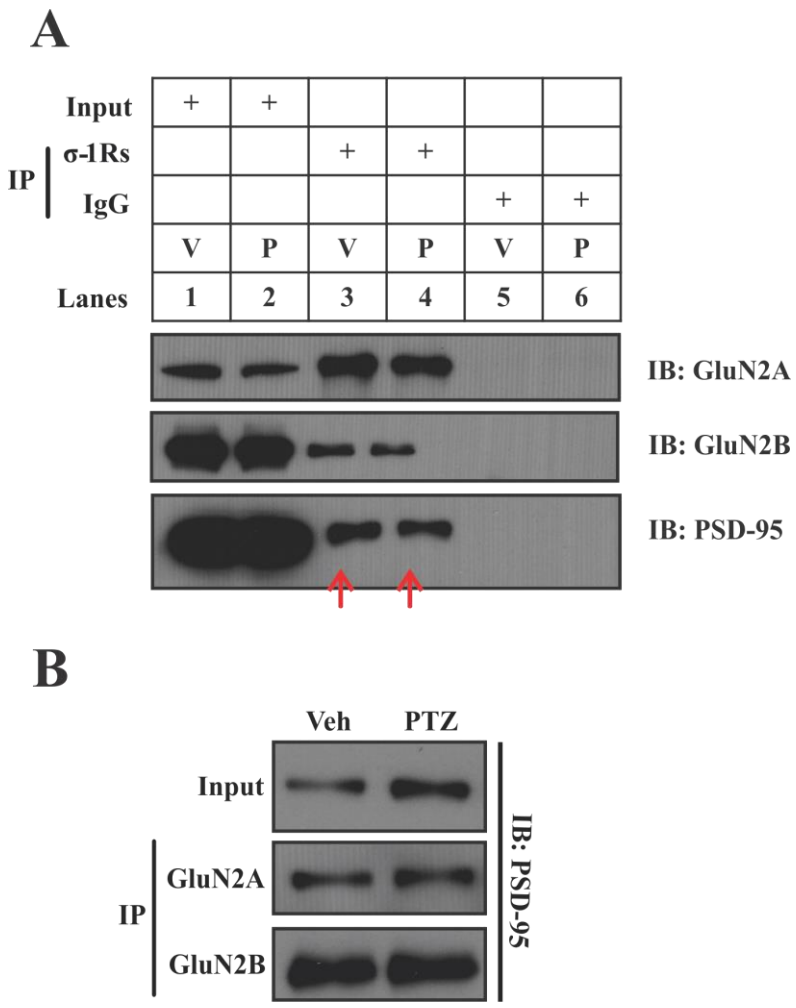
A
Input
IP
σ-1Rs
IgG
Lanes
+ + + + + +
V P V P V P
1 2 3 4 5 6
IB: GluN2A
IB: GluN2B
IB: PSD-95
B
Veh
PTZ
Input
IP
GluN2A
GluN2B
IB: PSD-95

FIGURE 15

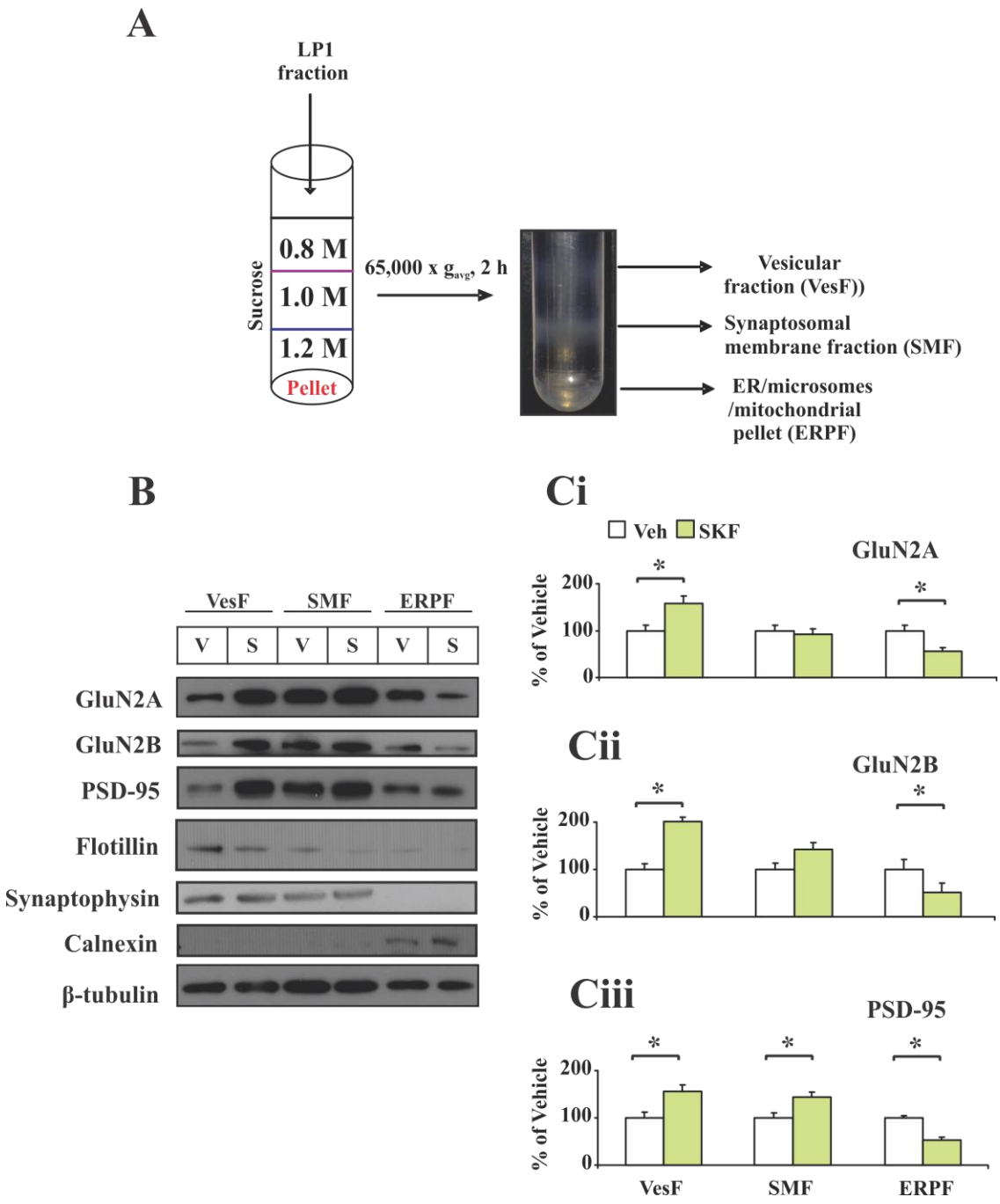
A
LP1 fraction
Sucrose
0.8 M
1.0 M
1.2 M
Pellet
65,000 x g$_{avg}$, 2 h
Vesicular fraction (VesF))
Synaptosomal membrane fraction (SMF)
ER/microsomes /mitochondrial pellet (ERPF)
B
VesF
SMF
ERPF
V
S
GluN2A
GluN2B
PSD-95
Flotillin
Synaptophysin
Calnexin
β-tubulin
Ci
Veh
SKF
GluN2A
% of Vehicle
200
100
0
Cii
GluN2B
Ciii
PSD-95
VesF
SMF
ERPF

FIGURE 16

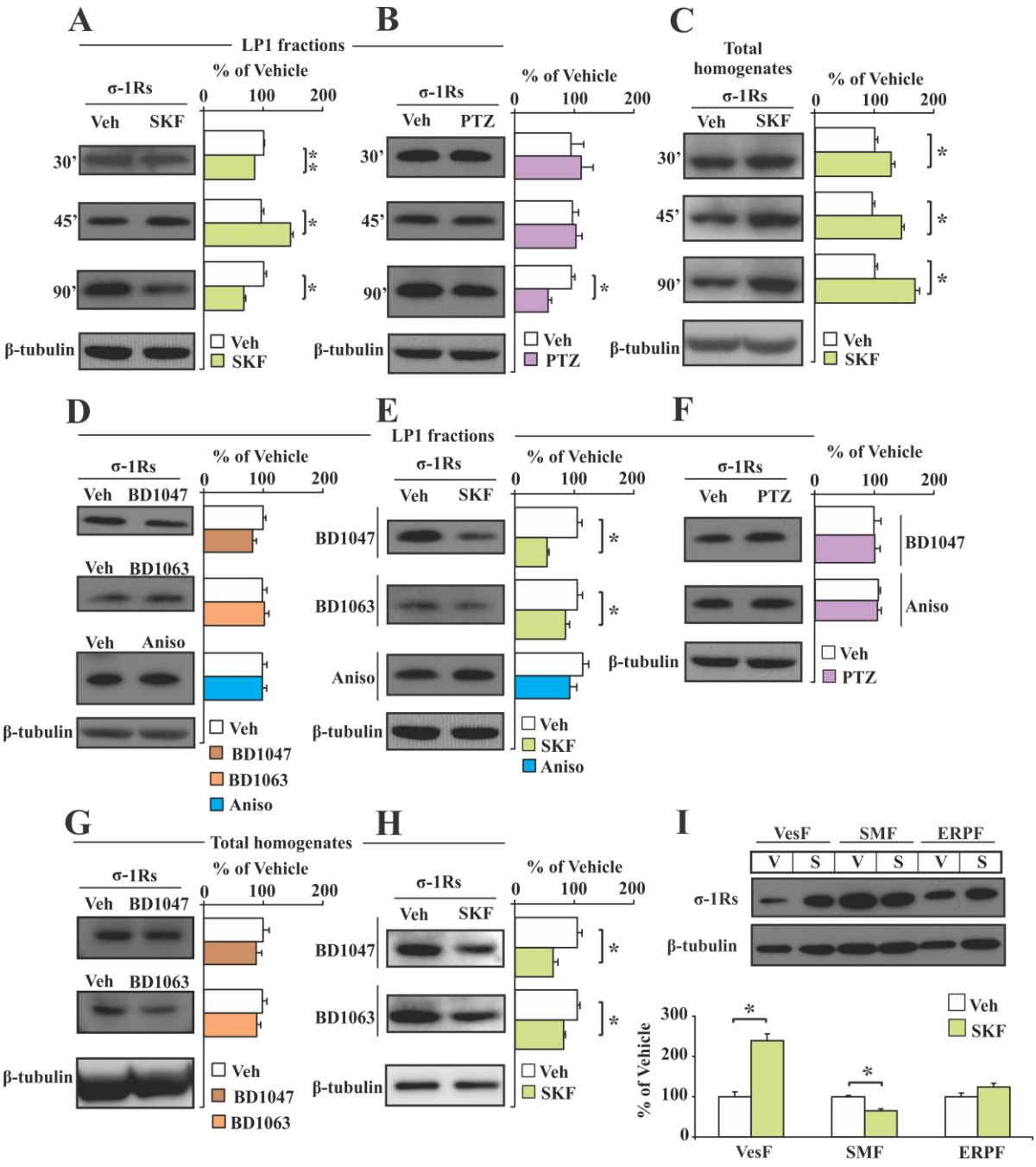
A
LP1 fractions
σ-1Rs
% of Vehicle
0 100 200
Veh SKF
30'
45'
90'
β-tubulin
Veh
SKF
B
σ-1Rs
% of Vehicle
0 100 200
Veh PTZ
30'
45'
90'
β-tubulin
Veh
PTZ
C
Total homogenates
σ-1Rs
% of Vehicle
0 100 200
Veh SKF
30'
45'
90'
β-tubulin
Veh
SKF
D
σ-1Rs
% of Vehicle
0 100 200
Veh BD1047
Veh BD1063
Veh Aniso
β-tubulin
Veh
BD1047
BD1063
Aniso
E
LP1 fractions
σ-1Rs
% of Vehicle
0 100 200
Veh SKF
BD1047
BD1063
Aniso
β-tubulin
Veh
SKF
Aniso
F
σ-1Rs
% of Vehicle
0 100 200
Veh PTZ
BD1047
Aniso
β-tubulin
Veh
PTZ
G
Total homogenates
σ-1Rs
% of Vehicle
0 100 200
Veh BD1047
Veh BD1063
β-tubulin
Veh
BD1047
BD1063
H
σ-1Rs
% of Vehicle
0 100 200
Veh SKF
BD1047
BD1063
β-tubulin
Veh
SKF
I
VesF SMF ERPF
V S V S V S
σ-1Rs
β-tubulin
Veh
SKF
% of Vehicle
300
200
100
0
VesF
SMF
ERPF

FIGURE 17

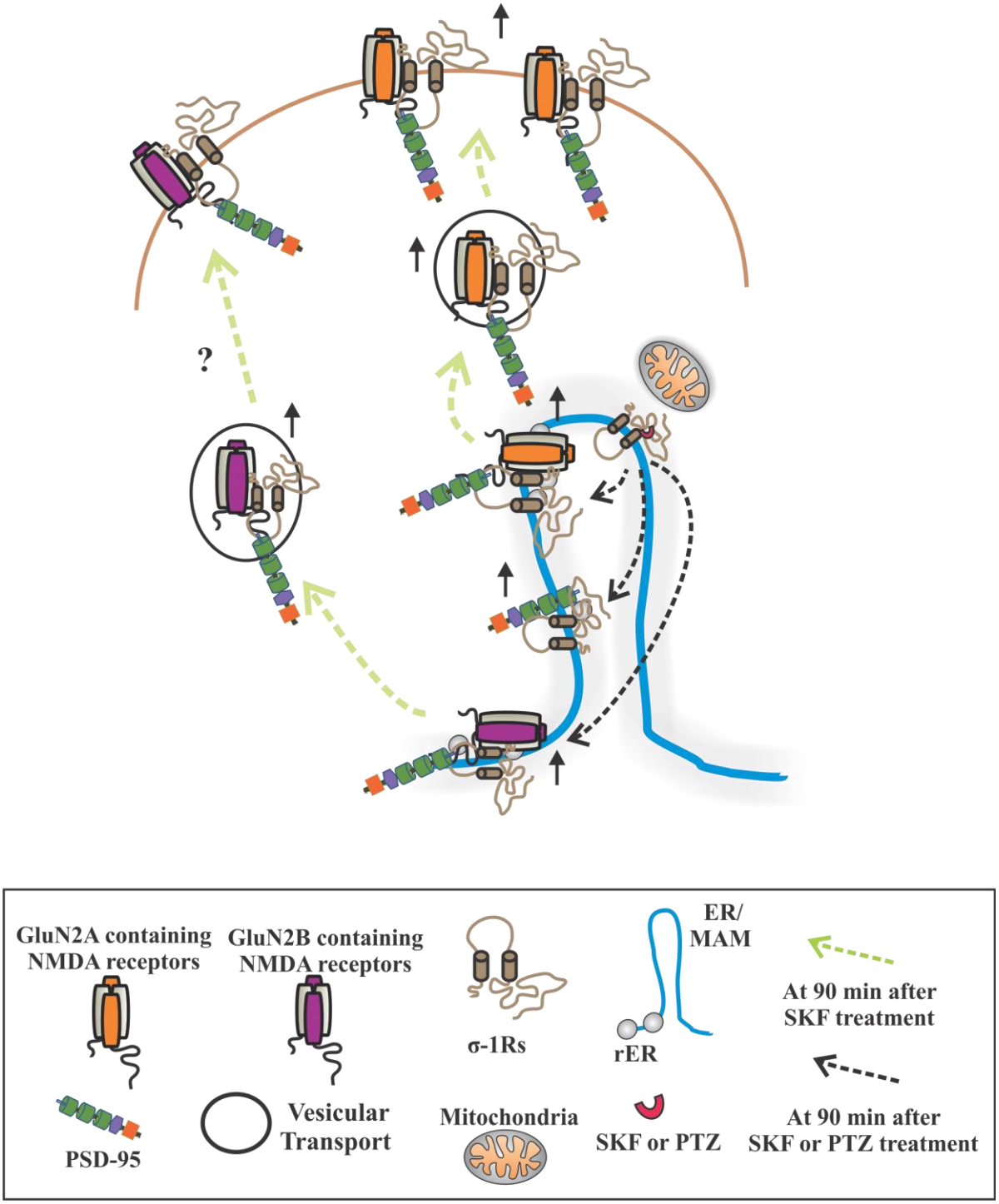
?
GluN2A containing NMDA receptors
GluN2B containing NMDA receptors
σ-1Rs
ER/ MAM
rER
At 90 min after SKF treatment
PSD-95
Vesicular Transport
Mitochondria
SKF or PTZ
At 90 min after SKF or PTZ treatment

FIGURE 18

TABLE I

Species	cDNA library size (bp)	Open reading frame of σ-1R gene (bp)	5'-noncoding region (bp)	No of exons and introns	3'-noncoding region (bp)	Chromosomal location	Classical TATA box at the start of transcription site	References
Human	1653	672	59	4 and 3	922	9p13	Absent	(84, 157)
Guinea Pig	1857	672	*	*	*	*	*	(56)
Rat	1582	672	30	*	880	5	*	(177)
Mouse	1567	672	21	4 and 3	874	A5-B2 of 4	Absent	(149, 179)

*-Information unknown

TABLE II

Species	Protein length (no. of amino acids)	Molecular weight (kDa)	Overall Sequence identity (I) and similarity (S) between human, guinea pig rat and mouse[#]	Assumed ER retention signal sequence	Glycosylatio-n site	Serine phosphoryla-tion sites (amino acids)	Tyrosine phosphoryla-tion site (amino acid)	Myristoylati-on site (amino acid)	References
Human	223	~28	>92% (I) and > 95% (S)	MQWAVGRR	None	98 and 182	142	75	(84, 149, 157)
Guinea pig	223	~25.3		MQWAVGRR	None	98 and 182	142	75	(149)
Rat	223	~28		MPWAVGRR	None	*	*	*	(177)
Mouse	223	~28		MPWAAGRR	None	99 and 182	143	76	(149, 179)

[#]-Source: NCBI, *-Information unknown

TABLE III

(+)-SKF 10,047 (2mg/kg, i.p.)							
		Veh	**30' post inj**	**Veh**	**45' post inj**	**Veh**	**90' post inj**
GluN1		100 ± 19.3	105 ± 10.8	100 ± 1.35	88.6 ± 5.73	100 ± 15.3	90.5 ± 15.3
GluN2A		100 ± 3.45	100 ± 4.81	100 ± 13.2	122 ± 12.8	100 ± 9.4	***205.5 ± 8.8****
GluN2B		100 ± 10.7	100 ± 6.94	100 ± 13.6	109 ± 13.6	100 ± 8.7	***208 ± 13.6****
GluA1		100 ± 4.34	115 ± 6.75	100 ± 3.08	107 ± 3.66	100 ± 12.2	94.1 ± 7.10
GluA2/3/4		100 ± 6.57	101 ± 7.32	100 ± 5.03	95.2 ± 6.14	100 ± 11.8	97.6 ± 10.8
PSD-95		100 ± 8.02	119 ± 5.31	100 ± 2.06	94.2 ± 4.66	100 ± 7.7	***161.7 ± 12.5****
(+)-Pentazocine (2mg/kg, i.p.)							
GluN1		100 ± 7.57	109 ± 6.75	100 ± 8.91	90.3 ± 7.51	100 ± 10.2	98.7 ± 14.2
GluN2A		100 ± 14.3	82.1 ± 12.6	100 ± 6.12	102 ± 9.02	100 ± 6.47	***138 ± 6.57****
GluN2B		100 ± 10.7	95.3 ± 9.97	100 ± 8.46	103 ± 8.65	100 ± 2.61	***128 ± 2.93****
GluA1		100 ± 20.5	125 ± 22.6	100 ± 10.1	88.2 ± 11.8	100 ± 17.1	108 ± 14.3
GluA2/3/4		100 ± 14.8	105 ± 9.68	100 ± 7.98	101 ± 7.99	100 ± 18.2	95.7 ± 16.2
PSD-95		100 ± 7.21	107 ± 9.68	100 ± 6.56	109 ± 7.81	100 ± 10.1	***153 ± 9.42****

TABLE IV

Changes in protein levels of σ-1Rs following different drug treatment							
Type of drug		**LP1 fractions**			**Total homogenates**		
		Length of treatment	**Levels**	**Possible mechanism**	**Length of treatment**	**Levels**	**Possible mechanism**
Agonists	SKF	30, 90 min 45 min	Decrease Increase	Translocation	30, 45, 90 min	Increase	Protein synthesis
	PTZ	30, 45 min 90 min	No change Decrease	Translocation			
Antagonists	BD1047	2 days	No change		No change	No change	
	BD1063	2 days	No change		No change	No change	
Antagonist plus agonist	BD1047 plus SKF	2 days 90 min	Decrease	Down-regulation	2 days 90 min	Decrease	Down-regulation
	BD1063 plus SKF	2 days 90 min	Decrease	Down-regulation	2 days 90 min	Decrease	Down-regulation
	BD1047 plus PTZ	2 days 90 min	No change				
Protein synthesis inhibitor plus or minus agonist	Anisomycin	2h 30 min	No change				
	Anisomycin plus SKF	2h 30 min	No change				
	Anisomycin plus PTZ	2h 30 min	No change				

TABLE V

Name	Structure	Calculation
(+)-SK&F 10047 hydrochloride (SKF) [2*S*-(2α,6α,11*R**]-1,2,3,4,5,6-hexahydr o-6,11-dimethyl-3-(2-propenyl)-2,6-methano-3-benza zocin-8-ol hydrochloride	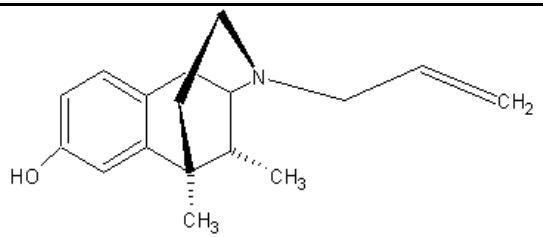 Molecular weight: 257.37 g	**1**. According to the previous work (126), 50 mg/kg i.p. injection of PTZ results in the availability of 3 mg/kg PTZ in the brain 90 min after the administration. **2**. We administered 2 mg/kg of PTZ. Therefore, the availability of PTZ to the brain should be 0.12 mg/kg. **3**. At the time of injection, each rat was 4-6 weeks of age and weighed approximately 200 g. This yielded a total availability of 0.024 mg of PTZ (0.12 mg/kg x 0.200 kg). Using the earlier report (98), the blood volume of the rat, based on its age and weight, was calculated to be 12.77 ml. **4**. Thus, the resulting concentration of PTZ in the brain is approximately 5.2 μM (0.024 mg/ 12.77 ml divided by 285.43 g/mole, adjusting for units). **5**. Overall, the brain concentration of the injected PTZ is approximately 4-6 μM as the weight of the animals varied between 150-250 g at 4-6 weeks of age.
(+)-Pentazocine hydrochloride (PTZ) (2*RS*,6*RS*,11*RS*)-6,11-dimethyl-3-(3-methylbut-2-en-1-yl)-1,2,3,4,5,6-hexahydro-2,6-methano-3-benzazocin-8-ol hydrochloride	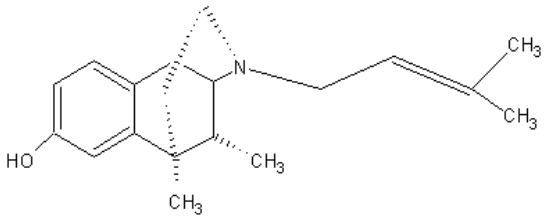 Molecular weight: 285.43 g	

APPENDICES

APPENDIX A: REFERENCES

1. **Aarts M, Liu Y, Liu L, Besshoh S, Arundine M, Gurd JW, Wang YT, Salter MW, and Tymianski M**. Treatment of ischemic brain damage by perturbing NMDA receptor- PSD-95 protein interactions. *Science* 298: 846-850, 2002.

2. **Abraham WC**. How long will long-term potentiation last? *Philos Trans R Soc Lond B Biol Sci* 358: 735-744, 2003.

3. **Al-Saif A, Al-Mohanna F, and Bohlega S**. A mutation in sigma-1 receptor causes juvenile amyotrophic lateral sclerosis. *Ann Neurol* 70: 913-919, 2011.

4. **Alonso G, Phan V, Guillemain I, Saunier M, Legrand A, Anoal M, and Maurice T**. Immunocytochemical localization of the sigma(1) receptor in the adult rat central nervous system. *Neuroscience* 97: 155-170, 2000.

5. **Amparan D, Avram D, Thomas CG, Lindahl MG, Yang J, Bajaj G, and Ishmael JE**. Direct interaction of myosin regulatory light chain with the NMDA receptor. *J Neurochem* 92: 349-361, 2005.

6. **Aoki C, Fujisawa S, Mahadomrongkul V, Shah PJ, Nader K, and Erisir A**. NMDA receptor blockade in intact adult cortex increases trafficking of NR2A subunits into spines, postsynaptic densities, and axon terminals. *Brain Res* 963: 139-149, 2003.

7. **Autry AE, Adachi M, Nosyreva E, Na ES, Los MF, Cheng PF, Kavalali ET, and Monteggia LM**. NMDA receptor blockade at rest triggers rapid behavioural antidepressant responses. *Nature* 475: 91-95, 2011.

8. **Awobuluyi M, Lipton SA, and Sucher NJ**. Translationally distinct populations of NMDA receptor subunit NR1 mRNA in the developing rat brain. *J Neurochem* 87: 1066-

1075, 2003.

9. **Aydar E, Palmer CP, Klyachko VA, and Jackson MB**. The sigma receptor as a ligand-regulated auxiliary potassium channel subunit. *Neuron* 34: 399-410, 2002.

10. **Balasuriya D, Stewart AP, Crottes D, Borgese F, Soriani O, and Edwardson JM**. The sigma-1 receptor binds to the Nav1.5 voltage-gated Na+ channel with four-fold symmetry. *J Biol Chem* 2012.

11. **Balasuriya D, Stewart AP, and Edwardson JM**. The sigma-1 Receptor Interacts Directly with GluN1 But Not GluN2A in the GluN1/GluN2A NMDA Receptor. *J Neurosci* 33: 18219-18224, 2013.

12. **Bard L, and Groc L**. Glutamate receptor dynamics and protein interaction: lessons from the NMDA receptor. *Mol Cell Neurosci* 48: 298-307, 2011.

13. **Bergeron R, de Montigny C, and Debonnel G**. Biphasic effects of sigma ligands on the neuronal response to N-methyl-D-aspartate. *Naunyn Schmiedebergs Arch Pharmacol* 351: 252-260, 1995.

14. **Bergeron R, de Montigny C, and Debonnel G**. Effect of short-term and long-term treatments with sigma ligands on the N-methyl-D-aspartate response in the CA3 region of the rat dorsal hippocampus. *Br J Pharmacol* 120: 1351-1359, 1997.

15. **Bergeron R, and Debonnel G**. Effects of low and high doses of selective sigma ligands: further evidence suggesting the existence of different subtypes of sigma receptors. *Psychopharmacology (Berl)* 129: 215-224, 1997.

16. **Bergeron R, Debonnel G, and De Montigny C**. Modification of the N-methyl-D-aspartate response by antidepressant sigma receptor ligands. *Eur J Pharmacol* 240: 319-323, 1993.

17. **Bermack JE, and Debonnel G**. The role of sigma receptors in depression. *J Pharmacol Sci* 97: 317-336, 2005.

18. **Blackstone CD, Moss SJ, Martin LJ, Levey AI, Price DL, and Huganir RL**. Biochemical characterization and localization of a non-N-methyl-D-aspartate glutamate receptor in rat brain. *J Neurochem* 58: 1118-1126, 1992.

19. **Bliss TV, and Lomo T**. Long-lasting potentiation of synaptic transmission in the dentate area of the anaesthetized rabbit following stimulation of the perforant path. *J Physiol* 232: 331-356, 1973.

20. **Bouchard P, and Quirion R**. [3H]1,3-di(2-tolyl)guanidine and [3H](+)pentazocine binding sites in the rat brain: autoradiographic visualization of the putative sigma1 and sigma2 receptor subtypes. *Neuroscience* 76: 467-477, 1997.

21. **Boyer PA, Skolnick P, and Fossom LH**. Chronic administration of imipramine and citalopram alters the expression of NMDA receptor subunit mRNAs in mouse brain. A quantitative in situ hybridization study. *J Mol Neurosci* 10: 219-233, 1998.

22. **Brenman JE, Christopherson KS, Craven SE, McGee AW, and Bredt DS**. Cloning and characterization of postsynaptic density 93, a nitric oxide synthase interacting protein. *J Neurosci* 16: 7407-7415, 1996.

23. **Brigman JL, Wright T, Talani G, Prasad-Mulcare S, Jinde S, Seabold GK, Mathur P, Davis MI, Bock R, Gustin RM, Colbran RJ, Alvarez VA, Nakazawa K, Delpire E, Lovinger DM, and Holmes A**. Loss of GluN2B-containing NMDA receptors in CA1 hippocampus and cortex impairs long-term depression, reduces dendritic spine density, and disrupts learning. *J Neurosci* 30: 4590-4600, 2010.

24. **Burchett SA, and Hicks TP**. The mysterious trace amines: protean neuromodulators

of synaptic transmission in mammalian brain. *Prog Neurobiol* 79: 223-246, 2006.

25. **Cagnotto A, Bastone A, and Mennini T**. [3H](+)-pentazocine binding to rat brain sigma 1 receptors. *Eur J Pharmacol* 266: 131-138, 1994.

26. **Carnally SM, Johannessen M, Henderson RM, Jackson MB, and Edwardson JM**. Demonstration of a direct interaction between sigma-1 receptors and acid-sensing ion channels. *BiophysJ* 98: 1182-1191, 2010.

27. **Chen L, Dai XN, and Sokabe M**. Chronic administration of dehydroepiandrosterone sulfate (DHEAS) primes for facilitated induction of long-term potentiation via sigma 1 (sigma1) receptor: optical imaging study in rat hippocampal slices. *Neuropharmacology* 50: 380-392, 2006.

28. **Chen WF, Chang H, Wong CS, Huang LT, Yang CH, and Yang SN**. Impaired expression of postsynaptic density proteins in the hippocampal CA1 region of rats following perinatal hypoxia. *Exp Neurol* 204: 400-410, 2007.

29. **Chen WS, and Bear MF**. Activity-dependent regulation of NR2B translation contributes to metaplasticity in mouse visual cortex. *Neuropharmacology* 52: 200-214, 2007.

30. **Chen Y, Hajipour AR, Sievert MK, Arbabian M, and Ruoho AE**. Characterization of the cocaine binding site on the sigma-1 receptor. *Biochemistry* 46: 3532-3542, 2007.

31. **Christopherson KS, Hillier BJ, Lim WA, and Bredt DS**. PSD-95 assembles a ternary complex with the N-methyl-D-aspartic acid receptor and a bivalent neuronal NO synthase PDZ domain. *J Biol Chem* 274: 27467-27473, 1999.

32. **Cobos EJ, Entrena JM, Nieto FR, Cendan CM, and Del Pozo E**. Pharmacology and therapeutic potential of sigma(1) receptor ligands. *Curr Neuropharmacol* 6: 344-366,

2008.

33. **Collingridge GL, and Bliss TV**. Memories of NMDA receptors and LTP. *Trends Neurosci* 18: 54-56, 1995.

34. **Crottes D, Guizouarn H, Martin P, Borgese F, and Soriani O**. The sigma-1 receptor: a regulator of cancer cell electrical plasticity? *Front Physiol* 4: 175, 2013.

35. **Crottes D, Martial S, Rapetti-Mauss R, Pisani DF, Loriol C, Pellissier B, Martin P, Chevet E, Borgese F, and Soriani O**. Sig1R protein regulates hERG channel expression through a post-translational mechanism in leukemic cells. *J Biol Chem* 286: 27947-27958, 2011.

36. **Debonnel G, Bergeron R, and de Montigny C**. Potentiation by dehydroepiandrosterone of the neuronal response to N-methyl-D-aspartate in the CA3 region of the rat dorsal hippocampus: an effect mediated via sigma receptors. *J Endocrinol* 150 Suppl: S33-42, 1996.

37. **Dhir A, and Kulkarni S**. Involvement of sigma (sigma1) receptors in modulating the anti-depressant effect of neurosteroids (dehydroepiandrosterone or pregnenolone) in mouse tail-suspension test. *J Psychopharmacol* 22: 691-696, 2008.

38. **Doucet MV, Harkin A, and Dev KK**. The PSD-95/nNOS complex: new drugs for depression? *Pharmacol Ther* 133: 218-229, 2012.

39. **Duman RS, and Aghajanian GK**. Synaptic dysfunction in depression: potential therapeutic targets. *Science* 338: 68-72, 2012.

40. **Dyck LE**. *Neuronal transport of trace amines: an overview*. Clifton, New Jersey: Humana Press, 1984.

41. **El-Husseini AE, Schnell E, Chetkovich DM, Nicoll RA, and Bredt DS**. PSD-95

involvement in maturation of excitatory synapses. *Science* 290: 1364-1368, 2000.

42. **Elias GM, and Nicoll RA**. Synaptic trafficking of glutamate receptors by MAGUK scaffolding proteins. *Trends Cell Biol* 17: 343-352, 2007.

43. **Fischer A, Sananbenesi F, Schrick C, Spiess J, and Radulovic J**. Distinct roles of hippocampal de novo protein synthesis and actin rearrangement in extinction of contextual fear. *J Neurosci* 24: 1962-1966, 2004.

44. **Fletcher EJ, Church J, Abdel-Hamid K, and MacDonald JF**. Blockade by sigma site ligands of N-methyl-D-aspartate-evoked responses in rat and mouse cultured hippocampal pyramidal neurones. *Br J Pharmacol* 116: 2791-2800, 1995.

45. **Fletcher EJ, Church J, Abdel-Hamid K, and MacDonald JF**. Selective reduction of N-methyl-D-aspartate-evoked responses by 1,3-di(2-tolyl)guanidine in mouse and rat cultured hippocampal pyramidal neurones. *Br J Pharmacol* 109: 1196-1205, 1993.

46. **Fontanilla D, Johannessen M, Hajipour AR, Cozzi NV, Jackson MB, and Ruoho AE**. The hallucinogen N,N-dimethyltryptamine (DMT) is an endogenous sigma-1 receptor regulator. *Science* 323: 934-937, 2009.

47. **Friedman HV, Bresler T, Garner CC, and Ziv NE**. Assembly of new individual excitatory synapses: time course and temporal order of synaptic molecule recruitment. *Neuron* 27: 57-69, 2000.

48. **Ganapathy ME, Prasad PD, Huang W, Seth P, Leibach FH, and Ganapathy V**. Molecular and ligand-binding characterization of the sigma-receptor in the Jurkat human T lymphocyte cell line. *J Pharmacol Exp Ther* 289: 251-260, 1999.

49. **Gardoni F, Mauceri D, Fiorentini C, Bellone C, Missale C, Cattabeni F, and Di Luca M**. CaMKII-dependent phosphorylation regulates SAP97/NR2A interaction. *J Biol*

Chem 278: 44745-44752, 2003.

50. **Gronier B, and Debonnel G**. Electrophysiological evidence for the implication of cholecystokinin in the modulation of the N-methyl-D-aspartate response by sigma ligands in the rat CA3 dorsal hippocampus. *Naunyn Schmiedebergs Arch Pharmacol* 353: 382-390, 1996.

51. **Guillaud L, Setou M, and Hirokawa N**. KIF17 dynamics and regulation of NR2B trafficking in hippocampal neurons. *J Neurosci* 23: 131-140, 2003.

52. **Guitart X, Codony X, and Monroy X**. Sigma receptors: biology and therapeutic potential. *Psychopharmacology (Berl)* 174: 301-319, 2004.

53. **Guitart X, Mendez R, Ovalle S, Andreu F, Carceller A, Farre AJ, and Zamanillo D**. Regulation of ionotropic glutamate receptor subunits in different rat brain areas by a preferential sigma(1) receptor ligand and potential atypical antipsychotic. *Neuropsychopharmacology* 23: 539-546, 2000.

54. **Hallett PJ, Collins TL, Standaert DG, and Dunah AW**. Biochemical fractionation of brain tissue for studies of receptor distribution and trafficking. *Curr Protoc Neurosci* Chapter 1: Unit 1 16, 2008.

55. **Han L, Campanucci VA, Cooke J, and Salter MW**. Identification of a single amino acid in GluN1 that is critical for glycine-primed internalization of NMDA receptors. *Mol Brain* 6: 36, 2013.

56. **Hanner M, Moebius FF, Flandorfer A, Knaus HG, Striessnig J, Kempner E, and Glossmann H**. Purification, molecular cloning, and expression of the mammalian sigma1-binding site. *Proc Natl Acad Sci U S A* 93: 8072-8077, 1996.

57. **Hardingham GE, and Bading H**. Synaptic versus extrasynaptic NMDA receptor

signalling: implications for neurodegenerative disorders. *Nat Rev Neurosci* 11: 682-696, 2010.

58. **Hardingham GE, Fukunaga Y, and Bading H**. Extrasynaptic NMDARs oppose synaptic NMDARs by triggering CREB shut-off and cell death pathways. *Nat Neurosci* 5: 405-414, 2002.

59. **Hayashi T, and Su TP**. Intracellular dynamics of sigma-1 receptors (sigma(1) binding sites) in NG108-15 cells. *J Pharmacol Exp Ther* 306: 726-733, 2003.

60. **Hayashi T, and Su TP**. The potential role of sigma-1 receptors in lipid transport and lipid raft reconstitution in the brain: implication for drug abuse. *Life Sci* 77: 1612-1624, 2005.

61. **Hayashi T, and Su TP**. Sigma-1 receptor chaperones at the ER-mitochondrion interface regulate Ca(2+) signaling and cell survival. *Cell* 131: 596-610, 2007.

62. **Hayashi T, and Su TP**. Sigma-1 receptor ligands: potential in the treatment of neuropsychiatric disorders. *CNS Drugs* 18: 269-284, 2004.

63. **Hayashi T, and Su TP**. Sigma-1 receptors (sigma(1) binding sites) form raft-like microdomains and target lipid droplets on the endoplasmic reticulum: roles in endoplasmic reticulum lipid compartmentalization and export. *J Pharmacol Exp Ther* 306: 718-725, 2003.

64. **Hayashi T, and Su TP**. Sigma-1 receptors at galactosylceramide-enriched lipid microdomains regulate oligodendrocyte differentiation. *Proc Natl Acad Sci U S A* 101: 14949-14954, 2004.

65. **Hayashi T, Tsai SY, Mori T, Fujimoto M, and Su TP**. Targeting ligand-operated chaperone sigma-1 receptors in the treatment of neuropsychiatric disorders. *Expert Opin*

Ther Targets 15: 557-577, 2011.

66. **Hedskog L, Pinho CM, Filadi R, Ronnback A, Hertwig L, Wiehager B, Larssen P, Gellhaar S, Sandebring A, Westerlund M, Graff C, Winblad B, Galter D, Behbahani H, Pizzo P, Glaser E, and Ankarcrona M**. Modulation of the endoplasmic reticulum-mitochondria interface in Alzheimer's disease and related models. *Proc Natl Acad Sci U S A* 110: 7916-7921, 2013.

67. **Helms JB, and Zurzolo C**. Lipids as targeting signals: lipid rafts and intracellular trafficking. *Traffic* 5: 247-254, 2004.

68. **Herrera Y, Katnik C, Rodriguez JD, Hall AA, Willing A, Pennypacker KR, and Cuevas J**. Sigma-1 receptor modulation of acid-sensing ion channel a (ASIC1a) and ASIC1a-induced Ca2+ influx in rat cortical neurons. *JPharmacolExpTher* 327: 491-502, 2008.

69. **Hollmann M, and Heinemann S**. Cloned glutamate receptors. *Annu Rev Neurosci* 17: 31-108, 1994.

70. **Huh KH, and Wenthold RJ**. Turnover analysis of glutamate receptors identifies a rapidly degraded pool of the N-methyl-D-aspartate receptor subunit, NR1, in cultured cerebellar granule cells. *J Biol Chem* 274: 151-157, 1999.

71. **Inoue A, Sugita S, Shoji H, Ichimoto H, Hide I, and Nakata Y**. Repeated haloperidol treatment decreases sigma(1) receptor binding but does not affect its mRNA levels in the guinea pig or rat brain. *Eur J Pharmacol* 401: 307-316, 2000.

72. **Ishiguro H, Ohtsuki T, Toru M, Itokawa M, Aoki J, Shibuya H, Kurumaji A, Okubo Y, Iwawaki A, Ota K, Shimizu H, Hamaguchi H, and Arinami T**. Association between polymorphisms in the type 1 sigma receptor gene and schizophrenia. *Neurosci Lett*

257: 45-48, 1998.

73. **Itzhak Y, and Alerhand S**. Differential regulation of sigma and PCP receptors after chronic administration of haloperidol and phencyclidine in mice. *FASEB J* 3: 1868-1872, 1989.

74. **Itzhak Y, and Stein I**. Regulation of sigma receptors and responsiveness to guanine nucleotides following repeated exposure of rats to haloperidol: further evidence for multiple sigma binding sites. *Brain Res* 566: 166-172, 1991.

75. **Itzhak Y, and Stein I**. Sigma binding sites in the brain; an emerging concept for multiple sites and their relevance for psychiatric disorders. *Life Sci* 47: 1073-1081, 1990.

76. **Iyengar S, Dilworth VM, Mick SJ, Contreras PC, Monahan JB, Rao TS, and Wood PL**. Sigma receptors modulate both A9 and A10 dopaminergic neurons in the rat brain: functional interaction with NMDA receptors. *Brain Res* 524: 322-326, 1990.

77. **Iyengar S, Mick S, Dilworth V, Michel J, Rao TS, Farah JM, and Wood PL**. Sigma receptors modulate the hypothalamic-pituitary-adrenal (HPA) axis centrally: evidence for a functional interaction with NMDA receptors, in vivo. *Neuropharmacology* 29: 299-303, 1990.

78. **Javitt DC**. Twenty-five years of glutamate in schizophrenia: are we there yet? *Schizophr Bull* 38: 911-913, 2012.

79. **Jeyifous O, Waites CL, Specht CG, Fujisawa S, Schubert M, Lin EI, Marshall J, Aoki C, de Silva T, Montgomery JM, Garner CC, and Green WN**. SAP97 and CASK mediate sorting of NMDA receptors through a previously unknown secretory pathway. *Nat Neurosci* 12: 1011-1019, 2009.

80. **Jha S, and Komar AA**. Birth, life and death of nascent polypeptide chains.

Biotechnol J 6: 623-640, 2011.

81. **Jiang G, Mysona B, Dun Y, Gnana-Prakasam JP, Pabla N, Li W, Dong Z, Ganapathy V, and Smith SB**. Expression, subcellular localization, and regulation of sigma receptor in retinal muller cells. *Invest Ophthalmol Vis Sci* 47: 5576-5582, 2006.

82. **Johannessen M, Ramachandran S, Riemer L, Ramos-Serrano A, Ruoho AE, and Jackson MB**. Voltage-gated sodium channel modulation by sigma-receptors in cardiac myocytes and heterologous systems. *AmJPhysiol Cell Physiol* 296: C1049-C1057, 2009.

83. **Katz JL, Su TP, Hiranita T, Hayashi T, Tanda G, Kopajtic T, and Tsai SY**. A Role for Sigma Receptors in Stimulant Self Administration and Addiction. *Pharmaceuticals (Basel)* 4: 880-914, 2011.

84. **Kekuda R, Prasad PD, Fei YJ, Leibach FH, and Ganapathy V**. Cloning and functional expression of the human type 1 sigma receptor (hSigmaR1). *Biochem Biophys Res Commun* 229: 553-558, 1996.

85. **Kim E, Cho KO, Rothschild A, and Sheng M**. Heteromultimerization and NMDA receptor-clustering activity of Chapsyn-110, a member of the PSD-95 family of proteins. *Neuron* 17: 103-113, 1996.

86. **Kim HW, Kwon YB, Roh DH, Yoon SY, Han HJ, Kim KW, Beitz AJ, and Lee JH**. Intrathecal treatment with sigma1 receptor antagonists reduces formalin-induced phosphorylation of NMDA receptor subunit 1 and the second phase of formalin test in mice. *Br J Pharmacol* 148: 490-498, 2006.

87. **Kim HW, Roh DH, Yoon SY, Seo HS, Kwon YB, Han HJ, Kim KW, Beitz AJ, and Lee JH**. Activation of the spinal sigma-1 receptor enhances NMDA-induced pain via PKC- and PKA-dependent phosphorylation of the NR1 subunit in mice. *BrJPharmacol* 154:

1125-1134, 2008.

88. **Kinoshita M, Matsuoka Y, Suzuki T, Mirrielees J, and Yang J**. Sigma-1 receptor alters the kinetics of Kv1.3 voltage gated potassium channels but not the sensitivity to receptor ligands. *Brain Res* 1452: 1-9, 2012.

89. **Kiraly DD, Lemtiri-Chlieh F, Levine ES, Mains RE, and Eipper BA**. Kalirin binds the NR2B subunit of the NMDA receptor, altering its synaptic localization and function. *J Neurosci* 31: 12554-12565, 2011.

90. **Kizu A, Yoshida Y, and Miyagishi T**. Rat cortical sigma receptors differentially regulated by pentazocine and haloperidol. *J Neural Transm Gen Sect* 83: 149-153, 1991.

91. **Kornau HC, Schenker LT, Kennedy MB, and Seeburg PH**. Domain interaction between NMDA receptor subunits and the postsynaptic density protein PSD-95. *Science* 269: 1737-1740, 1995.

92. **Kourrich S, Hayashi T, Chuang JY, Tsai SY, Su TP, and Bonci A**. Dynamic Interaction between Sigma-1 Receptor and Kv1.2 Shapes Neuronal and Behavioral Responses to Cocaine. *Cell* 152: 236-247, 2013.

93. **Kourrich S, Su TP, Fujimoto M, and Bonci A**. The sigma-1 receptor: roles in neuronal plasticity and disease. *Trends Neurosci* 35: 762-771, 2012.

94. **Kristiansen LV, Huerta I, Beneyto M, and Meador-Woodruff JH**. NMDA receptors and schizophrenia. *Curr Opin Pharmacol* 7: 48-55, 2007.

95. **Kulkarni SK, and Dhir A**. On the mechanism of antidepressant-like action of berberine chloride. *Eur J Pharmacol* 589: 163-172, 2008.

96. **Langa F, Codony X, Tovar V, Lavado A, Gimenez E, Cozar P, Cantero M, Dordal A, Hernandez E, Perez R, Monroy X, Zamanillo D, Guitart X, and Montoliu L**.

Generation and phenotypic analysis of sigma receptor type I (sigma 1) knockout mice. *Eur J Neurosci* 18: 2188-2196, 2003.

97. **Lau CG, and Zukin RS**. NMDA receptor trafficking in synaptic plasticity and neuropsychiatric disorders. *Nat Rev Neurosci* 8: 413-426, 2007.

98. **Lee HB, and Blaufox MD**. Blood volume in the rat. *J Nucl Med* 26: 72-76, 1985.

99. **Lei S, Czerwinska E, Czerwinski W, Walsh MP, and MacDonald JF**. Regulation of NMDA receptor activity by F-actin and myosin light chain kinase. *J Neurosci* 21: 8464-8472, 2001.

100. **Leitner ML, Hohmann AG, Patrick SL, and Walker JM**. Regional variation in the ratio of sigma 1 to sigma 2 binding in rat brain. *Eur J Pharmacol* 259: 65-69, 1994.

101. **Li Z, Zhou R, Cui S, Xie G, Cai W, Sokabe M, and Chen L**. Dehydroepiandrosterone sulfate prevents ischemia-induced impairment of long-term potentiation in rat hippocampal CA1 by up-regulating tyrosine phosphorylation of NMDA receptor. *Neuropharmacology* 51: 958-966, 2006.

102. **Liang X, and Wang RY**. Biphasic modulatory action of the selective sigma receptor ligand SR 31742A on N-methyl-D-aspartate-induced neuronal responses in the frontal cortex. *Brain Res* 807: 208-213, 1998.

103. **Lipton SA, and Rosenberg PA**. Excitatory amino acids as a final common pathway for neurologic disorders. *N Engl J Med* 330: 613-622, 1994.

104. **Liu L, Wong TP, Pozza MF, Lingenhoehl K, Wang Y, Sheng M, Auberson YP, and Wang YT**. Role of NMDA receptor subtypes in governing the direction of hippocampal synaptic plasticity. *Science* 304: 1021-1024, 2004.

105. **Lockhart BP, Soulard P, Benicourt C, Privat A, and Junien JL**. Distinct

neuroprotective profiles for sigma ligands against N-methyl-D-aspartate (NMDA), and hypoxia-mediated neurotoxicity in neuronal culture toxicity studies. *Brain Res* 675: 110-120, 1995.

106. **Machado-Vieira R, Ibrahim L, Henter ID, and Zarate CA, Jr.** Novel glutamatergic agents for major depressive disorder and bipolar disorder. *Pharmacol Biochem Behav* 100: 678-687, 2012.

107. **Malenka RC, and Bear MF**. LTP and LTD: an embarrassment of riches. *Neuron* 44: 5-21, 2004.

108. **Marquis KL, Paquette NC, Gussio RP, and Moreton JE**. Comparative electroencephalographic and behavioral effects of phencyclidine, (+)-SKF-10,047 and MK-801 in rats. *J Pharmacol Exp Ther* 251: 1104-1112, 1989.

109. **Martin WR, Eades CG, Thompson JA, Huppler RE, and Gilbert PE**. The effects of morphine- and nalorphine- like drugs in the nondependent and morphine-dependent chronic spinal dog. *J Pharmacol Exp Ther* 197: 517-532, 1976.

110. **Martina M, Turcotte ME, Halman S, and Bergeron R**. The sigma-1 receptor modulates NMDA receptor synaptic transmission and plasticity via SK channels in rat hippocampus. *J Physiol* 578: 143-157, 2007.

111. **Matsumoto RR, Bowen WD, Tom MA, Vo VN, Truong DD, and De Costa BR**. Characterization of two novel sigma receptor ligands: antidystonic effects in rats suggest sigma receptor antagonism. *Eur J Pharmacol* 280: 301-310, 1995.

112. **Mauceri D, Gardoni F, Marcello E, and Di Luca M**. Dual role of CaMKII-dependent SAP97 phosphorylation in mediating trafficking and insertion of NMDA receptor subunit NR2A. *J Neurochem* 100: 1032-1046, 2007.

113. **Maurice T**. Beneficial effect of the sigma(1) receptor agonist PRE-084 against the spatial learning deficits in aged rats. *Eur J Pharmacol* 431: 223-227, 2001.

114. **Maurice T, Hiramatsu M, Itoh J, Kameyama T, Hasegawa T, and Nabeshima T**. Behavioral evidence for a modulating role of sigma ligands in memory processes. I. Attenuation of dizocilpine (MK-801)-induced amnesia. *Brain Res* 647: 44-56, 1994.

115. **Maurice T, Hiramatsu M, Itoh J, Kameyama T, Hasegawa T, and Nabeshima T**. Low dose of 1,3-di(2-tolyl)guanidine (DTG) attenuates MK-801-induced spatial working memory impairment in mice. *Psychopharmacology (Berl)* 114: 520-522, 1994.

116. **Maurice T, Junien JL, and Privat A**. Dehydroepiandrosterone sulfate attenuates dizocilpine-induced learning impairment in mice via sigma 1-receptors. *Behav Brain Res* 83: 159-164, 1997.

117. **Maurice T, and Lockhart BP**. Neuroprotective and anti-amnesic potentials of sigma (sigma) receptor ligands. *Prog Neuropsychopharmacol Biol Psychiatry* 21: 69-102, 1997.

118. **Maurice T, and Privat A**. SA4503, a novel cognitive enhancer with sigma1 receptor agonist properties, facilitates NMDA receptor-dependent learning in mice. *Eur J Pharmacol* 328: 9-18, 1997.

119. **Maurice T, and Su TP**. The pharmacology of sigma-1 receptors. *Pharmacol Ther* 124: 195-206, 2009.

120. **Maurice T, Su TP, Parish DW, Nabeshima T, and Privat A**. PRE-084, a sigma selective PCP derivative, attenuates MK-801-induced impairment of learning in mice. *Pharmacol Biochem Behav* 49: 859-869, 1994.

121. **Mavlyutov TA, and Ruoho AE**. Ligand-dependent localization and intracellular

stability of sigma-1 receptors in CHO-K1 cells. *J Mol Signal* 2: 8, 2007.

122. **McCann DJ, Weissman AD, and Su TP**. Sigma-1 and sigma-2 sites in rat brain: comparison of regional, ontogenetic, and subcellular patterns. *Synapse* 17: 182-189, 1994.

123. **McKinney RA**. Excitatory amino acid involvement in dendritic spine formation, maintenance and remodelling. *J Physiol* 588: 107-116, 2010.

124. **Meador-Woodruff JH, Clinton SM, Beneyto M, and McCullumsmith RE**. Molecular abnormalities of the glutamate synapse in the thalamus in schizophrenia. *Ann N Y Acad Sci* 1003: 75-93, 2003.

125. **Meddows E, Le Bourdelles B, Grimwood S, Wafford K, Sandhu S, Whiting P, and McIlhinney RA**. Identification of molecular determinants that are important in the assembly of N-methyl-D-aspartate receptors. *J Biol Chem* 276: 18795-18803, 2001.

126. **Medzihradsky F, and Ahmad K**. The uptake of pentazocine into brain. *Life Sci I* 10: 711-720, 1971.

127. **Mei J, and Pasternak GW**. Molecular cloning and pharmacological characterization of the rat sigma1 receptor. *Biochem Pharmacol* 62: 349-355, 2001.

128. **Meunier J, and Hayashi T**. Sigma-1 receptors regulate Bcl-2 expression by reactive oxygen species-dependent transcriptional regulation of nuclear factor kappaB. *J Pharmacol Exp Ther* 332: 388-397, 2010.

129. **Migaud M, Charlesworth P, Dempster M, Webster LC, Watabe AM, Makhinson M, He Y, Ramsay MF, Morris RG, Morrison JH, O'Dell TJ, and Grant SG**. Enhanced long-term potentiation and impaired learning in mice with mutant postsynaptic density-95 protein. *Nature* 396: 433-439, 1998.

130. **Miki Y, Mori F, Kon T, Tanji K, Toyoshima Y, Yoshida M, Sasaki H, Kakita A,**

Takahashi H, and Wakabayashi K. Accumulation of the sigma-1 receptor is common to neuronal nuclear inclusions in various neurodegenerative diseases. *Neuropathology* 2013.

131. **Moebius FF, Striessnig J, and Glossmann H**. The mysteries of sigma receptors: new family members reveal a role in cholesterol synthesis. *Trends Pharmacol Sci* 18: 67-70, 1997.

132. **Monnet FP, Debonnel G, Bergeron R, Gronier B, and de Montigny C**. The effects of sigma ligands and of neuropeptide Y on N-methyl-D-aspartate-induced neuronal activation of CA3 dorsal hippocampus neurones are differentially affected by pertussin toxin. *Br J Pharmacol* 112: 709-715, 1994.

133. **Monnet FP, Debonnel G, Junien JL, and De Montigny C**. N-methyl-D-aspartate-induced neuronal activation is selectively modulated by sigma receptors. *Eur J Pharmacol* 179: 441-445, 1990.

134. **Morin-Surun MP, Collin T, Denavit-Saubie M, Baulieu EE, and Monnet FP**. Intracellular sigma1 receptor modulates phospholipase C and protein kinase C activities in the brainstem. *Proc Natl Acad Sci U S A* 96: 8196-8199, 1999.

135. **Morris RG, Anderson E, Lynch GS, and Baudry M**. Selective impairment of learning and blockade of long-term potentiation by an N-methyl-D-aspartate receptor antagonist, AP5. *Nature* 319: 774-776, 1986.

136. **Muller BM, Kistner U, Kindler S, Chung WJ, Kuhlendahl S, Fenster SD, Lau LF, Veh RW, Huganir RL, Gundelfinger ED, and Garner CC**. SAP102, a novel postsynaptic protein that interacts with NMDA receptor complexes in vivo. *Neuron* 17: 255-265, 1996.

137. **Musazzi L, Treccani G, Mallei A, and Popoli M**. The Action of Antidepressants on

the Glutamate System: Regulation of Glutamate Release and Glutamate Receptors. *Biol Psychiatry* 2012.

138. **Niethammer M, Kim E, and Sheng M**. Interaction between the C terminus of NMDA receptor subunits and multiple members of the PSD-95 family of membrane-associated guanylate kinases. *J Neurosci* 16: 2157-2163, 1996.

139. **Nishimura T, Ishima T, Iyo M, and Hashimoto K**. Potentiation of nerve growth factor-induced neurite outgrowth by fluvoxamine: role of sigma-1 receptors, IP3 receptors and cellular signaling pathways. *PLoS One* 3: e2558, 2008.

140. **Nowak G, Legutko B, Skolnick P, and Popik P**. Adaptation of cortical NMDA receptors by chronic treatment with specific serotonin reuptake inhibitors. *Eur J Pharmacol* 342: 367-370, 1998.

141. **Ohi K, Hashimoto R, Yasuda Y, Fukumoto M, Yamamori H, Umeda-Yano S, Kamino K, Ikezawa K, Azechi M, Iwase M, Kazui H, Kasai K, and Takeda M**. The SIGMAR1 gene is associated with a risk of schizophrenia and activation of the prefrontal cortex. *Prog Neuropsychopharmacol Biol Psychiatry* 35: 1309-1315, 2011.

142. **Ohmori O, Shinkai T, Suzuki T, Okano C, Kojima H, Terao T, and Nakamura J**. Polymorphisms of the sigma(1) receptor gene in schizophrenia: An association study. *Am J Med Genet* 96: 118-122, 2000.

143. **Ohno M, and Watanabe S**. Intrahippocampal administration of (+)-SKF 10,047, a sigma ligand, reverses MK-801-induced impairment of working memory in rats. *Brain Res* 684: 237-242, 1995.

144. **Pabba M**. The essential roles of protein-protein interaction in sigma-1 receptor functions. *Front Cell Neurosci* 7: 50, 2013.

145. **Pabba M, Hristova E, and Biscaro D**. The elusive roles of NMDA receptor amino-terminal domains. *J Physiol* 590: 5561-5562, 2012.

146. **Pal A, Chu UB, Ramachandran S, Grawoig D, Guo LW, Hajipour AR, and Ruoho AE**. Juxtaposition of the steroid binding domain-like I and II regions constitutes a ligand binding site in the sigma-1 receptor. *J Biol Chem* 283: 19646-19656, 2008.

147. **Pal A, Hajipour AR, Fontanilla D, Ramachandran S, Chu UB, Mavlyutov T, and Ruoho AE**. Identification of regions of the sigma-1 receptor ligand binding site using a novel photoprobe. *Mol Pharmacol* 72: 921-933, 2007.

148. **Palacios G, Muro A, Vela JM, Molina-Holgado E, Guitart X, Ovalle S, and Zamanillo D**. Immunohistochemical localization of the sigma1-receptor in oligodendrocytes in the rat central nervous system. *Brain Res* 961: 92-99, 2003.

149. **Pan YX, Mei J, Xu J, Wan BL, Zuckerman A, and Pasternak GW**. Cloning and characterization of a mouse sigma1 receptor. *J Neurochem* 70: 2279-2285, 1998.

150. **Paoletti P**. Molecular basis of NMDA receptor functional diversity. *Eur J Neurosci* 33: 1351-1365, 2011.

151. **Paoletti P, Bellone C, and Zhou Q**. NMDA receptor subunit diversity: impact on receptor properties, synaptic plasticity and disease. *Nat Rev Neurosci* 14: 383-400, 2013.

152. **Paul IA, Nowak G, Layer RT, Popik P, and Skolnick P**. Adaptation of the N-methyl-D-aspartate receptor complex following chronic antidepressant treatments. *J Pharmacol Exp Ther* 269: 95-102, 1994.

153. **Petralia RS, Al-Hallaq RA, and Wenthold RJ**. Trafficking and Targeting of NMDA Receptors. 2009.

154. **Pfeiffer BE, and Huber KM**. Current advances in local protein synthesis and

synaptic plasticity. *J Neurosci* 26: 7147-7150, 2006.

155. **Phan VL, Urani A, Sandillon F, Privat A, and Maurice T**. Preserved sigma1 (sigma1) receptor expression and behavioral efficacy in the aged C57BL/6 mouse. *Neurobiol Aging* 24: 865-881, 2003.

156. **Pollak DD, Herkner K, Hoeger H, and Lubec G**. Behavioral testing upregulates pCaMKII, BDNF, PSD-95 and egr-1 in hippocampus of FVB/N mice. *Behav Brain Res* 163: 128-135, 2005.

157. **Prasad PD, Li HW, Fei YJ, Ganapathy ME, Fujita T, Plumley LH, Yang-Feng TL, Leibach FH, and Ganapathy V**. Exon-intron structure, analysis of promoter region, and chromosomal localization of the human type 1 sigma receptor gene. *J Neurochem* 70: 443-451, 1998.

158. **Prybylowski K, Chang K, Sans N, Kan L, Vicini S, and Wenthold RJ**. The synaptic localization of NR2B-containing NMDA receptors is controlled by interactions with PDZ proteins and AP-2. *Neuron* 47: 845-857, 2005.

159. **Prybylowski K, Fu Z, Losi G, Hawkins LM, Luo J, Chang K, Wenthold RJ, and Vicini S**. Relationship between availability of NMDA receptor subunits and their expression at the synapse. *J Neurosci* 22: 8902-8910, 2002.

160. **Prybylowski K, and Wenthold RJ**. N-Methyl-D-aspartate receptors: subunit assembly and trafficking to the synapse. *J Biol Chem* 279: 9673-9676, 2004.

161. **Quirion R, Bowen WD, Itzhak Y, Junien JL, Musacchio JM, Rothman RB, Su TP, Tam SW, and Taylor DP**. A proposal for the classification of sigma binding sites. *Trends Pharmacol Sci* 13: 85-86, 1992.

162. **Rani CS, Qiang M, and Ticku MK**. Potential role of cAMP response element-

binding protein in ethanol-induced N-methyl-D-aspartate receptor 2B subunit gene transcription in fetal mouse cortical cells. *Mol Pharmacol* 67: 2126-2136, 2005.

163. **Roberts EB, and Ramoa AS**. Enhanced NR2A subunit expression and decreased NMDA receptor decay time at the onset of ocular dominance plasticity in the ferret. *J Neurophysiol* 81: 2587-2591, 1999.

164. **Roche KW, Standley S, McCallum J, Dune Ly C, Ehlers MD, and Wenthold RJ**. Molecular determinants of NMDA receptor internalization. *Nat Neurosci* 4: 794-802, 2001.

165. **Roh DH, Choi SR, Yoon SY, Kang SY, Moon JY, Kwon SG, Han HJ, Beitz AJ, and Lee JH**. Spinal neuronal NOS activation mediates sigma-1 receptor-induced mechanical and thermal hypersensitivity in mice: involvement of PKC-dependent GluN1 phosphorylation. *Br J Pharmacol* 163: 1707-1720, 2011.

166. **Roh DH, Kim HW, Yoon SY, Seo HS, Kwon YB, Kim KW, Han HJ, Beitz AJ, Na HS, and Lee JH**. Intrathecal injection of the sigma(1) receptor antagonist BD1047 blocks both mechanical allodynia and increases in spinal NR1 expression during the induction phase of rodent neuropathic pain. *Anesthesiology* 109: 879-889, 2008.

167. **Roh DH, Yoon SY, Seo HS, Kang SY, Moon JY, Song S, Beitz AJ, and Lee JH**. Sigma-1 receptor-induced increase in murine spinal NR1 phosphorylation is mediated by the PKCalpha and epsilon, but not the PKCzeta, isoforms. *Neurosci Lett* 477: 95-99, 2010.

168. **Ruoho AE, Chu UB, Ramachandran S, Fontanilla D, Mavlyutov T, and Hajipour AR**. The ligand binding region of the sigma-1 receptor: studies utilizing photoaffinity probes, sphingosine and N-alkylamines. *Curr Pharm Des* 18: 920-929, 2012.

169. **Ruscher K, Shamloo M, Rickhag M, Ladunga I, Soriano L, Gisselsson L, Toresson H, Ruslim-Litrus L, Oksenberg D, Urfer R, Johansson BB, Nikolich K, and**

Wieloch T. The sigma-1 receptor enhances brain plasticity and functional recovery after experimental stroke. *Brain* 134: 732-746, 2011.

170. **Sabeti J, Nelson TE, Purdy RH, and Gruol DL**. Steroid pregnenolone sulfate enhances NMDA-receptor-independent long-term potentiation at hippocampal CA1 synapses: role for L-type calcium channels and sigma-receptors. *Hippocampus* 17: 349-369, 2007.

171. **Sala C, Cambianica I, and Rossi F**. Molecular mechanisms of dendritic spine development and maintenance. *Acta Neurobiol Exp (Wars)* 68: 289-304, 2008.

172. **Sans N, Prybylowski K, Petralia RS, Chang K, Wang YX, Racca C, Vicini S, and Wenthold RJ**. NMDA receptor trafficking through an interaction between PDZ proteins and the exocyst complex. *Nat Cell Biol* 5: 520-530, 2003.

173. **Sans N, Wang PY, Du Q, Petralia RS, Wang YX, Nakka S, Blumer JB, Macara IG, and Wenthold RJ**. mPins modulates PSD-95 and SAP102 trafficking and influences NMDA receptor surface expression. *Nat Cell Biol* 7: 1179-1190, 2005.

174. **Sanz-Clemente A, Matta JA, Isaac JT, and Roche KW**. Casein kinase 2 regulates the NR2 subunit composition of synaptic NMDA receptors. *Neuron* 67: 984-996, 2010.

175. **Satoh F, Miyatake R, Furukawa A, and Suwaki H**. Lack of association between sigma receptor gene variants and schizophrenia. *Psychiatry Clin Neurosci* 58: 359-363, 2004.

176. **Schwarz S, Pohl P, and Zhou GZ**. Steroid binding at sigma-"opioid" receptors. *Science* 246: 1635-1638, 1989.

177. **Seth P, Fei YJ, Li HW, Huang W, Leibach FH, and Ganapathy V**. Cloning and functional characterization of a sigma receptor from rat brain. *J Neurochem* 70: 922-931,

1998.

178. **Seth P, Ganapathy ME, Conway SJ, Bridges CD, Smith SB, Casellas P, and Ganapathy V**. Expression pattern of the type 1 sigma receptor in the brain and identity of critical anionic amino acid residues in the ligand-binding domain of the receptor. *Biochim Biophys Acta* 1540: 59-67, 2001.

179. **Seth P, Leibach FH, and Ganapathy V**. Cloning and structural analysis of the cDNA and the gene encoding the murine type 1 sigma receptor. *Biochem Biophys Res Commun* 241: 535-540, 1997.

180. **Setou M, Nakagawa T, Seog DH, and Hirokawa N**. Kinesin superfamily motor protein KIF17 and mLin-10 in NMDA receptor-containing vesicle transport. *Science* 288: 1796-1802, 2000.

181. **Sharp JW**. Phencyclidine (PCP) acts at sigma sites to induce c-fos gene expression. *Brain Res* 758: 51-58, 1997.

182. **Shioda N, Ishikawa K, Tagashira H, Ishizuka T, Yawo H, and Fukunaga K**. Expression of a truncated form of the endoplasmic reticulum chaperone protein, sigma1 receptor, promotes mitochondrial energy depletion and apoptosis. *J Biol Chem* 287: 23318-23331, 2012.

183. **Standley S, Petralia RS, Gravell M, Hamilton R, Wang YX, Schubert M, and Wenthold RJ**. Trafficking of the NMDAR2B receptor subunit distal cytoplasmic tail from endoplasmic reticulum to the synapse. *PLoS One* 7: e39585, 2012.

184. **Steiner P, Higley MJ, Xu W, Czervionke BL, Malenka RC, and Sabatini BL**. Destabilization of the postsynaptic density by PSD-95 serine 73 phosphorylation inhibits spine growth and synaptic plasticity. *Neuron* 60: 788-802, 2008.

185. **Stephenson FA, Cousins SL, and Kenny AV**. Assembly and forward trafficking of NMDA receptors (Review). *Mol Membr Biol* 25: 311-320, 2008.

186. **Su TP**. Evidence for sigma opioid receptor: binding of [3H]SKF-10047 to etorphine-inaccessible sites in guinea-pig brain. *J Pharmacol Exp Ther* 223: 284-290, 1982.

187. **Su TP**. Sigma receptors. Putative links between nervous, endocrine and immune systems. *Eur J Biochem* 200: 633-642, 1991.

188. **Su TP, Hayashi T, Maurice T, Buch S, and Ruoho AE**. The sigma-1 receptor chaperone as an inter-organelle signaling modulator. *Trends Pharmacol Sci* 31: 557-566, 2010.

189. **Su TP, Hayashi T, and Vaupel DB**. When the endogenous hallucinogenic trace amine N,N-dimethyltryptamine meets the sigma-1 receptor. *Sci Signal* 2: pe12, 2009.

190. **Su TP, London ED, and Jaffe JH**. Steroid binding at sigma receptors suggests a link between endocrine, nervous, and immune systems. *Science* 240: 219-221, 1988.

191. **Suh YH, Terashima A, Petralia RS, Wenthold RJ, Isaac JT, Roche KW, and Roche PA**. A neuronal role for SNAP-23 in postsynaptic glutamate receptor trafficking. *Nat Neurosci* 13: 338-343, 2010.

192. **Takebayashi M, Hayashi T, and Su TP**. Nerve growth factor-induced neurite sprouting in PC12 cells involves sigma-1 receptors: implications for antidepressants. *J Pharmacol Exp Ther* 303: 1227-1237, 2002.

193. **Takebayashi M, Hayashi T, and Su TP**. Sigma-1 receptors potentiate epidermal growth factor signaling towards neuritogenesis in PC12 cells: potential relation to lipid raft reconstitution. *Synapse* 53: 90-103, 2004.

194. **Takizawa R, Hashimoto K, Tochigi M, Kawakubo Y, Marumo K, Sasaki T,**

Fukuda M, and Kasai K. Association between sigma-1 receptor gene polymorphism and prefrontal hemodynamic response induced by cognitive activation in schizophrenia. *Prog Neuropsychopharmacol Biol Psychiatry* 33: 491-498, 2009.

195. **Tam SW**. Naloxone-inaccessible sigma receptor in rat central nervous system. *Proc Natl Acad Sci U S A* 80: 6703-6707, 1983.

196. **Tang YP, Shimizu E, Dube GR, Rampon C, Kerchner GA, Zhuo M, Liu G, and Tsien JZ**. Genetic enhancement of learning and memory in mice. *Nature* 401: 63-69, 1999.

197. **Tchedre KT, Huang RQ, Dibas A, Krishnamoorthy RR, Dillon GH, and Yorio T**. Sigma-1 receptor regulation of voltage-gated calcium channels involves a direct interaction. *Invest Ophthalmol Vis Sci* 49: 4993-5002, 2008.

198. **Tchedre KT, and Yorio T**. sigma-1 receptors protect RGC-5 cells from apoptosis by regulating intracellular calcium, Bax levels, and caspase-3 activation. *Invest Ophthalmol Vis Sci* 49: 2577-2588, 2008.

199. **Tolias KF, Bikoff JB, Burette A, Paradis S, Harrar D, Tavazoie S, Weinberg RJ, and Greenberg ME**. The Rac1-GEF Tiam1 couples the NMDA receptor to the activity-dependent development of dendritic arbors and spines. *Neuron* 45: 525-538, 2005.

200. **Tovar KR, and Westbrook GL**. The incorporation of NMDA receptors with a distinct subunit composition at nascent hippocampal synapses in vitro. *J Neurosci* 19: 4180-4188, 1999.

201. **Traynelis SF, Wollmuth LP, McBain CJ, Menniti FS, Vance KM, Ogden KK, Hansen KB, Yuan H, Myers SJ, and Dingledine R**. Glutamate receptor ion channels: structure, regulation, and function. *Pharmacol Rev* 62: 405-496, 2010.

202. **Trullas R, and Skolnick P**. Functional antagonists at the NMDA receptor complex

exhibit antidepressant actions. *Eur J Pharmacol* 185: 1-10, 1990.

203. **Tsai SY, Hayashi T, Harvey BK, Wang Y, Wu WW, Shen RF, Zhang Y, Becker KG, Hoffer BJ, and Su TP**. Sigma-1 receptors regulate hippocampal dendritic spine formation via a free radical-sensitive mechanism involving Rac1xGTP pathway. *Proc Natl Acad Sci U S A* 106: 22468-22473, 2009.

204. **Tuerxun T, Numakawa T, Adachi N, Kumamaru E, Kitazawa H, Kudo M, and Kunugi H**. SA4503, a sigma-1 receptor agonist, prevents cultured cortical neurons from oxidative stress-induced cell death via suppression of MAPK pathway activation and glutamate receptor expression. *Neurosci Lett* 469: 303-308, 2010.

205. **Uchida N, Ujike H, Nakata K, Takaki M, Nomura A, Katsu T, Tanaka Y, Imamura T, Sakai A, and Kuroda S**. No association between the sigma receptor type 1 gene and schizophrenia: results of analysis and meta-analysis of case-control studies. *BMC Psychiatry* 3: 13, 2003.

206. **Uchida N, Ujike H, Tanaka Y, Sakai A, Yamamoto M, Fujisawa Y, Kanzaki A, and Kuroda S**. A variant of the sigma receptor type-1 gene is a protective factor for Alzheimer disease. *Am J Geriatr Psychiatry* 13: 1062-1066, 2005.

207. **Vastagh C, Gardoni F, Bagetta V, Stanic J, Zianni E, Giampa C, Picconi B, Calabresi P, and Di Luca M**. N-methyl-D-aspartate (NMDA) receptor composition modulates dendritic spine morphology in striatal medium spiny neurons. *J Biol Chem* 287: 18103-18114, 2012.

208. **Villard V, Meunier J, Chevallier N, and Maurice T**. Pharmacological interaction with the sigma1 (sigma1)-receptor in the acute behavioral effects of antidepressants. *J Pharmacol Sci* 115: 279-292, 2011.

209. **W.Hoffman GBaP**. *Biology of the NMDA receptor*. ©Taylor & Francis Group, LLC, 2009, p. 80-94.

210. **Walker JM, Bowen WD, Walker FO, Matsumoto RR, De Costa B, and Rice KC**. Sigma receptors: biology and function. *Pharmacol Rev* 42: 355-402, 1990.

211. **Wang SC, and Hung MC**. Nuclear translocation of the epidermal growth factor receptor family membrane tyrosine kinase receptors. *Clin Cancer Res* 15: 6484-6489, 2009.

212. **Wanisch K, and Wotjak CT**. Time course and efficiency of protein synthesis inhibition following intracerebral and systemic anisomycin treatment. *Neurobiol Learn Mem* 90: 485-494, 2008.

213. **Washbourne P, Liu XB, Jones EG, and McAllister AK**. Cycling of NMDA receptors during trafficking in neurons before synapse formation. *J Neurosci* 24: 8253-8264, 2004.

214. **Wenthold RSPaRJ**. *Biology of the NMDA receptor*. ©Taylor & Francis Group, LLC, 2009, p. 149-182.

215. **Wood MW, VanDongen HM, and VanDongen AM**. The 5'-untranslated region of the N-methyl-D-aspartate receptor NR2A subunit controls efficiency of translation. *J Biol Chem* 271: 8115-8120, 1996.

216. **Wu Z, and Bowen WD**. Role of sigma-1 receptor C-terminal segment in inositol 1,4,5-trisphosphate receptor activation: constitutive enhancement of calcium signaling in MCF-7 tumor cells. *J Biol Chem* 283: 28198-28215, 2008.

217. **Wyllie DJ, Livesey MR, and Hardingham GE**. Influence of GluN2 subunit identity on NMDA receptor function. *Neuropharmacology* 74: 4-17, 2013.

218. **Yamamoto H, Miura R, Yamamoto T, Shinohara K, Watanabe M, Okuyama S,**

Nakazato A, and Nukada T. Amino acid residues in the transmembrane domain of the type 1 sigma receptor critical for ligand binding. *FEBS Lett* 445: 19-22, 1999.

219. **Yang S, Bhardwaj A, Cheng J, Alkayed NJ, Hurn PD, and Kirsch JR**. Sigma receptor agonists provide neuroprotection in vitro by preserving bcl-2. *Anesth Analg* 104: 1179-1184, tables of contents, 2007.

220. **Yang ZJ, Carter EL, Torbey MT, Martin LJ, and Koehler RC**. Sigma receptor ligand 4-phenyl-1-(4-phenylbutyl)-piperidine modulates neuronal nitric oxide synthase/postsynaptic density-95 coupling mechanisms and protects against neonatal ischemic degeneration of striatal neurons. *Exp Neurol* 221: 166-174, 2010.

221. **Yin X, Takei Y, Kido MA, and Hirokawa N**. Molecular motor KIF17 is fundamental for memory and learning via differential support of synaptic NR2A/2B levels. *Neuron* 70: 310-325, 2011.

222. **Zambon AC, De Costa BR, Kanthasamy AG, Nguyen BQ, and Matsumoto RR**. Subchronic administration of N-[2-(3,4-dichlorophenyl) ethyl]-N-methyl-2-(dimethylamino) ethylamine (BD1047) alters sigma 1 receptor binding. *Eur J Pharmacol* 324: 39-47, 1997.

223. **Zhang H, and Cuevas J**. Sigma receptors inhibit high-voltage-activated calcium channels in rat sympathetic and parasympathetic neurons. *J Neurophysiol* 87: 2867-2879, 2002.

224. **Zhang Q, Fan JS, and Zhang M**. Interdomain chaperoning between PSD-95, Dlg, and Zo-1 (PDZ) domains of glutamate receptor-interacting proteins. *J Biol Chem* 276: 43216-43220, 2001.

225. **Zhang Y, Shi Y, Qiao L, Sun Y, Ding W, Zhang H, Li N, and Chen D**. Sigma-1 receptor agonists provide neuroprotection against gp120 via a change in bcl-2 expression in

mouse neuronal cultures. *Brain Res* 1431: 13-22, 2012.

PUBLICATIONS

frontiers in
NEUROANATOMY

OPINION ARTICLE
published: 28 August 2013
doi: 10.3389/fnana.2013.00027

Evolutionary development of the amygdaloid complex

Mohan Pabba *

Neurosciences Unit, Department of Cellular and Molecular Medicine, Faculty of Medicine, University of Ottawa, Ottawa, ON, Canada
**Correspondence: mpabb044@uottawa.ca; mpabba@ohri.ca*

Edited by:
Makoto Fukuda, Baylor College of Medicine, USA

Reviewed by:
Joshua Corbin, Children's National Medical Center, USA

Keywords: amygdala, anatomy, tetrapods, mammals, evolution

In the early 19th century, Burdach discovered an almond-shaped mass of gray matter in the anterior portion of the mammalian temporal lobe, which he called "amygdala" (Burdach, 1819–1822). The first anatomical description of the amygdala was made in 1867 by Meynert (1867). Subsequently, a large number of other nuclei were added to the amygdala to constitute what is now known as the "amygdaloid complex" (AC) (Johnston, 1923). Until this day, AC remains a subject of intense investigation in terms of content and evolutionary development since it is a much more complicated structure than what was previously thought. It is therefore, important to know the evolutionary developmental origin of AC before we can completely understand its function.

The AC is a multinuclear complex comprised of 13 nuclei. These nuclei are divided into three major groups: the basolateral, cortical-like, and centromedial. Other accessory nuclei such as the intercalated cell masses (I) and the amygdalo-hippocampus area have also been described. The basolateral group is comprised of the lateral nucleus (LA), basal nucleus (B), and accessory basal nucleus (AB) (Johnston, 1923). The cortical-like group of nuclei includes the nucleus of the lateral olfactory tract (NLOT), bed nucleus of the accessory olfactory tract (BAOT), anterior and posterior cortical nuclei (CoA and CoP, respectively), and periamygdaloid cortex (PAC). The centromedial nucleus consists of the central nucleus (CeA), medial nucleus (M), and amygdaloid part of the bed nucleus of stria terminalis (BST). The major remaining groups of AC are the amygdalohippocampal area (AHA) and intercalated nuclei (I) (Aggleton, 2000; Sah et al., 2003). These different nuclei of AC are connected within and also with various brain regions, and thus, process various types of information (e.g., olfactory and **Figure 1A**).

Swanson and Petrovich (1998) definition of amygdala as neither a structural nor a functional unit provides an attractive point to explore the evolutionary developmental aspects of AC because a growing number of evidence suggests AC as an evolutionarily conserved structure. Earlier, research on structural organization of AC in different amniotic vertebrates revealed a common pattern of organization, along with shared functional roles. Conversely, research on anamniotes provided little comparative information regarding structural organization of AC. However, recent studies have shown a homology between amygdaloid components of amniotes and anamniotes. To better understand the evolutionary and developmental history of a particular brain region, one needs to follow a "sequential (step by step) approach," which takes into account the developmental, topological, hodological, genetical, and functional history. Interestingly, recent data on AC of mammals, reptiles, and anurans suggest that the evolution of AC occurred as common traits of telencephlon, for example, regions of cortical amygdala such as nLOT and accessory olfactory bulb (AOB) (Remedios et al., 2007; Huilgol et al., 2013); but not as the sum of unrelated structures with different origins. The present understanding of AC in developmental and adult vertebrates suggests two major divisions of telencephlon: the pallium and the subpallium (Puelles et al., 2000; Martinez-Garcia et al., 2002; Moreno and Gonzalez, 2007b; Remedios et al., 2007). This dual view or origin makes AC a histogenetic complex structure of the adult brain, with extremely intense morphogenetic and migratory processes during the development in all tetrapods (Puelles et al., 2000). In mammals, the pallial component is composed of "cortical amygdala" and "basolateral amygdala." In turn, the subpallial component consists of the striatal component, central amygdala, and medial amygdala. This basic plan is shared by reptiles, birds, and also by anuran amphibians (Martinez-Garcia et al., 2002; Medina et al., 2004). Interestingly, this basic description is possible only in few mammalian tetrapods, but not in the non-mammalian amniotes and the anurans where they have no clear anatomical subdivisions. The existence of shared embryological AC components in all tetrapods provides clues to the presence of precursors of the amygdaloid nuclei from anamniotes (Moreno and Gonzalez, 2007b). The following sections deal with the current view on accepted and shared components of AC in tetrapods.

The amygdala is a part of a phylogentically conserved olfactory system, particularly the olfactory bulb, in vertebrate evolution in terms of embryological origin, neurochemistry, connectivity, and function (Martinez-Garcia et al., 2002; Huilgol et al., 2013). Additionally, a major part of amygdala is also an integral component of the vomeronasal system of the tetrapod (except avian) brain (Swanson and Petrovich, 1998; Moreno and Gonzalez, 2005a).

In mammals, the vomeronasal information passes via the AOB to medial (MeA) and cortical postero-medial amygdala (CoApm) (Swanson and Petrovich, 1998). In addition, the amygdala also receives information from the main olfactory bulb (MOB) and hypothalamus to modulate reproductive and defensive behaviors (Canteras et al., 1995). In reptiles and anurans, the existence of a well-developed "vomeronasal amygdala"

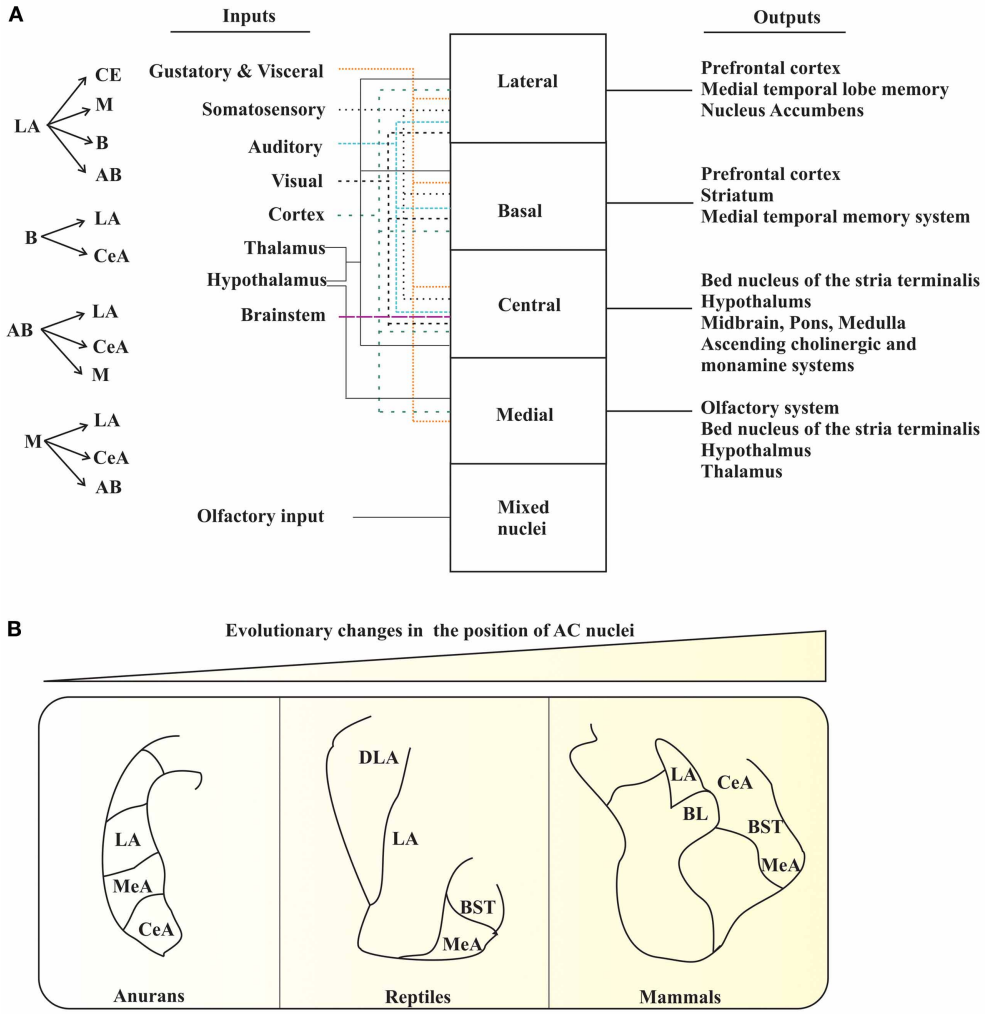

FIGURE 1 | AC of tetrapods. (A) The interconnections (*left panel*) and summary of the main inputs to AC and outputs from AC (*right panel*). The various types of inputs to AC are denoted with different types of colored arrows. **(B)** Pictorial diagram depicting the changes in the position of certain AC nuclei during the course of evolution. LA, lateral nucleus; MeA, medial nucleus; CeA, central nucleus; DLA, dorsal division of lateral nucleus; BST, bed nucleus of stria terminalis; BL, basolateral amygdala. The figure panels **(A)** and **(B)** are adapted and modified from Sah et al. (2003); Moreno and Gonzalez (2007b).

has also been reported (Moreno and Gonzalez, 2003), although no vomeronasal amygdaloid nuclei has been described in birds so far (Martinez-Garcia et al., 2006). Thus, in all tetrapods, the main secondary vomeronasal brain areas belong to AC.

In mammals, the olfactory amygdaloid system consists of the distinct cortical (CoA, CoP nuclei, etc.) and basolateral amygdala (BL, M, LA nuclei). LA receives major sensory input, and is important for emotional behavior (Ledoux et al., 1990). Studies on birds indicate the presence of nuclei that are comparable to CoP of the mammalian amygdala. These studies also revealed the possession of counterparts similar to BM and LA of the mammalian amygdala (Martinez-Garcia et al., 2006). In reptiles, studies on the olfactory system showed comparable functional circuitry with the mammalian BA complex. The anuran counterpart of the mammalian olfactory amygdala is LA (Moreno and Gonzalez, 2004). This part of the amygdala in anurans receives directly or indirectly olfactory, visual, auditory, somatosensory, vomeronasal, and gustatory information. The observed integration that occurs in AC of tetrapods is responsible for the acquisition of "emotional memory," which pertains to the survival of individuals during their defence against danger, their interaction with sexual partners, or their fight with an enemy (Ledoux, 2000). Therefore, the amygdala receives large sensory input information from olfactory and vomeronasal projections, and are conserved in tetrapods.

Studies on tetrapods showed CeA as the main receiver of a wide range of sensory information from other amygdaloid regions in addition to the thalamus and brain stem. Moreover, CeA is known to link and integrate the emotional and motor components of behavior (Han et al., 1997), behavioral responses to nociceptive and visceral pain (Han and Neugebauer, 2004), and

behavioral responses to stressful stimuli (Saha et al., 2000). CeA also mediates many of the autonomic, somatic, endocrine, and behavioral responses in different tetrapods. The autonomic amygdala provides a link between environmental stimuli and animal behavioral responses, and thus, provides an important significance in terms of evolutionary conservation.

Another conserved shared system of tetrapods is the strong amygdalo-hypothalamic connections (Martinez-Marcos et al., 1999; Moreno and Gonzalez, 2005a). In mammals, nuclei that project to hypothalamus through the stria terminalis arise from the medial and basolateral amygdala (Swanson and Petrovich, 1998). As in mammals, the amygdalo-hypothalamic projections of anurans (Moreno and Gonzalez, 2005b) also project through the stria terminalis. In anurans, the amygdalo-hypothalamic connections control functions mediated by the hypothalamus in response to pheromones and odors (Reiner and Karten, 1985; Swanson and Petrovich, 1998).

As in mammals, the amygdalo-hypothalamic projections of anurans, project through the stria terminalis. The main similarity with amniotes is the projection to the hypothalamus from comparable amygdaloid territories carrying vomeronasal, olfactory, and multimodal information (Reiner and Karten, 1985; Swanson and Petrovich, 1998). The situation of amygdalo-hypothalamic projections in birds is more complicated because of the lack of a well-developed olfactory/vomeronasal system.

On the other hand, studies that compare the distribution of neuronal markers (either proteins or genes/transcription factors) across the development of analogous AC nuclei from different species as well as within the same species have also provided valuable information on the evolution of AC. For instance, similarities in the molecular profiles of the pallium and subpallium of mice and chickens were obtained by comparing the nested expression domains of genes such as Dlx-2, Tbr-1, Pax-6, NKx-2.1, and Emx-1 (Puelles et al., 2000). Moreno and Gonzalez, using the distribution of somatostatin, nitric oxide synthase, etc. in anuran CeA and MeA in a series of studies, has predicted that these parts of AC could be related to AC of amniotes (Moreno and Gonzalez, 2005a, 2007a). Medina et al. demonstrated a possible existence of evolutionary relationship in various AC nuclei of mammals, reptiles and birds by testing the expression patterns of genes/transcription factors such as Lhx2, Lhx9, Pax6, Islet 1, NKx2, Lhx6, and Lhx5 in forebrain regions of these animals (Medina et al., 2011). Using the similarities and differences in the expression of Lhx1 and Lhx5, Abellan et al. suggested a common pattern of evolutionary conservation in telencephalon between mice and chickens during various stages of development (Abellan et al., 2010). By examining the distribution of Lhx2, Trb1, reelin, and CdK5, Remedios et al. estimated a possible developmental and evolutionary link between nLOT of AC and neocortex (Remedios et al., 2007; Subramanian et al., 2009). Another study from Tole's group, using migratory genetic markers (e.g., NP2 and AP2α), showed that the distinct halves of AOB [posterior and anterior (pAOB and aAOB)] has different developmental origins, and that pAOB could be a component of AC as it was positioned closely to MeA in anamniotes (*Xenopus*) (Huilgol et al., 2013). Finally, Barger et al. using a different approach, i.e., by comparing the percentage of neurons in individual nuclei of AC between humans and apes, suggested that during the course of human evolution, LA of AC has further progressed in humans (Barger et al., 2012).

CONCLUDING REMARKS

The classical hypothesis proposed by Edinger regarding the evolution of the brain attracted much attention (Edinger, 1908). He proposed that the telencephlon evolved in progressive stages of complexity and size, culminating to the human brain. He also stated that there is an "old brain" (the subpallium at the telencephalic base) followed by the addition of a "new brain" (the pallium at the top of the telencephlon). Nevertheless, this classical hypothesis provides evidence on the existence of a basic plan in the origin, regionalization, and organization of the forebrain of vertebrates. Based on the data pertaining to the organization of AC, there seems to have several important features that are common to all tetrapods: (1) it is formed by pallial and subpallial derivatives; (2) it is topographically situated in the ventrolateral caudal telencephalic hemispheres; (3) it has shared features in relation with different functional systems like the vomeronasal, olfactory, autonomic, and multimodal systems along with an intricate intra-amygdaloid network; (4) it is the origin of important hypothalamic projections; (5) it has a common embryological origin for several prominent features of AC; (6) it has the presence of a main output for autonomic system; finally, (7) it has abundant local circuit neurons that are shared by most amniotes. Thus, in the light of recent findings on AC (Remedios et al., 2007; Butler et al., 2011; Huilgol et al., 2013) also strongly support the idea that tetrapods share the same basic plan.

The increase in size of the pallium, especially in mammals, has an evolutionary importance. The current spatial arrangements of the mammalian AC are still found in living anurans. Therefore, it is now obvious that these "new evolutionary nuclei" would have pushed the "most conserved nuclei" (Moreno and Gonzalez, 2007b). It explains why mammals have the central, medial, and basolateral nuclei occupying the most medial positions, whereas the cortical amygdaloid nuclei occupy the most lateral positions (**Figure 1B**) (Moreno and Gonzalez, 2007b). Consequently, the brain of ancestral tetrapods developed an elaborate AC in response to new requirements imposed on them as a part of the transition from water-to-land. Therefore, the basic organization of the brain system, at least in the case of the AC, is still recognizable in all existing tetrapods, and can be compared with that of mammals.

ACKNOWLEDGMENTS

I am thankful to Dr. Richard Bergeron, Dr. Marzia Martina, and Wissam B. Nassrallah for their helpful feedback on the manuscript.

REFERENCES

Abellan, A., Vernier, B., Retaux, S., and Medina, L. (2010). Similarities and differences in the forebrain expression of Lhx1 and Lhx5 between chicken and mouse: insights for understanding telencephalic development and evolution. *J. Comp. Neurol.* 518, 3512–3528. doi: 10.1002/cne.22410

Aggleton, J. (2000). *The Amygdala: A Functional Analysis*. Oxford: Academic Press.

Barger, N., Stefanacci, L., Schumann, C. M., Sherwood, C. C., Annese, J., Allman, J. M.,

et al. (2012). Neuronal populations in the basolateral nuclei of the amygdala are differentially increased in humans compared with apes: a stereological study. *J. Comp. Neurol.* 520, 3035–3054. doi: 10.1002/cne.23118

Burdach, K. F. (1819–1822). *Vom Baue und Leben des Gehims. 2 vols.* Leipzig: Dyk'sche Buchhdl.

Butler, A. B., Reiner, A., and Karten, H. J. (2011). Evolution of the amniote pallium and the origins of mammalian neocortex. *Ann. N.Y. Acad. Sci.* 1225, 14–27. doi: 10.1111/j.1749-6632.2011.06006.x

Canteras, N. S., Simerly, R. B., and Swanson, L. W. (1995). Organization of projections from the medial nucleus of the amygdala: a PHAL study in the rat. *J. Comp. Neurol.* 360, 213–245. doi: 10.1002/cne.903600203

Edinger, L. (1908). The relations of comparative anatomy to comparative psychology. *J. Comp. Neurol. Pscychol.* 18, 437–457. doi: 10.1002/cne.920180502

Han, J. S., McMahan, R. W., Holland, P., and Gallagher, M. (1997). The role of an amygdalonigrostriatal pathway in associative learning. *J. Neurosci.* 17, 3913–3919.

Han, J. S., and Neugebauer, V. (2004). Synaptic plasticity in the amygdala in a visceral pain model in rats. *Neurosci. Lett.* 361, 254–257. doi: 10.1016/j.neulet.2003.12.027

Huilgol, D., Udin, S., Shimogori, T., Saha, B., Roy, A., Aizawa, S., et al. (2013). Dual origins of the mammalian accessory olfactory bulb revealed by an evolutionarily conserved migratory stream. *Nat. Neurosci.* 16, 157–165. doi: 10.1038/nn.3297

Johnston, J. B. (1923). Further contributions to the study of the evolution of the fore-brain. *J. Comp. Neurol.* 35, 371–482. doi: 10.1002/cne.900350502

Ledoux, J. E. (2000). Emotion circuits in the brain. *Annu. Rev. Neurosci.* 23, 155–184. doi: 10.1146/annurev.neuro.23.1.155

Ledoux, J. E., Cicchetti, P., Xagoraris, A., and Romanski, L. M. (1990). The lateral amygdaloid nucleus: sensory interface of the amygdala in fear conditioning. *J. Neurosci.* 10, 1062–1069.

Martinez-Garcia, F., Martinez-Marcos, A., and Lanuza, E. (2002). The pallial amygdala of amniote vertebrates: evolution of the concept, evolution of the structure. *Brain Res. Bull.* 57, 463–469. doi: 10.1016/S0361-9230(01)00665-7

Martinez-Garcia, F., Novejarque, A., and Lanuza, E. (2006). "*Evolution of the* amygdala in vertebrates," in *Evolution of Nervous Systems*. Vol. 2, ed J. H. Kaas (Elsevier Inc.), 255–334.

Martinez-Marcos, A., Lanuza, E., and Halpern, M. (1999). Organization of the ophidian amygdala: chemosensory pathways to the hypothalamus. *J. Comp. Neurol.* 412, 51–68.

Medina, L., Bupesh, M., and Abellan, A. (2011). Contribution of genoarchitecture to understanding forebrain evolution and development, with particular emphasis on the amygdala. *Brain Behav. Evol.* 78, 216–236. doi: 10.1159/000330056

Medina, L., Legaz, I., Gonzalez, G., De Castro, F., Rubenstein, J. L., and Puelles, L. (2004). Expression of Dbx1, Neurogenin 2, Semaphorin 5A, Cadherin 8, and Emx1 distinguish ventral and lateral pallial histogenetic divisions in the developing mouse claustroamygdaloid complex. *J. Comp. Neurol.* 474, 504–523. doi: 10.1002/cne.20141

Meynert, T. (1867). Der Bau der Grosshirnrinde und seine ortlichen verschiedenheiten, nebst einem pathologisch-anatomischen Corollarium. *Vjschr. Psychiat.* 1, 77–93, 126–170, 198–217.

Moreno, N., and Gonzalez, A. (2003). Hodological characterization of the medial amygdala in anuran amphibians. *J. Comp. Neurol.* 466, 389–408. doi: 10.1002/cne.10887

Moreno, N., and Gonzalez, A. (2004). Localization and connectivity of the lateral amygdala in anuran amphibians. *J. Comp. Neurol.* 479, 130–148. doi: 10.1002/cne.20298

Moreno, N., and Gonzalez, A. (2005a). Central amygdala in anuran amphibians: neurochemical organization and connectivity. *J. Comp. Neurol.* 489, 69–91. doi: 10.1002/cne.20611

Moreno, N., and Gonzalez, A. (2005b). Forebrain projections to the hypothalamus are topographically organized in anurans: conservative traits as compared with amniotes. *Eur. J. Neurosci.* 21, 1895–1910. doi: 10.1111/j.1460-9568.2005.04025.x

Moreno, N., and Gonzalez, A. (2007a). Development of the vomeronasal amygdala in anuran amphibians: hodological, neurochemical, and gene expression characterization. *J. Comp. Neurol.* 503, 815–831. doi: 10.1002/cne.21422

Moreno, N., and Gonzalez, A. (2007b). Evolution of the amygdaloid complex in vertebrates, with special reference to the anamnio-amniotic transition. *J. Anat.* 211, 151–163. doi: 10.1111/j.1469-7580.2007.00780.x

Puelles, L., Kuwana, E., Puelles, E., Bulfone, A., Shimamura, K., Keleher, J., et al. (2000). Pallial and subpallial derivatives in the embryonic chick and mouse telencephalon, traced by the expression of the genes Dlx-2, Emx-1, Nkx-2.1, Pax-6, and Tbr-1. *J. Comp. Neurol.* 424, 409–438.

Reiner, A., and Karten, H. J. (1985). Comparison of olfactory bulb projections in pigeons and turtles. *Brain Behav. Evol.* 27, 11–27. doi: 10.1159/000118717

Remedios, R., Huilgol, D., Saha, B., Hari, P., Bhatnagar, L., Kowalczyk, T., et al. (2007). A stream of cells migrating from the caudal telencephalon reveals a link between the amygdala and neocortex. *Nat. Neurosci.* 10, 1141–1150. doi: 10.1038/nn1955

Saha, S., Batten, T. F., and Henderson, Z. (2000). A GABAergic projection from the central nucleus of the amygdala to the nucleus of the solitary tract: a combined anterograde tracing and electron microscopic immunohistochemical study. *Neuroscience* 99, 613–626. doi: 10.1016/S0306-4522(00)00240-2

Sah, P., Faber, E. S., Lopez De Armentia, M., and Power, J. (2003). The amygdaloid complex: anatomy and physiology. *Physiol. Rev.* 83, 803–834.

Subramanian, L., Remedios, R., Shetty, A., and Tole, S. (2009). Signals from the edges: the cortical hem and antihem in telencephalic development. *Semin. Cell Dev. Biol.* 20, 712–718. doi: 10.1016/j.semcdb.2009.04.001

Swanson, L. W., and Petrovich, G. D. (1998). What is the amygdala. *Trends Neurosci.* 21, 323–331. doi: 10.1016/S0166-2236(98)01265-X

Received: 09 July 2013; accepted: 06 August 2013; published online: 28 August 2013.

Citation: Pabba M (2013) Evolutionary development of the amygdaloid complex. Front. Neuroanat. 7:27. doi: 10.3389/fnana.2013.00027

This article was submitted to the journal Frontiers in Neuroanatomy.

frontiers in
CELLULAR NEUROSCIENCE

OPINION ARTICLE
published: 23 April 2013
doi: 10.3389/fncel.2013.00050

The essential roles of protein–protein interaction in sigma-1 receptor functions

Mohan Pabba*

Neurosciences Unit, Department of Cellular and Molecular Medicine, Faculty of Medicine, University of Ottawa, Ottawa, ON, Canada
**Correspondence: mpabb044@uottawa.ca; mpabba@ohri.ca*

Edited by:
Christophe Altier, University of Calgary, Canada

Reviewed by:
Christophe Altier, University of Calgary, Canada

σ-1R is the well-known subtype of σ-Rs that were originally proposed in 1976 (Martin et al., 1976). σ-1R is a 223 amino acid integral membrane protein consisting of a short N-terminus, a large C-terminus tail, and two transmembrane domains: one at the N-terminus and the other in the middle of the protein (Su et al., 2010). σ-1Rs are distributed throughout the brain. At the subcellular level, σ-1Rs are mainly localized at the endoplasmic reticulum (ER)/mitochondrial associated membranes (MAM) and at very low levels in post-synaptic thickenings of the neuron (Alonso et al., 2000; Su et al., 2010). σ-1Rs at ER/MAM membranes exist in clustered globular structures that are enriched with cholesterol and neutral lipids (Hayashi and Su, 2003, 2005). Several categories of drugs bind to σ-1Rs, for example: cocaine, dihydroepiandrosterone, dimethyl tryptamine (DMT), psychotomimetic compounds, and haloperidol (antagonist). The steroids and DMT were proposed to act as endogenous ligands for the σ-1R. Studies from various laboratories performed on heterologous, *in vivo* and *ex vivo* systems by employing multidisciplinary techniques demonstrated that the σ-1R interacts with numerous cellular components (Su et al., 2010), e.g., different classes of ion channels, kinases, G-protein coupled receptors (GPCRs), etc. The σ-1R associates with voltage-gated ion channels, e.g., Na^+, K^+, and Ca^{2+}. Interaction of the σ-1R with voltage-gated K^+ and Ca^{2+} channels results in either inhibition or enhancement in the activities of these ion channels, whereas σ-1R interaction with voltage-gated Na^+ channels results in inhibition of the channel activity (Kourrich et al., 2012). On the other hand, σ-1R enhances the activity of *N*-methyl-D-aspartate receptors (NMDARs) (a ligand-gated ion channel) and dopamine D_1 receptors (a GPCR) (Monnet et al., 1990; Navarro et al., 2010). The σ-1R modulation of D_1R is through protein–protein interactions (Navarro et al., 2010). However, it is yet to be determined whether σ-1R modulates the NMDAR function through protein–protein interactions. Nevertheless, a recent study demonstrated that σ-1R inhibits the activity of small conductance Ca^{2+}-activated K^+-channels (SK channels), and consequently potentiates the NMDAR function (Martina et al., 2007). It is still unknown if there is any physical association between SK channels and σ-1Rs.

How does the σ-1R, being an intracellular protein, modulate the functions of numerous cellular components that are present at the plasma membrane? The prevailing hypothesis is that under resting conditions, at ER/MAM, σ-1Rs are associated with chaperone called BiP. Upon activation of σ-1Rs by their agonists (at concentrations ∼ equal to or less than 10 times their K_i value), σ-1R dissociates from BiP and modulates the function of inositol triphosphate (IP3) receptors. The σ-1R modulation of IP3 receptor function consequently affects Ca^{2+} influx and signaling into the mitochondria (Hayashi and Su, 2007). However, if σ-1R agonists are present at high concentrations (∼>10 times their K_i value) or during the ER stress, σ-1R dissociates from BiP and translocates to the plasma membrane or plasmalemma and modulates the activities of various cellular components via protein–protein interactions (Su et al., 2010). While this model is promising, several outstanding questions remain to be addressed with respect to σ-1Rs and their association with cellular components, especially different classes of ion channels (**Figure 1**). For instance, first, it needs to be clarified whether the σ-1R modulates multiple cellular components at the plasma membrane or at the plasmalemma of neurons (Su et al., 2010). Second, it is unclear at the moment if the σ-1R associates with ion channels (e.g., voltage-gated Na^+ or K^+ channels) at the ER/MAM, and after association, whether or not the entire complex (σ-1R-ion channel) is translocated to the plasma membrane. Third, investigations from different laboratories demonstrated that the treatment of animals with several σ-1R ligands alter the behavior of animals in various behavioral paradigms such as cocaine-induced behavioral response, NMDAR-antagonism induced amnesia, etc. Hence, it remains to be investigated if there is any link between σ-1Rs association with voltage-gated and/or ligand-gated ion channels, and the alteration in animal behavior, at least in the above-mentioned conditions. Forth, how the σ-1R modulates the functions of voltage-gated and ligand-gated ion channels heterogeneously and to a varying degree remains elusive. Although there can be multiple factors involved, the following reasons could play an important role in differential regulation of voltage-gated and ligand-gated ion channels by σ-1Rs. (a) Recently, it is shown that the σ-1R could exist in dimers (Chu et al., 2013); therefore, do the dimers of σ-1R associate with ion channels? (b) What is the stoichiometry of the σ-1R interaction with ion channels? (c) Several lines of evidence demonstrate that there exist subtypes within the σ-1Rs (Bergeron and Debonnel, 1997; Shioda et al., 2012); thus, do these subtypes display differences in association with ion channels? (d) What is the conformational crystal structure of the σ-1R

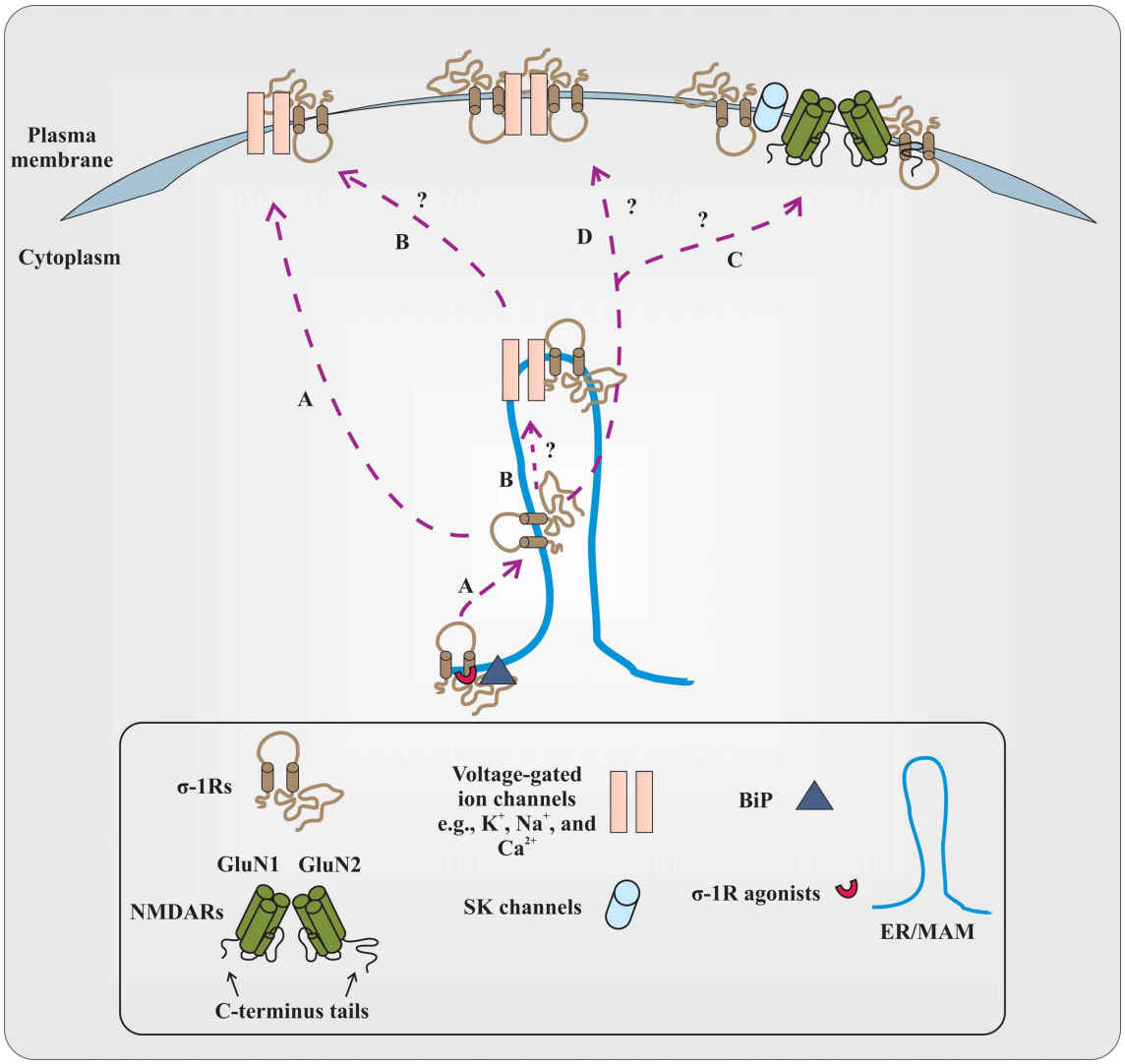

FIGURE 1 | Proposed and elusive mechanism(s) of σ-1R modulation of the function of voltage-gated and ligand-gated ion channels. (A) The prevailing hypothesis is that activation of σ-1Rs with high concentrations of their agonists (red colored semi-circle) causes σ-1Rs two transmembrane domains (black colored line boundaries and respective tails in a light brown color), at the ER/MAM, to dissociate from the chaperone called BiP (dark gray colored triangle). The dissociated σ-1Rs translocate to the plasma membrane or plasmalemma and in a subtype dependent manner, either inhibit or enhance the function of ion channels by forming protein-protein interactions. **(B)** It remains to be identified if the dissociated σ-1Rs associate with ion channels at the ER/MAM, and after association, whether or not the entire complex is translocated toward the plasma membrane. The study from Kourrich et al. (2013) supports this possibility, at least with voltage-gated K^+-channel Kv1.2. **(C)** It is unclear if dissociated and translocated σ-1Rs associate with SK channels or NMDARs. The functional NMDARs are tetrameric assembles of two obligatory GluN1 subunits with either two GluN2 subunits (different combinations of GluN2 subunits) or GluN3 subunits. For representation, the dimer form of NMDARs (GluN1 and GluN2 subunits) and their C-terminus tails are presented in the figure. The N-terminus domain of NMDAR subunits and GluN3 subunits are not shown. **(D)** The other possibilities that remain unexplored are whether the dimers of the σ-1R interact with ion channels, and the stoichiometry of interaction between the σ-1R and ion channels.

in association with either voltage-gated or ligand-gated ion channels? (e) Which amino acid residues or motif(s) in the σ-1R determine the σ-1R association with various classes of ion channels? (f) Which polar and non-polar amino acid residues of the σ-1R influence the biophysical properties of σ-1R-associated ion channels? The crystallographic data could provide enough evidence regarding the residues and domains of the σ-1R involved in physical association with ion channels. Additionally, it could also provide information regarding the differences in associations between σ-1Rs and various ion channels, if there are any. Finally, are there any spatial requirements for the σ-1R to associate with ion channels, given σ-1R-modulated ion channels (e.g., voltage-gated Na^+ and K^+ channels) have some overlapping distribution in the neuron (Trimmer and Rhodes, 2004)?

However, a recent study by employing a multidisciplinary approach elegantly

demonstrated that the σ-1R's interaction with voltage-gated K^+ channel Kv1.2 plays an important role in the cocaine-induced locomotor sensitization (Kourrich et al., 2013). Using pharmacological blockers and knockdown of σ-1Rs, Kourrich et al. (2013) first identified that σ-1Rs are involved in cocaine-induced long-lasting neuronal and behavioral adaptation. Then, by employing electrophysiological recordings as well as biochemical studies on *ex vivo* tissue and heterologous cells, they confirmed that the σ-1R's interaction with voltage-gated K^+ channel Kv1.2 contributes/participates in the behavioral response (locomotor sensitization) to cocaine. Studies from Kourrich et al. (2013) have provided valuable information in terms of the σ-1R's association with ion channels, at least with voltage-gated K^+-channels such as: (a) the σ-1R could possibly associate with these ion channels at the ER/MAM, and then the entire complex is trafficked toward the plasma membrane; (b) the potential link between σ-1R association with these ion channels and alteration in the behavior of animals; and importantly, (c) the structural orientation of the σ-1R at the plasma membrane during the association with these ion channels, for example, both N-terminus and C-terminus tails of the σ-1R are extracellular. Additionally, this study also provided first direct and unequivocal evidence for the presence of σ-1Rs at the plasma membrane. Nonetheless, even though Kourrich et al. (2013) demonstrated that both N-terminus and C-terminus tails of the σ-1R are extracellular, the orientation of the σ-1R *in vivo* needs to be confirmed. Also, future studies are necessary to test if the σ-1R's interaction with other ion channels alters the behavior of animals similar to what is shown by Kourrich et al. (2013). For example, is there any interaction between σ-1Rs and NMDARs that could ameliorate the behavioral phenotype observed in mouse models of amnesia induced by the blockade of NMDARs (Maurice et al., 1994)?

It is essential to identify and understand the molecular details of the σ-1R association with cellular components (Su et al., 2010) such as different classes of ion channels, kinases, GPCRs, etc. Gaining substantial knowledge on the details about σ-1Rs and their structural determinants responsible for association with ion channels as well as other cellular components could help decipher the σ-1R's role in pathological conditions such as addiction, amnesia, frontotemporal degeneration in motor neuron disease (FTLD-MND), etc. (Hayashi et al., 2011). Furthermore, insights on molecular features of the σ-1R interactions with various classes of ion channels provide the opportunity to understand the critical role of σ-1Rs in neuronal plasticity (Su et al., 2010; Kourrich et al., 2012). Defining the intricacies underlying the relationship between σ-1Rs and their interacting partners during physiological and pathological conditions will form a venue for the development of novel therapeutic strategies.

ACKNOWLEDGMENTS

I am thankful to Wissam B. Nassrallah for helpful feedback on the manuscript.

REFERENCES

Alonso, G., Phan, V., Guillemain, I., Saunier, M., Legrand, A., Anoal, M., et al. (2000). Immunocytochemical localization of the sigma(1) receptor in the adult rat central nervous system. *Neuroscience* 97, 155–170.

Bergeron, R., and Debonnel, G. (1997). Effects of low and high doses of selective sigma ligands: further evidence suggesting the existence of different subtypes of sigma receptors. *Psychopharmacology (Berl.)* 129, 215–224.

Chu, U. B., Ramachandran, S., Hajipour, A. R., and Ruoho, A. E. (2013). Photoaffinity labeling of the sigma-1 receptor with N-[3-(4-Nitrophenyl)propyl]-N-dodecylamine: evidence of receptor dimers. *Biochemistry* 52, 859–868.

Hayashi, T., and Su, T. P. (2003). Sigma-1 receptors (sigma(1) binding sites) form raft-like microdomains and target lipid droplets on the endoplasmic reticulum: roles in endoplasmic reticulum lipid compartmentalization and export. *J. Pharmacol. Exp. Ther.* 306, 718–725.

Hayashi, T., and Su, T. P. (2005). The potential role of sigma-1 receptors in lipid transport and lipid raft reconstitution in the brain: implication for drug abuse. *Life Sci.* 77, 1612–1624.

Hayashi, T., and Su, T. P. (2007). Sigma-1 receptor chaperones at the ER-mitochondrion interface regulate Ca(2+) signaling and cell survival. *Cell* 131, 596–610.

Hayashi, T., Tsai, S. Y., Mori, T., Fujimoto, M., and Su, T. P. (2011). Targeting ligand-operated chaperone sigma-1 receptors in the treatment of neuropsychiatric disorders. *Expert Opin. Ther. Targets* 15, 557–577.

Kourrich, S., Hayashi, T., Chuang, J. Y., Tsai, S. Y., Su, T. P., and Bonci, A. (2013). Dynamic interaction between sigma-1 receptor and Kv1.2 shapes neuronal and behavioral responses to cocaine. *Cell* 152, 236–247.

Kourrich, S., Su, T. P., Fujimoto, M., and Bonci, A. (2012). The sigma-1 receptor: roles in neuronal plasticity and disease. *Trends Neurosci.* 35, 762–771.

Martin, W. R., Eades, C. G., Thompson, J. A., Huppler, R. E., and Gilbert, P. E. (1976). The effects of morphine- and nalorphine- like drugs in the nondependent and morphine-dependent chronic spinal dog. *J. Pharmacol. Exp. Ther.* 197, 517–532.

Martina, M., Turcotte, M. E., Halman, S., and Bergeron, R. (2007). The sigma-1 receptor modulates NMDA receptor synaptic transmission and plasticity via SK channels in rat hippocampus. *J. Physiol.* 578, 143–157.

Maurice, T., Hiramatsu, M., Itoh, J., Kameyama, T., Hasegawa, T., and Nabeshima, T. (1994). Behavioral evidence for a modulating role of sigma ligands in memory processes. I. Attenuation of dizocilpine (MK-801)-induced amnesia. *Brain Res.* 647, 44–56.

Monnet, F. P., Debonnel, G., Junien, J. L., and De Montigny, C. (1990). N-methyl-D-aspartate-induced neuronal activation is selectively modulated by sigma receptors. *Eur. J. Pharmacol.* 179, 441–445.

Navarro, G., Moreno, E., Aymerich, M., Marcellino, D., McCormick, P. J., Mallol, J., et al. (2010). Direct involvement of sigma-1 receptors in the dopamine D1 receptor-mediated effects of cocaine. *Proc. Natl. Acad. Sci. U.S.A.* 107, 18676–18681.

Shioda, N., Ishikawa, K., Tagashira, H., Ishizuka, T., Yawo, H., and Fukunaga, K. (2012). Expression of a truncated form of the endoplasmic reticulum chaperone protein, sigma1 receptor, promotes mitochondrial energy depletion and apoptosis. *J. Biol. Chem.* 287, 23318–23331.

Su, T. P., Hayashi, T., Maurice, T., Buch, S., and Ruoho, A. E. (2010). The sigma-1 receptor chaperone as an inter-organelle signaling modulator. *Trends Pharmacol. Sci.* 31, 557–566.

Trimmer, J. S., and Rhodes, K. J. (2004). Localization of voltage-gated ion channels in mammalian brain. *Annu. Rev. Physiol.* 66, 477–519.

Received: 05 April 2013; accepted: 05 April 2013; published online: 23 April 2013.
Citation: Pabba M (2013) The essential roles of protein–protein interaction in sigma-1 receptor functions. Front. Cell. Neurosci. 7:50. doi: 10.3389/fncel.2013.00050

JPn Neuroscience
The Journal of Physiology

JOURNAL CLUB

The elusive roles of NMDA receptor amino-terminal domains

Mohan Pabba, Elitza Hristova and Dante Biscaro
Neurosciences Unit, Department of Cellular and Molecular Medicine, Faculty of Medicine, University of Ottawa, 451 Smyth Rd, Ottawa, Ontario, Canada K1H 8M5

Email: mpabba@ohri.ca or mpabb044@uottawa.ca

The influx of ions into the neuron forms the requisite step for the passage of information from one neuron to the other neuron. The functional units of the neuron – ion channels – carry out this essential step efficiently and in a highly coordinated manner. Generally, a neuron expresses a variety of ion channels that permit the movement of specific ions. However, the fidelity for the flow of specific ions through a particular ion channel is often defined by the biophysical properties of that ion channel such as activation and inactivation, etc. Interestingly, many of the biophysical properties of an ion channel are acquired by protein domains of that ion channel. This form of dependence on multiple intrinsic factors for given biophysical properties gets complicated if that ion channel has numerous protein domains and each protein domain functions as a semiautonomous entity. The *N*-methyl-D-aspartate receptors (NMDARs) are one such particular ion channel that has distinct profiles of biophysical properties due to the presence of several different semiautonomous protein domains (Traynelis *et al.* 2010).

NMDARs are glutamate-gated cation channels that are ubiquitously expressed in various regions of the brain and are involved in synaptic transmission. Structurally, NMDARs are hetero-tetramers of subunits GluN1, GluN2 and GluN3. In order to form a functional NMDAR ion channel complex, assemblies of two GluN1 subunits together with either two GluN2 subunits or a combination of GluN2 and GluN3 subunits are required. However, the presence of isoforms in each NMDAR subunit results in the existence of a large repertoire of NMDAR subunit combinations giving rise to functionally distinct NMDARs. The GluN2 family includes four members (GluN2A–D) encoded by four different genes, while the GluN3 family includes two members (GluN3A and B) encoded by two separate genes. In contrast to GluN2 and GluN3 subunits, the GluN1 subunit is encoded by a single gene but due to alternative mRNA splicing of three exons (5, 21 and 22) leads to eight possible isoforms for GluN1 (GluN1–1a to 4a and GluN1–1b to 4b). The isoforms 'b' has an additional stretch of 21 amino acids in the amino-terminal region of the GluN1 subunit that is encoded by exon 5. The exon 21 encodes a 37-amino-acid segment at the C-terminus while the exon 22 encodes a 38-amino-acid segment also at the C-terminus of the GluN1 subunit. The distribution and expression patterns of all NMDAR isoforms vary at different brain regions and throughout development. Each NMDAR subunit is a modular protein that contains four distinct semiautonomous domains: the amino-terminal domain (ATD; roughly divided into two halves, R1 and R2), the ligand-binding domain (LBD; formed from amino-acid segments S1 and S2), the transmembrane domain (TMD) and the C-terminal domain (CTD). The ATD and LBD are extracellular while the CTD is intracellular (Traynelis *et al.* 2010). Studies performed by employing electrophysiological, pharmacological and molecular biological strategies on native tissues and on heterologously expressed NMDAR subunits (different isoform combinations that are either wild type, chimeric, mutant and truncated versions) have provided the essential roles of these protein domains in conferring NMDARs with unique functional and heterogeneous biophysical properties. These properties can be broadly grouped into two main categories (Paoletti, 2011): (a) permeation properties, which are mainly acquired due to the TMD, include single-channel conductances and their block by extracellular Mg^{2+} ions, and (b) gating properties, which include sensitivity to various agonists and antagonists, activation and deactivation kinetics, channel mean open time and maximal open probability, and channel shut times, etc. Initially, the LBD and TMD were believed to be solely responsible for most of the gating properties, and therefore both exogenous and endogenous compounds would modulate the function of NMDARs by binding to these domains. However, more recent studies have shown that the ATD is equally if not more important than the LBD and TMD in influencing gating properties of NMDARs.

How can the ATD of NMDAR subunits influence various biophysical properties of NMDARs? The detailed mechanisms of the ATD's role in NMDAR function are less well understood, but modelling, functional and crystallographic data support the hypothesis that the ATD has indirect effects on the LBD and TMD of the NMDAR complex. An oversimplified and generalized model is that R1 and R2 of the ATD oscillate between open, closed and various intermediate conformational states at rest as well as under conditions during and after binding to allosteric modulators, consequently influencing the subsequent downstream protein domains, i.e. the LBD and TMD (Gielen *et al.* 2009). But there exists many differences in interactions, orientations and structural rearrangements under different conditions within the ATD of NMDAR subunits resulting in observing heterogeneity in ATD modulation of NMDAR function. Taken together, the ATDs of NMDAR subunits have significant role on biophysical and pharmacological properties of NMDARs. Briefly, electrophysiological studies performed on truncated, chimeric and mutated ATDs of GluN2-containing NMDARs have shown alterations in channel maximal open probability, and deactivation and desensitization kinetics, at least, at GluN2A- or GluN2B-containing NMDARs. Furthermore, many studies have shown the role of the GluN1–1a (the most widely used GluN1 variant) ATD in influencing the biophysical properties of the GluN2-containing NMDAR subunits. For example, the GluN1–1a subunit expressed with GluN2D-containing NMDARs in a heterologous system exhibited low open probability, variations in deactivation and desensitization kinetics, etc (Gielen *et al.* 2009; Yuan *et al.* 2009). Despite the knowledge available on the ATD of NMDAR subunits, it still remains unclear how GluN1 splice variants influence biophysical and pharmacological properties of various

 DOI: 10.1113/jphysiol.2012.243311

GluN2 subunit-containing NMDARs, in particular, GluN2D-containing NMDARs.

However, in a recent study in *The Journal of Physiology*, Vance *et al.* (2012), by employing the heterologous expression approach, have dissected the role of GluN1 splice variants, specifically the GluN1–1b isoform, on the biophysical and pharmacological properties of GluN1/GluN2D-containing NMDARs. They found that inclusion of a 21-amino-acid stretch in the ATD of the GluN1 subunit (i.e. the GluN1–1b isoform) increases open probability and deactivation kinetics, and decreases agonist potencies of GluN1/GluN2D-containing NMDARs as opposed to GluN1–1a isoform-containing GluN1/GluN2D receptors. Moreover, they extended their approach in characterizing and comparing the effects of other GluN1 splice variants (i.e. GluN1–1a to 4a and GluN1–1b to 4b) on biophysical and pharmacological properties of GluN1/GluN2D-containing NMDARs. Interestingly, they found that Lys211 encoded in exon 5 mediates most of the effects on agonist potencies as well as deactivation kinetics of GluN1/GluN2D-containing NMDARs. Finally, they proposed a model that fits with the single channel and macroscopic properties of GluN1/GluN2D receptors. Although Vance *et al.* (2012) have yet again demonstrated the exceptional role of the ATD in influencing NMDAR function, it is still not well understood how a 21-amino-acid stretch in the ATD can induce such major effects on biophysical and pharmacological properties of GluN1/GluN2D receptors. This could be due in part to the lack of structural data on the ATD in full-length NMDA receptors. However, Vance *et al.* (2012) have predicted that Lys211 in the ATD of GluN1–1b subunits plays an important role in intra-subunit interaction with GluN2D receptors, thus observing lower agonist potencies and rapid deactivation time course in their study.

Nevertheless, in spite of such significant progress in understanding the role(s) of the ATD in modulating NMDAR function, several questions remain unanswered (Hansen *et al.* 2010). For instance, how does the ATD of NMDAR subunits exerts its role in assembly, targeting and trafficking of NMDARs? Second, how does the modification of NMDAR subunit ATD consensus sites for *N*-glycosylation impact biophysical properties of NMDARs? Third, an increasing amount of evidence suggests that the *in vivo* composition of NMDARs is not always a binary assembly of GluN1/GluN2 (A–D) or GluN1/GluN3 (A–B), but that NMDARs can also exist as triheteromeric subunit assemblies (GluN1/GluN2 (A–D)/GluN3 (A–B)). Therefore, what is the role of the ATD in influencing the biophysical properties of triheteromeric NMDARs? Finally, it has been demonstrated that the ATD of NMDAR subunits interacts with a variety of extracellular synaptic proteins. However, it is unclear if these interactions have any influence on ATD modulation of NMDAR function (Hansen *et al.* 2010).

It is necessary to understand the role(s) of the ATD as well as other protein domains in proper functioning of NMDARs because these receptors play a critical role in several physiological and pathological processes. NMDARs are highly permeable to Ca^{2+} ions and this property allows NMDARs to operate as efficient integrators of synaptic activity and the activation of a multitude of intracellular signalling cascades. The influx of Ca^{2+} ions via NMDARs into a postsynaptic neuron has a tremendous impact on that neuron because the amplitude and time course of the calcium transient (which mainly depends on the biophysical properties of NMDARs) results in altering intracellular signalling events that are central for inducing the process of long-term potentiation (Traynelis *et al.* 2010). Unfortunately, the excess influx of calcium ions through NMDARs leads to deleterious effects on the postsynaptic neuron under conditions such as ischaemic stroke where overstimulation of NMDARs occurs. Furthermore, inappropriate activation or function of NMDARs protein domains can lead to certain chronic pathologies such as epilepsy and schizophrenia (Lau & Zukin, 2007; Traynelis *et al.* 2010). Also, given the ambiguous roles for various protein domains of NMDARs in a multitude of neurodegenerative disorders, studies such as that of Vance *et al.* (2012) significantly contribute to our understanding of the previously unappreciated role of the ATD in NMDAR physiology. In conclusion, a better understanding of the molecular determinants underling the proper function of NMDARs creates the potential for therapeutic intervention while revealing new insights into multiple brain pathologies that involve predominantly NMDAR dysfunction.

References

Gielen M, Siegler RB, Mony L, Johnson JW & Paoletti P (2009). Mechanism of differential control of NMDA receptor activity by NR2 subunits. *Nature* **459**, 703–707.

Hansen KB, Furukawa H & Traynelis SF (2010). Control of assembly and function of glutamate receptors by the amino-terminal domain. *Mol Pharmacol* **78**, 535–549.

Lau CG & Zukin RS (2007). NMDA receptor trafficking in synaptic plasticity and neuropsychiatric disorders. *Nat Rev Neurosci* **8**, 413–426.

Paoletti P (2011). Molecular basis of NMDA receptor functional diversity. *Eur J Neurosci* **33**, 1351–1365.

Traynelis SF, Wollmuth LP, McBain CJ, Menniti FS, Vance KM, Ogden KK, Hansen KB, Yuan H, Myers SJ & Dingledine R (2010). Glutamate receptor ion channels: structure, regulation, and function. *Pharmacol Rev* **62**, 405–496.

Vance KM, Hansen KB & Traynelis SF (2012). GluN1 splice variant control of GluN1/GluN2D NMDA receptors. *J Physiol* **590**, 3857–3875.

Yuan H, Hansen KB, Vance KM, Ogden KK & Traynelis SF (2009). Control of NMDA receptor function by the NR2 subunit amino-terminal domain. *J Neurosci* **29**, 12045–12058.

SYNAPSE 65:1181–1195 (2011)

Chronically Saturating Levels of Endogenous Glycine Disrupt Glutamatergic Neurotransmission and Enhance Synaptogenesis in the CA1 Region of Mouse Hippocampus

WAFAE BAKKAR,[1,2] CHUN-LEI MA,[3] MOHAN PABBA,[1,2] PAMELA KHACHO,[1,2] YONG-LI ZHANG,[1] EMILIE MULLER,[1] MARZIA MARTINA,[4] AND RICHARD BERGERON[1,2,5]*

[1]*Ottawa Hospital Research Institute, Ottawa, Ontario, Canada*
[2]*Department of Cellular and Molecular Medicine, University of Ottawa, Ottawa, Ontario, Canada*
[3]*Department of Physiology Binzhou Medical College, Yantai Campus #346 Guanhai Road, Laishan District, Yantai City. Shandong Province, 264003, China*
[4]*National Research Council of Canada, Ottawa, Ontario, Canada*
[5]*Department of Psychiatry, University of Ottawa, Ottawa, Ontario, Canada*

KEY WORDS glutamate; NMDA receptor; mEPSC; glycine encephalopathy; whole-cell patch-clamp; Ifenprodil

ABSTRACT Glycine serves a dual role in neurotransmission. It is the primary inhibitory neurotransmitter in the spinal cord and brain stem and is also an obligatory coagonist at the excitatory glutamate, *N*-methyl-D-aspartate receptor (NMDAR). Therefore, the postsynaptic action of glycine should be strongly regulated to maintain a balance between its inhibitory and excitatory inputs. The glycine concentration at the synapse is tightly regulated by two types of glycine transporters, GlyT1 and GlyT2, located on nerve terminals or astrocytes. Genetic studies demonstrated that homozygous (GlyT1−/−) newborn mice display severe sensorimotor deficits characterized by lethargy, hypotonia, and hyporesponsivity to tactile stimuli and ultimately die in their first postnatal day. These symptoms are similar to those associated with the human disease glycine encephalopathy in which there is a high level of glycine in cerebrospinal fluid of affected individuals. The purpose of this investigation is to determine the impact of chronically high concentrations of endogenous glycine on glutamatergic neurotransmission during postnatal development using an in vivo mouse model (GlyT1+/−). The results of our study indicate the following; that compared with wild-type mice, CA1 pyramidal neurons from mutants display significant disruptions in hippocampal glutamatergic neurotransmission, as suggested by a faster kinetic of NMDAR excitatory postsynaptic currents, a lower reduction of the amplitude of NMDAR excitatory postsynaptic currents by ifenprodil, no difference in protein expression for NR2A and NR2B but a higher protein expression for PSD-95, an increase in their number of synapses and finally, enhanced neuronal excitability. **Synapse 65:1181–1195, 2011.** © 2011 Wiley-Liss, Inc.

INTRODUCTION

Aside from its role in protein synthesis and metabolism, glycine is a well-established inhibitory neurotransmitter, particularly in the spinal cord and brain stem where it activates strychnine-sensitive ionotropic glycine receptors (GlyRs) (Legendre, 2001; Betz and Laube, 2006; Kirsch, 2006). In addition to its inhibitory function, numerous studies performed in the last two decades showed that glycine is implicated in neurotransmission mediated by glutamate, the major excitatory neurotransmitter in the nervous

Additional Supporting Information may be found in the online version of this article.

V.B. and C.-L. M. have contributed equally to the manuscript

Contract grant sponsor: March of Dimes Foundation; Contract grant number: 6-FY06-327; Contract grant sponsor: Richard Bergeron is also a recipient of the New Investigator Award from the Canadian Institutes of Health Research

*Correspondence to: Richard Bergeron, Ottawa Hospital Research Institute, 725 Parkdale Avenue, Ottawa, ON, Canada K1Y 4E9. E-mail: rbergeron@ohri.ca

Received 3 February 2011; Accepted 18 May 2011

DOI 10.1002/syn.20956

Published online 1 June 2011 in Wiley Online Library (wileyonlinelibrary.com).

system that acts as a coagonist at the *N*-methyl-D-aspartate receptor (NMDAR) (Johnson and Ascher, 1987; Kleckner and Dingledine, 1988; Mayer, Vyklicky, and Clements, 1989; Thomson, Walker, and Flynn, 1989; Gabernet et al., 2005; Bergeron, Meyer, Coyle, and Greene, 1998; Berger, Dieudonne, and Ascher, 1998). It is important to mention that several studies also indicate that D-serine could be the more important coagonist at NMDAR, particularly in the hippocampus (Schell, Molliver, and Snyder, 1995).

Similar to other neurotransmitters, glycine gradients in the nervous system are tightly regulated by specialized transmembrane proteins known as glycine transporters (GlyTs) (Smith et al., 1992; Liu et al., 1992; Zafra et al., 1995; Borowsky, Mezey, and Hoffman, 1993; Liu et al., 1993; Lopez-Corcuera, Alcantara, Vazquez, and Aragon, 1993; Guastella et al., 1992; Jursky and Nelson, 1996; Adams, et al., 1995; Zafra et al., 1995; Eulenburg, Armsen, Betz, and Gomeza, 2005). These ion-driven reuptake pumps have two different genes which code for two GlyT subtypes, GlyT1 and GlyT2 (Borowsky, Mezey, and Hoffman, 1993). The in vivo role of GlyTs contributes to the overall activity of inhibitory GlyRs and glutamatergic neurotransmission as recently demonstrated using genetically altered mice (Gomeza et al., 2003; Gomeza et al., 2003; Aragon and Lopez-Corcuera, 2005). Homozygote GlyT1-/- mice die on their first day of birth (Gomeza et al., 2003; Tsai et al., 2004) due to over-activation of GlyRs, whereas heterozygote (GlyT1+/−) animals develop relatively normally but show a disruption in glutamatergic neurotransmission in the forebrain (Martina et al., 2005; Gabernet et al., 2005; Yee et al., 2006).

NMDARs play a central role in synaptic transmission and plasticity (Lau and Zukin, 2007). These ionotropic receptors, which are gated by glutamate (Cull-Candy, Brickley, and Farrant, 2001; Papadia and Hardingham, 2007), incorporate different subunits from a repertoire of three subtypes: NR1, NR2, and NR3, to form heterotetrameric complexes. There are eight NR1 splice variants, four NR2 subunits (A-D), and two NR3 subunits (A and B). The consensus is that NMDARs on CA1 pyramidal cells (CA1 PCs) are tetraheteromers, typically composed of two glycine-binding NR1 subunits and two glutamate-binding NR2 subunits (Anson et al., 1998; Waxman and Lynch, 2005). NR1 is essential for a functional NMDAR, whereas the identity of the NR2 subunit is critical in determining many biophysical and pharmacological properties of the receptor. Although NR2B is the predominant subunit at the synapse early in postnatal development (Monyer et al., 1992; Monyer Laurie, Sakmann, and Seeburg, 1994; Stocca and Vicini, 1998), NR2A expression, which produces the NMDAR current with the fastest kinetics, increases during the postnatal period (Sans, Petralia, Wang, Blahos, Hell, and Wenthold, 2000; Stephenson, 2001).

The purpose of this investigation is to determine the impact of chronic high levels of glycine on different parameters of glutamatergic NMDAR-mediated neurotransmission during the postnatal development in the CA1 region of the mouse hippocampus, using the in vivo mouse model (GlyT1+/−).

Abbreviations

ACSF	artificial cerebrospinal fluid
AMPA	α-amino-3-hydroxy-5-methylisoxazole-4-propionic acid
APV	amino-phosphoro-valeric acid
CNS	central nervous system
GABA	γ-aminobutyric acid
GlyT	glycine transporter
GMS	glycine modulatory site
IR	immunoreactivity
NBQX	1,2,3,4-tetrahydro-6-nitro-2,3-dioxobenzo[f]quinoxaline-7-sulfonamide
NFPS	glycine transporter antagonist type 1
NMDAR	*N*-methyl-D-aspartate receptor
PBS	phosphate buffer saline
QX-314	*N*-ethyl bromide
TTX	tetrodotoxin
WT	wild type mice
EPSC	excitatory postsynaptic current
EDTA	ethylenediaminetetracetic acid
TBS	tris-buffered saline.

EXPERIMENTAL PROCEDURES

Genotyping

All mice used for this investigation were backcrossed at least nine generations to the 129/SvEvTac background, as previously described (Tsai et al., 2004). Genotyping of GlyT1+/− mice has been previously described (Martina et al., 2005; Imamura, Ma, Pabba, and Bergeron, 2008). Briefly, polymerase chain reaction (PCR) amplification of genomic DNA was prepared from mouse tissue. Mouse tail samples were incubated in proteinase K (0.5 mg/ml; Sigma, St. Louis, MO) at 50°C overnight and were centrifuged (20 min) at 1600 g. The supernatant was then added to a double volume of isopropanol to precipitate the genomic DNA. The supernatant was removed and the DNA was washed with 70% ethanol and allowed to dry. DNA was resuspended in 300 μl of water of which 1 μl was added to the PCR mixture.

PCR analysis was done using *Taq* DNA polymerase (Invitrogen Corporation, Carlsbad, CA). Reaction products were run on a 1% agarose gel and visualized using ethidium bromide. Primer sequences (5′-3′) were: Primer 1 GCCTTGGGAAAAGCGCCTCC; Primer 2 CCCCTACTTCATCATGCTGATC; Primer 3 CACCTACCAGTAGTTGCCTT. Cycling conditions (GeneAmp 2400, Perkin-Elmer, Foster City, CA) were 2 min at 95°C followed by 36 cycles at 94°C (melting) for 30 s, 57°C (annealing) for 30 s, and 72°C (extension) for 1 min 40 s.

The reaction solution contained Mg^{2+} (1.5 mM), dNTPs (0.2 mM each), oligonucleotide primers (0.625 μM for Primer 1 and 0.25 μM for Primer 3), *Taq* polymerase (2.5 units), reaction buffer (10×; 2 μl), and 1 μl of solubilized genomic DNA (20 μl final volume) in distilled water. Each mouse was genotyped using one reaction as previously shown (Tsai, Ralph-Williams, Martina et al., 2004). WT mice showed a single band at 1.3 Kb,reas whe the GlyT1+/− mice had an additional band at 1.0 Kb.

Electrophysiology

Hippocampal slices preparation

Prior to decapitation, the animals were anesthetized with isofluorane in agreement with the guidelines of the Canadian Council of Animal Care. The brain was removed and placed in the oxygenated (95% O_2 and 5% CO_2) artificial cerebrospinal fluid (ACSF) at 4°C containing (mM): 126 NaCl, 2.5 KCl, 1 $MgCl_2$, 26 $NaHCO_3$, 1.25 NaH_2PO_4, 2 $CaCl_2$, and 10 glucose. The ACSF solution was adjusted to. an osmolarity of 300 mOsml/L and the pH adjusted to 7.2. Acute coronal brain slices (300 μm) containing the hippocampus were obtained from GlyT1+/− and WT mice at 2, 3, 4, and 8 weeks of age with a vibrating microtome (Leica VT 1000S, Nassloch, Germany). The slices were then transferred to a chamber containing oxygenated ACSF and maintained at room temperature for at least 1 h prior to the recording.

Data recording and analysis

Electrical stimulation of the Schaffer collaterals with a bipolar microelectrode positioned in the stratum radiatum evoked postsynaptic responses. The stimulation was delivered every 12 s with a pulse duration of 100 μs. The stimulation intensity was set in order to obtain an NMDAR-mediated excitatory postsynaptic current (NMDAR EPSC) amplitude of 30-60 pA at a membrane holding potential of −65 mV.

To minimize the current attenuation of NMDAR EPSC, we performed voltage-clamp experiments with pipettes filled with a solution containing (mM) 130 Cs^+ methanesulphonate, 10 Hepes, 2 $MgCl_2$, 2 ATP-Mg, 0.5 GTP, 1 lignocaine (lidocaine) *N*-ethyl bromide (QX-314), and 2 EGTA. For recordings of spontaneous activity, 0.2 mM EGTA was used instead of 2. To isolate the NMDAR-mediated component of evoked responses, we used ACSF containing a low concentration of $MgCl_2$ (0.1 mM) with osmolarity maintained by $CaCl_2$ (2.9 mM) and added (μM): five 1,2,3,4-tetrahydro-6-nitro-2,3-dioxobenzo[f]quinoxaline-7-sulfonamide (NBQX), 50 picrotoxin, 10 CGP 52,432, and 1 strychnine, to block α-amino-3-hydroxy-5-methylisoxazole-4-propionic acid (AMPA), γ-aminobutyric acid (GABA) $GABA_A$, $GABA_B$ and GlyRs, respectively. All chemicals and drugs were purchased from Sigma-Aldrich, with the exception of NBQX, which was purchased from Tocris Bioscience (Ellisville, MO).

Decay kinetics of NMDAR EPSCs were analyzed on the average of 20 to 25 traces. The decays were fitted with double exponential functions: $y = A_f e^{-t/\tau} + A_s e^{-t/\tau}$ in which A is amplitude, τ is decay time constant, and the subscript f and s denote fast and slow components, respectively. Weighted time constants (τ_{mean}) were calculated using the equation: $\tau_{mean} = [A_f/(A_f + A_s)]\ \tau_f + [A_s/(A_s + A_f)]\ \tau_s$ (Stocca and Vicini, 1998; Stocca and Vicini, 1998).

Miniature EPSCs (mEPSCs) were recorded in presence of tetrodotoxin (TTX; 1 μM). Amino-phosphonovaleric acid (APV) and NBQX were not included in the ACSF. Results were analyzed off-line using the mini analysis program written by Justin Lee (Synaptosoft Inc., Decatur, GA). Data were collected using pClamp 9 software (Axon Instrument, Foster City, CA). Analysis was performed off-line with Clampfit 9.0 software (Axon Instruments).

Current-clamp experiments were performed using mutant and WT mice at 4 and 8 weeks of age. These current-clamp experiments required an internal solution containing the same chemicals as described above with the exception of QX-314 which was omitted and 130 Cs^+ methanesulphonate was replaced by 130 K+- gluconate. The ACSF contained a low Mg^{2+} concentration of $MgCl_2$ (0.1 mM), bicuculline (20 μM), picrotoxin (50 μM), CGP-52,532 (10 μM), strychnine (1 μM), and NBQX (5 μM).

Morphological identification of CA1 PCs

In some experiments, the recording pipette was filled with 2 mM Lucifer Yellow. The slices were removed from the chamber after recordings and fixed in 4% paraformaldehyde in a 0.1 M phosphate buffer solution (PBS; 0.1 M, pH 7.2) for 1 to 3 days. Slices were then washed with dimethyl-sulfoxide for 1 h. An LSM 510 confocal laser-scanning microscope (Zeiss, Germany) was used to visualize the CA1 PCs using 10× and 40× water immersion objectives. A three-dimensional structure of the neurons was obtained from the z-series data using the confocal system software. The scanned neurons were reconstructed with Adobe Photoshop7.0 (San Jose, CA) and the dendritic branches were counted manually.

Immunoblotting

Mice were sacrificed under anesthesia using isoflurane, in agreement with the guidelines of the Canadian Council of Animal Care. The hippocampal region (CA1 area) from each hemisphere was dissected on ice and homogenized by dounce tissue homogenizer

using ice-cold TEVP lysis buffer (10 mM Tris-HCl, 5 mM Sodium fluoride (NaF), 5 mM Sodium orthovanadate (Na_3VO_4), 5 mM ethylenediaminetetracetic acid (EDTA), pH 7.4). The hippocampal tissue of 24 different animals (12 mutant and 12 WT mice) was pooled in two different groups. For the NR2A and NR2B subunits, the CA1 regions from 24 different animals (four mutant and four WT mice at 2, 4, and 8 weeks of age) were dissected on ice and homogenized by dounce tissue homogenizer using ice-cold TEVP lysis buffer (10 mM Tris-HCl, 5 mM sodium fluoride (NaF), 5 mM sodium Orthovanadate (Na_3VO_4), 5 mM EDTA, pH 7.4. The lysed tissue was centrifuged at 5000 g for 10 min at 4°C. Twenty-four animals at 2, 4, and 8 weeks of age (12 mutant and 12 WT mice) were also used for the PSD-95 protein measurement.

The pellet (P1) containing nuclei and other debris was discarded and the supernatant (S1) was collected. The S1 was then centrifuged at 15,000 rpm for 15 min at 4°C and the resulting pellet (P2) was collected by discarding the supernatant (S2). The collected pellet (P2) was dissolved in ice-cold TEVP buffer containing a Mini-EDTA free protease inhibitor cocktail tablet (Roche, Basel, Switzerland), 1 mM phenylmethylsulphonyl fluoride, 1% Nonidet P-40, 0.5% Sodium deoxycholate and 0.1% SDS. Protein concentration was determined using a BCA protein assay and bovine serum albumin was used as a standard (Pierce, Biotechnology Inc., Rockford, IL).

Fifty micrograms of membrane proteins from GlyT1+/− and WT mice were diluted with sample loading buffer (10% SDS, 100 μM dithiothreitol (DTT), 10% glycerol (v/v), 0.001% bromophenol blue, 25 mM Tris pH 6.8) and boiled for 3 min at 95°C. The proteins were separated in 7.5% SDS-polyacrylamide gel. Subsequently, proteins were transferred to a polyvinylidene difluoride (PVDF) membrane using a mini trans-blot cell (Bio-Rad, Hercules CA). Membranes were then blocked with 5% nonfat milk in tris-buffered saline (TBS; 50 mM Tris pH 8.0, 148 mM NaCl) for 1 h at room temperature.

Membranes were incubated overnight at 4°C with primary antibodies diluted in 5% nonfat milk in TBS. The antibody dilution used was 1:1000 for rabbit polyclonal anti-NR2A antibodies; 1:7500 for rabbit polyclonal anti-NR2B antibodies; 1:4000 for rabbit polyclonal anti-PSD-95 antibodies; 1:5000 for rabbit polyclonal anti-GAPDH antibodies. The antibodies for NR2A, NR2B and GAPDH were purchased from Abcam, Cambridge, MA, whereas the antibody for PSD-95 was purchased from Cell Signaling Technology, Beverly, MA.

The membranes were washed 3 times in TBS containing 0.1% NP-40 for a total of 20 min, and then incubated with goat antirabbit IgG secondary antibody which is conjugated with horseradish peroxidase (1:3000; Santa Cruz Biotechnology, Inc, CA) for 1 h at room temperature. The membranes were washed again and then incubated in ECL solution (Amersham Biosciences, Baie d'Urfé, QC, Canada). The bands were visualized on Amersham Hyperfilm (Amersham Biosciences).

Immunohistochemistry

GlyT1+/− and age matching WT mice (4 and 8 weeks of age) were anesthetized with an overdose of pentobarbital (60 mg/kg) and intracardiacally perfused with 4% paraformaldehyde in PBS solution. After 30 min postfixation at 4°C, the brain was put into 30% sucrose/PBS solution until it sunk. The brain was then frozen at −80°C. The brain was sliced with a cryostat (Leica CM 3050S, Nassloch, Germany) to obtain hippocampal coronal slices of 14 μm. The slices were quenched with 50 mM NH_4Cl in PBS for 30 min and permeabilized with 0.2% triton and 0.25% fish gelatin in PBS for 30 min to enhance the penetration of the primary antibody and reduce nonspecific binding. The slices were then incubated with a mouse antisynaptophysin (1:750; Sigma) and guinea pig anti-VGLUT 1, 2, 3 (VGLUTs; 1:500; Millipore/Chemicon, Temecula, CA) primary antibodies in 0.25% gelatin and 0.2% triton PBS solution (PBSGT) overnight at 4°C. The slices were then rinsed thoroughly in PBSGT and subsequently incubated with secondary antibodies: Cy3-conjugated goat antimouse IgG (1:500; Jackson ImmunoResearch Laboratories, Inc., West Grove, PA) and an FITC-conjugated goat antiguinea pig (1:250; Jackson ImmunoResearch) in PBSGT for 2 h at room temperature. Slices were rinsed and mounted with Vectashield mounting medium (Vector Laboratories Inc., Burlingame, CA). Control slices, minus the primary antibodies were examined for background staining.

Confocal microscopy and imaging

We acquired fluorescent images of hippocampal slices using an LSM 510 confocal laser-scanning microscope (Zeiss, Germany) with a 63× oil-immersion objective (numerical aperture 1.4) at the resolution of 1024 × 1024 pixels. The stratum pyramidale of the CA1 region of the hippocampus were scanned twice to optimize the signal-to-noise ratio. Three parallel regions of each slice were selected for quantification and the density of clusters was determined by using Image J software (NIH, Bethesda, MD).

Statistical analysis

Student's t tests (two-tailed) or Kolmogorov-Smirnov two-sample test were used to determine the statistical significance of the results. All values are

TABLE I. Decay time constants of NMDAR EPSCs in GlyT1+/− and WT mice

	Control					Ifenprodil
(*n*)	τ_s (ms)	τ_f (ms)	A_s (%)	A_f (%)	τ_{mean} (ms)	τ_{mean} (ms)
2 weeks						
WT (18)	648 ± 49.33	114.0 ± 12.74	26.4 ± 2.18	73.6 ± 2.19	234.7 ± 13.93	151.0 ± 8.80 (7)
GlyT1+/− (18)	457 ± 30.20*	71.8 ± 4.85*	29.5 ± 2.23	70.5 ± 2.28	185.9 ± 10.9*	151.6 ± 9.60 (13)
3 weeks						
WT (18)	654 ± 55.33	111.9 ± 9.48	21.4 ± 2.16	75.2 ± 2.16	205.3 ± 10.92	161.2 ± 10.03 (9)
GlyT1+/− (19)	548 ± 7.20*	83.4 ± 1.37*	20.8 ± 0.61	79.2 ± 0.58	171.6 ± 2.14*	165.4 ± 8.15 (15)
4 weeks						
WT (15)	563 ± 28.53	84.74 ± 4.48	18.3 ± 1.87	81.6 ± 1.68	167.7 ± 5.58	122.1 ± 4.40 (6)
GlyT1+/− (20)	465 ± 31.50*	71.31 ± 3.77*	17.2 ± 1.84	82.8 ± 1.84	139.3 ± 6.91*	124.9 ± 5.94 (9)
8 weeks						
WT (18)	559 ± 27.47	83.89 ± 3.43	14.9 ± 1.68	85.1 ± 1.68	152.4 ± 5.45	115.6 ± 6.10 (7)
GlyT1+/− (18)	411 ± 20.20*	76.44 ± 2.78*	19.6 ± 1.68	80.4 ± 1.88	138.2 ± 3.90*	123.8 ± 14.01 (7)

Values are mean ± SEM. NMDAR EPSCs were recorded in absence (control) and presence of ifenprodil (3 μM). The slow and fast decay components are designated by τ_s and τ_f, respectively, and the weighted time constant by τ mean.
*Significant difference between WT and GlyT1+/− mice ($p < 0.05$).

expressed as means ± SEM, and a *P* value of <0.05 was considered significant.

RESULTS

Biophysical properties of NMDAR EPSCs in GlyT1+/− and WT mice during postnatal development

Previous data from our laboratory showed that in GlyT1+/− mice (12-13 weeks of age), the glycine modulatory site of the NMDAR at the synapse is saturated as suggested by the finding that exogenous application of glycine (10 μM) or D-serine (10 μM) does not modify the amplitude of NMDAR EPSC, whereas the same dose of glycine enhances NMDAR EPSC amplitude by approximately 40% in WT mice (Tsai et al., 2004). We have also previously reported that NMDAR EPSCs in GlyT1+/− mice (12-13 weeks of age) have faster decay kinetics compared to their age matching WT mice (Martina et al., 2005). We recorded NMDAR EPSCs in hippocampal CA1 PCs from both GlyT1+/− and WT mice at 2, 3, 4, and 8 weeks of age in order to explore whether this difference originates early in the postnatal period.

No significant differences were noted in the 10-90% rise time of NMDAR EPSCs between mutant and WT mice at 2 (GlyT1+/−: 18.03 ± 1.86 ms, $n = 20$; WT: 21.6 ± 2.45 ms, $n = 11$), 3 (GlyT1+/−: 26.51 ± 5.83 ms, $n = 11$; WT: 24.01 ± 7.02 ms, $n = 12$), 4 (GlyT1+/−: 26.7 ± 3.9 ms, $n = 21$; WT: 22.1 ± 3.4 ms, $n = 9$), and 8 (GlyT1+/−: 18.36 ± 2.22 ms, $n = 7$; WT: 19.6 ± 2.6 ms, $n = 7$) weeks of age. However, the averaged τ_s and τ_f of GlyT1 ± mice at all ages are consistently faster than those of WT mice (Table I). The weighted time constant is significantly faster in GlyT1+/− compared to that of WT mice (Figs. 1A and 1B; Table I). From these data, we cannot conclude that this is a higher expression of NR2A or a lower expression of NR2B subunits in the CA1 region of mutant mice, however, one could argue that this possibility should be addressed.

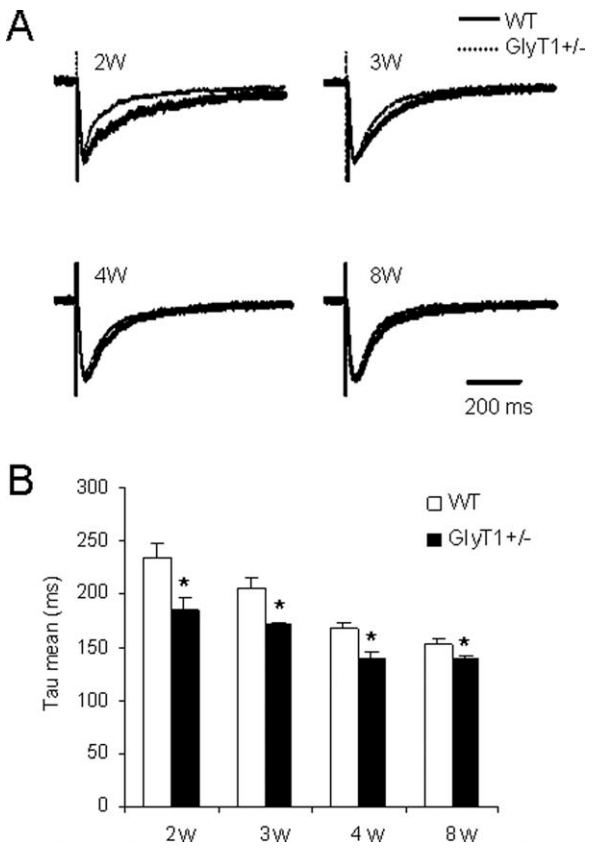

Fig. 1. Biophysical properties of NMDAR EPSCs recorded from CA1 PCs of GlyT1+/− and WT mice. **A**: Traces of NMDAR EPSCs recorded from CA1 PCs of GlyT1+/− (dashed line) and WT (thick line) mice at 2 (2W), 3 (3W), 4 (4W), and 8 (8W) weeks of age. **B**: Histogram showing the weighted time constants (τ_{mean}) of NMDAR EPSCs of CA1 PCs in GlyT1+/− (full bar) and WT mice (empty bar) at 2, 3, 4, and 8 postnatal weeks. *Indicates statistically significant differences in the τ_{mean} between GlyT1+/− and WT mice ($P < 0.05$).

Antagonistic effect of Ifenprodil on NMDAR EPSCs in GlyT1+/− and WT mice during postnatal development

A limited number of drugs can selectively distinguish between certain subunits of NMDARs, of which

ifenprodil is the most characterized. This drug has an IC_{50} that is approximately 400-fold lower for NR2B subunit compared to that of other NMDAR subunits (Williams, 1993). The antagonistic effect of ifenprodil on NMDAR EPSCs correlates with developmental changes in NMDAR composition such that NMDAR activity in immature neurons is almost completely inhibited by ifenprodil (Kew, Richards, Mutel, and Kemp, 1998; Sinor et al., 2000). Because higher levels of endogenous glycine in GlyT1+/− mice could reduce the antagonistic effect of ifenprodil, we used 3 μM of ifenprodil, a concentration that is glycine independent (Legendre and Westbrook, 1991).

Immunoblotting for NR2A, NR2B, PSD-95 in the CA1 region in GlyT1+/− and WT mice during postnatal development

We found that the reduction in the amplitude of NMDAR EPSCs induced by ifenprodil is significantly smaller in GlyT1+/− mice at 2, 3, 4 and 8 weeks of ages compared to their WT littermates ($P < 0.05$; Figs. 2A and 2B). This occurrence may reflect a lower expression of NR2B in mutant mice. Nevertheless, ifenprodil significantly reduces the NMDAR EPSC amplitudes of CA1 PCs in GlyT1+/− mice by 51.99 ± 5.60% ($n = 12$; $P < 0.05$) at 2 weeks, 45.01 ± 2.51% ($n = 23$; $P < 0.05$) at 3 weeks, 38.13 ± 4.32% ($n = 14$; $P < 0.05$) at 4 weeks, and 32.61 ± 5.61% ($n = 8$; $P < 0.05$) at 8 weeks of age, as well we noted further reduction of NMDAR EPSC amplitudes of WT by 67.91 ± 4.63% ($n = 18$; $P < 0.05$) at 2 weeks, 57.66 ± 2.99% ($n = 14$; $P < 0.05$) at 3 weeks, 52.05 ± 5.17% ($n = 12$; $P < 0.05$) at 4 weeks, and 47.15 ± 4.66% ($n = 10$; $P < 0.05$) at 8 weeks of age.

Since NR2B-containing NMDARs have slower decay kinetics compared to NR2A-containing NMDARs, we speculate that ifenprodil could also reduce the τ_{mean} and consequently accelerate NMDAR EPSC decay. Indeed, we find that ifenprodil drastically reduces the values of the τ_{mean} in both GlyT1+/− and WT mice at all ages examined (Fig. 2C and Table I). However, the τ_{mean} of WT mice significantly reduces upon ifenprodil treatment compared GlyT1+/− mice ($P < 0.05$).

Differences observed in the antagonistic effect of ifenprodil on NMDAR EPSC amplitudes and the decay kinetics between the two types of mice suggest a lower expression of NR2B or a higher expression of NR2A in GlyT1+/− mice. To test this hypothesis, we performed immunoblotting experiments to measure NR2A and NR2B protein expression in the CA1 region of the hippocampus of GlyT1+/− and WT mice at 2, 4, and 8 weeks of age (Fig. 3). Consistent with the literature, our results show that NR2B protein expression remains relatively unchanged during postnatal development (Liu, Murray, and Jones, 2004; von Engelhardt, Doganci, Seeburg, and Monyer, 2009),

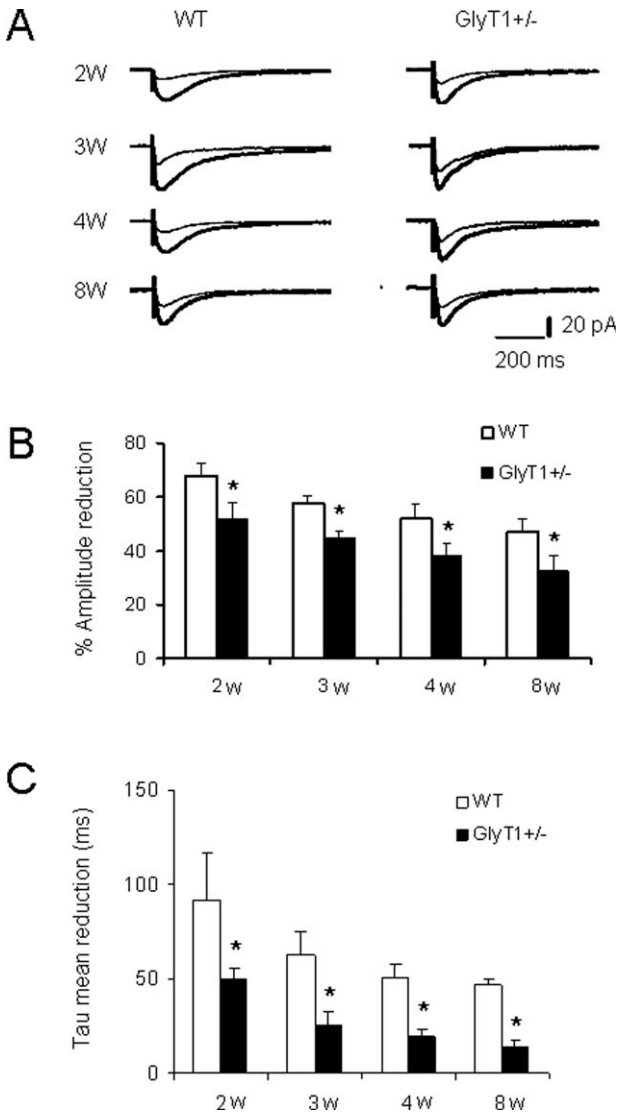

Fig. 2. Effect of ifenprodil on NMDAR EPSCs of CA1 PCs in GlyT1+/− and WT mice. **A**: Traces of NMDAR EPSCs recorded from CA1 PCs in GlyT1+/− and WT mice in the absence (thick line) and presence of ifenprodil (3 μM; thin line). **B**: Histogram showing the effect of ifenprodil on the amplitude of NMDAR EPSCs in GlyT1+/− (full bar) and WT mice (empty bar) at 2, 3, 4, and 8 weeks of age. Note that the antagonistic effect of ifenprodil on NMDAR EPSC amplitude decreased with age in both GlyT1+/− and WT mice. **C:** Histogram showing the effect of ifenprodil on Tau mean reduction in GlyT1+/− (full bar) and WT mice (empty bar) at 2, 3, 4, and 8 weeks of age. *Indicates statistically significant differences between GlyT1+/− and WT mice ($P < 0.05$).

whereas NR2A protein expression becomes more prominent with ages (Monyer et al., 1992; Monyer, et al., 1994; Stocca and Vicini, 1998). However, when comparing GlyT1+/− mice to WT littermates of the same age, no significant difference is observed in the protein expression of either NR2A or NR2B; $n = 4$ for each group.

We also investigated PSD-95 expression, a protein that exists at the excitatory postsynaptic region is known to be coupled with NMDARs, especially with

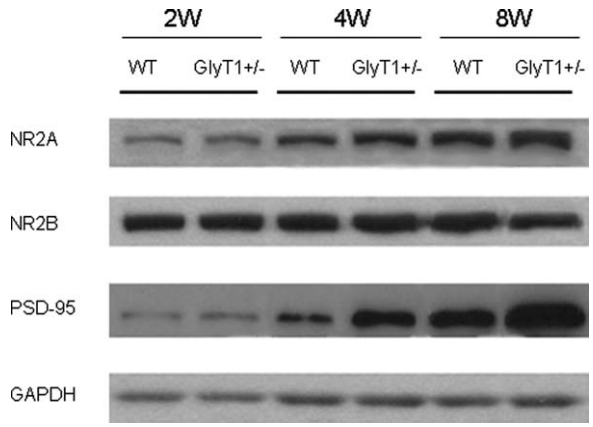

Fig. 3. Expression of NR2A and NR2B protein in whole hippocampus of GlyT1+/− and WT mice. Whole hippocampus (n = 24) was used to determine the protein expression of NR2A, NR2B, and PSD-95 in mutant and WT mice at 2, 4, and 8 weeks of age. During postnatal development, NR2A and PSD-95 protein expression increases with age. When comparing both types of mice, we find a higher expression of PSD-95 protein in GlyT1+/− mice, whereas there is no obvious increase in NR2A protein expression. NR2B protein expression remains relatively constant. GAPDH was used as an internal control for protein loading.

those containing the NR2A subunit (Elias et al., 2008). This protein plays a pivotal role in preventing NR2A-containing NMDARs to internalize (Lin et al., 2004; Rao and Craig, 1997). In both types of mice, we found a PSD-95 protein expression increase with age during postnatal development. Moreover, compared to WT mice, there is a significantly higher protein expression of PSD-95 in mutants at 4 and 8 weeks of age (n = 4 for each group; Fig. 3). Overall, our data suggest that PSD-95 in mutant mice anchors NR2A-containing NMDARs at the synapse, thereby explaining the faster decay kinetics observed in GlyT1+/− animals.

Morphological properties of CA1 PCs in GlyT1+/− and WT mice during postnatal development

We previously reported that there was no significant difference in the morphology of CA1 PCs between GlyT1+/− and WT adult mice (12-13 weeks of age). However, in that case no quantification of dendritic branches was performed (Martina et al., 2005; Martina et al., 2005). To further characterize the morphological properties of CA1 PCs in GlyT1+/− and WT mice during postnatal development (2, 3, 4, and 8 weeks of age) we labeled them by filling the recording electrodes with Lucifer Yellow. We obtained the morphology of CA1 PCs using confocal microscopy following the electrophysiological recordings.

Our findings show that the number of apical and basal dendritic segments in CA1 PCs is significantly higher in mutant compared to WT mice at 2, 3, and 4 weeks of age (Fig. 4 and Table II), whereas no significant difference is observed at 8 weeks of age. These data suggest that during the early stages of postnatal development, CA1 PCs in GlyT1+/− mice undergo morphological changes which may impact network excitability.

Miniature excitatory postsynaptic currents in GlyT1+/− and WT mice during postnatal development

We studied mEPSCs to investigate whether in GlyT1+/− mice, changes in the number of functional synaptic contacts could occur during postnatal development. The averaged amplitude of mEPSCs indicates a single quantum of transmitter release at an individual synapse (or number of postsynaptic glutamatergic receptors), whereas their frequency corresponds to the number/density of synapses (El Husseini et al., 2000) or to the probability of release (Hopf, Waters, Mehta, and Smith, 2002).

Our findings indicate that in GlyT1+/− mice, the average of mEPSC amplitudes (pA) at 2 weeks (7.89 ± 0.24, n = 8), 3 weeks (7.95 ± 0.29, n = 11), 4 weeks (8.67 ± 0.24, n = 7), and 8 weeks (8.71 ± 0.27, n = 6) of age is not significantly different compared to WT mice at 2 (8.26 ± 0.35, n = 6; $P > 0.05$), 3 (8.66 ± 0.30, n = 6; $P > 0.05$), 4 (8.64 ± 0.43, n = 10; $P > 0.05$), and 8 weeks (9.10 ± 0.24, n = 6; $P > 0.05$; Figs. 5A, 5B, and 5D and Supporting Information Fig. 1) of age. These results suggest that there is no difference in the number of glutamatergic postsynaptic receptors (AMPARs and NMDARs) between GlyT1+/− and WT mice.

Interestingly, our observations show that the frequency (Hz) of mEPSCs is significantly higher in GlyT1+/− mice at 4 (0.627 ± 0.06, n = 7) and 8 weeks (0.654 ± 0.07, n = 6) of age compared with their matching WT littermates (4 weeks: 0.455 ± 0.03, n = 10; $P < 0.05$; 8 weeks: 0.520 ± 0.06, n = 6; $P < 0.05$; Figs. 5A, 5C, and 5E and Supporting Information Fig. 2). In contrast, there is no significant difference in the frequency of mEPSCs at 2 and 3 weeks of age between GlyT1+/− (2 weeks: 0.310 ± 0.05, n = 8; 3 weeks: 0.560 ± 0.07, n = 11) and WT mice (2 weeks: 0.284 ± 0.07, n = 6; $P > 0.05$; 3 weeks: 0.470 ± 0.08, n = 6; $P > 0.05$; Kolmogorov-Smirnov test).

We conducted the paired-pulse (PP) protocol to determine the release probability to test whether the high frequency of mEPSC in mutant mice (at 4 and 8 weeks of age) was not due to a higher release of glutamate from presynaptic terminals, (Hsia, Malenka, and Nicoll, 1998; Wasling, Hanse, and Gustafsson, 2004). We performed PP stimulation to Schaffer collateral terminals using a pulse interval of 40, 80, and 100 ms and recorded the NMDAR-mediated paired-response in CA1 PCs. We found that there was a significantly higher PP ratio in GlyT1+/− mice at 3, 4, and 8 weeks of age compared to those of WT litter-

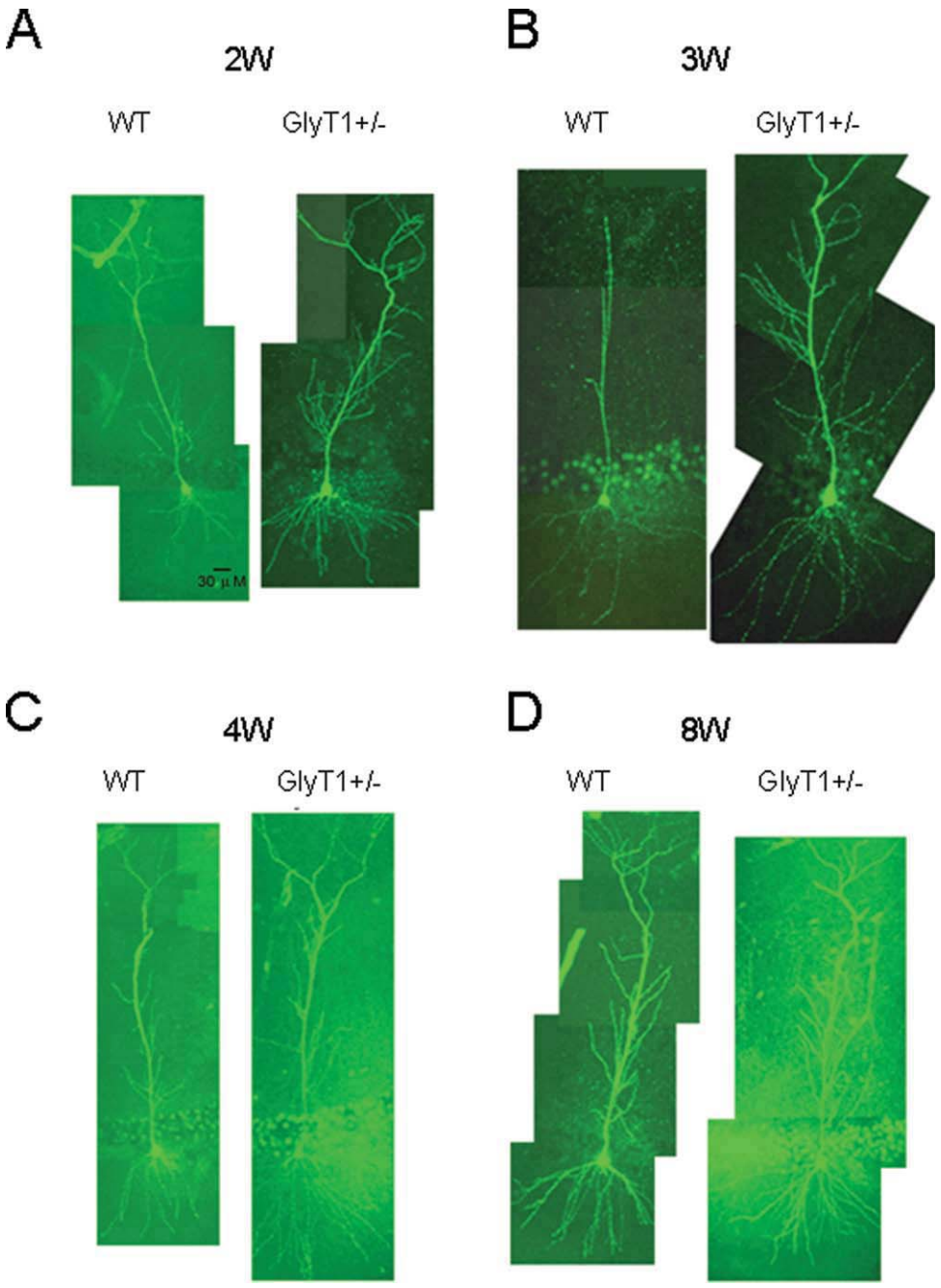

Fig. 4. Morphological properties of CA1 PCs in GlyT1+/− and WT mice during different stages of postnatal development (**A**–**D**) Lucifer yellow-labeled CA1 PCs obtained from GlyT1+/− and WT mice at 2, 3, 4 and 8 weeks of age showed that mutants have a higher number of dendritic branching than WT littermates (see Table II for details). [Color figure can be viewed in the online issue, which is available at wileyonlinelibrary.com.]

mates (Supporting Information Fig. 1; $P < 0.05$). This suggests a lower release probability in GlyT1+/− compared to WT mice (Supporting Information Fig. 1) and may argue in favor of a higher density of synapses in mutant mice at 4 and 8 weeks of age. It is worth mentioning that the above findings, such as the amplitude and frequency of the mEPSCs as well as the paired pulse ratio are not reversed by the GlyR antagonist strychnine at the dose of 1 μM but are blocked by APV (20 μM).

Synaptic organization in GlyT1+/− and WT mice

NMDAR activation is required for early synapse formation and neural development. Blocking NMDAR

TABLE II. Morphological properties of CA1 PCs labeled with Lucifer yellow in GlyT1+/− and WT mice during different stages of postnatal development

	Apical dendrites				Basal dendrites		
(n)	II	III	IV	V	I	II	III
2 weeks							
WT	8.42 ± 1.05 (12‖	11.83 ± 1.55 (12)	6.45 ± 0.62 (11)	7.33 ± 1.76 (3)	3.90 ± 0.31 (10)	7.40 ± 0.58 (10)	11.89 ± 1.41 (9)
GlyT1+/−	6.25 ± 0.99 (16)	16.25 ± 1.54 (16)*	10.88 ± 2.32 (16)*	5.78 ± 0.94 (9)	4.36 ± 0.28 (11)	9.45 ± 0.59 (11)*	12.88 ± 1.36 (8)
3 weeks							
WT	6.67 ± 1.86 (3)	10.0 ± 1.0 (2)	4 (1)	n/a	3.50 ± 1.50 (2)	9.50 ± 3.5 (2)	10.40 ± 4.0 (2)
GlyT1+/−	12.78 ± 0.9 (9)*	21.44 ± 1.5 (9)*	9.63 ± 1.55 (8)	5.0 ± 1.0 (2)	4.62 ± 0.52 (8)	11.75 ± 1.68 (8)	14.88 ± 0.67 (8)*
4 weeks							
WT	8.0 ± 0.82 (6)	10.17 ± 1.62 (6)	4.33 ± 0.76 (6)	5.75 ± 0.85 (4)	3.80 ± 0.37 (5)	9.00 ± 0.89 (5)	7.60 ± 1.33 (5)
GlyT1+/−	12.50 ± 2.1 6 (6)*	15.33 ± 1.84 (6)*	9.17 ± 1.64 (6)*	7.60 ± 1.21 (5)	4.20 ± 0.49 (5)	9.4 ± 1.33 (5)	14.0 ± 2.07 (5)*
8 weeks							
WT	7.00 ± 4.9 (7)	11.10 ± 1.12 (7)	6.86 ± 1.32 (7)	6.50 ± 0.26 (2)	4.28 ± 0.43 (7)	10.14 ± 0.19 (7)	11.86 ± 0.19 (7)
GlyT1+/−	8.86 ± 2.20 (7)	13.14 ± 1.14 (7)	7.14 ± 1.03 (7)	7.00 ± 0.54 (2)	4.14 ± 0.46 (7)	9.0 ± 0.82 (7)	13.43 ± 1.46 (7)

Values are mean ± SEM. CA1 PCs labeled with Lucifer yellow were recorded frome GlyT1+/− and WT mice at 2, 3, 4, and 8 weeks of age. We identified (I) as the first dendritic segments leaving the soma, (II) the dendritic segments branching from (I), (III) the dendritic segments branching from (II), etc.
*Significant difference between GlyT1+/− and WT mice ($P < 0.05$).

activity inhibits dendritic arbor growth (Rajan and Cline, 1998). We performed double immunostaining using synaptophysin, a protein involved in the presynaptic exocytosis machinery and vesicular glutamate transporter subtypes (VGLUT1, 2, 3; VGLUTs), the specific molecular markers of glutamatergic vesicles to compare the density of excitatory synapses at Schaffer collaterals/CA1 synapses between GlyT1+/− and WT mice at 4 and 8 weeks of age. Colocalization of synaptophysin and VGLUTs formed bright fluorescent clusters that are uniformly distributed in the *stratum pyramidale* in both GlyT1+/− and WT mice (Figs. 6A–6D). The density of synaptophysin and VGLUTs clusters as well the density of coclusters is much higher in GlyT1+/− mice at 4 and 8 weeks of age compared with that of WT littermates (Supporting Information Figs. 4A–4C). These findings suggest a higher density of excitatory presynaptic terminals and further suggest a higher number of synaptic contacts at Schaffer collaterals/CA1 synapses in mutant mice.

Neuronal excitability in GlyT1+/− and WT mice

Thus far, the results of our study suggest that in the hippocampal network of mutant mice, there is a higher level of synaptic contact which could lead to higher excitability. In the last series of experiments, we sought to investigate this hypothesis by assessing the firing frequency of action potentials of CA1 PCs at 4 and 8 weeks in both types of mice. If indeed the neuronal network is more excitable in mutant mice, the frequency of action potentials should increase when compared to WT mice. We recorded CA1 pyramidal neurons in current-clamp mode. Cs methanesulfonate was not used because it would inhibit potassium channels. For these experiments, K+ gluconate was used instead of Cs methanesulfonate. As illustrated in Figures 7A and 7B, there is a significant increase in the frequency of action potentials in GlyT1+/− mice at 4 and 8 weeks. Interestingly, we do not find any significant change in resting membrane potential. Moreover, in both GlyT1+/− and WT mice at 8 weeks of age, the firing frequency was reduced upon bath application of the competitive NMDAR antagonist, APV (Fig. 7C).

DISCUSSION

In this study, using GlyT1+/− mice, we investigated the impact of chronic high levels of endogenous glycine on important parameters of glutamatergic neurotransmission involving NMDARs. Our results indicate that throughout postnatal development, compared with control animals, mutant mice undergo major changes with respect to the pharmacological properties and functionality of NMDARs in CA1 PCs. More precisely, differences observed in GlyT1+/− mice are the following: (1) a faster decay kinetic of NMDAR EPSCs; (2) a reduction of the antagonistic effect of ifenprodil; (3) a higher protein expression of PSD-95; (4) an increase in dendritic branching and glutamatergic presynaptic terminals; (5) a higher frequency of mEPSC; and (6) higher network excitability.

During early postnatal development, NMDARs at the synapse are predominantly composed of NR2B subunits, whereas NR2A subunits are gradually inserted into the synapse at maturation (Monyer, et al., 1994; Sheng et al., 1994; Flint et al., 1997), a transition that is reflected by the acceleration of the decay kinetics of NMDAR EPSCs (Hestrin, 1992; Cathala, Misra, and Cull-Candy, 2000) and the loss of ifenprodil sensitivity (Tovar and Westbrook, 1999; Williams, 2001). Accordingly, in both mutant and WT mice, we observed a developmental decrease in the decay kinetics of NMDAR EPSCs, however, GlyT1+/− mice exhibited significantly faster decay kinetics compared with WT littermates at all studied ages. Consist-

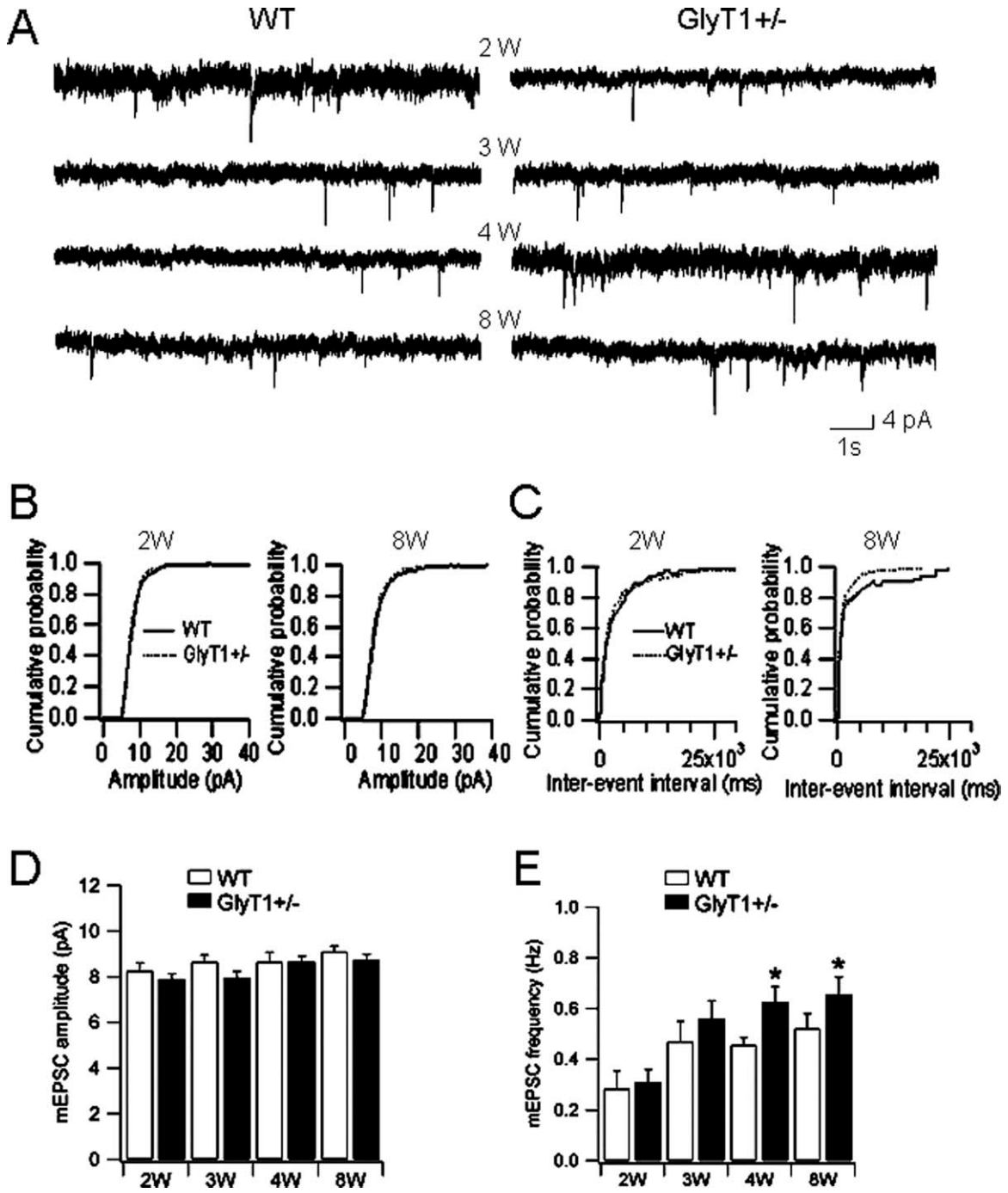

Fig. 5. mEPSCs of CA1 PCs in GlyT1+/− and WT mice during postnatal development. **A**: mEPSCs recorded from CA1 PCs of GlyT1+/− (right panel) and WT (left panel) mice at 2, 3, 4, and 8 weeks of age. **B** and **D**: Both types of mice had no significant difference in mEPSCs amplitudes at 2, 3, 4, and 8 weeks of age. **C** and **E**: The frequency of mEPSCs was significantly higher in mutants at 4 and 8 weeks of age. *Indicates statistically significant differences between GlyT1+/− and WT mice ($P < 0.05$).

ent with previous reports (Monyer et al., 1994; Sheng et al., 1994; Flint et al., 1997), the results of our immunoblotting experiments confirmed an increase in NR2A protein expression with age in both GlyT1+/− and WT mice. However, our results did not reveal any significant difference in protein expression of NR2A between GlyT1+/− and WT mice at any studied time points. Our observation that decay kinetics of NMDAR EPSCs is faster in mutant mice cannot be explained by a difference in NR2A or NR2B protein expression. In agreement with other studies (Stocca and Vicini, 1998), our data from immunoblotting experiments revealed that NR2B protein expression remains relatively constant despite the faster decay kinetics of

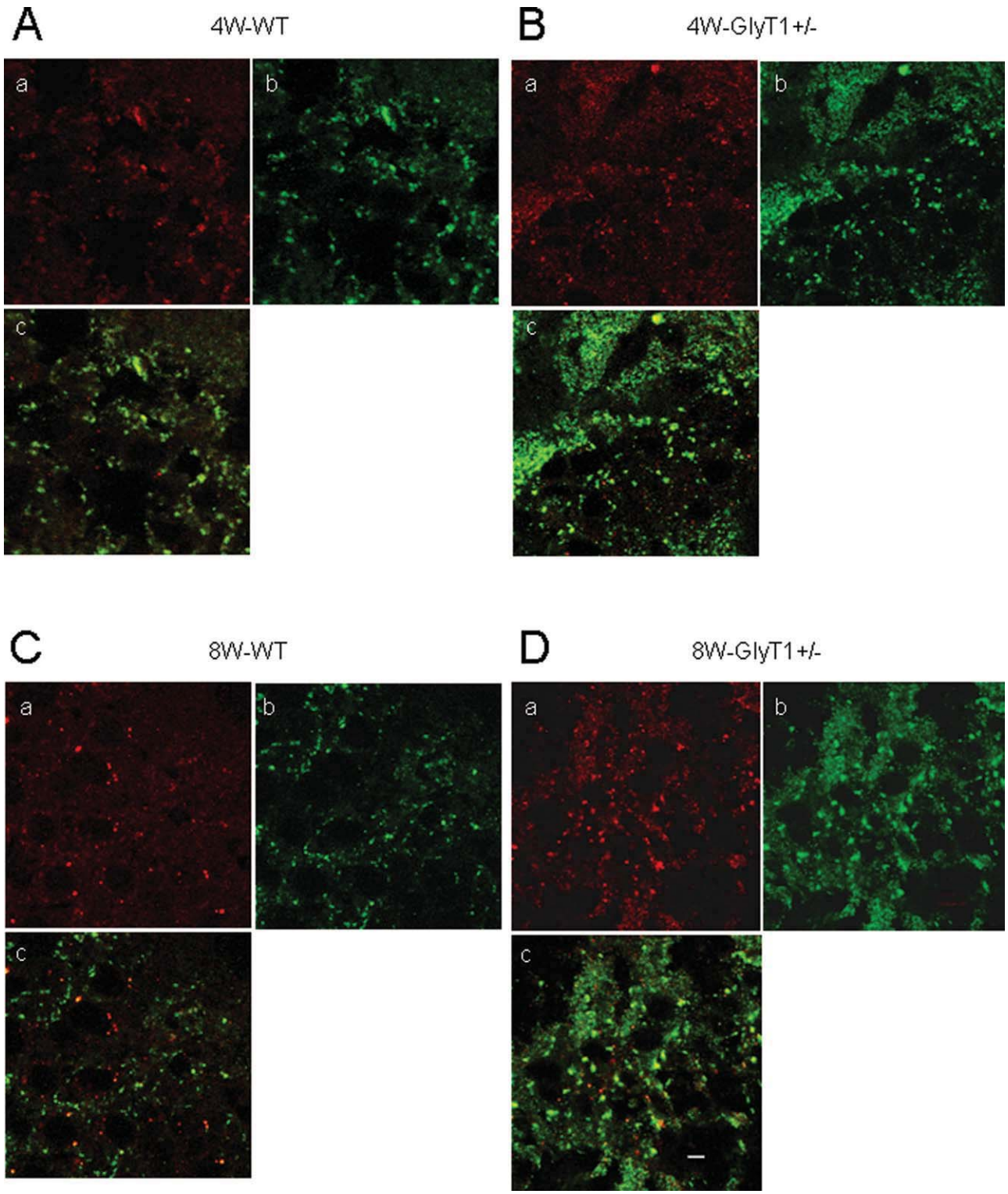

Fig. 6. Immunohistochemistry detection of synaptophysin and VGLUTs in the *stratum pyramidale* of GlyT1+/− and WT mice at 4 and 8 weeks of age. **A–D**: Immunofluorescent confocal sections of CA1 PCs layer in the hippocampus, double labeled for (a) synaptophysin, (b) VGLUTs in GlyT1+/− and WT mice at 4 and 8 weeks of age and (c) merged image. Scale bar is 5 μm. [Color figure can be viewed in the online issue, which is available at wileyonlinelibrary.com.]

NMDAR EPSCs and the decrease in ifenprodil sensitivity, suggesting that NR2A subunits are inserted into these synapses forming heteromerics complexes.

A core component of the postsynaptic density at excitatory synapses during postnatal development is that PSD-95 protein expression parallels that of

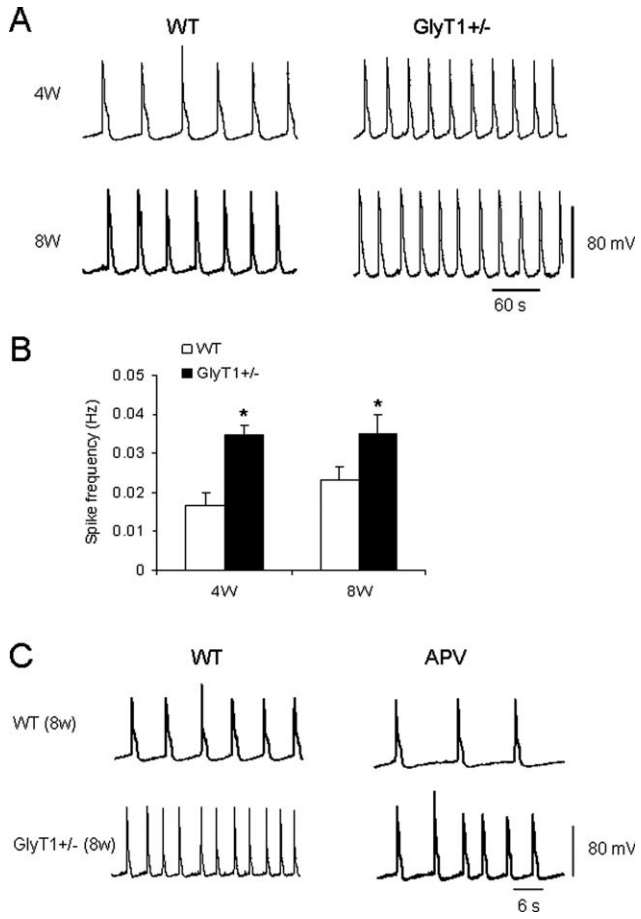

Fig. 7. Neuronal excitability in GlyT1+/− and WT mice. **A**: Traces representing spontaneous NMDAR-dependent activity in CA1 PCs recorded in current-clamp mode. We observed a higher frequency of action potentials in mutants compared to WT mice at 4 and 8 weeks of age. **B**: Bar histogram shows a significantly higher frequency of action potentials in GlyT1+/− mice compared with WT littermates. **C**: The action potential frequency in mutants (8W) and WT animals (8W) was reduced upon bath application of NMDAR antagonist APV (50 μM). *Indicates statistically significant differences between GlyT1+/− and WT mice ($P < 0.05$).

NR2A. Indeed, a past study shows that over-expression of PSD-95 in cultured cerebellar granule cells promotes NR2A synaptic expression (Losi et al., 2003). Therefore, the faster decay kinetics observed in GlyT1+/− mice could be explained by the increased expression of PSD-95, which is involved in the trafficking and stabilization of NR2A subunits at the synapse (Elias et al., 2008). Previous reports have already shown the molecular mechanisms that could be involved in the phenomenon (Tovar and Westbrook, 1999; Fox, Henley, and Isaac, 1999; MacDonald, Jackson, and Beazely, 2006; Hoffmann, Gremme, Hatt, and Gottmann, 2000).

We observed that throughout postnatal development, GlyT1+/− mice exhibited a higher number of dendritic branching (Fig. 4 and Table II) as well as a higher density of excitatory glutamatergic synapses (Fig. 6 and Supporting Information Fig. 4) in the CA1 region of the hippocampus compared to WT mice. Indeed, the results of our investigation are consistent with those of previous reports in which focal application of glutamate lead to a dramatic increase in the length of the shaft filopodia leading to dendritic growth and branching during neuronal development (Portera-Cailliau, Pan, and Yuste, 2003). Moreover, numerous studies highlight that neuronal activity mediated by the NMDARs promotes dendritic arbor growth (Niell, Meyer, and Smith, 2004; Sin, Haas, Ruthazer, and Cline, 2002), whereas blocking NMDARs reduces dendritic growth (Rajan and Cline, 1998). Recently, Cline and coworkers showed that NR2A and NR2B subunits have specific functions in the morphological development of tectal neurons in the living Xenopus and found that NR2A but not NR2B increased dendritic branch clusters (Ewald, Keuren-Jensen, Aizenman, and Cline, 2008). GlyT1+/− mice exhibited a higher degree of synaptic connectivity (Fig. 5 and Supporting Information Fig. 2) as well as a higher degree of network excitability in the CA1 region of the hippocampus compared to WT mice (Fig. 7). Several mechanisms could explain this occurrence. First, the higher synaptic expression of NR2A in mutants endows the NMDAR channel with a higher open probability (Po; 5-fold higher) as well as a higher peak open probability than NR2B-containing NMDARs (Erreger et al., 2005; Mellor, Nicoll, and Schmitz, 2002), resulting in a higher degree of synaptic excitability. Second, NR2A-containing NMDARs have a faster glutamate unbinding rate (30-fold faster) than NR2B-containing NMDARs; this attribute reduces the degree of receptor desensitization, thereby enabling the receptor to respond promptly to repetitive synaptic signal inputs, especially during high frequency stimulation (Erreger et al., 2005). Finally, the morphological findings in our study, e.g., the higher number of postsynaptic dendritic branching in GlyT1+/− mice and higher density of synapses, provide the postsynaptic neurons with a stronger ability for integration of multiple synaptic inputs by temporal and spatial summation, altogether facilitating the generation of action potentials (Xu, Ye, Poo, and Zhang, 2006; Hausser, Spruston, and Stuart, 2000; Magee, 2000). These mechanisms could explain, at least in part, the higher network excitability encountered in mutant mice.

One of the more interesting and intriguing findings of our work is that there is a higher expression of PSD-95 protein in the hippocampus of mutant compared with WT mice. PSD-95 has been particularly studied because in the central nervous system it is one of the major constituents of excitatory PSDs (Chen et al., 2005), and it is directly involved in synaptic plasticity (Migaud et al., 1998). It is well documented that this abundant postsynaptic scaffold, PSD-95, regulates the formation of excitatory

synapses. PSD-95 is essential for synaptogenesis and for neurons to establish correct connectivity. PSD-95 protein plays major roles in synapse organization and function (Funke, Dakoji, and Bredt, 2005). Overexpression of PSD-95 in neurons is associated with modifications in the properties of synaptic transmission and has also been proposed to affect synapse maturation and stabilization (El-Husseini, Schnell, Chetkovich, Nicoll and Bredt, 2000) and, thus, synapse number. Acute knockdown of PSD-95 reduces the development of synaptic structures (Ehrlich, Klein, Rumpel, and Malinow, 2007), and PSD-95 mutant mice exhibit variations in spine densities in several brain regions (Vickers et al., 2006).

Morphological properties of excitatory synapses upon over-expression of PSD-95 reveals important new functions of this protein in regulating spine synapse formation and plasticity. The expression of PSD-95 resulted in changes in spine shape, a marked increase of the spine volume, and an enlargement of the PSD, resulting in the formation of synapses with complex and perforated or segmented PSDs. The effect is very significant because, on average, the PSD area increased by a factor of six to eight, and the spine volume increased about 3-fold, emphasizing the close relationship existing between spine volume and PSD size (Harris and Stevens, 1989). Moreover, PSD-95 has diverse synaptic functions. One such function is to interact with membrane proteins and regulate their synaptic localization. PSD-95 seems to stabilize interacting membrane proteins at synapses by suppressing their lateral diffusion or internalization (Roche et al., 2001; Prybylowski et al., 2005). In addition to its role in protein trafficking, PSD-95 can regulate the functional properties of interacting membrane proteins, as shown by PSD-95-dependent changes in the gating of NMDA receptors (Lin et al., 2006).

Glycinergic neurotransmission is known to control motor functions and arousal states (Legendre, 2001; Betz et al., 2006) while glutamatergic neural pathways are involved in the regulation of cognitive processes such as learning and memory storage (Citri and Malenka, 2008; MacDonald, Jackson, and Beazely, 2006; Citri and Malenka, 2008). Presumably, GlyT1 disruption affects one or more of these processes. This could likely play a role in glycine encephalopathy (GE) pathophysiology. This disease is believed to result from a shortage of an enzyme that normally breaks down glycine in the body. This defect allows excess glycine to build up in tissues and organs, particularly in the brain, leading to serious medical complications. Typically, neonatal individuals suffering from GE display a number of neuropsychological symptoms including hypotonia, convulsions and even coma, while mental retardation, psychomotor limitations, and behavioral abnormalities are usually observed later during childhood (Hayasaka et al., 1982; Hayasaka, Tada, Fueki, and Aikawa, 1990; Agamanolis, Potter, and Lundgren, 1993; Kikuchi, Motokawa, Yoshida, and Hiraga, 2008). Most GE individuals die as newborns but the rare ones that survive demonstrate lack of neurological development, intractable seizures and many neuropsychiatric symptoms including learning disabilities and mental retardation (Applegarth and Toone, 2001; Toone, et al., 2003; Applegarth and Toone, 2004).

GlyT1 knockout mouse models (Gomeza et al., 2003; Tsai et al., 2004) suggest the intriguing possibility that mutations in the corresponding gene in humans could cause GE. It is tempting to speculate that many of the symptoms present in GE patients could be explained by some of the new findings that we are reporting in our study. However, it is worth mentioning that all animal models of any human disease must be viewed with some scepticism. Indeed, homozygous GlyT1 deficient mice display most of the symptoms observed in individuals with GE, however, one would argue that the phenotype of heterozygous GlyT1 mice is relatively normal compared with WT mice. Indeed, GlyT1+/− are quite healthy, rarely exhibit seizures and perform relatively well in the Morris Water Maze (Tsai et al., 2004). However, GlyT1+/− mice have higher levels of glycine in their brain, blood, and urine, similar to what has been reported in GE patients that survive until early adulthood (Agamanolis, Potter, and Lundgren, 1993; Hardingham, 2009; Gomeza et al., 2003). NMDAR antagonists as a first line treatment for patients with GE have been used by several groups (Ohya, et al., 1991). The results of our investigations are indeed in support of this approach. However, one should never minimize the potential side effects of this type of treatment and the use of NMDAR antagonists should be done with caution.

ACKNOWLEDGMENTS

The authors thank Dr J.T. Coyle for providing the transgenic mice and Adrian Wong for his critical input. We also thank Chris Métivier and Jonathan Boyd for technical assistance.

REFERENCES

Adams RH, Sato K, Shimada S, Tohyama M, Puschel AW, Betz H. 1995. Gene structure and glial expression of the glycine transporter GlyT1 in embryonic and adult rodents. J Neurosci 15:2524–2532.

Agamanolis DP, Potter JL, Lundgren DW. 1993. Neonatal glycine encephalopathy: biochemical and neuropathologic findings. Pediatr Neurol 9:140–143.

Anson LC, Chen PE, Wyllie DJ, Colquhoun D, Schoepfer R. 1998. Identification of amino acid residues of the NR2A subunit that control glutamate potency in recombinant NR1/NR2A NMDA receptors. J Neurosci 18:581–589.

Applegarth DA, Toone JR. 2001. Nonketotic hyperglycinemia (glycine encephalopathy): laboratory diagnosis. Mol Genet Metab 74:139–146.

Applegarth DA, Toone JR. 2004. Glycine encephalopathy (nonketotic hyperglycinaemia) : review and update. J Inherit Metab Dis 27:417–422.
Aragon C, Lopez-Corcuera B. 2005. Glycine transporters: crucial roles of pharmacological interest revealed by gene deletion. Trends Pharmacol Sci 26:283–286.
Berger AJ, Dieudonne S, Ascher P. 1998. Glycine uptake governs glycine site occupancy at NMDA receptors of excitatory synapses. J Neurophysiol 80:3336–3340.
Bergeron R, Meyer TM, Coyle JT, Greene RW. 1998. Modulation of N-methyl-D-aspartate receptor function by glycine transport. Proc Natl Acad Sci U S A 95:15730–15734.
Betz H, Gomeza J, Armsen W, Scholze P, Eulenburg V. 2006. Glycine transporters: essential regulators of synaptic transmission. Biochem Soc Trans 34:55–58.
Betz H, Laube B. 2006. Glycine receptors: Recent insights into their structural organization and functional diversity. J Neurochem 97:1600–1610.
Borowsky B, Mezey E, Hoffman BJ. 1993. Two glycine transporter variants with distinct localization in the CNS and peripheral tissues are encoded by a common gene. Neuron 10:851–863.
Cathala L, Misra C, Cull-Candy S. 2000. Developmental profile of the changing properties of NMDA receptors at cerebellar mossy fiber-granule cell synapses. J Neurosci 20:5899–5905.
Chen X, Vinade L, Leapman RD, Petersen JD, Nakagawa T, Phillips TM, Sheng M, Reese TS. 2005. Mass of the postsynaptic density and enumeration of three key molecules. Proc Natl Acad Sci U S A 102:11551–11556.
Citri A, Malenka RC. 2008. Synaptic plasticity: Multiple forms, functions, and mechanisms. Neuropsychopharmacology 33:18–41.
Cull-Candy S, Brickley S, Farrant M. 2001. NMDA receptor subunits: Diversity, development and disease. Curr Opin Neurobiol 11:327–335.
Ehrlich I, Klein M, Rumpel S, Malinow R. 2007. PSD-95 is required for activity-driven synapse stabilization. Proc Natl Acad Sci U S A 104:4176–4181.
El Husseini AE, Schnell E, Chetkovich DM, Nicoll RA, Bredt DS. 2000. PSD-95 involvement in maturation of excitatory synapses. Science 290:1364–1368.
Elias GM, Elias LA, Apostolides PF, Kriegstein AR, Nicoll RA. 2008. Differential trafficking of AMPA and NMDA receptors by SAP102 and PSD-95 underlies synapse development. Proc Natl Acad Sci U S A 105:20953–20958.
Erreger K, Dravid SM, Banke TG, Wyllie DJ, Traynelis SF. 2005. Subunit-specific gating controls rat NR1/NR2A and NR1/NR2B NMDA channel kinetics and synaptic signalling profiles. J Physiol 563:345–358.
Eulenburg V, Armsen W, Betz H, Gomeza J. 2005. Glycine transporters: essential regulators of neurotransmission. Trends Biochem Sci 30:325–333.
Ewald RC, Keuren-Jensen KR, Aizenman CD, Cline HT. 2008. Roles of NR2A and NR2B in the development of dendritic arbor morphology in vivo. J Neurosci 28:850–861.
Flint AC, Maisch US, Weishaupt JH, Kriegstein AR, Monyer H. 1997. NR2A subunit expression shortens NMDA receptor synaptic currents in developing neocortex. J Neurosci 17:2469–2476.
Fox K, Henley J, Isaac J. 1999. Experience-dependent development of NMDA receptor transmission. Nat Neurosci 2:297–299.
Funke L, Dakoji S, Bredt DS. 2005. Membrane-associated guanylate kinases regulate adhesion and plasticity at cell junctions. Annu Rev Biochem 74:219–245.
Gabernet L, Pauly-Evers M, Schwerdel C, Lentz M, Bluethmann H, Vogt K, Alberati D, Mohler H, Boison D. 2005. Enhancement of the NMDA receptor function by reduction of glycine transporter-1 expression. Neurosci Lett 373:79–84.
Gomeza J, Hulsmann S, Ohno K, Eulenburg V, Szoke K, Richter D, Betz H. 2003. Inactivation of the glycine transporter 1 gene discloses vital role of glial glycine uptake in glycinergic inhibition. Neuron 40:785–796.
Gomeza J, Ohno K, Hulsmann S, Armsen W, Eulenburg V, Richter DW, Laube B, Betz H. 2003. Deletion of the mouse glycine transporter 2 results in a hyperekplexia phenotype and postnatal lethality. Neuron 40:797–806.
Guastella J, Brecha N, Weigmann C, Lester HA, Davidson N. 1992. Cloning, expression, and localization of a rat brain high-affinity glycine transporter. Proc Natl Acad Sci U S A 89:7189–7193.
Hardingham GE. 2009. Coupling of the NMDA receptor to neuroprotective and neurodestructive events. Biochem Soc Trans 37:1147–1160.
Harris KM, Stevens JK. 1989. Dendritic spines of CA 1 pyramidal cells in the rat hippocampus: serial electron microscopy with reference to their biophysical characteristics. J Neurosci 9:2982–2997.
Hausser M, Spruston N, Stuart GJ. 2000. Diversity and dynamics of dendritic signaling. Science 290:739–744.
Hayasaka K, Narisawa K, Satoh T, Tateda H, Metoki K, Tada K, Hiraga K, Aoki T, Kawakami T, Akamatsu H, Matsuo N. 1982. Glycine cleavage system in ketotic hyperglycinemia: a reduction of H-protein activity. Pediatr Res 16:5–7.
Hayasaka K, Tada K, Fueki N, Aikawa J. 1990. Prenatal diagnosis of nonketotic hyperglycinemia: enzymatic analysis of the glycine cleavage system in chorionic villi. J Pediatr 116:444–445.
Hestrin S. 1992. Developmental regulation of NMDA receptor-mediated synaptic currents at a central synapse. Nature 357:686–689.
Hoffmann H, Gremme T, Hatt H, Gottmann K. 2000. Synaptic activity-dependent developmental regulation of NMDA receptor subunit expression in cultured neocortical neurons. J Neurochem 75:1590–1599.
Hopf FW, Waters J, Mehta S, Smith SJ. 2002. Stability and plasticity of developing synapses in hippocampal neuronal cultures. J Neurosci 22:775–781.
Hsia AY, Malenka RC, Nicoll RA. 1998. Development of excitatory circuitry in the hippocampus. J Neurophysiol 79:2013–2024.
Imamura Y, Ma CL, Pabba M, Bergeron R. 2008. Sustained saturating level of glycine induces changes in NR2B-containing-NMDA receptor localization in the CA1 region of the hippocampus. J Neurochem 105:2454–2465.
Johnson JW, Ascher P. 1987. Glycine potentiates the NMDA response in cultured mouse brain neurons. Nature 325:529–531.
Jursky F, Nelson N. 1996. Developmental expression of the glycine transporters GLYT1 and GLYT2 in mouse brain. J Neurochem 67:336–344.
Kew JN, Richards JG, Mutel V, Kemp JA. 1998. Developmental changes in NMDA receptor glycine affinity and ifenprodil sensitivity reveal three distinct populations of NMDA receptors in individual rat cortical neurons. J Neurosci 18:1935–1943.
Kikuchi G, Motokawa Y, Yoshida T, Hiraga K. 2008. Glycine cleavage system: reaction mechanism, physiological significance, and hyperglycinemia. Proc Jpn Acad Ser B Phys Biol Sci 84:246–263.
Kirsch J. 2006. Glycinergic transmission. Cell Tissue Res 326:535–540.
Kleckner NW, Dingledine R. 1988. Requirement for glycine in activation of NMDA-receptors expressed in Xenopus oocytes. Science 241:835–837.
Lau CG, Zukin RS. 2007. NMDA receptor trafficking in synaptic plasticity and neuropsychiatric disorders. Nat Rev Neurosci 8:413–426.
Legendre P. 2001. The glycinergic inhibitory synapse. Cell Mol Life Sci 58:760–793.
Legendre P, Westbrook GL. 1991. Ifenprodil blocks N-methyl-D-aspartate receptors by a two-component mechanism. Mol Pharmacol 40:289–298.
Lin Y, Jover-Mengual T, Wong J, Bennett MV, Zukin RS. 2006. PSD-95 and PKC converge in regulating NMDA receptor trafficking and gating. Proc Natl Acad Sci U S A 103:19902–19907.
Lin Y, Skeberdis VA, Francesconi A, Bennett MV, Zukin RS. 2004. Postsynaptic density protein-95 regulates NMDA channel gating and surface expression. J Neurosci 24:10138–10148.
Liu QR, Lopez-Corcuera B, Mandiyan S, Nelson H, Nelson N. 1993. Cloning and expression of a spinal cord- and brain-specific glycine transporter with novel structural features. J Biol Chem 268:22802–22808.
Liu QR, Nelson H, Mandiyan S, Lopez-Corcuera B, Nelson N. 1992. Cloning and expression of a glycine transporter from mouse brain. FEBS Lett 305:110–114.
Liu XB, Murray KD, Jones EG. 2004. Switching of NMDA receptor 2A and 2B subunits at thalamic and cortical synapses during early postnatal development. J Neurosci 24:8885–8895.
Lopez-Corcuera B, Alcantara R, Vazquez J, Aragon C. 1993. Hydrodynamic properties and immunological identification of the sodium- and chloride-coupled glycine transporter. J Biol Chem 268:2239–2243.
Losi G, Prybylowski K, Fu Z, Luo J, Wenthold RJ, Vicini S. 2003. PSD-95 regulates NMDA receptors in developing cerebellar granule neurons of the rat. J Physiol 548:21–29.
MacDonald JF, Jackson MF, Beazely MA. 2006. Hippocampal long-term synaptic plasticity and signal amplification of NMDA receptors. Crit Rev Neurobiol 18:71–84.
Magee JC. 2000. Dendritic integration of excitatory synaptic input. Nat Rev Neurosci 1:181–190.
Martina M, Turcotte ME, Halman S, Tsai G, Tiberi M, Coyle JT, Bergeron R. 2005. Reduced glycine transporter type 1 expression

leads to major changes in glutamatergic neurotransmission of CA1 hippocampal neurones in mice. J Physiol 563:777–793.
Mayer ML, Vyklicky L Jr, Clements J. 1989. Regulation of NMDA receptor desensitization in mouse hippocampal neurons by glycine. Nature 338:425–427.
Mellor J, Nicoll RA, Schmitz D. 2002. Mediation of hippocampal mossy fiber long-term potentiation by presynaptic Ih channels. Science 295:143–147.
Migaud M, Charlesworth P, Dempster M, Webster LC, Watabe AM, Makhinson M, He Y, Ramsay MF, Morris RG, Morrison JH, O'Dell TJ, Grant SG. 1998. Enhanced long-term potentiation and impaired learning in mice with mutant postsynaptic density-95 protein. Nature 396:433–439.
Monyer H, Burnashev N, Laurie DJ, Sakmann B, Seeburg PH. 1994. Developmental and regional expression in the rat brain and functional properties of four NMDA receptors. Neuron 12:529–540.
Monyer H, Sprengel R, Schoepfer R, Herb A, Higuchi M, Lomeli H, Burnashev N, Sakmann B, Seeburg PH. 1992. Heteromeric NMDA receptors: Molecular and functional distinction of subtypes. Science 256:1217–1221.
Niell CM, Meyer MP, Smith SJ. 2004. In vivo imaging of synapse formation on a growing dendritic arbor. Nat Neurosci 7:254–260.
Ohya Y, Ochi N, Mizutani N, Hayakawa C, Watanabe K. 1991. Nonketotic hyperglycinemia: treatment with NMDA antagonist and consideration of neuropathogenesis. Pediatr Neurol 7:65–68.
Papadia S, Hardingham GE. 2007. The dichotomy of NMDA receptor signaling. Neuroscientist 13:572–579.
Portera-Cailliau C, Pan DT, Yuste R. 2003. Activity-regulated dynamic behavior of early dendritic protrusions: evidence for different types of dendritic filopodia. J Neurosci 23:7129–7142.
Prybylowski K, Chang K, Sans N, Kan L, Vicini S, Wenthold RJ. 2005. The synaptic localization of NR2B-containing NMDA receptors is controlled by interactions with PDZ proteins and AP-2. Neuron 47:845–857.
Rajan I, Cline HT. 1998. Glutamate receptor activity is required for normal development of tectal cell dendrites in vivo. J Neurosci 18:7836–7846.
Rao A, Craig AM. 1997. Activity regulates the synaptic localization of the NMDA receptor in hippocampal neurons. Neuron 19:801–812.
Roche KW, Standley S, McCallum J, Dune Ly C, Ehlers MD, Wenthold RJ. 2001. Molecular determinants of NMDA receptor internalization. Nat Neurosci 4:794–802.
Sans N, Petralia RS, Wang YX, Blahos J, Hell JW, Wenthold RJ. 2000. A developmental change in NMDA receptor-associated proteins at hippocampal synapses. J Neurosci 20:1260–1271.
Schell MJ, Molliver ME, Snyder SH. 1995. D-serine, an endogenous synaptic modulator: localization to astrocytes and glutamate-stimulated release. Proc Natl Acad Sci U S A 92:3948–3952.
Sheng M, Cummings J, Roldan LA, Jan YN, Jan LY. 1994. Changing subunit composition of heteromeric NMDA receptors during development of rat cortex. Nature 368:144–147.
Sin WC, Haas K, Ruthazer ES, Cline HT. 2002. Dendrite growth increased by visual activity requires NMDA receptor and Rho GTPases. Nature 419:475–480.
Sinor JD, Du S, Venneti S, Blitzblau RC, Leszkiewicz DN, Rosenberg PA, Aizenman E. 2000. NMDA and glutamate evoke excitotoxicity at distinct cellular locations in rat cortical neurons in vitro. J Neurosci 20:8831–8837.
Smith KE, Borden LA, Hartig PR, Branchek T, Weinshank RL. 1992. Cloning and expression of a glycine transporter reveal colocalization with NMDA receptors. Neuron 8:927–935.
Stephenson FA. 2001. Subunit characterization of NMDA receptors. Curr Drug Targets 2:233–239.
Stocca G, Vicini S. 1998. Increased contribution of NR2A subunit to synaptic NMDA receptors in developing rat cortical neurons. J Physiol 507(Pt 1):13–24.
Thomson AM, Walker VE, Flynn DM. 1989. Glycine enhances NMDA-receptor mediated synaptic potentials in neocortical slices. Nature 338:422–424.
Toone JR, Applegarth DA, Levy HL, Coulter-Mackie MB, Lee G. 2003. Molecular genetic and potential biochemical characteristics of patients with T-protein deficiency as a cause of glycine encephalopathy (NKH). Mol Genet Metab 79:272–280.
Tovar KR, Westbrook GL. 1999. The incorporation of NMDA receptors with a distinct subunit composition at nascent hippocampal synapses in vitro. J Neurosci 19:4180–4188.
Tsai G, Ralph-Williams RJ, Martina M, Bergeron R, Berger-Sweeney J, Dunham KS, Jiang Z, Caine SB, Coyle JT. 2004. Gene knockout of glycine transporter 1: Characterization of the behavioral phenotype. Proc Natl Acad Sci U S A 101:8485–8490.
Vickers CA, Stephens B, Bowen J, Arbuthnott GW, Grant SG, Ingham CA. 2006. Neurone specific regulation of dendritic spines in vivo by post synaptic density 95 protein (PSD-95). Brain Res 1090:89–98.
von Engelhardt J, Doganci B, Seeburg PH, Monyer H. 2009. Synaptic NR2A- but not NR2B-containing NMDA receptors increase with blockade of ionotropic glutamate receptors. Front Mol Neurosci 2:1–14.
Wasling P, Hanse E, Gustafsson B. 2004. Developmental changes in release properties of the CA3-CA1 glutamate synapse in rat hippocampus. J Neurophysiol 92:2714–2724.
Waxman EA, Lynch DR. 2005. N-methyl-D-aspartate receptor subtypes: Multiple roles in excitotoxicity and neurological disease. Neuroscientist 11:37–49.
Williams K. 1993. Ifenprodil discriminates subtypes of the N-methyl-D-aspartate receptor: selectivity and mechanisms at recombinant heteromeric receptors. Mol Pharmacol 44:851–859.
Williams K. 2001. Ifenprodil, a novel NMDA receptor antagonist: Site and mechanism of action. Curr Drug Targets 2:285–298.
Xu NL, Ye CQ, Poo MM, Zhang XH. 2006. Coincidence detection of synaptic inputs is facilitated at the distal dendrites after long-term potentiation induction. J Neurosci 26:3002–3009.
Yee BK, Balic E, Singer P, Schwerdel C, Grampp T, Gabernet L, Knuesel I, Benke D, Feldon J, Mohler H, Boison D. 2006. Disruption of glycine transporter 1 restricted to forebrain neurons is associated with a procognitive and antipsychotic phenotypic profile. J Neurosci 26:3169–3181.
Zafra F, Aragon C, Olivares L, Danbolt NC, Gimenez C, Storm-Mathisen J. 1995. Glycine transporters are differentially expressed among CNS cells. J Neurosci 15:3952–3969.
Zafra F, Gomeza J, Olivares L, Aragon C, Gimenez C. 1995. Regional distribution and developmental variation of the glycine transporters GLYT1 and GLYT2 in the rat CNS. Eur J Neurosci 7:1342–1352.

Journal of Neurochemistry

JOURNAL OF NEUROCHEMISTRY | 2008 | 105 | 2454–2465 doi: 10.1111/j.1471-4159.2008.05324.x

Sustained saturating level of glycine induces changes in NR2B-containing-NMDA receptor localization in the CA1 region of the hippocampus

Yukio Imamura,[1] Chun-Lei Ma,[1] Mohan Pabba and Richard Bergeron

Department of Cellular and Molecular Medicine, Department of Psychiatry, University of Ottawa, Ottawa Health Research Institute, Ottawa, Ontario, Canada

Abstract

Post-synaptic actions of glycine are terminated by specialized transporters. There are two genes encoding glycine transporters, GlyT1 and GlyT2. Glycine acts as a co-agonist at *N*-methyl-D-aspartate glutamatergic receptors (NMDARs). Blockage of GlyT1 enhances NMDAR function by controlling ambient glycine concentrations. Using whole-cell patch-clamp recordings of acute hippocampal slices, we investigated NMDAR kinetics of CA1 pyramidal neurons of mice expressing 50% of GlyT1 (GlyT1+/–). In this study, we report that the glycine modulatory site of the NMDAR at CA1 synapses is saturated in GlyT1+/– but not in wild-type (WT) mice. We also found that the effect of ifenprodil, a highly selective NR2B-containing-NMDAR antagonist, is significantly reduced at CA1 synapses in GlyT1+/– compared to WT mice while immunoblotting experiments do not show significant differences for NR1, NR2A-B-C-D subunits in both types of mice, suggesting alteration in NR2B-containing-NMDAR localization under a state of chronic saturating level of endogenous glycine. Using a pharmacological approach with MK-801 and DL-TBOA, we discriminated synaptic *vis-à-vis* extra-synaptic NMDARs. We found that NR2B-containing-NMDARs are expressed at a higher level in the extra-synaptic area of CA1 pyramidal neurons from GlyT1+/– compared to WT mice. Our results demonstrate that chronic saturating level of glycine induces significant changes in NMDAR localization and kinetic. Therefore, results from our study should help to gain a better understanding of the role of glycine in pathological conditions.

Keywords: extra-synaptic NMDA receptors, glutamate, ifenprodil, whole-cell patch-clamp recording.

J. Neurochem. (2008) **105**, 2454–2465.

At central synapses, glutamate is the main excitatory neurotransmitter. Once released from pre-synaptic terminals, glutamate activates a number of different glutamatergic receptors one of which is the NMDAR. NMDARs are oligomeric ligand-gated ion channels formed by the assembly of different subunits. Biophysical studies of NMDARs outline its complex pharmacology with multiple modulatory binding sites. NMDARs are critical players in excitatory synaptic transmission, synaptic plasticity, and have specialized characteristics including voltage-dependent block by magnesium, calcium permeability, and slow deactivation kinetics. One of the peculiar properties of NMDARs is that they require the binding of two different agonists for gating. In addition to glutamate, glycine/D-serine acts as obligatory co-agonists for NMDAR activation.

In the forebrain, NMDARs contain two essential NR1 subunits paired with two NR2 subunits, implying four subunits within the functional channel (Laube *et al.* 1998). The NR1 subunit is expressed throughout the CNS and is essential for NMDAR-channel activity. The NR2 subunit, when co-expressed with NR1, determines the pharmacological profile, the gating properties, and the Mg^{2+} sensitivity (Vicini *et al.* 1998). There are four NR2 subunits (A–D), but NR2A and NR2B (which form high conductance channels) predominate in the forebrain (Yamakura and Shimoji 1999). At the synapse, NR2B subunits are more abundant early in

Received October 11, 2007; revised manuscript received February 25, 2008; accepted February 27, 2008.

Address correspondence and reprint requests to Richard Bergeron, Ottawa Health Research Institute, Department of Cellular and Molecular Medicine, Department of Psychiatry, University of Ottawa, 725 Parkdale Avenue, Ottawa, Ontario, Canada K1Y 4E9. E-mail: rbergeron@ohri.ca

[1]Both authors contributed equally to the manuscript.

Abbreviations used: ACSF, artificial cerebrospinal fluid; AMPAR, α-amino-3-hydroxy-5-methylisoxazole-4-propionic acid receptor; EPSC, excitatory post-synaptic current; GlyT1, glycine transporter type 1; GlyT1+/–, heterozygote mice for GlyT1 gene; NMDARs, *N*-methyl-D-aspartate glutamatergic receptors; TBS, Tris-buffered saline.

life, whereas NR2A expression increases with development. As the NR2A subunit produces NMDAR current with the fastest kinetics (Stocca and Vicini 1998), the increasing speed of NMDAR current decay kinetics over post-natal development is likely because of its increased expression (Vicini *et al.* 1998). NR1 and NR2 subunits harbor the glycine and glutamate binding sites, respectively (Monyer *et al.* 1992; Wafford *et al.* 1995; Ivanovic *et al.* 1998). Although the binding sites for glutamate and glycine are on different subunits, the presence of one influences the binding of the other (Regalado *et al.* 2001). Notably, it is the type of NR2 subunit co-assembled with NR1 that determines NMDAR affinity for glycine (Kew *et al.* 1998). Glycine has approximately a 10-fold higher affinity for NR2B-, NR2C-, or NR2D-containing than for NR2A-containing NMDARs (Danysz and Parsons 1998). Moreover, NMDARs are found not only at the synapse but also extra-synaptically (Clark and Cull-Candy 2002).

We have previously reported, using whole-cell voltage-clamp recordings, that the glycine modulatory site of the NMDAR is saturated in heterozygote mice for GlyT1 (GlyT1+/−) but not in WT mice, since the application of glycine (10 μM) did not enhance the amplitude of the isolated NMDAR current in GlyT1+/− while increasing the amplitude of the isolated NMDAR current by approximately 40% in WT mice (Tsai *et al.* 2004; Martina *et al.* 2005). We have also observed a significant reduction in the antagonistic effect of the highly NR1/NR2B-selective antagonist, ifenprodil, on the amplitude of the isolated NMDAR current in CA1 pyramidal neurons from GlyT1+/− compared to WT mice (Martina *et al.* 2005). Moreover, we found a faster kinetic of the synaptic NMDAR current in GlyT1+/− mice, suggesting a lower expression of NR2B or a higher expression of NR2A subunits in GlyT1+/− mice.

These results raise an important issue concerning the impact of sustained saturating level of glycine on NMDAR amplitude or kinetic. Does the saturating level of glycine promote a loss of NR2B-containing-NMDAR expression or a different ratio of NR2A/NR2B expression in the CA1 region of the hippocampus of GlyT1+/− compared to WT mice? Is there a differential compartmentalization or subcellular redistribution of NR2A/NR2B subunits between GlyT1+/− and WT mice? Using whole-cell patch-clamp recording of acute hippocampal slices from 11–12 weeks of age GlyT1+/− and WT mice, we investigated the impact of sustained saturating level of endogenous glycine on NMDAR localization and kinetic of CA1 pyramidal neurons.

Materials and methods

Genotyping

All genotyping of mice was performed using polymerase chain reaction (PCR) amplification of genomic DNA prepared from mouse tissue as described in our previous manuscript (Martina *et al.* 2005). Throughout our experimental series, only GlyT1+/− and their matching WT mice at 11–12 weeks of age were used.

Immunoblotting

Mice were killed under anesthesia using isoflurane, in agreement with the guidelines of the Canadian Council of Animal Care. The hippocampal region (CA1 area) from each hemisphere was dissected on ice and homogenized by dounce tissue homogenizer using ice-cold tobacco etch virus protease (TEVP) lysis buffer (10 mM Tris–HCl, 5 mM sodium fluoride (NaF), 5 mM sodium orthovanadate (Na_3VO_4), 5 mM Ethylenediaminetetracetic acid (EDTA), pH 7.4). The hippocampal tissue of 16 different animals (16 mutant and 16 WT mice) was pooled in two different groups. The lysed tissue was centrifuged 1000 *g* for about 5 min at 4°C. The pellet (P1) containing nuclei and other debris were discarded by collecting the supernatant (S1). S1 was subjected to centrifugation of 15 000 rpm, 15 min at 4°C and the resulting pellet (P2) was collected by discarding the supernatant (S2). The collected pellet was dissolved in ice-cold TEVP buffer containing complete, Mini-EDTA free protease inhibitor cocktail tablet (Roche, Basel, Switzerland), 1 mM phenylmethylsulphonyl fluoride, 1% Nonidet P-40, 0.5% sodium deoxycholate, 0.1% sodium dodecyl sulfate (SDS) and subjected to short centrifugation of 2–3 min at 15 000 rpm. After centrifugation, the supernatant (S3) were collected and protein concentration was determined using a BCA protein assay and bovine serum albumin as standard (Pierce Biotechnology, Inc., Rockford, IL, USA). Please note that the region of the hippocampus that was chosen for the immunoblotting since it is the whole-cell recordings were made from this brain area. NR1 antibodies were purchased from Cell Signaling Technology, Inc. (Danvers, MA, USA, Cat. No. 4204); NR2A, 2B and 2C antibodies were purchased from Abcam (Cambridge, MA, USA, Cat. No. ab14596, ab14400, ab110); NR2D antibodies were purchased from Santa Cruz Biotechnology, Inc. (Santa Cruz, CA, USA, Cat. No. sc-10727).

Fifty microgram aliquots of membrane proteins was diluted with sample loading buffer (10% SDS, 100 μM dithiothreitol, 10% glycerol, 0.001% (w/v) bromophenol blue, 25 mM Tris pH 6.8) and boiled at 95°C for 3 min. Boiled samples from WT and GlyT1+/− mice were randomly paired-wised and proteins were separated on 7.5% SDS-polyacrylamide gel and transferred to a polyvinylidene difluoride membrane using a trans-blot semi-dry transfer cell (Bio-Rad, Hercules CA, USA). Membranes were then blocked with 5% milk in Tris-buffered saline (50 mM Tris pH 8.0, 148 mM NaCl) for 1 h at 20°C. Subsequently, membranes were then incubated with primary antibodies diluted in 5% milk in Tris-buffered saline (TBS) (1 : 1000 for rabbit polyclonal anti-NR1 antibodies; 1 : 5000 for rabbit polyclonal anti-NR2A antibodies; 1 : 7500 for rabbit polyclonal anti-NR2B antibodies; 1 : 1000 for rabbit polyclonal anti NR2C antibodies; 1 : 500 for rabbit polyclonal anti-NR2D antibodies; 1 : 5000 for rabbit polyclonal anti-GAPDH antibodies) for overnight at 4°C, washed three times in TBS containing 0.1% NP-40 for a total of 20 min, incubated with horseradish peroxidase-conjugated secondary antibody (Santa Cruz Biotechnology, Cat. No. sc-2004) diluted in 5% milk in TBS (1 : 5000) for 1 h at 20°C and washed three times in TBS containing 0.1% NP-40 for a total of 20 min. Membranes were then incubated in enhanced chemiluminescence solution (Amersham Biosciences, Inc., Baie d'Urfée, QC, Canada) and bands visualized on Amersham Hyperfilm (Amersham Biosciences, Inc.).

Whole-cell patch-clamp recording

We performed the electrophysiological experiments using acute brain slices. Coronal brain slices (300 μm containing the hippocampus) were obtained from mice (11–12 weeks of age). Prior to decapitation, the animals were anesthetized with isofluorane in agreement with the guidelines of the Canadian Council of Animal Care. The brain was removed and placed in an oxygenated (95% O_2/5% CO_2) physiological solution, artificial cerebrospinal fluid (ACSF) at 4°C, containing (mM): NaCl (126), KCl (2.5), $MgCl_2$ (1), $NaHCO_3$ (26), NaH_2PO_4 (1.25), $CaCl_2$ (2) and D-glucose (10). The osmolarity of the ACSF was adjusted to 300 mOsmol-1 and the pH to 7.2. A block containing the region of interest was prepared, and sections (300 μm) were obtained with a vibrating microtome (Leica VT 1000S, Leica Microsystems GmbH, Wetzlar, Germany). The slices were stored for 1 h in an oxygenated chamber at room temperature prior to the experiments. The recordings were performed with borosilicate electrodes filled with a solution containing (in mM) Cs-methansufonate (120), TEA-Cl (10), HEPES (10), EGTA (0.6), $MgCl_2$ (2), Mg2-ATP (2), Na-GTP (0.5) and QX-314 (0.5). The pH was adjusted to 7.2 and the osmolarity to 280–290 mOsmol-1. The recording pipettes had a resistance of 3–6 MΩ when filled with this solution. The series resistance was monitored during the experiment and the data were discarded when the series resistance was changed more than 15% of the original level.

Voltage-clamp recordings were obtained with a Multiclamp 700A amplifier (Axon Instruments, Foster City, CA, USA) under visual control using differential interference contrast and infrared video microscopy (IR-DIC; Leica DMLFSA, Germany). Whole-cell currents were recorded at room temperature from individual pyramidal neurons of the CA1 region of the hippocampus voltage–clamped at −65 mV.

The CA3 input to CA1 pyramidal neurons, mediated by the Schaffer collaterals, is glutamatergic (Amaral and Witter 1989). Post-synaptic responses were evoked by electrical stimulation of the Schaffer collaterals with a bipolar microelectrode positioned in the stratum radiatum. The stimulation pulse was delivered every 15 s (i.e., 0.067 Hz) with the pulse duration of 100 μs. The stimulation intensity was set to obtain the excitatory post-synaptic current (EPSC) amplitude of 60–70 pA.

The recordings were first obtained in normal ACSF. To isolate the NMDAR-mediated EPSC, we used an ACSF containing a low concentration of $MgCl_2$ (0.1 mM) with osmolarity maintained by $CaCl_2$, and the α-amino-3-hydroxy-5-methylisoxazole-4-propionic acid receptor (AMPAR) antagonist 1,2,3,4-tetrahydro-6-nitro-2,3-dioxobenzoquinoxaline-7-sulphonamide (NBQX), the $GABA_A$ receptor antagonist picrotoxin, the $GABA_B$ receptor antagonist 3-[[(3,4-dichlorophenyl)methyl]amino]propyl]diethoxymethyl)phosphinic acid (CGP 52432), and the glycine receptor antagonist strychnine. When required, dizocilpine (MK-801) and amino-phosphoro-valeric acid (APV) were bath-applied.

To facilitate the blocking of synaptic NMDAR currents by MK-801, the interval of stimuli was changed from 15 to 5 s during MK-801 application. The concentration of drugs applied in the perfusate was (μM): NBQX (10), picrotoxin (50), CGP 52432 (10), strychnine (0.5), MK-801 (30), DL-TBOA (30) and ifenprodil (5). All drugs were purchased from Sigma–Aldrich, with the exception of DL-TBOA (Tocris, Bristol, UK). Baseline NMDAR currents were normalized by the average of 5 min control recordings (average of 20–25 traces).

Kinetic analysis was performed on averaged EPSCs (usually 20–25 consecutive traces). The rise time constants of NMDAR currents were measured by fitting the single exponential function by using Clampfit. The decay time constants were measured by fitting the exponential functions: $y = A_f e^{-t/\tau_f} + A_s e^{-t/\tau_s}$ for double and $y = A_1 \exp^{-t/\tau}$ for single exponential decay, where A is the amplitude, τ is the decay time constant, and the subscript f and s denote fast and slow components, respectively. Weighted time constants (τ_{mean}) were calculated using the equation: $\tau_{mean} = [A_f/(A_f + A_s)]\tau_f + [A_s/(A_s + A_f)]\tau_s$ (Stocca and Vicini 1998).

The Data were made with Microsoft Excel or Igor Pro (WaveMetrics, Inc.). Results are presented as means ± SE. Data were compared statistically by Student's *t*-tests and significance was defined as $p < 0.05$.

Results

We used an *in vivo* animal model with reduced expression of the GlyT1 gene. Since homozygote GlyT1-/− mice die during the first postnatal day (Gomeza *et al.* 2003; Tsai *et al.* 2004), only GlyT1+/− mice and their matching wild-type (WT) mice were used for this investigation. These transgenic mice (genetic background: C57Black6) are valuable models to investigate NMDAR amplitude and kinetic under a state of sustained saturating level of glycine.

No significant difference between GlyT1+/− and WT mice was observed in protein expression levels of NR1, NR2A-B-C-D in the hippocampus

The different antagonistic effect to ifenprodil to the amplitude of the NMDAR current raised one intriguing question. Could this lower antagonistic effect of ifenprodil on the amplitude of the NMDAR current be due to a lower expression of NR2B subunit between the two types of mice? In this first experimental series, we determined the level of NR2B but also for NR1, NR2A-C and D subunits. The level of expression of NR1, NR2A-B-C- D subunit proteins in the hippocampus in both types of mice between 11–12 weeks of age was investigated by western blot analysis using subunit specific antibodies. Our results did not reveal any significant difference in the level of protein expression for NR1, NR2A, NR2B, NR2C, and NR2D subunits between the two types of mice, WT ($n = 16$) and GlyT1+/− ($n = 16$) mice (Fig. 1) as is evident by the verification of internal marker GAPDH, suggesting that the abnormal high level of glycine does not promote any significant change in the level of expression of NR1-NR2A-B-C-D -containing-NMDAR subunit in the hippocampus of GlyT1+/− compared to WT mice.

Glycine modulatory site of NMDAR of CA1 pyramidal neurons was saturated in GlyT1+/− but not in WT mice

We have previously reported, using whole-cell voltage-clamp recordings, that the glycine modulatory site of NMDAR is

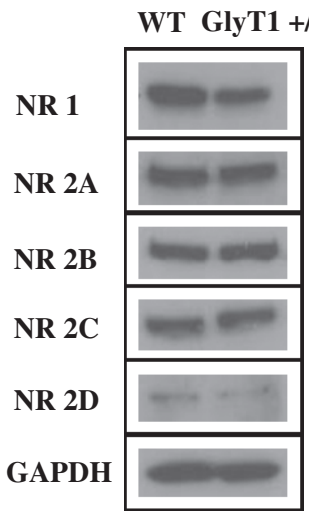

Fig. 1 Western blot analysis of hippocampus for NR2A and NR2B subunits between GlyT1+/– and WT mice. (a) NR1, NR2A, NR2B, NR2C, and NR2D immunoreactive bands. Western blot analysis of protein samples (50 μg) prepared from hippocampal CA1 region of GlyT1+/– and WT mice. The protein samples were separated on 7.5% SDS-polyacrylamide gels, transferred to PVDF membrane and probed with respective NMDAR subunit(s) primary antibodies. Note that no significant difference in protein expression levels for NMDAR subunits was detected between GlyT1+/– and WT mice (number of animals used: n = 16 for each).

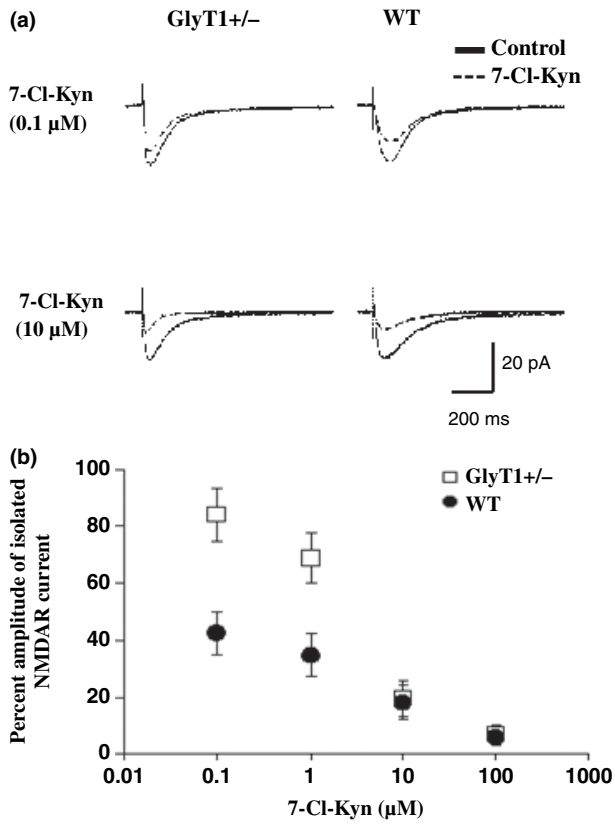

Fig. 2 Dose–response curve of the effect of 7-chlorokynurenic acid, a selective and potent antagonist for the glycine modulatory site of the NMDAR. We determined the antagonistic effect of 7-chlorokynurenic acid by calculating the percent reduction on the amplitude of the isolated NMDAR current in both types of mice. Experiments were performed in voltage-clamp mode, at −65 mV in a low Mg^{2+} solution. The higher doses 7-chlorokynurenic acid that are required to block the isolated NMDAR current in GlyT1+/– mice suggest a higher level of ambient glycine at Schaffer collaterals/CA1 synapses in GlyT1+/– compared to WT mice.

saturated in GlyT1+/– but not in WT mice since the application of glycine (10 μM) did not enhance the amplitude of NMDAR current in GlyT1+/– while increasing the amplitude of NMDAR current by approximately 40% in WT mice (Tsai *et al.* 2004; Martina *et al.* 2005).

In this series of experiments, we compared the antagonistic effect of 7-chlorokynurenic acid on the NMDAR current amplitude by recording CA1 pyramidal neurons from mutant and WT mice. NMDAR current was pharmacologically isolated as described in the experimental procedures. Experiments were performed blinded to the investigator and the genotyping was revealed only after the analysis was completed. NMDAR current amplitude was determined at baseline. The effect of the selective glycine modulatory binding site antagonist, 7-chlorokynurenic acid (Kemp *et al.* 1988) was measured at four different doses. We determined the antagonistic effect of 7-chlorokynurenic acid by calculating the percent reduction on the amplitude of the isolated NMDAR current in both types of mice. Experiments were performed in voltage-clamp mode, at −65 mV in a low Mg^{2+} solution (see Materials and methods).

Application of 7-chlorokynurenic acid at the doses of 10 μM and 100 μM did not induce significant differences in the amplitude reduction in NMDAR current of CA1 pyramidal neurons between the two types of mice (Fig. 2). However, we found that at the doses of 0.1 and 1 μM, 7-chlorokynurenic acid induced a smaller amplitude reduction in the isolated NMDAR current of CA1 pyramidal neurons in GlyT1+/– compared to WT mice. These results strengthen our hypothesis that there is a higher level of endogenous glycine at the extracellular milieu at the CA1 region of the hippocampus in GlyT1+/– mice in comparison to WT mice (Fig. 2).

Pharmacological paradigm was used to isolate of extra-synaptic NMDARs

Since there is no significant difference in the expression of NR1, NR2A-B-C-D subunits in the hippocampus between mutant and WT mice, we hypothesized that the lower reduction in the amplitude of the isolated NMDAR current at the synapse induced by ifenprodil in GlyT1+/– compared to WT mice could be explained by a lower density of synaptic NR2B-containing-NMDAR subunits of CA1 pyramidal

neurons of GlyT1+/− mice. To selectively activate extra-synaptic NMDARs, we performed the experiment in three steps.

First, we stimulated the Schaffer collaterals and induced EPSC every 15 s. NMDAR component of EPSC was pharmacologically isolated using selective antagonists for AMPAR, $GABA_A$, $GABA_B$, and glycine receptor, in a low Mg^{2+} solution. The concentration of drugs applied in the perfusate was (μM): NBQX (10), picrotoxin (50), CGP 52432 (10), strychnine (0.5), MK-801 (30), DL-TBOA (30) and ifenprodil (5). The recording of NMDAR current during the first 5 min was normalized at 100% and used as the control value.

Second, we took advantage of the unique property of the 'irreversible' open channel blocker MK-801, a use-dependent antagonist with a high-affinity for the phencyclidine site within the NMDAR channel (Huettner and Bean 1988). Following a baseline recording of 10 min, MK-801 (30 μM) was included in ACSF. MK-801 blocked selectively synaptic NMDARs that opened in response to synaptically released glutamate. Repeated electrical stimulation in the presence of MK-801 (every 5 s) progressively blocked NMDAR-mediated synaptic activity. Because MK-801 is a use-dependent NMDAR antagonist, we used a 5 s interval for the electrical stimulation only when MK-801 was applied in the ACSF in order to block more rapidly the synaptic NMDARs. In all other situations, the electrical stimulation interval was always performed at every 15 s. Application of MK-801 in the ACSF induced a rapid decline in the amplitude of the NMDAR current after 15 min: 6.93 ± 0.93% $n = 5$ in GlyT1+/− mice and 7.74 ± 0.96%, $n = 5$ in WT mice. The residual current remained stable following the removal of MK-801 from the ACSF even after 30 min: 6.42 ± 0.88%, $n = 5$ in GlyT1+/− mice and 7.23 ± 0.94% $n = 5$ in WT mice (Fig. 3a and b). Because MK-801 dissociates very slowly from NMDARs at −65 mV (Huettner and Bean 1988), NMDARs bound to MK-801 were no longer contributing to the amplitude of the isolated NMDAR current.

Third, following the removal of MK-801 from the ACSF, we applied a glutamate reuptake antagonist, DL-TBOA (30 μM) and the electrical stimulation interval was readjusted back to every 15 s. Under these conditions, glutamate can diffuse at extra-synaptic sites away from synaptic contacts and activate the extra-synaptic NMDAR population (Clements *et al.* 1992). We found that the application of DL-TBOA induces a recovery in the current amplitude presumably *via* activation of extra-synaptic NMDARs (98.54 ± 12.31%, $n = 5$ in GlyT1+/− and 95.22 ± 14.92%, $n = 4$ in WT mice (Fig. 3c and d). We also found that the amplitude of the current induced following application of DL-TBOA, was blocked by the highly potent competitive NMDAR antagonist, APV (100 μM; Fig. 3e and f). These results suggest that the extra-synaptic currents were indeed mediated by NMDARs and not the result of activation of other ion currents.

We compared the results obtained with MK-801 (30 μM) with APV (100 μM). We observed a more rapid decline of the amplitude of the isolated synaptic NMDAR currents when APV (100 μM) was included in the ACSF, since APV is a competitive NMDAR antagonist compared to MK-801 which is a use dependent antagonist. In contrast to the experiments performed with MK-801, following the removal of APV (100 μM) from the ACSF, the amplitude of the isolated synaptic NMDAR current recovered rapidly in WT mice: (1) 99.53 + 4.51%, baseline synaptic NMDAR current; (2) 6.24 + 1.21% following application of APV in the ACSF; (3) 82.96 + 12.23% after removal of APV from the ACSF, $n = 4$ (Fig. 4a). In GlyT1+/− mice: (1) 99.93 + 2.68%, baseline synaptic NMDAR; (2) 9.23 + 0.45%, following application of APV in the ACSF; (3) 90.23 + 3.56%, after removal of APV from the ACSF, $n = 5$ (Fig. 4b). Even though APV is a very potent competitive antagonist for the glutamate binding site on the NMDAR, we also observed a residual current in GlyT1+/− and in WT mice (Fig. 4a and b) similar to the one observed following application of MK-801 (Fig. 3a and b).

The residual current remaining following the block of synaptic NMDAR current by MK-801 is intriguing. We used two different approaches to determine whether that current could be blocked. First, in WT mice, application of APV (100 μM) was tested on the residual current following application of MK-801 in the ACSF. Interestingly, APV (100 μM) did not modify significantly the remaining current [8.57 ± 0.59%; following application of MK-801 in the ACSF and 7.58 ± 0.70% following application of APV in the ACSF; $n = 6$, $p = 0.64$ (Fig. 4c)]. The effect of APV (100 μM) was also determined in GlyT1+/− mice. We observed that the amplitude of the residual current was 7.94 ± 0.72% following application of MK-801 in the ACSF and 8.73 ± .61%, following application of APV; $n = 6$, $p = 0.27$ (Fig. 4d). Second, we investigated the effect of MK-801 (100 μM) on the amplitude of the isolated NMDAR at two different voltages (−65 mM, data not shown and −30 mV). Even though at −30 mV, all NMDARs should be opened, we observed a residual current at that voltage (Fig. 4e and f) similar to the one observed at −65 mV (Fig. 4c and d). These results strongly suggest that the residual current is not mediated by NMDAR but may arise from a baseline noise of the recording or the lack of complete penetration of MK-801 through the slice.

No significant difference was observed in paired pulse ratio between WT and GlyT1+/− mice

Perfusion of the slice with DL-TBOA blocked the glutamate transporters and increased the extracellular level of glutamate. This increase in glutamate at the extracellular milieu may not only activate the extra-synaptic NMDARs but also

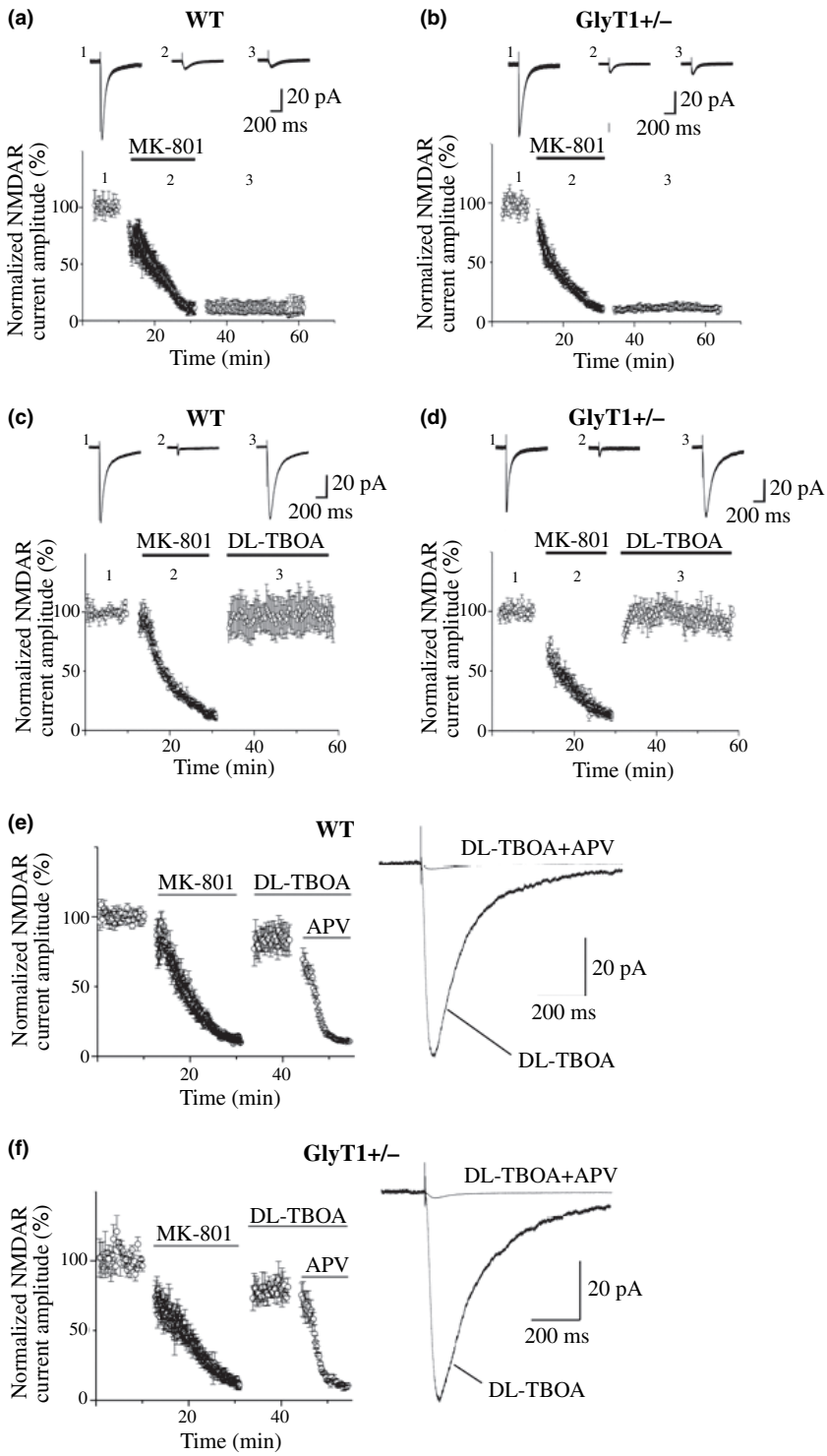

Fig. 3 Stability of NMDAR currents following removal of MK-801 (a and b) and activated extra-synaptic currents during the administration of DL-TBOA (c and d). (a and b) Plots of normalized NMDAR current reduction induced by MK-801 (30 μM) in GlyT1+/– ($n = 5$) and WT ($n = 5$) mice. Representative traces are shown at the time points as indicated (1, control; 2, MK-801; 3, after removal of MK-801). Please note that following the removal of MK-801 from the ACSF, the remaining current was stable over a period of 30 min. (c and d) DL-TBOA activates of extra-synaptic NMDAR currents in GlyT1+/– ($n = 5$) and WT ($n = 4$) mice. Synaptic NMDAR current was blocked by MK-801 (30 μM) and application of DL-TBOA (30 μM) induced spillover of glutamate in the extra-synaptic area, which in turn activated extra-synaptic NMDARs. Representative traces are shown at the time points as indicated (1, control; 2, MK-801; 3, DL-TBOA). Bars: 20 pA, 200 ms. (e and f) DL-TBOA activated extra-synaptic NMDAR currents (thick line), which in turn were blocked by APV (100 μM; thin line). Please note that no significant difference in the amplitude of the isolated NMDAR current was observed between GlyT1+/– and WT mice. Bars: 20 pA, 200 ms.

metabotropic glutamatergic receptors located pre- and post-synaptically. In such conditions, pre-synaptic release probability may be affected (Benquet *et al.* 2002). We performed a series of experiments to rule out this possibility. We used the pair-pulse paradigm to determine the release probability. A change in the ratio of the NMDAR current amplitude would suggest that the application of DL-TBOA changed the rate of pre-synaptic release probability. Our results demonstrate that the paired-pulse paradigm did not show any significant differences in the ratio of NMDAR current amplitude in both types of mice (4.56 ± 0.25: 50 ms; 2.92 ± 0.31: 100 ms; 1.89 ± 0.16: 200 ms; 1.09 ± 0.11:

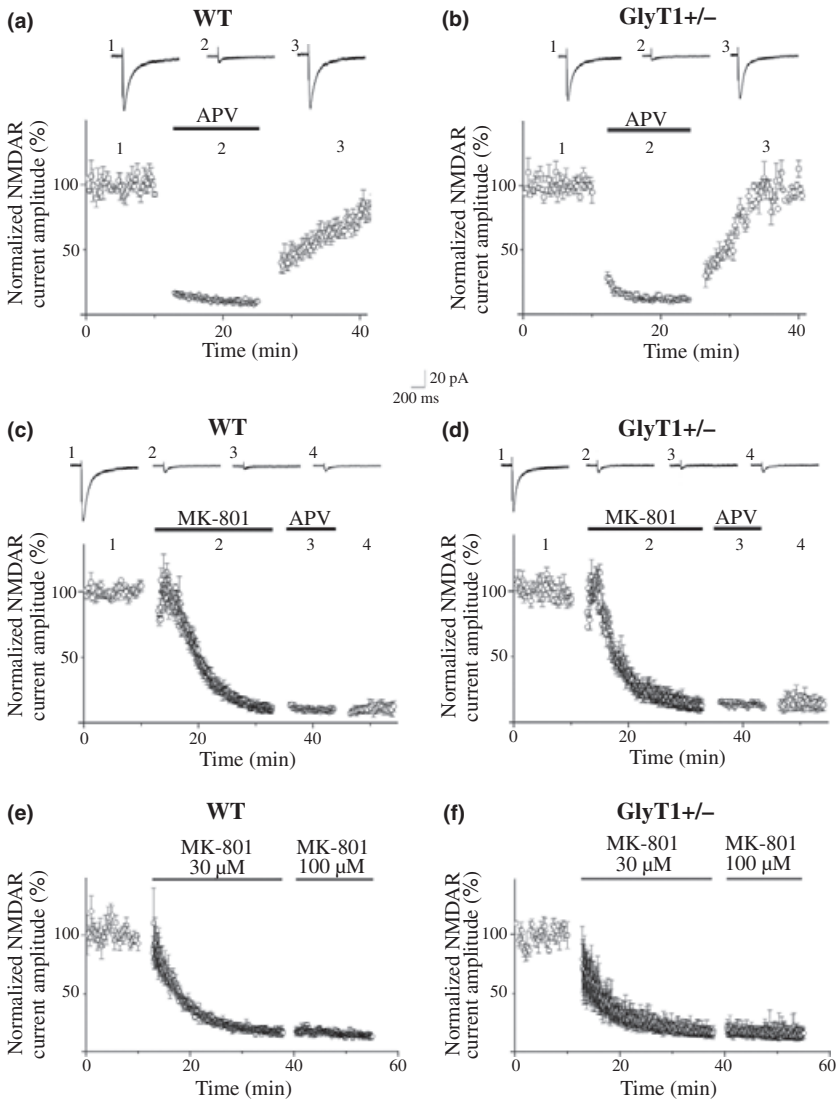

Fig. 4 Synaptic NMDARs in CA1 pyramidal neurons from GlyT1+/– mice and WT mice. Synaptic NMDAR currents in CA1 pyramidal neurons were obtained by electrical stimulation of Schaffer collateral fibers using a bipolar electrode. Recordings were made in voltage-clamp mode at *Vm* = –65 mV. (a and b) Synaptic NMDAR current recorded in low Mg^{2+} ACSF (0.1 mM) from GlyT1+/– ($n = 5$) and WT ($n = 4$) was blocked by APV (100 μM). (c and d) Plots of synaptic NMDAR current inhibition by MK-801 (30 μM) in GlyT1+/– ($n = 7$) and in WT ($n = 7$). Following the removal of MK-801 from low Mg^{2+} ACSF, the remaining currents were still detectable upon the administration of APV (100 μM). Please note that following the removal of APV from the ACSF (c and d) did not modify significantly the amplitude of the residual current. Representative traces shown in each inset are indicated at the time point of each plot. Bars: 20 pA, 200 ms. (e and f) The effect of higher dose (100 μM) of MK-801 on the amplitude of the isolated NMDAR current was also determined at –30 mV in both types of mice in a low Mg solution (see Materials and methods). The results indicate that there is not a significant difference in the amplitude of the residual current following the application of MK-801. The results further suggest that the remaining current is likely not mediated by NMDARs but may only represent the fact that penetration of the slice by MK-801 is not completely achieved.

500 ms; 0.91 ± 0.06: 1 s; $n = 6$ for GlyT1+/– mice and 4.55 ± 1.05: 50 ms; 3.08 ± 0.47: 100 ms; 1.81 ± 0.25: 200 ms; 0.96 ± 0.01: 500 ms; 0.85 ± 0.05: 1 s; $n = 6$ for WT mice; data not shown), suggesting that pre-synaptic release probability is not modified by the increase of glutamate following application of DL-TBOA, at least at the dose that we used. We also performed the paired-pulse ratio experiments using AMPAR EPSC before and following application of DL-TBOA in both types of mice. Some investigators use the AMPAR-EPSC as a standard for paired pulse paradigm. Paired-pulse paradigms were performed at 100 and 50 ms intervals before and after the application of DL-TBOA. Our results do not suggest any significant difference in the paired-pulse ratio of AMPAR EPSC before and after application of DL-TBOA and between 100 or 200 ms intervals, in agreement with the result obtained in the NMDAR EPSC ratio (Fig. 5).

Ifenprodil antagonism in extra-synaptic area was higher in GlyT1+/– mice

We selectively activated extra-synaptic NMDARs of CA1 pyramidal neurons from both types of mice using the paradigm described above. We determined the antagonism induced by ifenprodil by measuring the amplitude reduction in the isolated NMDAR current. We found that the percent reduction in the amplitude of the isolated NMDAR current was significantly greater in GlyT1+/–compared to the WT mice (50.12 ± 4.03%; $n = 9$ for GlyT1+/– mice; $p < 0.05$ and 32.82 ± 6.17%; $n = 8$ for WT; Fig. 6), suggesting a higher density of NR2B-containing-NMDARs in the extra-synaptic area in GlyT1+/– compared to WT mice. One may argue that the concentration of endogenous glycine could effect the antagonism of ifenprodil on extra-synaptic NMDARs. To address this possibility, we repeated the same experimental series in presence of a saturating dose of

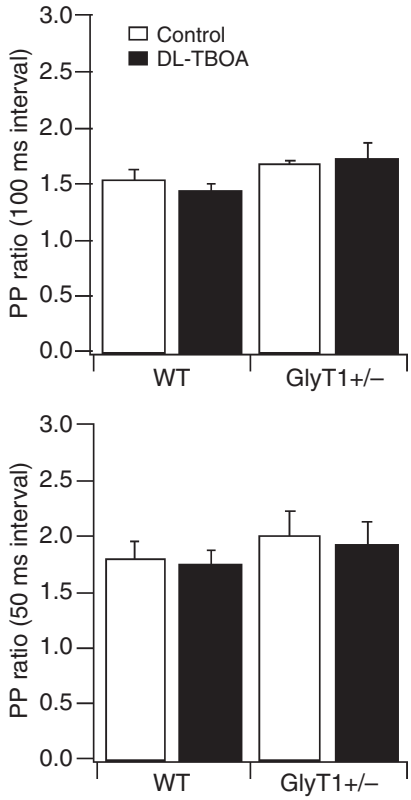

Fig. 5 Paired-pulse ratio in extra-synaptic AMPAR currents. Paired pulse ratio reflects neurotransmitter release probability. Representative traces of extra-synaptic AMPAR current in paired-pulse stimuli with the interval of 50 and 100 ms: No significant difference in paired-pulse ratio was observed between WT (n = 5) and GlyT1+/– mice (n = 5).

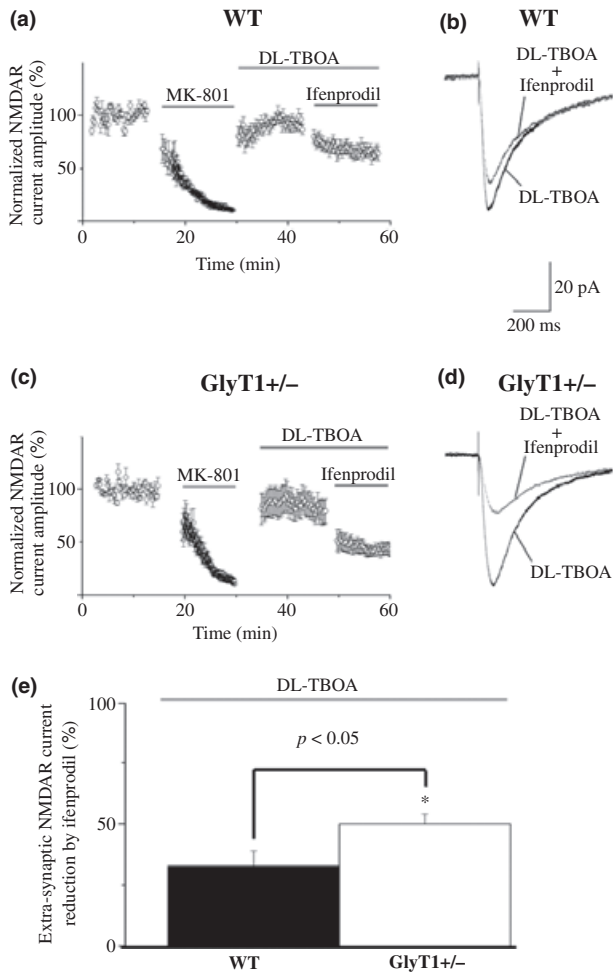

Fig. 6 Reduction rate of extra-synaptic NMDAR currents by ifenprodil (specific NR2B antagonist) is larger in GlyT1+/– pyramidal neurons. Ifenprodil antagonized extra-synaptic NR2B-containing-NMDAR. Representative traces of extra-synaptic NMDAR current from WT mice (a) and from GlyT1+/– mice (c) during application of DL-TBOA (thick line), and DL-TBOA + ifenprodil (thin line) are superimposed. Sample traces showing activation of extra-synaptic NMDAR current and reduction in extra-synaptic NMDAR current in WT mice (b) and GlyT1+/– mice (d) by 5 μM ifenprodil are shown. (e) Ifenprodil reduced the amplitude of the extra-synaptic NMDAR current by 32.8 ± 6.17% in WT (n = 8) and 50.1 ± 4.03% in GlyT1+/– (n = 9). Bars: 20 pA, 200 ms.

glycine (10 μM). In these conditions, we also observed a greater reduction in ifenprodil (10 μM) on the amplitude of the NMDAR current in mutant compared to WT mice (data not shown).

Deactivation kinetics of synaptic NMDAR currents from GlyT1+/– mice were faster in synaptic NMDARs but slower in extra-synaptic NMDARs

Finally, we characterized the kinetics of NMDARs in both types of mice. Indeed, another convincing argument that favors a difference in NMDAR subunit makeup between the GlyT1+/– and WT mice could be a difference in the kinetics of the isolated NMDAR current between synaptic *vis-à-vis* extra-synaptic sites in both types of mice. If indeed NR2B-containing-NMDARs moved from synaptic to extra-synaptic area in mutant, one would expect a slower NMDAR kinetic in the extra-synaptic areas of mutant. Data are summarized in Table 1. These results show that the kinetics of the synaptic NMDAR current from CA1 pyramidal neurons is faster in GlyT1+/– compared to WT mice. In contrast, the kinetics of the extra-synaptic NMDAR-mediated currents from CA1 pyramidal neurons is slower in GlyT1+/– compared to WT mice (255.32 ± 20.57 ms, n = 14 in GlyT1+/– mice and 180.49 ± 9.00 ms, n = 14 in WT mice: $p < 0.05$; Table 1). These results suggest higher density of NR2B-containing-NMDARs in the extra-synaptic area of GlyT1+/– mice.

All together, our results suggest a '*displacement*' of NR2B-containing-NMDAR subunits from the synaptic to the extra-synaptic area under a state of chronic saturating level of glycine.

Table 1 Rise and decay time constants of NMDAR currents in WT and GlyTl+/− CA1 pyramidal neurons recorded in low Mg^{2+} ACSF (0.1 mM) at −65 mV

	Synaptic				Ifenprodil-synaptic			
	τ_{rise}	τ_f	τ_s	τ_{mean}	τ_{rise}	τ_f	τ_s	τ_{mean}
Synaptic								
WT	10.40 ± 0.56 *n* = 28	70.18 ± 2.44 *n* = 28	469.11 ± 31.06 *n* = 28	135.33 ± 5.49 *n* = 28	14.74 ± 2.45 *n* = 6	61.22 ± 3.24 *n* = 6	376.01 ± 18.28 *n* = 6	107.50 ± 3.40 *n* = 6
GlyT1+/−	8.78 ± 0.40 *n* = 25	63.47 ± 1.77 *n* = 25	393.01 ± 21.90* *n* = 25	113.70 ± 5.50* *n* = 25	11.50 ± 0.81 *n* = 5	60.25 ± 1.15 *n* = 5	377.25 ± 26.07 *n* = 5	109.21 ± 2.75 *n* = 5
	DL-TBOA				DL-TBOA+Ifenprodil			
	τ_{rise}	τ_f	τ_s	τ_{mean}	τ_{rise}	τ_f	τ_s	τ_{mean}
Extra-synaptic								
WT	33.02 ± 2.68 *n* = 14	94.12 ± 4.07 *n* = 14	496.11 ± 34.29 *n* = 14	180.49 ± 9.00 *n* = 14	33.82 ± 1.60 *n* = 8	80.62 ± 6.48 *n* = 8	423.17 ± 42.12 *n* = 8	160.14 ± 17.23 *n* = 8
GlyT1+/−	37.21 ± 3.11 *n* = 14	133.75 ± 11.84* *n* = 14	682.89 ± 45.43* *n* = 14	255.32 ± 20.57* *n* = 14	37.14 ± 0.95 *n* = 8	110.34 ± 22.56 *n* = 8	316.53 ± 23.16 *n* = 8	215.42 ± 19.75 *n* = 8

Electrically evoked NMDAR currents were recorded in a low Mg2 + ACSF (0.1 mM) in presence of NBQX (10 μM), picrotoxin (50 μM), strychnine (0.5 μM), MK-801 (30 μM), DL-TBOA (30 μM), and ifenprodil (5 μM). Following blockade of synaptic NMDAR, extra-synaptic NMDAR was activated by DL-TBOA. Each component is designated as rise time constants of the NMDAR currents by τ_{rise} and the weighted time constant by τ_{mean}. Values are mean ± SE. * Significant differences were observed between WT and GlyT1+/− mice ($p < 0.05$).

Discussion

In the present study, we report that the sustained saturating level of endogenous glycine impacts on the NMDAR kinetic of CA1 pyramidal neurons. The assumption that there is a higher level of endogenous glycine in mutant mice was confirmed by a dose-response curve comparing the antagonistic effect of 7-chlorokynurenic acid in both types of mice. Faster kinetics of synaptic NMDARs in mutant mice may suggest a change in NMDAR subunit makeup. However, the results of immunoblotting experiments do not demonstrate any significant changes in the level of protein expression for NR1, NR2A, and NR2B. We hypothesized that a displacement of NR2A- or NR2B-containing NMDAR from synaptic to extra-synaptic. Our challenge was then to find an experimental design that could allow the discrimination of the two populations (synaptic and extra-synaptic) of NMDARs. We took advantage of the unique property of irreversible block of NMDARs by MK-801 and the potent effect of DL-TBOA to induce glutamate spillover to extra-synaptic areas. Using that pharmacological paradigm, we found that at the extra-synaptic area, the antagonistic effect of ifenprodil was significantly higher in GlyT1+/− compared to WT mice, suggesting a displacement of NR2B-containing-NMDAR subunits from the synaptic to extra-synaptic site in GlyT1+/− mice.

NMDARs are localized in both synaptic and extra-synaptic areas, but they are found at higher density within the synapse (Clark and Cull-Candy 2002). Shortly after birth, synaptic NMDARs of cortical neurons display relatively large and long-duration NMDAR-mediated EPSC (Barth and Malenka 2001; Lu *et al.* 2001) and have a low open probability (Rosenmund *et al.* 1995; Chen *et al.* 1999; Popescu and Auerbach 2003). However, during postnatal development, the decay of synaptic NMDAR kinetic becomes faster (Monyer *et al.* 1994; Crair and Malenka 1995). These changes are accompanied by a decline in the ability of the highly NR1/NR2B-selective antagonist ifenprodil to reduce NMDAR current (Legendre and Westbrook 1991; Williams 1993; Quinlan *et al.* 1999). After the peak of synaptogenesis, the NR1/NR2A complex, characterized by rapid offset kinetics, dominates at the synapse, while the NR1/NR2B complex, characterized by slow kinetics, predominates in the extra-synaptic area (Rumbaugh and Vicini 1999; Tovar and Westbrook 1999; Li *et al.* 2002). The activation of extra-synaptic NMDARs by glutamate escaping from the synaptic cleft during episodes of high synaptic activity (Conti and Weinberg 1999; Kullmann 1999) suggests that they may have a different role (Sattler *et al.* 2000; Vanhoutte and Bading 2003; Scimemi *et al.* 2004). Moreover, extra-synaptic NMDARs are the target for astrocytic glutamate release (Fellin *et al.* 2004). While extra-synaptic NMDAR-mediated signaling may contribute to the overall dynamics of neuronal synchrony, its presence raises a series of intriguing questions on its possible role in pathological changes (Hardingham *et al.* 2002). It has been proposed that extra-synaptic NMDARs are important mediators of excitotoxicity, whereas synaptic NMDARs appear neuroprotective

(Prybylowski and Wenthold 2004). Another major difference between synaptic and extra-synaptic NMDARs is that the former colocalize and interact with many signaling proteins that are concentrated within the post-synaptic compartment (Ziff 1997).

The use of MK-801 to block synaptic NMDAR has been previously reported. Work from Westbrook laboratory has shown that in immature hippocampal neuron cultures, NMDAR EPSC exhibits a slow recovery following MK-801 blockade of synaptic NMDARs (Tovar and Westbrook 2002). It has been suggested that this may be due to a lateral movement of extra-synaptic NMDARs into the synapse (Tovar and Westbrook 2002; Triller and Choquet 2003; Groc *et al.* 2004). However, this phenomenon has not been investigated in mature neurons from acute hippocampal slices. Moreover, MK-801 dissociating from synaptic NMDAR channels over time also needed to be considered. We carefully addressed these two possibilities and our results illustrated in Fig. 3 do not support the observations from immature neurons in culture.

The nature of the remaining current observed after the block of synaptic NMDARs by MK-801 is puzzling. In all experiments performed in the present investigation, there was always a residual current of approximately 10%. Application of APV (100 μM) and MK-801 (100 μM) on that residual current did not modify significantly its amplitude. Indeed, when we compared the amplitude between APV and MK-801 for each mouse line, the statistical values were: in GlyT1+/− mice, $p = 0.64$, $n = 6$ and in WT mice, $p = 0.27$, $n = 6$ (Fig. 5c and d). Using the paradigm described in our manuscript, we recorded more than 1000 neurons so far in which synaptic NMDARs were inactivated with MK-801 and we always observed the same finding. This is in contrast to the recordings made on slices from cultures where the thicknesses are much less (approximately 40 μm). In such conditions, the penetration of MK-801 through the slice is facilitated.

We have established a rigorous experimental approach to discriminate synaptic from extra-synaptic NMDARs. To do so, we induced glutamate 'spillover' using a glutamate reuptake blocker. It has been reported that glutamate 'spillover' is observed between Schaffer collateral fiber synapses onto CA1 pyramidal neurons only when glutamate transporters are blocked (Diamond and Jahr 2000; Diamond 2001, 2002). Moreover, NMDARs are especially sensitive to the phenomenon of glutamate 'spillover' due to their high affinity for glutamate and their slow desensitization (Kullmann and Asztely 1998; Rusakov and Kullmann 1998; Lozovaya *et al.* 1999). Finally, a recent study suggests that at the Schaffer collateral/CA1 synapse, NR2B-containing-NMDARs are activated by glutamate 'spillover' while NR2A-containing-NMDARs do not share such 'spillover' signals (Scimemi *et al.* 2004). This is of particular interest since our experimental paradigm is designed to investigate the difference between NR2B subunits in the synaptic cleft compared to the extra-synaptic pool between the two types of mice. Our results shown in Fig. 4 strongly suggest that at these synapses, DL-TBOA induces glutamate spillover and activates solely extra-synaptic NMDARs since the recovering EPSC is abolished by the application of APV (100μM).

Deactivation time constant for current mediated by NR1/NR2A assemblies is comprised of tens of milliseconds, compared to hundreds of milliseconds for NR1/NR2B, and several seconds for NR1/NR2D (Vicini *et al.* 1998; Wyllie *et al.* 1998). A recent study has shown that NR2D-containing-NMDARs are present in the adult mouse hippocampus (Lozovaya *et al.* 2004) but only extra-synaptically. One can argue that the slower kinetic of extra-synaptic NMDAR current that we observed in GlyT1+/− mice may be due, at least in part, to the contribution of NR2D. However, immunohistochemical studies from adult murine hippocampal formation indicate that NR2D-like immunoreactivity is totally excluded from CA1 pyramidal bodies (Thompson *et al.* 2002).

One of the very important scaffolding proteins known to interact with NMDAR is PSD-95 (Kornau *et al.* 1995; Niethammer *et al.* 1996; Liao *et al.* 2000; Roy *et al.* 2002; Rutter *et al.* 2002; Lavezzari *et al.* 2003). Recently, it has been reported that PSD-95 interacts with GlyT1 and impairs its internalization (Cubelos *et al.* 2005). Indeed, biochemical evidence suggests a physical interaction of GlyT1 and PSD-95 by the C-terminal sequence of the transporter. We performed immunoblotting experiments using a selective antibody for PSD-95. Interestingly, we found that the expression of PSD-95 was approximately 50% less in mutant compared to the WT mice ($n = 6$, data not shown). Even though it has been reported that deletion of the gene for PSD-95, synaptic NMDAR currents, subunit expression, and morphology are all unaffected in the mutant mice (Migaud *et al.* 1998), it appears that PSD-95 is important in coupling NMDAR. It is generally agreed that the role of PSD-95 is likely to be restricted to the control expression of synaptic AMPAR as its over-expression seems to have minimal effect on NMDAR synaptic current amplitude (Lim *et al.* 2003; Beique *et al.* 2004). It is unclear at this point to what extent which acute manipulation of PSD-95 expression (over-expression or RNAi strategies (Nakagawa *et al.* 2004; Kim and Sheng 2004) might have a more subtle effect on NMDAR expression.

The *in vivo* animal model used for this investigation may be an excellent model to study a disease that is known to be related to a chronic high level of glycine. Glycine encephalopathy is an autosomal recessive disorder in which the level of glycine is elevated in the blood and CSF of afflicted individuals. Glycine concentration is markedly elevated in the brain tissue (Agamanolis *et al.* 1993). Most patients die soon after birth, and those who survive manifest severe

neurological deficits such as psychomotor retardation and convulsions that are difficult to treat (Agamanolis *et al.* 1993). It has been proposed that neonatal glycine encephalopathy may be due to excessive post-synaptic inhibition. However, attempts to reverse this inhibition with strychnine, an antagonist of glycine receptor, have been unsuccessful. Interestingly, oral administration of NMDAR antagonists, such as ketamine, improved the patient's condition and this is correlated with electroencephalographic findings (Ohya *et al.* 1991). Moreover, early treatment with NMDAR antagonists appeared to reduce late neurological complications (Boneh *et al.* 1996). Our findings further support the role of NMDARs in this pathological condition.

Conflict of interest

The authors declare that no conflict of interest exists.

Acknowledgements

We thank Dr. Joseph T. Coyle from Harvard Medical School for providing the transgenic mice, Dr. Marzia Martina for reading the manuscript, Christian Metivier, Marie-Eve B.-Turcotte for technical support, and Linda Richard for secretarial assistance. This work is supported by grants awarded to Richard Bergeron from the Canadian Institutes of Health Research (MOP-79360) and by March of Dimes Foundation (#6-FY06-327).

References

Agamanolis D. P., Potter J. L. and Lundgren D. W. (1993) Neonatal glycine encephalopathy: biochemical and neuropathologic findings. *Pediatr. Neurol.* **9**, 140–143.

Amaral D. G. and Witter M. P. (1989) The three-dimensional organization of the hippocampal formation: a review of anatomical data. *Neuroscience* **31**, 571–591.

Barth A. L. and Malenka R. C. (2001) NMDAR EPSC kinetics do not regulate the critical period for LTP at thalamocortical synapses. *Nat. Neurosci.* **4**, 235–236.

Beique J. C., Campbell B., Perring P., Hamblin M. W., Walker P., Mladenovic L. and Andrade R. (2004) Serotonergic regulation of membrane potential in developing rat prefrontal cortex: coordinated expression of 5-hydroxytryptamine (5-HT)1A, 5-HT2A, and 5-HT7 receptors. *J. Neurosci.* **24**, 4807–4817.

Benquet P., Gee C. E. and Gerber U. (2002) Two distinct signaling pathways upregulate NMDA receptor responses via two distinct metabotropic glutamate receptor subtypes. *J. Neurosci.* **22**, 9679–9686.

Boneh A., Degani Y. and Harari M. (1996) Prognostic clues and outcome of early treatment of nonketotic hyperglycinemia. *Pediatr. Neurol.* **15**, 137–141.

Chen N., Luo T. and Raymond L. A. (1999) Subtype-dependence of NMDA receptor channel open probability. *J. Neurosci.* **19**, 6844–6854.

Clark B. A. and Cull-Candy S. G. (2002) Activity-dependent recruitment of extrasynaptic NMDA receptor activation at an AMPA receptor-only synapse. *J. Neurosci.* **22**, 4428–4436.

Clements J. D., Lester R. A., Tong G., Jahr C. E. and Westbrook G. L. (1992) The time course of glutamate in the synaptic cleft. *Science* **258**, 1498–1501.

Conti F. and Weinberg R. J. (1999) Shaping excitation at glutamatergic synapses. *Trends Neurosci.* **22**, 451–458.

Crair M. C. and Malenka R. C. (1995) A critical period for long-term potentiation at thalamocortical synapses. *Nature* **375**, 325–328.

Cubelos B., Gonzalez-Gonzalez I. M., Gimenez C. and Zafra F. (2005) The scaffolding protein PSD-95 interacts with the glycine transporter GLYT1 and impairs its internalization. *J. Neurochem.* **95**, 1047–1058.

Danysz W. and Parsons A. C. (1998) Glycine and N-methyl-D-aspartate receptors: physiological significance and possible therapeutic applications. *Pharmacol. Rev.* **50**, 597–664.

Diamond J. S. (2001) Neuronal glutamate transporters limit activation of NMDA receptors by neurotransmitter spillover on CA1 pyramidal cells. *J. Neurosci.* **21**, 8328–8338.

Diamond J. S. (2002) A broad view of glutamate spillover. *Nat. Neurosci.* **5**, 291–292.

Diamond J. S. and Jahr C. E. (2000) Synaptically released glutamate does not overwhelm transporters on hippocampal astrocytes during high-frequency stimulation. *J. Neurophysiol.* **83**, 2835–2843.

Fellin T., Pascual O., Gobbo S., Pozzan T., Haydon P. G. and Carmignoto G. (2004) Neuronal synchrony mediated by astrocytic glutamate through activation of extrasynaptic NMDA receptors. *Neuron* **43**, 729–743.

Gomeza J., Hulsmann S., Ohno K., Eulenburg V., Szoke K., Richter D. and Betz H. (2003) Inactivation of the glycine transporter 1 gene discloses vital role of glial glycine uptake in glycinergic inhibition. *Neuron* **40**, 785–796.

Groc L., Heine M., Cognet L., Brickley K., Stephenson F. A., Lounis B. and Choquet D. (2004) Differential activity-dependent regulation of the lateral mobilities of AMPA and NMDA receptors. *Nat. Neurosci.* **7**, 695–696.

Hardingham G. E., Fukunaga Y. and Bading H. (2002) Extrasynaptic NMDARs oppose synaptic NMDARs by triggering CREB shut-off and cell death pathways. *Nat. Neurosci.* **5**, 405–414.

Huettner J. E. and Bean B. P. (1988) Block of N-methyl-D-aspartate-activated current by the anticonvulsant MK-801: selective binding to open channels. *Proc. Natl Acad. Sci. USA* **85**, 1307–1311.

Ivanovic A., Reilander H., Laube B. and Kuhse J. (1998) Expression and initial characterization of a soluble glycine binding domain of the N-methyl-D-aspartate receptor NR1 subunit. *J. Biol. Chem.* **273**, 19933–19937.

Kemp J. A., Foster A. C., Leeson P. D., Priestley T., Tridgett R., Iversen L. L. and Woodruff G. N. (1988) 7-Chlorokynurenic acid is a selective antagonist at the glycine modulatory site of the N-methyl-D-aspartate receptor complex. *Proc. Natl Acad. Sci. USA* **85**, 6547–6550.

Kew J. N., Richards J. G., Mutel V. and Kemp J. A. (1998) Developmental changes in NMDA receptor glycine affinity and ifenprodil sensitivity reveal three distinct populations of NMDA receptors in individual rat cortical neurons. *J. Neurosci.* **18**, 1935–1943.

Kim E. and Sheng M. (2004) PDZ domain proteins of synapses. *Nat. Rev. Neurosci.* **5**, 771–781.

Kornau H. C., Schenker L. T., Kennedy M. B. and Seeburg P. H. (1995) Domain interaction between NMDA receptor subunits and the postsynaptic density protein PSD-95. *Science* **269**, 1737–1740.

Kullmann D. M. (1999) Excitatory synapses. Neither too loud nor too quiet. *Nature* **399**, 111–112.

Kullmann D. M. and Asztely F. (1998) Extrasynaptic glutamate spillover in the hippocampus: evidence and implications. *Trends Neurosci.* **21**, 8–14.

Laube B., Kuhse J. and Betz H. (1998) Evidence for a tetrameric structure of recombinant NMDA receptors. *J. Neurosci.* **18**, 2954–2961.

Lavezzari G., McCallum J., Lee R. and Roche K. W. (2003) Differential binding of the AP-2 adaptor complex and PSD-95 to the C-ter-

minus of the NMDA receptor subunit NR2B regulates surface expression. *Neuropharmacology* **45**, 729–737.

Legendre P. and Westbrook G. L. (1991) Ifenprodil blocks N-methyl-D-aspartate receptors by a two-component mechanism. *Mol. Pharmacol.* **40**, 289–298.

Li B., Chen N., Luo T., Otsu Y., Murphy T. H. and Raymond L. A. (2002) Differential regulation of synaptic and extra-synaptic NMDA receptors. *Nat. Neurosci.* **5**, 833–834.

Liao G. Y., Kreitzer M. A., Sweetman B. J. and Leonard J. P. (2000) The postsynaptic density protein PSD-95 differentially regulates insulin- and Src-mediated current modulation of mouse NMDA receptors expressed in Xenopus oocytes. *J. Neurochem.* **75**, 282–287.

Lim I. A., Merrill M. A., Chen Y. and Hell J. W. (2003) Disruption of the NMDA receptor-PSD-95 interaction in hippocampal neurons with no obvious physiological short-term effect. *Neuropharmacology* **45**, 738–754.

Lozovaya N. A., Kopanitsa M. V., Boychuk Y. A. and Krishtal O. A. (1999) Enhancement of glutamate release uncovers spillover-mediated transmission by N-methyl-D-aspartate receptors in the rat hippocampus. *Neuroscience* **91**, 1321–1330.

Lozovaya N. A., Grebenyuk S. E., Tsintsadze T. S., Feng B., Monaghan D. T. and Krishtal O. A. (2004) Extrasynaptic NR2B and NR2D subunits of NMDA receptors shape 'superslow' afterburst EPSC in rat hippocampus. *J. Physiol.* **558**, 451–463.

Lu H. C., Gonzalez E. and Crair M. C. (2001) Barrel cortex critical period plasticity is independent of changes in NMDA receptor subunit composition. *Neuron* **32**, 619–634.

Martina M., Turcotte M. E., Halman S., Tsai G., Tiberi M., Coyle J. T. and Bergeron R. (2005) Reduced glycine transporter type 1 expression leads to major changes in glutamatergic neurotransmission of CA1 hippocampal neurones in mice. *J. Physiol.* **563**, 777–793.

Migaud M., Charlesworth P., Dempster M. *et al.* (1998) Enhanced long-term potentiation and impaired learning in mice with mutant postsynaptic density-95 protein. *Nature* **396**, 433–439.

Monyer H., Sprengel R., Schoepfer R., Herb A., Higuchi M., Lomeli H., Burnashev N., Sakmann B. and Seeburg P. H. (1992) Heteromeric NMDA receptors: molecular and functional distinction of subtypes. *Science* **256**, 1217–1221.

Monyer H., Burnashev N., Laurie D. J., Sakmann B. and Seeburg P. H. (1994) Developmental and regional expression in the rat brain and functional properties of four NMDA receptors. *Neuron* **12**, 529–540.

Nakagawa T., Futai K., Lashuel H. A., Lo I., Okamoto K., Walz T., Hayashi Y. and Sheng M. (2004) Quaternary structure, protein dynamics, and synaptic function of SAP97 controlled by L27 domain interactions. *Neuron* **44**, 453–467.

Niethammer M., Kim E. and Sheng M. (1996) Interaction between the C terminus of NMDA receptor subunits and multiple members of the PSD-95 family of membrane-associated guanylate kinases. *J. Neurosci.* **16**, 2157–2163.

Ohya Y., Ochi N., Mizutani N., Hayakawa C. and Watanabe K. (1991) Nonketotic hyperglycinemia: treatment with NMDA antagonist and consideration of neuropathogenesis. *Pediatr. Neurol.* **7**, 65–68.

Popescu G. and Auerbach A. (2003) Modal gating of NMDA receptors and the shape of their synaptic response. *Nat. Neurosci.* **6**, 476–483.

Prybylowski K. and Wenthold R. J. (2004) N-Methyl-D-aspartate receptors: subunit assembly and trafficking to the synapse. *J. Biol. Chem.* **279**, 9673–9676.

Quinlan E. M., Philpot B. D., Huganir R. L. and Bear M. F. (1999) Rapid, experience-dependent expression of synaptic NMDA receptors in visual cortex in vivo. *Nat. Neurosci.* **2**, 352–357.

Regalado M. P., Villarroel A. and Lerma J. (2001) Intersubunit cooperativity in the NMDA receptor. *Neuron* **32**, 1085–1096.

Rosenmund C., Feltz A. and Westbrook G. L. (1995) Synaptic NMDA receptor channels have a low open probability. *J. Neurosci.* **15**, 2788–2795.

Roy B. C., Kohu K., Matsuura K., Yanai H. and Akiyama T. (2002) SPAL, a Rap-specific GTPase activating protein, is present in the NMDA receptor-PSD-95 complex in the hippocampus. *Genes Cells* **7**, 607–617.

Rumbaugh G. and Vicini S. (1999) Distinct synaptic and extrasynaptic NMDA receptors in developing cerebellar granule neurons. *J. Neurosci.* **19**, 10603–10610.

Rusakov D. A. and Kullmann D. M. (1998) Extrasynaptic glutamate diffusion in the hippocampus: ultrastructural constraints, uptake, and receptor activation. *J. Neurosci.* **18**, 3158–3170.

Rutter A. R., Freeman F. M. and Stephenson F. A. (2002) Further characterization of the molecular interaction between PSD-95 and NMDA receptors: the effect of the NR1 splice variant and evidence for modulation of channel gating. *J. Neurochem.* **81**, 1298–1307.

Sattler R., Xiong Z., Lu W. Y., MacDonald J. F. and Tymianski M. (2000) Distinct roles of synaptic and extrasynaptic NMDA receptors in excitotoxicity. *J. Neurosci.* **20**, 22–33.

Scimemi A., Fine A., Kullmann D. M. and Rusakov D. A. (2004) NR2B-containing receptors mediate cross talk among hippocampal synapses. *J. Neurosci.* **24**, 4767–4777.

Stocca G. and Vicini S. (1998) Increased contribution of NR2A subunit to synaptic NMDA receptors in developing rat cortical neurons. *J. Physiol.* **507**(Pt 1), 13–24.

Thompson C. L., Drewery D. L., Atkins H. D., Stephenson F. A. and Chazot P. L. (2002) Immunohistochemical localization of N-methyl-D-aspartate receptor subunits in the adult murine hippocampal formation: evidence for a unique role of the NR2D subunit. *Brain Res. Mol. Brain Res.* **102**, 55–61.

Tovar K. R. and Westbrook G. L. (1999) The incorporation of NMDA receptors with a distinct subunit composition at nascent hippocampal synapses in vitro. *J. Neurosci.* **19**, 4180–4188.

Tovar K. R. and Westbrook G. L. (2002) Mobile NMDA receptors at hippocampal synapses. *Neuron* **34**, 255–264.

Triller A. and Choquet D. (2003) Synaptic structure and diffusion dynamics of synaptic receptors. *Biol. Cell* **95**, 465–476.

Tsai G., Ralph-Williams R. J., Martina M., Bergeron R., Berger-Sweeney J., Dunham K. S., Jiang Z., Caine S. B. and Coyle J. T. (2004) Gene knockout of glycine transporter 1: Characterization of the behavioral phenotype. *Proc. Natl Acad. Sci. USA* **101**, 8485–8490.

Vanhoutte P. and Bading H. (2003) Opposing roles of synaptic and extrasynaptic NMDA receptors in neuronal calcium signalling and BDNF gene regulation. *Curr. Opin. Neurobiol.* **13**, 366–371.

Vicini S., Wang J. F., Li J. H., Zhu W. J., Wang Y. H., Luo J. H., Wolfe B. B. and Grayson D. R. (1998) Functional and pharmacological differences between recombinant N-methyl-D-aspartate receptors. *J. Neurophysiol.* **79**, 555–566.

Wafford K. A., Kathoria M., Bain C. J., Marshall G., le Bourdelles B., Kemp J. A. and Whiting P. J. (1995) Identification of amino acids in the N-methyl-D-aspartate receptor NR1 subunit that contribute to the glycine binding site. *Mol. Pharmacol.* **47**, 374–380.

Williams K. (1993) Ifenprodil discriminates subtypes of the N-methyl-D-aspartate receptor: selectivity and mechanisms at recombinant heteromeric receptors. *Mol. Pharmacol.* **44**, 851–859.

Wyllie D. J., Behe P. and Colquhoun D. (1998) Single-channel activations and concentration jumps: comparison of recombinant NR1a/NR2A and NR1a/NR2D NMDA receptors. *J. Physiol.* **510**(Pt 1), 1–18.

Yamakura T. and Shimoji K. (1999) Subunit- and site-specific pharmacology of the NMDA receptor channel. *Prog. Neurobiol.* **59**, 279–298.

Ziff E. B. (1997) Enlightening the postsynaptic density. *Neuron* **19**, 1163–1174.

